ISTANBUL TECHNICAL UNIVERSITY ★ GRADUATE SCHOOL OF SCIENCE ENGINEERING AND TECHNOLOGY

UNSCENTED KALMAN FILTER BASED SATELLITE ORBIT DETERMINATION ON THE GPS AND SINGLE STATION ANTENNA MEASUREMENTS

M.Sc. THESIS

Melih ATA

Department of Aeronautics and Astronautics Engineering

Aeronautics and Astronautics Engineering Programme

JUNE 2013

ISTANBUL TECHNICAL UNIVERSITY ★ GRADUATE SCHOOL OF SCIENCE ENGINEERING AND TECHNOLOGY

UNSCENTED KALMAN FILTER BASED SATELLITE ORBIT DETERMINATION ON THE GPS AND SINGLE STATION ANTENNA MEASUREMENTS

M.Sc. THESIS

Melih Ata
(511111124)

Department of Aeronautics and Astronautics Engineering

Aeronautics and Astronautics Engineering Programme

Thesis Advisor: Prof. Dr. Cengiz HACIZADE

JUNE 2013

İSTANBUL TEKNİK ÜNİVERSİTESİ ★ FEN BİLİMLERİ ENSTİTÜSÜ

UYDU YÖRÜNGELERİNİN GPS VE TEK YER İSTASYONU ÖLÇÜMLERİYLE SEZGİSİZ KALMAN SÜZGECİ TEMELLİ BELİRLENMESİ

YÜKSEK LİSANS TEZİ

Melih ATA
(511111124)

Uçak ve Uzay Mühendisliği Anabilim Dalı

Uçak ve Uzay Mühendisliği Programı

Tez Danışmanı: Prof. Dr. Cengiz HACIZADE

HAZİRAN 2013

Melih Ata, a M.Sc. student of ITU Graduate School of Science Engineering and Technology 511111124, successfully defended the thesis entitled “UNSCENTED KALMAN FILTER BASED SATELLITE ORBIT DETERMINATION ON THE GPS AND SINGLE STATION ANTENNA MEASUREMENTS”, which he prepared after fulfilling the requirements specified in the associated legislations, before the jury whose signatures are below.

Thesis Advisor : **Prof. Dr. Cengiz HACIZADE** ....
Istanbul Technical University

Jury Members : **Assist. Prof. Dr. Turgut Berat KARYOT** ....
Istanbul Technical University

Assist. Prof. Dr. Ali Fuat ERGENÇ ....
Istanbul Technical University

Date of Submission : 02 May 2013
Date of Defense : 06 June 2013

To my family,

FOREWORD

The purpose of the study is actualizing orbit determination of satellites by using different system measurements such as single ground station antenna and Global Positioning System via estimation mechanisms as Unscented and Robust Unscented Kalman Filters. Antenna measurement bias estimation mechanism with Linear Kalman Filter by using antenna and Global Positioning System measurements is also an important object for the study.

I would like to thank to my advisor Prof. Dr.Çingiz Haciyev for his advise and support during my studying.
I am also grateful to my parents who always support me in every period of my life.

April 2013 Melih ATA
(Astronautical Engineer)

TABLE OF CONTENTS

Page

ABBREVIATIONS

OD	: Orbit Determination
GPS	: Global Positioning System
SSA	: Single Station Antenna
SSN	: Space Surveillance Network
GEO	: Geostationary Orbit
LEO	: Low Earth Orbit
KF	: Kalman Filter
LKF	: Linear Kalman Filter
LSE	: Least Squares Estimation
EKF	: Extended Kalman Filter
UT	: Unscented Transformation
UKF	: Unscented Kalman Filter
RUKF	: Robust Unscented Kalman Filter
MNSF	: Measurement Noise Scale Factor
SMNSF	: Single Measurement Noise Scale Factor
MMNSF	: Multiple Measurement Noise Scale Factor
Est	: Estimation
Inc	: Increment
Cont	: Continuous
Out	: Output
Abs	: Absolute
VSAT	: Very Small Aperture Terminal
USAT	: Ultra Small Aperture Terminal
NAVSTAR	: Navigation Signal Time and Range
TIMATION	: Time and Navigation
C/A	: Coarse Acquisition
P	: Precise Code
ECI	: Earth- Centered- Inertial
ECEF	: Earth- Centered –Earth- Fixed
ENU	: East- North- Up

LIST OF TABLES

Page

LIST OF FIGURES

Page

LIST OF SYMBOLS

$\mathbf{x(k)}$: n dimensional state vector
$\boldsymbol{\emptyset}\mathbf{(k+1,k)}$: nxn dimensional system transition matrix
$\mathbf{w(k)}$: r dimensional random Gauss noise vector
$\mathbf{E}$: Statistical expected value operator
$\boldsymbol{\delta}\mathbf{(kj)}$: Cronecker symbol
$\mathbf{G(k+1,k)}$: nxr dimensional transition matrix of system noise
$\mathbf{y(k)}$: s dimensional measurement vector
$\mathbf{H(k)}$: sxn dimensional measurement matrix of system
$\mathbf{v(k)}$: s dimensional measurement noise vector
$\mathbf{\hat{x}\ (k|k)}$: Estimation value
$\mathbf{K(k)}$: Optimal gain matrix
$\mathbf{P(k|k)}$: Correlation matrix of filtering error
$\mathbf{P(k|k-1)}$: Correlation matrix of extrapolation error
$\mathbf{k|k-1}$: The values which are predicted in the previous step
$\mathbf{k,k}$: Estimation via using all measurements
$\mathbf{R(k)}$: Measurement noise correlation matrix
$\mathbf{Q(k)}$: System noise correlation matrix
$\mathbf{\bar{x}}$: Mean value
$\mathbf{P_{xx}}$: Mean covariance
$\mathbf{W_i}$: Weight
$\mathbf{\bar{y}}$: Mean value of transformed points
$\mathbf{P_{yy}}$: Mean covariance of transformed points
$\mathbf{\widehat{X}(k|k)}$: Mean of sigma points
$\mathbf{n}$: State number
$\boldsymbol{\kappa}$: Scaling parameter
$\mathbf{X_0(k|k)}$: Sigma points
$\mathbf{X_i(k|k)}$: Sigma points
$\mathbf{X_{i+n}(k|k)}$: Sigma points
$\mathbf{\widehat{X}(k+1|k)}$: Predicted mean
$\mathbf{P(k+1|k)}$: Predicted covariance
$\mathbf{\widehat{Y}(k+1|k)}$: Predicted observation vector
$\mathbf{P_{YY}(k+1|k)}$: Observation covariance matrix
$\mathbf{P_{XY}(k+1|k)}$: Cross correlation matrix
$\mathbf{Y(k+1)}$: Measurementvector
$\mathbf{v(k+1)}$: Residual term
$\mathbf{P_{vv}(k+1|k)}$: Innovation covariance
$\mathbf{\widehat{X}\ (k+1|k+1)}$: Estimated state vector
$\mathbf{P(k+1|k+1)}$: Estimated covariance matrix
$\mathbf{S(k)}$: Scale factor
$\mathbf{tr(.)}$: Trace
$\boldsymbol{\mu}$: Width of the moving window
$\mathbf{S^*}$: Scale matrix

$\mathbf{S_{ii}}$: i^{th} diagonal element of the matrix $S(k)$
$\boldsymbol{\gamma_0}$: The system is normally operating
$\boldsymbol{\gamma_1}$: There is a malfunction in the estimation system
$\boldsymbol{\beta(k+1)}$: Statistical value
$\boldsymbol{\chi^2_{\alpha,s}}$: Threshold value
$\mathbf{m}$: Width of the moving window
$\boldsymbol{\gamma}$: Kepler constant
$\mathbf{x, y, z}$: Descartes coordinates of the spacecraft in the ECI coordinate frame
$\mathbf{V_x\ \ V_y\ \ V_z}$: Velocities of spacecraft in ECI coordinate frame
$\mathbf{r}$: Range between spacecraft's and Earth's center of masses
$\mathbf{M}$: Mass of the Earth
$\boldsymbol{\Delta t}$: Sampling time
$\mathbf{u, v, w}$: Velocities in x, y, and z directions
$\mathbf{w_{(.)}}$: Gaussian white noise with zero mean
$\boldsymbol{\rho}$: Range from the antenna to the spacecraft
$\boldsymbol{\alpha}$: Azimuth angle
$\boldsymbol{\beta}$: Elevation angle
$\boldsymbol{\rho_E, \rho_N, \rho_U}$: Components of range in the East-North- Up coordinate system
$\mathbf{Z(k)}$: Measurement vector
$\mathbf{h(x(k), k)}$: Nonlinear measurement model
$\boldsymbol{\lambda}$: Latitude
$\boldsymbol{\sigma^2_x, \sigma^2_y, \sigma^2_z}$: Variances of the calculated x, y, z coordinates' errors
$\boldsymbol{\sigma^2_\rho, \sigma^2_\alpha, \sigma^2_\beta}$: Variances of the measurement errors of antenna
$\boldsymbol{\theta}$: Rotation angle of the ECEF system around the Earth's rotation axis
$\mathbf{d_{2000}}$: Duration from the epoch at the beginning of the year 2000
$\mathbf{Re}$: Earth's radius
$\boldsymbol{\rho_x\ \ \rho_y\ \ \rho_z}$: Range components in ECI coordinate frame
$\mathbf{X_0}$: Initial state vector
$\boldsymbol{\sigma_{Vx}, \sigma_{Vy}, \sigma_{Vz}}$: Standard deviations for velocity components
$\boldsymbol{\Delta x,\ \Delta y,\ \Delta z}$: Position errors of antenna system
$\mathbf{x_{GPS}, y_{GPS}, z_{GPS}}$: Direct GPS position mesurements
$\mathbf{x_{antenna}, y_{antenna}, z_{antenna}}$: Indirect antenna position measurements
$\mathbf{Z_{\Delta x}, Z_{\Delta y}, Z_{\Delta z}}$: Error measurement vector components
$\boldsymbol{\Delta x_m, \Delta y_m, \Delta z_m}$: System errors in terms of position components
$\mathbf{\hat{x}_{antenna}, \hat{y}_{antenna}, \hat{z}_{antenna}}$: Estimated positions
$\mathbf{W_x, W_y, W_z}$: Gauss distributed noises
$\boldsymbol{\sigma^2_{W_x}, \sigma^2_{W_y}, \sigma^2_{W_z}}$: Standard deviations of Gauss distributed noise

UNSCENTED KALMAN FILTER BASED SATELLITE ORBIT DETERMINATION ON THE GPS AND SINGLE STATION ANTENNA MEASUREMENTS

SUMMARY

Orbits of satellites can be determined via usage of position or velocity measurements of navigation systems with respect to the dynamic models of the satellites. Measurement of satellite parameters such as positions, velocities or angles requires to use navigation equipments such as Global Positioning System (GPS) and Earth stations which include single or multiple antenna systems. For orbit determination, it is needed to apply an estimation method for orbit determination parameters, too. One of the most well-known estimation methods is Kalman Filter.

Study basically involves five main estimation procedures. First estimation procedure is a two-stage approach for estimation of Geostationary Orbit (GEO) satellite's position and velocity by single station antenna tracking data with Unscented Kalman Filter (UKF). Second procedure is the estimation of Low Earth Orbit (LEO) satellite's position and velocity by direct GPS measurements with Unscented Kalman Filter. Third and fourth estimation procedures are using Robust Unscented Kalman Filters with Single Measurement Noise Scale Factor and Multiple Measurement Noise Scale Factors in case of measurement malfunctions such as continuous bias, noise increment and zero output for both of the antenna and GPS measurements. The last procedure is to estimate antenna measurement bias via integration of antenna and GPS measurements with Linear Kalman Filter.

In this study, a two-stage approach for estimation of satellite's position and velocity by single station antenna tracking data with UKF is proposed. In the first stage, direct nonlinear antenna measurements are transformed to linear x-y-z coordinate measurements of satellite's position, and statistical characteristics of orbit determination errors are analyzed. Variances of orbit parameters' errors are chosen as the accuracy criteria. In the second stage, the outputs of the first stage are improved by the designed Unscented Kalman Filter (UKF) for estimation of the satellite's position and velocity on indirect linear x-y-z measurements. In simulations, position and velocity values of a geostationary satellite are found via proposed two-stage procedure. Simulations proved that two-stage estimation method straightened the single station antenna tracking data very well.

Unscented Kalman Filter which uses position and velocity measurements of GPS for estimation of LEO satellite parameters is proposed. The difference of this application from UKF with indirect single station antenna measurements, is using the direct measurements. GPS directly measures the position and velocities of the satellite. Therefore, UKF uses the directly obtained measurements and it does not require hard transformations to obtain indirect measurements from real antenna measurements. Simulations showed that the method straightened the GPS tracking data successfully.

Robust Unscented Kalman Filter (RUKF) algorithms with the filter gain correction for the case of measurement malfunctions are introduced. By the use of defined variables named as measurement noise scale factor, the faulty measurements are taken into the consideration with a small weight and the estimations are corrected without affecting the characteristic of the accurate ones. In the presented RUKFs, the filter gain correction is performed only in the case of malfunctions in the measurement system and in all other cases procedure is run optimally with regular UKF. Checkout is satisfied via a kind of statistical information. In order to achieve that, the fault detection procedure is introduced.

Two different RUKF algorithms, one with single scale factor and one with multiple scale factors, are proposed and applied for the two-stage approach to estimate position and velocity parameters of Geostationary Orbit satellite with indirect single station antenna measurements and estimate the position and velocity parameters of Low Earth Orbit Satellite with GPS measurements. The results of these algorithms are compared for different types of measurement faults in different estimation scenarios and recommendations about their applications are given. For two-stage approach application with antenna measurements, simulation results showed that the effect of azimuth angle on all indirect measurements caused an unexpected result as RUKF with SMNSF and MMNSF results are close to each other. On the other hand, simulation results showed that, the performance of RUKF with MMNSF is better than RUKF with SMNSF for application with GPS measurements.

Complementary Kalman Filter which integrates single station antenna system and GPS is proposed to estimate antenna position bias. A constant bias which affects indirect position measurements of antenna is added to azimuth measurement. Then, x, y and z position biases are estimated. According to results, complementary Kalman Filter successfully estimated antenna measurement biases. Simulations indicated that the integration of single station antenna and GPS via Complementary Kalman Filter is a reliable procedure to estimate antenna measurement biases.

UYDU YÖRÜNGELERİNİN GPS VE TEK YER İSTASYONU ÖLÇÜMLERİYLE SEZGİSİZ KALMAN SÜZGECİ TEMELLİ BELİRLENMESİ

ÖZET

Uyduların yörüngeleri, navigasyon sistemlerinin konum ve hız ölçümlerinin kullanılmasıyla, uydu dinamik modeline göre belirlenebilir. Konum ve hız gibi uydu parametrelerinin ölçülmesi, Küresel Konumlandırma Sistemi (GPS) ve tek ya da çoklu anten sistemleri içeren yer istasyonları gibi navigasyon sistemlerinin kullanılmasını gerektirir. Bunun yanında, yörünge parametrelerinin ilerideki değerlerini tahmin edebilmek için kestirim yöntemleri uygulamak gereklidir. En çok bilinen kestirim yöntemlerinden biri Kalman Süzgeci'dir.

Kalman Süzgeci'ni lineer olmayan sistemlere uygulamak zordur. Genişletilmiş Kalman Süzgeci otuz yıldan fazladır filtreleme çözüm metodu olarak kullanılmaktadır. Geleneksel Kalman Süzgeci'nin nonlineer modellerde kullanılabilmesini sağlayan Genişletilmiş Kalman Süzgeci, nonlineer modelleri lineerleştirmek için bir çözümdür. Fakat bu sürecin iki tane sorunu vardır. Yerel doğrusallık kabulleri kırılırsa, stabil olmayan süzgeçler üretilebilir. Genişletilmiş Kalman Süzgeci'nin önemli süreçlerinden biri olan Jakobian matrisi hesaplaması zor bir uygulamadır. Üstelik, Genişletilmiş Kalman Süzgeci'nin uygulanması ve ayarlanması da zordur. Genişletilmiş Kalman Süzgeci'nin kısıtlama ve zorluklarıyla başa çıkabilmek için Sezgisiz dönüşümü isimli yeni bir metod geliştirilmiştir. Bu metod, nonlineer dönüşümleri ile ortalama ve kovaryansı çoğaltır. Genişletilmiş Kalman Süzgeci ile kıyaslandığında Sezgisiz Kalman Süzgeci'nin daha iyi sonuçlar verdiği ve uygulanmasının daha kolay olduğu belirlenmiştir. Çalışmada da Sezgisiz dönüşümünü kullanan Sezgisiz Kalman Süzgeci önerilerek algoritmaları tanıtılmış ve ve yörünge belirleme süreçlerinde kestirim tekniği olarak kullanılmıştır.

Çalışmada, yörünge belirlemede kullanılan enstrumanlar olan yer istasyonları antenleri ile Küresel Konumlandırma Sistemi (GPS)'nin özellikleri, çalışma prensipleri ve sistem elemanları ile ilgili teorik bilgiler verilmiştir. Yer istasyonu anteni yer sabit yörünge uydusu için kullanılmıştır. Yer sabit yörünge uyduları 35786 kilometre irtifada, dairesel yörüngeli uydulardır ve yörünge periyodu Dünya'nın bir yıldız günü için dönüş periyoduna eşittir. GPS ise düşük Dünya yörüngesi uydusu için kullanılmıştır. Düşük Dünya yörüngesi uyduları, yaklaşık olarak 2000 kilometre altı irtifada bulunan uydulardır.

Çalışmada kullanılacak olan kestirim yöntemlerinin seçimi önemlidir. Bunun yanında, yörünge takibinde kullanılacak yörünge belirleme sistemleri ve bu sistemlerin hangi tip uydular için kullanılacağı da önemlidir. Seçilen sistem türü ve takip edilecek uydu türüne göre sistemlerden birden fazla sayıda kullanılması gerekebilir. Örneğin, bir düşük Dünya yörünge uydusu Dünya'nın dönüşüne göre hızlı hareket edeceğinden tek yer istasyonu ile takibi zordur. Bu nedenle birden çok yer istasyonu kullanımı daha uygun olur. İstasyoner yörüngeli uyduların takibi ise

daha kolaydır. Tek yer istasyonu veya farklı bir sistem tek başına bu tip uydular için kullanılabilir. Çalışmada yer sabit yörünge uydusu için tek yer istasyonu kullanımı buna bir örnektir.

Çalışma, ana hatlarıyla ve temel olarak beş kestirim sürecinden oluşur. İlk kestirim işlemi, yer sabit yörünge uydusunun konum ve hızlarının tek yer istasyonundan alınan veriler kullanılarak Sezgisiz Kalman Süzgeci (UKF) yardımıyla iki aşamalı yaklaşımla kestirilmesidir. İkinci kestirim süreci, alçak yörünge uydusunun konum ve hızlarının direkt olarak GPS'den alınan ölçümlerle yine Sezgisiz Kalman Süzgeci tabanlı olarak belirlenmesidir. Üçüncü ve dördüncü kestirim süreçleri sırasıyla anten ve GPS ölçümleri için tek ölçüm gürültü ölçek faktörlü ve çoklu ölçüm gürültü ölçek faktörlü dayanıklı Sezgisiz Kalman Süzgeçlerinin, ölçümlerde sürekli sapma, ölçüm gürültüsü artması ve sıfır çıkış hataları durumunda kullanılmasıdır. Beşinci ve son kestirim süreci ise tek yer istasyonu ve GPS ölçümlerinin Lineer Kalman Süzgeci temelinde birleştirilmesiyle, anten ölçümlerindeki sapma hatalarının kestirilmesidir.

Çalışmada ilk olarak, uydunun konum ve hızlarının tek yer istasyonu ölçüm verileriyle Sezgisiz Kalman Süzgeci temelinde kestirilebilmesi için iki aşamalı yaklaşım önerilmiştir. İlk aşamada, direkt lineer olmayan anten ölçümleri uydunun endirek ölçümleri olan lineer x-y-z konum koordinatlarına çevrilmiştir ve yörünge belirleme hatalarının istatistiksel karakteristiği analiz edilmiştir. Yörünge parametrelerinin varyansları doğruluk kriteri olarak seçilmiştir. İkinci aşamada, ilk aşamada elde edilen sonuçlar, uydunun konum ve hızlarının endirek x-y-z konum ölçümleriyle kestirilebilmesi için tasarlanan Sezgisiz Kalman Süzgeci vasıtasıyla iyileştirilmiş ve geliştirilmiştir. Simulasyonlarda, yer sabit yörünge uydusunun konum ve hızları önerilen iki aşamalı süreç ile bulunmuştur. Simulasyonlar, iki aşamalı yöntemin tek yer istasyonu izleme verisini iyi bir şekilde düzelttiğini göstermiştir. Süzgecin kestirilen parametreler için hata ve varyans miktarları antenle takip edilen bir yer sabit yörünge uydusu için makul düzeydedir.

İkinci olarak, GPS konum ve hız ölçümlerini alçak yörünge uydusunun parametre kestirimi için kullanan Sezgisiz Kalman Süzgeci önerilmiştir. Bu uygulamanın endirek tek yer istasyonu anteni ölçümleri ile Sezgisiz Kalman Süzgeci temelinde yapılan uygulamadan farkı, direk ölçümleri kullanmaktır. GPS uyduların konum ve hızlarını direk olarak kendisi ölçer. Bu nedenle, Sezgisiz Kalman Süzgeci direk olarak elde edilmiş ölçümleri kullanır ve antende olduğu gibi endirek ölçüm elde etmek için yapılan dönüşüm işlemlerine ihtiyaç duymaz. Simulasyonlar, yöntemin GPS ölçümlerini iyileştirerek alçak yörünge uydusunun konum ve hızlarını iyi bir doğrulukla kestirdiğini göstermiştir. Süzgecin kestirilen parametreler için hata ve varyans miktarları GPS ile takip edilen bir alçak yörünge uydusu için gayet iyidir. Anten ile yer sabit yörünge takibi uygulamasında elde edilen hata ile varyans sonuçları ile GPS ile alçak yörünge uydusuna yapılan uygulamanın hata ve varyans sonuçları kıyaslandığında, GPS'nin direk ölçümleriyle yapılan kestirimin daha iyi sonuçlar verdiği görülmüştür.

Çalışmada, ölçüm arızaları durumu için süzgeç kazancı düzeltimli dayanıklı Sezgisiz Kalman Süzgeç algoritmaları tanıtılmıştır. Ölçüm gürültü ölçek faktörü olarak adlandırılan değişkenlerin kullanılmasıyla, hatalı ölçümler küçük ağırlıkla dikkate alınır ve kestirimler doğru olanların karakteristiğini etkilemeyecek şekilde düzeltilir. Tek ölçüm gürültü ölçek faktörü süzgeç kazancına eklenen bir adet terimden oluşurken, çoklu ölçüm gürültü ölçek faktörü birçok değişkenden oluşan ve süzgeç kazancının gerekli ve önemli terimlerini düzelten bir ölçek matrisidir. Önerilen dayanıklı Sezgisiz Kalman Süzgeçlerinde, süzgeç kazanç düzeltmesi yalnız ölçüm sisteminde hata olması durumu için uygulanmıştır ve diğer tüm durumlarda süreç optimal olarak normal Sezgisiz Kalman Süzgeci ile çalışmıştır. Kontrol işlemi, bir tür istatistiksel veri yardımıyla yerine getirilmiştir. Bunu yapabilmek amacıyla, hata belirleme işlemi tanıtılmıştır.

Biri tek ölçek faktörlü ve diğeri de çoklu ölçek faktörlü olma üzere iki adet dayanıklı Sezgisiz Kalman Süzgeci algoritmaları önerilmiş ve sırasıyla önce endirek tek yer istasyonu anten ölçümleriyle iki aşamalı yaklaşımla yer sabit yörünge uydusunun ve sonra GPS ölçümleriyle alçak yörünge uydusunun konum ve hızlarının kestirilebilmesi için uygulanmıştır. Algoritmaların sonuçları farklı kestirim senaryolarında ölçümlerde sürekli sapma, ölçüm gürültüsünün artışı ve sıfır ölçüm çıkışı gibi farklı tip ölçüm hataları için karşılaştırılmış ve uygulamaları ile ilgili öneriler verilmiştir. Anten ölçümleri ile yapılan iki aşamalı yaklaşım için, simulasyon sonuçları, açıklık açısına eklenen sapmanın tüm endirek ölçümler üzerinde beklenmeyen kötü bir etki yarattığını göstermiştir. Buna göre tek ölçüm gürültü ölçek faktörlü ve çoklu ölçüm gürültü ölçek faktörlü dayanıklı Sezgisiz Kalman Süzgeçleri birbirine yakın sonuçlar vermiştir. Normalde çoklu ölçek faktörlü algoritmanın tek ölçek faktörlü algoritmaya kıyasla daha iyi sonuç vermesi beklenebilirdi. Bu sonuç ile bu uygulamada karşılaşılmamasının sebebi ölçüm hatalarının direk ölçüm olan açıklık açısına uygulanması, fakat adaptif filtrenin açıklık açısının dolaylı olarak etkilediği ve endirek ölçümler olan konum ve hızlara uygulanmış olmasıdır Diğer taraftan, GPS ölçümleri ile yapılan uygulama sonuçlarına göre, çoklu ölçüm gürültü ölçek faktörlü süzgeç tek ölçüm gürültü ölçek faktörlü süzgece kıyasla daha iyi sonuç vermiştir. Tek ölçüm ölçek faktörlü dayanıklı Sezgisiz Kalman Süzgecinin çok değişkenli ve süzgeç performansının her bir parametre için farklılık gösterdiği kompleks sistemler için sağlıklı bir çözüm olmadığı gözlemlenmiştir. Burada normalde beklenebileceği üzere, çoklu ölçek faktörlü algoritma tek ölçek faktörlü algoritmaya kıyasla daha iyi sonuç vermiştir. Çünkü ölçüm arızası da direk ölçümlere uygulamış, süzgeçte direk olarak arızanın verildiği parametreleri düzeltmeye çalışmıştır.

Önerilen dayanıklı Sezgisiz Kalman Süzgeci yaklaşımları hataların prior istatistiksel karakteristiğini gerektirmez ve bu yaklaşımlar hem lineer hem de lineer olmayan sistemler için kullanılabilir. Ayrıca, sunulan dayanıklı Sezgisiz Kalman Süzgeci algoritmaları daha önceden var olan dayanıklı Sezgisiz Kalman Süzgeci algoritmalarına göre pratik uygulamalar için daha kolaydır. Bu karakteristikler, tanımlanan dayanıklı Sezgisiz Kalman Süzgeci algoritmalarını uydu hızları ve konumları için güvenilir parametre kestirimi sağlama noktasında son derece önemli yapar.

Anten konum ölçümü sapmalarını kestirebilmek amacıyla, tek yer istasyonu anten sistemi ile GPS'yi birleştiren Lineer Kalman Süzgeci tabanlı tümleştirici Kalman Süzgeci önerilmiştir. Anten açıklık açısı ölçümüne, endirek ölçümler olan konum bileşenlerini de etkileyen sabit miktarlı bir sapma eklenmiştir. Daha sonra, x, y ve z konumları için sapma miktarları kestirilmiştir. Simulasyon sonuçlarına göre, tümleştirici Kalman Süzgeci anten ölçüm sapmalarını başarılı bir şekilde kestirmiştir ve tek yer istasyonu anteni ile GPS ölçümlerinin tümleştirici Kalman Süzgeci ile birleştirilmesinin anten ölçüm sapmaları kestirimi için güvenilir bir süreç olduğunu göstermiştir.

1. INTRODUCTION

Orbit determination is the process of finding the best approximation of a satellite or spacecraft's position over time using observations of its position or velocity, where its motion is described by imperfect dynamic models.

In orbit determination of a spacecraft, the dynamic system and the measurement equations are of nonlinear nature. It is a nonlinear problem, in which the disturbing forces are not easily modeled. The problem consists of estimating variables that completely describe the body's trajectory in space, processing a set of information related to the considered body [1]. A tracking antenna on Earth or sensors as GPS receivers, magnetometers, etc. can perform such observations.

The work [2] describes an optimal iterative algorithm capable of determining the orbital parameters by using the antenna pointing angles, which are recorded in the tracking of the passing satellite. The algorithm is optimal in the sense that it minimizes the noise effects of the noisy measurements and the numerical uncertainties of the propagation. The method is originated from the Least Squares Estimation (LSE) algorithm, which, by using the theory of the Extended Kalman Filter (EKF), is suitably modified to reduce the disturbances on the estimation error.

Orbit determination accuracy improvement for a geostationary satellite with single station antenna tracking data is investigated in [3]. In this study, an operational orbit determination (OD) system for the geostationary satellite mission requires accurate satellite positioning data to accomplish image navigation registration on the ground. Ranging and tracking data, which is provided by a single ground station, is used to determine the orbit of the geostationary satellite in normal operation. However, the orbital longitude of the geostationary satellite is so close to those of satellite tracking sites that emerging geometric singularity affects observability [4]. Applying an azimuth bias estimation using the ranging and tracking data provided by two stations is a method to solve for the azimuth bias of a single station in singularity. Using only single-station data with the correction of the azimuth bias, OD succeeds to achieve three-sigma position accuracy of the order of 1.5 km root-sum square.

Localization of spacecraft is usually very accurate when GPS measurements are available [5]. The problem becomes more challenging when GPS signals are not available, for instance in high-Earth orbits or in long range missions such as Earth-to-Moon transfers. In these cases, spacecraft navigation is often handled by ground-based tracking stations, thus making it unfeasible for low-cost spacecraft missions. In order to make spacecraft fully autonomous, it is necessary to devise self-localization and navigation algorithms relying on measurements provided by onboard sensors. In [6], the problem of spacecraft self-localization is addressed using angular measurements. A dynamic model of the spacecraft accounting for several perturbing effects, such as Earth and Moon gravitational field asymmetry and errors associated with the Moon ephemerides, is employed. It is assumed that the navigation system is able to estimate the spacecraft's attitude (by using a star tracker sensor), and the spacecraft is equipped with line-of-sight sensors providing measurements of elevation and azimuth of the Moon and the Earth with respect to the spacecraft reference system. Range measurements, which are often difficult to obtain or are not sufficiently reliable, are not required.

In [7], a comparison of Extended Kalman Filter (EKF) and Unscented Kalman Filter (UKF) for spacecraft localization via angle measurements is performed. In the study, performances of two nonlinear estimators are compared for the localization of a spacecraft. It is assumed that range measurements are not available, and the localization problem is tackled on the basis of angle-only measurements. The dynamic model of the spacecraft is the same as in [6]. The measurement process is based on elevation and azimuth of Moon and Earth with respect to the spacecraft reference system. The position and velocity of the spacecraft are estimated using both EKF and UKF. The behaviors of the filters are compared on two sample missions: Earth-to-Moon transfer and geostationary orbit raising.

Orbit determination techniques in [8] are used to estimate the position and velocity of a debris object in orbit using range, azimuth, and elevation measurements obtained from Space Surveillance Network (SSN) sensors. The continuous-discrete Extended Kalman filter is used to estimate the debris' orbit.

In [9], the non-recursive batch filter has been presented and utilized for satellite orbit determination. Using the unscented transformation, a non-recursive batch filter is developed without any traditional linearization process. For the orbit determination system, the range, azimuth, and elevation angles of the satellite measured by ground tracking stations are used as observations. For evaluation and verification of the presented batch filter's performance, the results are compared with those of the batch least squares filter for various initial errors in position and velocity, measurement sampling periods, and measurement errors. For relatively small initial errors or short measurement sampling periods or small measurement errors, the accuracy of the orbit determination is similar in both the filters. Under large initial errors or long measurement sampling periods or large measurement errors, the presented non-recursive batch filter yields more robust and stable convergence than the existing batch least squares filter.

A robustly adaptive Kalman filter based on variance component estimation is proposed for orbit determination of a maneuvered Geostationary Orbit (GEO) satellite [10]. The main idea is to use robust estimation to resist the influence of measurement outliers and use an adaptive factor to control the effect of dynamic model errors. Simulations with the Chinese ground tracking network for a maneuvered GEO satellite were conducted to verify the performance of the proposed orbit determination technique. The results show that it can efficiently control both the influence of outliers and that of thrust force, and can provide high and reliable orbit accuracy.

The Global Positioning System (GPS) offers an attractive alternative to ground-based tracking systems for use in many Earth satellite orbit determination applications [11]. Many missions require an accuracy on the order of 100-200 m. The current civilian version of GPS can determine instantaneous position with an accuracy on the order of 10 meters when operating in stand-alone mode. This performance is available for virtually all users up to an altitude of 3,200 km. These facts give rise to the possibility of doing autonomous GPS-based satellite navigation for many Earth orbiting missions. The accuracy depends on the level of uncertainty in the orbital dynamics model. The system can also operate in a geosynchronous orbit, but its peak per-axis error degrades to 7 km if the filter neglects Solar and Lunar gravity terms, and the geosynchronous receiver must use an ovenized crystal oscillator as its clock.

In [12], Spaceborne GPS receivers are used for real-time navigation by most low Earth orbit (LEO) satellites. In general, the position and velocity accuracy of GPS navigation solutions without a dynamic filter are 25 m (1r) and 0.5 m/s (1r), respectively. However, GPS navigation solutions, which consist of position, velocity, and GPS receiver clock bias, have many abnormal excursions from the normal error range for space operation. These excursions lessen the accuracy of attitude control and onboard time synchronization. In the research, a new onboard orbit determination algorithm designed with the Unscented Kalman filter (UKF) was developed to improve the performance. Because the UKF is able to obtain the posterior mean and covariance accurately by using the second-order Taylor series expansion through the sampled sigma points that are propagated by using the true nonlinear system, its performance can be better than that of the Extended Kalman filter (EKF), which uses the linearized state transition matrix to predict the covariance. The comparison of the orbit determination results using EKF and UKF shows that orbit determination using the UKF yields better results than that using the EKF.

The purpose of the [13] was to determine the accuracy of GPS use for a Geostationary Orbit (GEO) satellite. Current missions at GEO altitude mainly use traditional ranging for orbit determination. With changing mission requirements and the increase in the number of GEO missions, utilizing GPS signals is becoming an increasingly attractive alternative for position and timing determination. GPS use at GEO is primarily limited by the availability of the spillover from the GPS earth coverage signal. The availability of the GPS signal at GEO is determined by the GPS block specific antenna patterns and the GEO satellite's receiver antenna. This analysis specifically examined the effects of the GPS constellation availability antenna gain patterns, and GPS receiver clock stability on position and timing accuracies at GEO.

The purpose of the [14] is to present a development of a non linear Kalman filter, based on the sigma point unscented transformation, aiming at real time satellite orbit determination using actual GPS measurements. If the dynamic system and the observation model are linear, the conventional Kalman filter may be used as an estimation algorithm. However, not rarely, the dynamic systems and the measurements equations are of non linear nature. For solving such problems, convenient extensions of the Kalman filter have been sought. In this work, the differential equations describing the orbital motion and the GPS measurements equations will be placed in a suitable form. They will be adapted for the unscented filter, using the sigma point Kalman filter.

A positioning method for the GPS receiver used in fuse with single antenna as compared to the traditional multi-antenna model is proposed in [15] . For that purpose, the intermediate frequency signal received by the single antenna is modeled and simulated, and a positioning method with partial GPS signals is proposed. Based on the positioning method with partial GPS signals and Kalman filter theory, positioning mechanisms for the GPS receiver used in fuse with single antenna are researched. The simulation result shows that the method can avoid the complicated design and fixing of the multi-antenna needed in traditional GPS receivers used in fuse, can reduce the difficulty of designing the tracking loop, and can also improve the anti-jamming ability in the practical application.

In general, for the orbit determination purpose, the Kalman filtering technique is used. Antenna tracking data can be processed by Kalman filter in various methods [1-10]. Because the antenna measurements (azimuth, elevation, and range) are non-linear with respect to the state variables, the process of location estimation of spacecraft by using antenna tracking data is non-linear and can only be solved by EKF or UKF. UKF can also be used to determine orbits with GPS [12,14]. Mostly, Low Earth Orbit (LEO) satellites are used in studies about GPS. Some studies research the availability of GPS usage for GEO satellites [11,13]. GPS can be used for LEO and GEO satellites. The reason of the search for GPS usage for GEO satellites is to obtain more accurate orbit parameters and reduce the orbit determination errors. Some researchs about GPS accuracy are given in [11]. There are also studies which fuse or integrate two different navigation sources such as antenna and GPS or multiplying the number of ground stations to increase accuracy and tracking ability [15].

In this study, orbit determination systems such as ground station antenna and GPS are introduced in chapter 2. In chapter 3, Kalman Filter is defined and the type of Kalman Filter algorithms as Linear Discrete Kalman Filter, Unscented Kalman Filter and Robust Unscented Kalman Filters with adaptive factors are presented. Two-stage estimation of satellite’s position and velocity by single station antenna tracking data is proposed in chapter 4. UKF application for estimation of position and velocity parameters of LEO satellite with GPS measurements is also presented. Robust Unscented Kalman Filters (RUKF) with Single Measurement Noise Scale Factor (SMNSF) and Multiple Measurement Noise Scale Factor (MMNSF) are introduced and applied to orbit determination with single station and antenna measurements for three fault scenarios such as continuous bias, noise increment and zero output. Results and comparisons of Regular UKF and Robust filters are actualized in chapter 4, too. In chapter 5, Linear Kalman Filter is used to estimate antenna measurement bias for positions via using integration of single station antenna and GPS. All results are summarized in conclusion section in chapter 6.

2. ORBIT DETERMINATION SYSTEMS

2.1 Earth Station and Antenna

An earth station system includes an antenna, tracking system, receiver, transmitter, multiplexer (combiner), and terrestrial links via a modem (or codec) (figure 2.1).

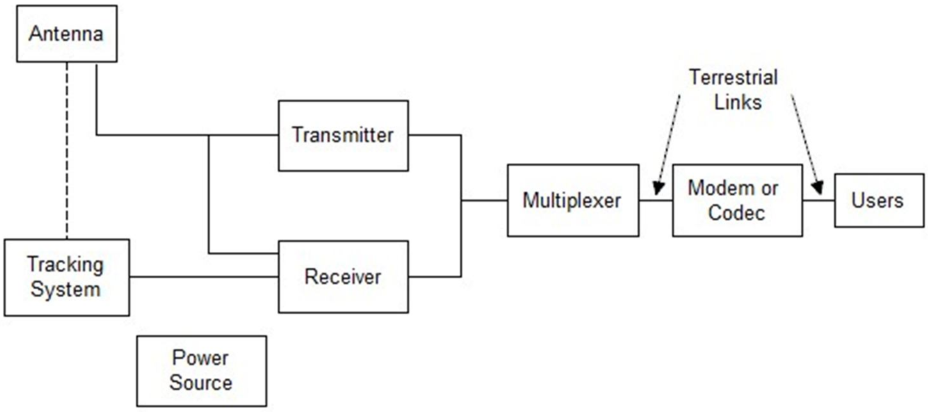

Figure 2.1: Block diagram of an earth station.

An antenna is a transducer between electromagnetic waves in space and voltages or currents in a transmission line. When transmitting, the antenna converts electrical signals into radio waves; a receiving antenna reverses the process and transforms radio waves back into electrical signals. Most antennas are passive, simply metal structures that launch or collect radio waves [17].

An essential operation in communicating by satellite is the acquisition (locating) of the satellite by the earth terminal antenna and the subsequent tracking of the satellite. Initial acquisition depends upon an exact knowledge of the position of the satellite. In combination with the geographic location of the earth terminal, knowing the position of the satellite enables you to compute accurate antenna pointing information. The degree of difficulty in locating and tracking a satellite is determined largely by what type orbit the satellite is in [18].

The locating and tracking of a synchronous satellite is relatively simple. This is because the satellite appears to be stationary. Locating a near-synchronous satellite is also relatively simple because of the slow relative motion of the satellite. However, the movement of a near-synchronous satellite is enough that accurate tracking is required to keep the narrow beam antenna pointed toward the satellite. Satellites in medium altitude circular orbits or in elliptical orbits are more difficult to acquire and to track because of the rapid changes in position [18].

There are many types of antennas and many different variations on the basic types, but their mode of operation is essentially the same [16]. That is, a radiofrequency transmitter excites electric currents in the conductive surface layers of the antenna and radiates an electromagnetic wave. If the same antenna is used with a receiver, the converse process applies; that is, an incident radiowave excites currents in the antenna, which are conducted to the receiver. The ability of an antenna to work both ways is termed the principle of reciprocity.

Three basic types of antennas are the reflector, lens, and phased array. A reflector antenna is the most desirable candidate for satellite antennas because of its light weight, structural simplicity, and design maturity [16]. Horns are frequently used as feeds to illuminate reflector antennas, which typically provide narrow beams. A lens antenna is the counterpart of the reflector from the optical property point of view. It can be made rotationally symmetric to preserve good optical characteristics. It has no feed blockage and compactness; however, it is heavier at low-frequency applications and has lens surface mismatch. A phased-array antenna is a class of array antennas that provides beam agility by effecting a progressive change of phase between successive radiators. An antenna array is a family of individual radiators whose characteristics are determined by the geometric position of the radiators and the amplitude and phase of their excitation. A phased-array antenna has a number of advantages over a lens or reflector antenna. This is due to the distribution of power amplification at the elementary radiation level, higher aperture efficiency, no spillover loss, no aperture (feed) blockage, and better reliability. The helical antenna has inherent broadband properties, possessing desirable pattern, polarization, and impedance characteristics over a relatively wide frequency range and may radiate in several modes [16].

The antenna subsystem requires separate tracking equipment, which provides precise pointing of the antenna at the satellite. With small earth stations where the antenna’s bandwidth is large, precision tracking equipment is not necessary. The antenna tracking system can be programmed to point to preassigned direction(s) automatically and can also be directed manually.

Earth stations with large antennas 10 to 60m in diameter are called long earth stations [16]. This type is often required to provide for high-capacity telephone, data, or television transmission. In general, the larger the antenna, the greater the traffic capacity of the station. Small earth stations are antennas with diameters between 1 and 10 m. They are commonly sighted on the roofs or in the gardens of domestic and commercial buildings. Small earth stations provide capabilities for reception of broadcast television and or connection for thin-route telephony systems in remote regions. Very small aperture (VSAT) earth stations are networks of satellite earth terminals, each of which has an antenna diameter between 0.3 and 0.9 m: hence the name very small. VSAT networks are usually arranged in a star configuration in which small aperture terminals each communicate via the satellite to a large central earth station known as a hub station. Any aperture smaller than VSAT is called an ultra-small aperture terminal (USAT). Nearly all earth station antennas with a diameter greater than 4m are of the paraboloidal-reflector Cassegrain type.

Three commonly used direction-finding systems in earth stations are monopulse, step track, and programmable steering. The operating principle of all direction-finding systems is based on a comparison of the actual beam axis, aligned in the direction of arrival of signals, with two received radiation patterns: one of the actual beam axis and the other from a satellite.

There are subtle differences in the operation of the three direction finding systems [16].

1. Monopulse: In monopulse tracking, multiple feed elements are used to obtain multiple received signals. The relative signal levels the various feed elements receive are compared to provide azimuth and elevation pointing error signals. The error signals are then used to activate the servo control system controlling antenna pointing. The monopulse method is used in systems that utilize polarization isolation, when greater satellite tracking precision is necessary, for example, in INTELSAT antennas.

2. Step track method: In the step track method, the radiation pattern of the antenna is shifted discretely in small steps. The position corresponding to the peak signal is

determined by measuring the sign of the difference of the signal levels before and after a step. The differential yields the step size for the next change in position alternately in azimuth and elevation. The iteration process is interrupted when the position is optimum, that is, when the differential is negligibly small. The advantages of the step track method are its simplicity and relative low cost. Its disadvantage is its low speed.

3. Programmable steering method: In this technique, antenna pointing is based upon knowledge of the relative motion of the satellite with respect to the earth station. A mathematical function, together with the known geographical coordinates of the earth station, is programmed and used to update the antenna pointing without reference to a signal received from the satellite. This technique is independent of earth station's performance and link parameters, yet it is relatively complex to achieve considerable precision accuracy.

In general, whichever scheme is implemented and in order to prevent the pointing loss, the main lobe of the earth station's antenna must be pointed automatically or manually at the satellite with the greatest possible accuracy [16]. This operation is performed by the tracking system that, by means of its various control loops, ensures that the position errors of the antenna main beam (e.g., due to wind or satellite drift) from the ideal satellite position are compensated. The antenna tracking system together with the tracking servo system, the drive electronics, the electric drives, and the antenna form a closed control loop. The servo system processes the error signals supplied by the tracking receiver and prepares them for the drive electronics that control the dc motors on the antenna axis. The electric drive supplies the drive torque through mechanical gears to the antenna axis and compensates the gears' backlash by producing bias torque.

2.2 Global Positioning System (GPS)

The NAVSTAR (Navigation Signal Time and Range) Global Positioning System is a space based navigation system. Users from whole Earth can access to the system during all day. GPS was designed for solutions to global navigation aims such as terrestrial, near terrestrial or on orbit. Users can access position and velocity estimations in three dimension via GPS. User must have a GPS receiver to be able to use the system. In brief, GPS receiver takes the range estimation data from at least four GPS satellites. These range estimations are usually used in Kalman Filter to determine the position of GPS receiver and estimate the clock bias [19].

Developer of the GPS system is United States Department of Defense [19]. Maintenance services for GPS are also performed by Department of Defense. Origin of GPS system bases on U.S. Navy Transit program. Object of this program is to use a satellite consellation for navigation and positioning via transmission of radio signals with satellites. U.S. Navy Transit program started in the 1950's and U.S. Air Force began to work on its own research in the 1960's. At the end of the Navy Transit program, Navy Navigation Satellite System was released to nonmilitary users in 1976. It supplied the desired space based navigation system but system had some drawbacks such as large time gaps in coverage and inaccurate position estimation. Due to these unexpected problems, U.S. Navy and Air Force decided to make additional researchs for more advanced navigation system. Then, Navy developed TIMATION (time and navigation). It was two dimensional and it could not estimate highly dynamic situations. Air Force developed proram 621B, too. It could estimate positions in high dynamic environments but it had some drawbacks again. Both of efforts performed by Navy and Air Force were integrated into a single program performed by Air Force in 1973. New program is named as Defense Navigation Satellite System. In December 1973, this program was accepted and renamed as Navstar/Global Positioning System..

GPS can be used for military applications such as inertial guidance systems, weapon delivery, targeting operations, guidance, rendezvous, command and control, antisubmarine warfare and reconnaissance. GPS can also be used for civilian purposes such as precision aircraft and general aviation navigation, land vehicle and ship navigation, search and rescue, geodesy, geology, mapping, surveying and mineral exploration [19].

GPS consists of three parts as space segment, control segment and user segment [20]. Space segment includes 24 operational satellites and 3 on orbit spares. 24 operational satellites are spread over six orbital planes (four satellites in each plane). These orbits are circular orbits with 20200 kilometers altitude and 55 degree inclination angle. Period of these orbits are around 11 hours 56 minutes. Feature of these orbits is allowing at least four satellites to be visible permanently from everywhere on the Earth.

Eight Block II satellites, 18 Block IIA satellites and a Block IIR satellite create the total 27 orbit configuration. Block I satellites which are the first generation satellites are not in service. The second generation Block II satellites provided GPS consellation to serve fully. Block IIA and Block IIR are the sequential generation satellites that started to work in the GPS system in 1989 [20].

Control segment includes five monitoring stations, three ground antennas and a Master Control Station (located in Colorado Springs at Falcon Air Force Base) (figure 2.2). Master Control Station handles the data obtained and transmitted by monitoring stations and determines satellite orbits. It also updates each satellite's navigation message. Ground antennas transmit the updated navigation messages to each satellites once per day. User segment includes [20] antennas and receivers to use for determination of position , velocity and precise time for user.

One way ranging from GPS satellites which are also spreading their estimated positions, is the basic navigation method of the GPS. Ranges are measured to four GPS satellites at the same time. This is done via matching the coming signal with user generated replica signal and measuring the received phase against the user's crystal clock. Latitude, longitude, altitude and user clock correction can be determined by measurement with four satellites. Future positions of satellites are estimated via range measurements obtained by monitoring stations. The master control station estimates satellite positions and clock corrections by using prediction algorithms [21].

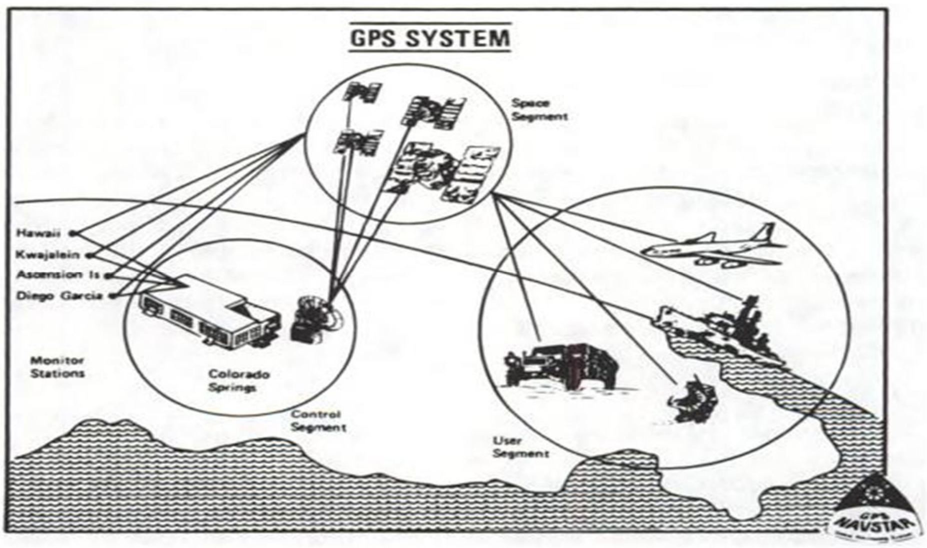

Figure 2.2: GPS system configuration [21].

GPS signal is broadcast on two frequencies in the L-band. These frequencies are L1 (1565.42 Mhz) and L2 (1227.60 Mhz). Coarse acquisition (C/A) code and the precise P code are carried by L1.

The C/A code is modulated at a frequency of 1.023 MHz and it is 1023 bits long [21]. It is the principal civilian ranging signal. It is always broadcast clearly (not encrypted). It is also used to obtain much longer P-code. Usage is this type of signal is named as Standard Positioning Service which is always available. The C/A code is only available on L1.

P or Precise Code is a very long code (nearly segments of a 200 day code). It is broadcast ten times at the level of C/A as 10.23 Mhz. The code ranging signal is more precise than the C/A's because of its higher modulation bandwidth. This provides to decrease the level of noise in the received signal. However, it can not fix the faults caused by biases. Using the P signal is called as Precise Positioning Service. This signal is encrypted via military service not to be used by unconfirmed people. This supplied that the unpredictable code can not be spoofed. Name of this feature is antispoof. After encrypting, P code takes the form of Y code. P/Y code receivers are the receivers which can decrypt Y code. As a result, most of the civilian people can only use Standard Positioning Service.

In addition, military operators can be able to reduce the accuracy of the C/A code by desynchronizing the satellite clock or incorporating the small errors in broadcast ephemeris. This process is called as Selective Availability. Amount of these range errors are around 20m and they results in rms horizontal position errors of about 50m, one sigma [21].

Broadcast ephemeris includes the orbits of satellites and parameters which define satellite positions in a specific time interval [22]. System satellites are continuously tracked via five satellite control stations (Ascension, Diego Garcia, Kwajalein, Hawaii, Colorado Springs) . They locate on available positions on Earth and they have very precious clocks. Data collected by each station is transmitted to main control station (Colorado Springs). Satellite orbits are calculated by evaluation of collected data and positions of them are estimated for specific time in the future. Main control station sends the ephemeris data to satellites with ground antennas.

Precise ephemeris is used to determine satellite orbits and positions with observation data obtained by tracking stations apart from GPS control stations. For instance; one of the satellite tracking networks CIGNET has Earth tracking stations which provide to obtain satellite orbit data precisely in the specific time. This data is transmitted to permanent tracking stations via international computer links. Data obtained by this ephemeris can only be used by official institutions. The main difference between broadcast ephemeris and precise ephemeris is data acquisition times. Broadcast ephemeris obtains the data at the same time with observation. Precise ephemeris obtains data a few weeks after observations [22].

3. KALMAN FILTER

Within the significant toolbox of mathematical tools that can be used for stochastic estimation from noisy sensor measurements, one of the most well-known and often-used tools is what is known as the Kalman filter [23]. The Kalman filter takes it's name from the founder Rudolph E. Kalman.

The Kalman filter is essentially a set of mathematical equations that implement a predictor-corrector type estimator that is optimal in the sense that it minimizes the estimated error covariance when some presumed conditions are met. Since the time of its introduction, the Kalman filter has been the subject of extensive research and application, particularly in the area of autonomous or assisted navigation. This is likely due in large part to advances in digital computing that made the use of the filter practical, but also to the relative simplicity and robust nature of the filter itself. Rarely do the conditions necessary for optimality actually exist, and yet the filter apparently works well for many applications in spite of this situation [23].

Kalman Filter can be used for [22] decreasing measurement errors and determination of better values of measured parameters, integration of multiple data sources (sensor fusion), estimation of unknown system parameters or state vector and detection of system faults.

Depending on the process, it can be required to know the estimation of state value. If state is estimated in future time, this process is named as prediction. If estimation is done via using the all existing measurements, this process is called as filtering [22]. Kalman filtering includes two steps;

1) Time update: Estimation of state vector and error covariance by using system model and statistics.

2) Measurement update: Developing the estimation which gives the filtered state.

3.1 The Discrete Kalman Filter

When a discrete linear system is handled, system's dynamic state equation defines the system mobility and measurement equation expresses the manufacturing system of measurement [22].

Equations of a linear system;

State equation;

$$x(k+1) = \emptyset(k+1,k)x(k) + G(k+1,k)w(k) \quad \textbf{(3.1)}$$

Measurement equation;

$$y(k) = H(k)x(k) + v(k) \quad \textbf{(3.2)}$$

Here, $x(k)$ is the n dimensional state vector, $\emptyset(k+1,k)$ is nxn dimensional system transition matrix , $w(k)$ is r dimensional random Gauss noise vector with zero mean and $E[w(k)w^T(j)] = Q(k)\delta(kj)$ covariance matrix, E is statistical expected value operator , $\delta(kj)$ is Cronecker symbol [23].

$$\delta(kj) = \begin{cases} 1, k = j, \\ 0, k \neq j \end{cases} \quad \textbf{(3.3)}$$

$G(k+1,k)$ is nxr dimensional transition matrix of system noise, $y(k)$ is s dimensional measurement vector, $H(k)$ is sxn dimensional measurement matrix of system, $v(k)$ is s dimensional measurement noise vector with zero mean and $E[v(k)v^T(j)] = R(k)\delta(kj)$ covariance matrix [22].

Initially, mean of $x(0)$ is $\bar{x}(0)$ and covariance matrix of $x(0)$ is $P(0)$. There is not any correlation between system noise $w(k)$ and measurement noise $v(k)$.

$$E[w(k)v^T(j)] = 0, \forall k, j \quad \textbf{(3.4)}$$

The Kalman filter estimates a process by using a form of feedback control: the filter estimates the process state at some time and then obtains feedback in the form of (noisy) measurements. As such, the equations for the Kalman filter fall into two groups: time update equations and measurement update equations. The time update equations are responsible for projecting forward (in time) the current state and error covariance estimates to obtain the a priori estimates for the next time step [23].

The algorithm of discrete Kalman Filter can be written as [22];

Estimation value equation;

$$\hat{x}\,(k|k) = \emptyset(k,k-1)\hat{x}(k-1|k-1) + K(k)[y(k) - H(k)\emptyset(k,k-1)\hat{x}(k-1|k-1)] \quad \textbf{(3.5)}$$

$$\hat{x}\,(k|k) = \hat{x}\,(k|k-1) + K(k)\tilde{z}(k|k-1) \quad \textbf{(3.6)}$$

Here, $K(k)$ is the optimal gain matrix of the filter.

$$K(k) = P(k|k)H^{T}(k)R^{-1}(k) \quad \textbf{(3.7)}$$

$$K(k) = P(k|k-1)H^{T}(k)[H(k)P(k|k-1)H^{T}(k) + R(k)]^{-1} \quad \textbf{(3.8)}$$

Correlation matrix of filtering error;

$$P(k|k) = P(k|k-1) - P(k|k-1)H^{T}(k)[H(k)P(k|k-1)P(k|k-1)H^{T}(k) + R(k)]^{-1}\,xH(k)P(k|k-1) \quad \textbf{(3.9)}$$

Correlation matrix of extrapolation error;

$$P(k|k-1) = \emptyset(k,k-1)P(k-1|k-1)\emptyset^{T}(k,k-1) + G(k,k-1)Q(k-1)G^{T}(k,k-1) \quad \textbf{(3.10)}$$

With initial conditions; $\hat{x}\,(0|0) = \bar{x}(0), P(0|0) = P(0)$.

The equations below can also be written for Kalman Gain $K(k)$ and correlation matrix of filtering error $P(k|k)$as;

$$K(k) = P(k|k)H^{T}(k)R^{-1}(k) \quad \textbf{(3.11)}$$

$$P(k|k) = \big(I - K(k)H(k)\big)P(k|k-1) \quad \textbf{(3.12)}$$

$$P(k|k) = [P^{-1}(k|k-1) + H^{T}(k)R^{-1}(k)H(k)]^{-1} \quad \textbf{(3.13)}$$

$$P(k|k) = P(k|k-1)[I + H^{T}(k)R^{-1}(k)H(k)P(k|k-1)]^{-1} \quad \textbf{(3.14)}$$

$k|k-1$ directory shows the values which are predicted in the previous step, k,k directory shows the estimation via using all measurements including $y(k)$ at k time. Initial values of $\bar{x}(0)$ and $P(0)$, $Q(k)$ system noise correlation matrix and $R(k)$ measurement noise correlation matrix must be given to run the filter.

3.2 Unscented Kalman Filter

Simplicity, optimality, tractability and robustness are the main features for Kalman Filter to be used as a method to track and estimate [24]. It is difficult to implement Kalman Filter to the nonlinear systems. Extended Kalman Filter (EKF) has been using as a filtering solution for over thirty years. Extended Kalman Filter that provides to use traditional Kalman Filter for nonlinear models, is a solution to linearise the nonlinear models. However, this process has two well-known drawbacks [24]. If local linearity assumptions are broken, unstable filters can be produced. As a difficult application, computation of Jacobian matrices is one of the significant processes of EKF. Moreover, application and tuning of EKF are difficult. It is also dependable for systems which are almost linear on the time scale of the update intervals.

To cope with the EKF's constraints, a new method named as the unscented transformation (UT) was developed [25]. It is as a method to propagate mean and covariance information through nonlinear transformations. When it is compared with the EKF applications, it can be seen that UT is more accurate, easier to implement, and uses the same order of calculations as linearization.

The unscented transformation is a new, novel method for calculating the statistics of a random variable which undergoes a nonlinear transformation [24]. It is founded on the intuition that it is easier to approximate a Gaussian distribution than it is to approximate an arbitrary nonlinear function or transformation. The approach is illustrated in Figure 3.1 [24]. A setof points (or sigma points) are chosen so that their sample mean and sample covariance are $\bar{x}$ and P_{xx}. The nonlinear function is applied to each point in turn to yield a cloud of transformed points and $\bar{y}$ and P_{yy} are the statistics of the transformed points.

Although this method bares a superficial resemblance to Monte Carlo-type methods, there is an extremely important and fundamental difference. The samples are not drawn at random but rather according to a specific, deterministic algorithm. Since the problems of statistical convergence are not an issue, high order information about the distribution can be captured using only a very small number of points.

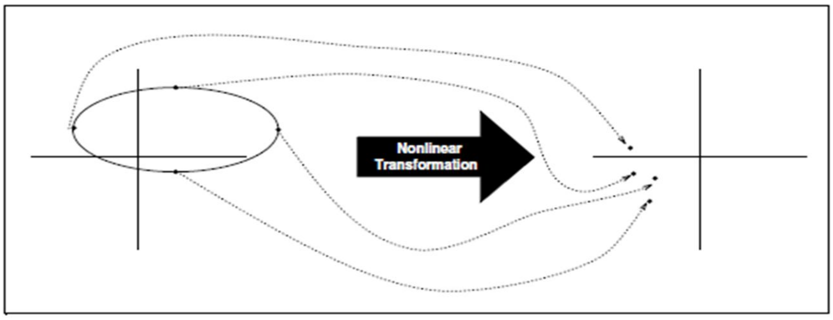

Figure 3.1: The principle of the unscented transform [24].

The n dimensional random variable x with mean $\bar{x}$ and covariance P_{xx} is approximated by $2n + 1$ weighted points given by,

$$\chi_0 = \bar{x} \qquad W_0 = \kappa/(n+\kappa) \tag{3.15}$$

$$\chi_i = \bar{x} + (\sqrt{(n+\kappa)P_{xx}})_i \qquad W_i = 1/2(n+\kappa) \tag{3.16}$$

$$\chi_{i+n} = \bar{x} - (\sqrt{(n+\kappa)P_{xx}})_i \qquad W_{i+n} = 1/2(n+\kappa) \tag{3.17}$$

Where $\kappa \epsilon R$, $(\sqrt{(n+\kappa)P_{xx}})_i$ is the ith row or column of the matrix square root of $(n+\kappa)P_{xx}$ and W_i is the weight which is associated with the ith point. The transformation procedure is as follows:

1. Instantiate each point through the function to yield the set of transformed sigma points,

$$y_i = f[\chi_i] \tag{3.18}$$

2. The mean is given by the weighted average of the transformed points,

$$\bar{y} = \sum_{i=0}^{2n} W_i y_i \tag{3.19}$$

3. The covariance is the weighted outer product of the transformed points,

$$P_{yy} = \sum_{i=0}^{2n} W_i \{y_i - \bar{y}\} \{y_i - \bar{y}\}^T \tag{3.20}$$

Given its properties of superior estimation accuracy and ease of implementation, the unscented transform is better suited than linearisation for filtering applications as shown in figure 3.2 [26].

As seen in the figure 3.2, mean and covariance computed via Extended Kalman Filter have not very good convergence characteristics. Results found by Unscented transformation have better convergence characteristics than the results determined with EKF.

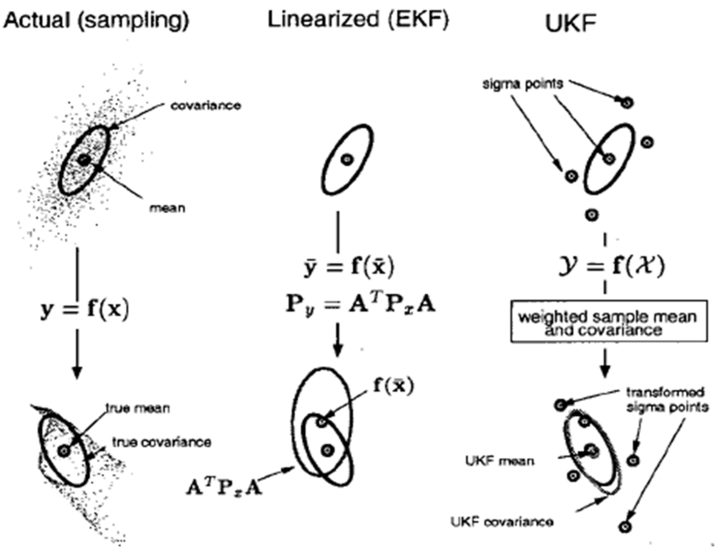

Figure 3.2: Example of mean and covariance propagation [26].

In order to utilize Kalman filter for nonlinear systems without any linearization step, the unscented transform and so Unscented Kalman Filter is one of the techniques. UKF uses the unscented transform, a deterministic sampling technique, to determine a minimal set of sample points (or sigma points) from the a priori mean and covariance of the state. Then, these sigma points go through nonlinear transformation. The posterior mean and the covariance are obtained from these transformed sigma points [27,28].

As it is stated, UKF procedure begins with the determination of $2n + 1$ sigma points with a mean of $\widehat{X}(k|k)$ and a covariance of $P(k|k)$. For an n dimensional state vector, these sigma points are obtained by,

$$X_0(k|k) = \widehat{X}(k|k) \tag{3.21}$$

$$X_i(k|k) = \widehat{X}(k|k) + (\sqrt{(n+\kappa)[P(k|k) + Q(k)]})_i \tag{3.22}$$

$$X_{i+n}(k|k) = \widehat{X}(k|k) - (\sqrt{(n+\kappa)[P(k|k) + Q(k)]})_i \tag{3.23}$$

where, $X_0(k|k)$, $X_i(k|k)$and $X_{i+n}(k|k)$ are sigma points, $Q(k)$ is the process noise covariance matrix, n is the state number and k is the scaling parameter which is used for fine tuning and the heuristic is to chose that parameter as $n + \kappa = 3$ [27]. Also, i is given as $i = 1 \ldots . n$.

Next step of the UKF process is transforming each sigma point by using system dynamics,

$$X_i(k+1|k) = f[X_i(k|k), k], \tag{3.24}$$

Then these transformed values are utilized for gaining the predicted mean and the covariance [29],

$$\hat{X}(k+1|k) = \frac{1}{n+\kappa}\left\{\kappa X_0(k+1|k) + \frac{1}{2}\sum_{i=1}^{2n} X_i\,(k+1|k)\right\}, \quad \textbf{(3.25)}$$

$$P(k+1|k) = \frac{1}{n+\kappa}\left\{\left[\kappa X_0(k+1|k) - \hat{X}\,(k+1|k)\right]\left[X_0(k+1|k) - \hat{X}\,(k+1|k)\right]^T\right.$$

$$\left.\frac{1}{2}\sum_{i=1}^{2n}[X_i\,(k+1/k) - \hat{X}\,(k+1/k)][X_i(k+1/k) - \hat{X}\,(k+1/k)]^T\right\} \quad \textbf{(3.26)}$$

Here, $\hat{X}\,(k+1|k)$ is the predicted mean and $P(k+1|k)$ is the predicted covariance. As the measurement equation is linear, measurement update can be performed with the same equations as the classical Kalman filter. The predicted observation vector is,

$$\hat{Y}(k+1|k) = H(k+1)\hat{X}\,(k+1|k) \quad \textbf{(3.27)}$$

Where, $H(k+1)$ is the measurement matrix. After that, observation covariance matrix is determined as,

$$P_{YY}(k+1|k) = H(k+1)P(k+1|k)H^T(k+1) \quad \textbf{(3.28)}$$

On the other hand the cross correlation matrix can be obtained as,

$$P_{XY}(k+1|k) = P(k+1|k)H^T(k+1) \quad \textbf{(3.29)}$$

Following part is the update phase of UKF algorithm. At that phase, first by using measurements, $Y(k+1)$, residual term (or innovation sequence) $v(k+1)$ is found as the difference between the actual observation and the predicted observation:

$$v(k+1) = Y(k+1) - \hat{Y}(k+1/k), \quad \textbf{(3.30)}$$

The innovation covariance is,

$$P_{vv}(k+1|k) = P_{YY}(k+1|k) + R(k+1)$$

$$= H(k+1)P(k+1|k)H^T(k+1) + R(k+1) \quad \textbf{(3.31)}$$

Here $R(k+1)$ is the measurement noise covariance matrix. Kalman gain is computed via equation of,

$$K(k+1) = P_{XY}(k+1|k)P_{vv}^{-1}(k+1|k) \quad \textbf{(3.32)}$$

At last, updated states and covariance matrix are determined by,

$$\hat{X}\,(k+1|k+1) = \hat{X}\,(k+1|k) + K(k+1)v(k+1), \quad \textbf{(3.33)}$$

$$P(k+1|k+1) = P(k+1|k) - P_{XY}(k+1|k)P_{vv}^{-1}(k+1|k)P_{XY}^{T}k+1|k) \quad \textbf{(3.34)}$$

or

$$P(k+1|k+1) = P(k+1|k) - K(k+1)P_{vv}(k+1|k)\,K^{T}(k+1) \quad \textbf{(3.35)}$$

Here, $\hat{X}(k+1|k+1)$ is the estimated state vector and $P(k+1|k+1)$ is the estimated covariance matrix.

3.3 Robust Unscented Kalman Filter with Single Measurement Noise Scale Factor

In case of normal operation of the measurement system, filter works correctly. However when there is a malfunction in the estimation system such as abnormal measurements, step-like changes or sudden shifts in the measurement channel etc. filter fails and estimation outputs become faulty [30].

Therefore, a robust algorithm must be introduced such that the filter makes itself insensitive to measurements in case of malfunctions and corrects estimation process without affecting good estimation behaviour.

Robust algorithm affects characteristic of filter only when the condition of the measurement system does not correspond to the model used in the synthesis of the filter. Otherwise, filter works with regular algorithm (3.24- 3.35) in an optimal way. Adaptation occurs as a change in the covariance matrix of the innovation sequence,

$$P_{vv}(k+1|k) = P_{YY}(k+1|k) + S(k)R(k+1) \quad \textbf{(3.36)}$$

where $S(k)$ is the scale factor calculated in the base of innovation sequence, $v(k+1)$, analyses. In robust case filter gain becomes,

$$K(k+1) = P_{XY}(k+1|k)[P_{YY}(k+1|k) + S(k)R(k+1)]^{-1}, \quad \textbf{(3.37)}$$

The gain matrix is changed when the condition of,

$$tr\{v(k+1)v^{T}(k+1)\} \geq tr\{P_{YY}(k+1|k) + R(k+1)\} \quad \textbf{(3.38)}$$

is the point at issue. Here $tr(.)$ is the trace of the related matrix. Left hand side of (3.38) represents the real filtration error while the right hand side is the accuracy of the innovation sequence known as a result of priori information [30]. When the predicted observation vector $\hat{y}(k+1|k)$ is reasonably different from measurement vector, $y(k+1)$, real filtration error exceeds the theoretical one. Hence, gain matrix must be fixed hereafter by the use of robust algorithm and so scale factor $S(k)$. In order to calculate the measurement noise scale factor equality of,

$$\mathrm{tr}[v(k+1)v^T(k+1)] = \mathrm{tr}[P_{YY}(k+1|k) + S(k)R(k+1)] \quad \textbf{(3.39)}$$

is used. Equation (3.39) can be rewritten as,

$$\mathrm{tr}[v(k+1)v^T(k+1)] = \mathrm{tr}[P_{YY}(k+1|k)] + S(k)\mathrm{tr}[R(k+1)] \quad \textbf{(3.40)}$$

If the knowledge of ,

$$\mathrm{tr}[v(k+1)v^T(k+1)] = v^T(k+1)v(k+1) \quad \textbf{(3.41)}$$

is taken into consideration, (3.40) becomes,

$$v^T(k+1)v(k+1) = \mathrm{tr}[P_{YY}(k+1|k)] + S(k)\mathrm{tr}[R(k+1)] \quad \textbf{(3.42)}$$

As a result, single noise measurement scale factor (SMNSF) can be obtained as,

$$S(k) = \frac{v^T(k+1)v(k+1) - \mathrm{tr}[P_{YY}(k+1|k)]}{\mathrm{tr}[R(k+1)]} = \frac{v^T(k+1)v(k+1) - \mathrm{tr}[H(k+1)P(k+1|k)H^T(k+1)]}{\mathrm{tr}[R(k+1)]} \quad \textbf{(3.43)}$$

Scale factor increases in case of malfunctions. As it can be seen from (3.36) and (3.37), that makes up an increment in covariance matrix of innovation sequence and a decrement in Kalman gain. Consequently, faulty measurements are regarded with a small weight in the estimation process and filter outputs are not affected.

3.4 Robust Unscented Kalman Filter with Multiple Measurement Noise Scale Factors

As it is discussed, robustness of the filter may be secured by using single measurement noise scale factor as a corrective term on the filter gain. However that is not a healthy procedure as long as the filter performance differs for each state for the complex systems with multivariable [31]. The preferred method is using a matrix built of multiple measurement noise scale factors (MMNSF) to fix the relevant term of the Kalman gain matrix, individually [32].

Robust algorithm affects characteristic of filter only when the condition of the measurement system does not correspond to the model used in the synthesis of the filter. Otherwise, filter works with regular algorithm (3.24)-(3.35) in an optimal way. However, when there is a measurement malfunction in the estimation system, the real error will exceed the theoretical one. Hence, if the matrix built of MMNSF, $S(k)$, is added into the algorithm as,

$$\frac{1}{\mu}\sum_{j=k-\mu+1}^{k} v^T(k+1)v(k+1) = P_{YY}(k+1|k) + S(k)R(k+1), \quad \textbf{(3.44)}$$

where, μ is the width of the moving window.

Then, $S(k)$ can be determined by the formula of,

$$S(k) = \left\{\frac{1}{\mu}\sum_{j=k-\mu+1}^{k} v(k+1)v^T(k+1) - P_{YY}(k+1|k)\right\} R^{-1}(k+1) \quad \textbf{(3.45)}$$

$$= \left\{\frac{1}{\mu}\sum_{j=k-\mu+1}^{k} v(k+1)v^T(k+1) - H(k+1)P(k+1|k)H^T(k+1)\right\} R^{-1}(k+1)$$

In case of normal operation, the scale matrix will be a unit matrix as $S(k) = I$. Here I represents the unit matrix.

Nonetheless, as μ is a limited number because of the number of the measurements and the computations performed with computer implies errors such as the approximation errors and the round off errors; $S(k)$ matrix, found by using (3.45) may not be diagonal and may have diagonal elements which are "negative" or less than "one" (actually, that is physically impossible).

Therefore, in order to avoid such situation, composing scale matrix by the following rule is suggested:

$$S^* = \mathrm{diag}(s_1^*, s_2^*, \ldots, s_n^*) \quad \textbf{(3.46)}$$

where,

$$s_i^* = \max\{1, S_{ii}\} \qquad i = 1, n. \quad \textbf{(3.47)}$$

Here, S_{ii} represents the i^{th} diagonal element of the matrix $S(k)$. Apart from that point, if the measurements are faulty, $S^*(k)$ will change and so affect the Kalman gain matrix;

$$K(k+1) = P_{XY}(k+1|k)[P_{yy}(k+1|k) + S^*(k)R(k+1)]^{-1} \quad \textbf{(3.48)}$$

In case of any kinds of malfunctions, the related element of the scale matrix, which corresponds to the faulty component of the measurement vector, increases and that brings out a smaller Kalman gain, which reduces the effect of the faulty innovation term on the state update process (3.34). As a result, accurate estimation results can be obtained even in case of measurement malfunctions.

Remark that, the covariance of the estimation error of RUKF increases in comparison with regular UKF due to the scale factor S_k. Therefore, robust algorithms are used only in case of faulty measurements and in all other cases procedure is run optimally with regular Unscented Kalman filter. Checkout is satisfied via a kind of statistical information. In order to achieve that, following two hypotheses may be introduced:

- γ_0; the system is normally operating
- γ_1; there is a malfunction in the estimation system.

Failure detection is realized by the use of following statistical function,

$$\beta(k+1) = \sum_{t=k-m+1}^{k}\{v^T(k+1)[P_{YY}(k+1|k) + R(k+1)]^{-1}v(k+1)\} \quad \textbf{(3.49)}$$

where m is the width of the moving window.

This statistical function has χ^2 distribution with s degree of freedom where s is the dimension of the innovation vector.

If the level of significance, α is selected as,

$$P\{\chi^2 > \chi^2_{\alpha,s}\} = \alpha; \qquad 0 < \alpha < 1, \quad \textbf{(3.50)}$$

the threshold value, $\chi^2_{\alpha,s}$ can be determined. Hence, when the hypothesis γ_1 is correct, the statistical value of $\beta(k+1)$ will be greater than the threshold value $\chi^2_{\alpha,s}$, i.e.:

$$\gamma_0 : \beta(k+1) \leq \chi^2_{\alpha,s} \qquad \forall k \quad \textbf{(3.51)}$$

$$\gamma_1 : \beta(k+1) > \chi^2_{\alpha,s} \qquad \exists k \quad \textbf{(3.52)}$$

4. UNSCENTED AND ROBUST UNSCENTED KALMAN FILTER APPLICATIONS FOR ORBIT DETERMINATION

4.1 The Mathematical Model of the Spacecraft Orbital Motion

Kepler equations system is one of the systems that can define elliptic orbits of spacecraft. This equations system includes 3 equations in differential form [33]:

$$\frac{d^2x}{dt^2} = -\gamma M \frac{x}{r^3} \tag{4.1}$$

$$\frac{d^2y}{dt^2} = -\gamma M \frac{y}{r^3} \tag{4.2}$$

$$\frac{d^2z}{dt^2} = -\gamma M \frac{z}{r^3} \tag{4.3}$$

where $\gamma = 6.67x10^{-11} m^3/kgs^2$ is the Kepler constant, x, y, and z are the Descartes coordinates of the spacecraft in Earth-Centered-Inertial (ECI) coordinate frame, $r = \sqrt{x^2 + y^2 + z^2}$ is the range between spacecraft's center of mass and Earth's center of mass, $M = 5.976x10^{24}$ kg is the mass of the Earth. Write the equations (4.1)-(4.3) in form of six difference equations as;

$$u_{i+1} = u_i - \Delta t\, \gamma M \frac{x_i}{r_i^3} + w_u \tag{4.4}$$

$$v_{i+1} = v_i - \Delta t\, \gamma M \frac{y_i}{r_i^3} + w_v \tag{4.5}$$

$$w_{i+1} = w_i - \Delta t\, \gamma M \frac{z_i}{r_i^3} + w_w \tag{4.6}$$

$$x_{i+1} = x_i + \Delta t u_i + w_x \tag{4.7}$$

$$y_{i+1} = x_i + \Delta t v_i + w_y \tag{4.8}$$

$$z_{i+1} = x_i + \Delta t w_i + w_z \tag{4.9}$$

In the equations; Δt is the sampling time, u, v, and w are the velocities in x, y, and z directions, respectively, $w_{(.)}$ is the Gaussian white noise with zero mean. As a result, it is possible to propagate the orbital position of the spacecraft for a desired time period by using these 6 equations.

By means of a ground tracking antenna, the distance from the antenna to the spacecraft (ρ), and the azimuth (α) and elevation (β) angles of the spacecraft are measured. The measurement equations are expressed as follows,

$$\rho = \sqrt{\rho_E^2 + \rho_N^2 + \rho_U^2} \quad \textbf{(4.10)}$$

$$\alpha = \tan^{-1}\frac{\rho_E}{\rho_N} \quad \textbf{(4.11)}$$

$$\beta = \sin^{-1}\frac{\rho_U}{\rho} \quad \textbf{(4.12)}$$

Here, ρ_E, ρ_N and ρ_U are the components of ρ in the East-North- Up (Zenith) (ENU) coordinate system.

4.2 Unscented Kalman Filter For Estimation Of Satellite Position and Velocity Based on Indirect Position Mesurements via Single Station Antenna

4.2.1 Problem statement

Consider the mathematical model of satellite's orbital motion in matrix form as;

$$X(k+1) = f\big(X(k)\big) + GW(k) \quad \textbf{(4.13)}$$

Where $X(k)$ is the state vector, $W(k)$ is the system noise, G is the transition matrix of the system noise.

The state vector of the orbital motion of satellite can be written in the following form;

$$X = [x \;\; y \;\; z \;\; u \;\; v \;\; w]^T, \quad \textbf{(4.14)}$$

The non-linear measurement equation is,

$$Z(k) = h(x(k), k) + V(k) \quad \textbf{(4.15)}$$

where $Z(k)$ is the measurement vector, $h(x(k), k)$ is a nonlinear measurement model mapping current state to measurements, $V(k)$ is the random measurement noise. It is assumed that both noise vectors $W(k)$ and $V(k)$ are white Gaussian.

As seen from (4.13) and (4.15), both the equations of system and measurements are nonlinear. Inputting the position components of the satellite in ECI reference frame calculated from the real range measurements in ENU reference frame to the filter leads to a linear measurement function. The conventional approach of inputting directly the real range-azimuth-elevation measurements to the filter results in a highly nonlinear measurement function, which increases the computational load significantly.

Below, two-stage estimation of satellite's position and velocity by single station antenna tracking data, where the measurement nonlinearities are eliminated, is proposed. In first stage, the direct nonlinear antenna measurements are transformed to the linear x-y-z coordinate measurements of satellite's position, and their errors' variances are evaluated. In the second stage, the solutions of the first stage are improved by UKF for estimation of the satellite position and velocity on indirect linear x-y-z measurements. The simulation results show that the proposed two-stage procedure satisfies both better estimation accuracy and convergence characteristics.

4.2.2 Determination of the satellite position by single station antenna tracking data

In general, for the orbit determination purpose, the Kalman filtering technique is used. Accuracy of the Kalman filter depends on the measurement accuracy significantly. Therefore, it is important to derive formulas for the accuracy (variances) of indirect x-y-z position measurements.

Satellite coordinates are determined with single point (ground station) by the help of this method and difficult calculations are not needed. Following formulas are used to calculate satellite's coordinates in the ENU coordinate frame [22,34];

$$\rho_E = \rho\cos\beta\sin\alpha \quad \textbf{(4.16)}$$

$$\rho_N = \rho\cos\beta\cos\alpha \quad \textbf{(4.17)}$$

$$\rho_U = \rho\sin\beta \quad \textbf{(4.18)}$$

Range ρ, azimuth α and elevation β angles are determined by radiolocation measurements. After accomplishing the successive coordinate transformations on the measured position between ENU and Earth-Centered-Earth-Fixed (ECEF) and between ECEF and ECI [34,35], the calculated indirect position measurements x, y, z of the satellite in ECI is obtained as a function of the real measurements ρ, α, β in ENU coordinate frame as follows;

$$x = -\rho\cos\beta\sin\alpha\sin\theta - \rho\cos\beta\cos\alpha\sin\lambda\cos\theta + \rho\sin\beta\cos\lambda\cos\theta + R_E\cos\lambda\cos\theta \quad \textbf{(4.19)}$$

$$y = \rho\cos\beta\sin\alpha\cos\theta - \rho\cos\beta\cos\alpha\sin\lambda\sin\theta + \rho\sin\beta\cos\lambda\sin\theta + R_E\cos\lambda\sin\theta \quad \textbf{(4.20)}$$

$$z = \rho\cos\beta\cos\alpha\cos\lambda + \rho\sin\beta\sin\lambda + R_E\sin\lambda \quad \textbf{(4.21)}$$

4.2.3 Variance analysis of the position errors

In this sub-section, formulas for the error analysis of the satellite's orbit determination will be presented. Variances of orbit parameters are chosen as the accuracy criteria, and the accuracy of algorithm (4.19-4.21) is considered for construction of the covariance matrix of measurement noise, R in EKF.

The method to calculate the accuracy of satellite's position enables determining possibility characteristics of the position data's error depending on the type of ground station, location of ground station, and measurement accuracy of navigation parameters [22,36]. Establishing ground stations optimally and choosing the most accurate position determining area are possible as a result of the needed calculations. In some cases, due to the difficulty of the calculations and the need for huge preparations, approximate accuracy values of the coordinates are used to determine the accuracy of the position data. The coordinates of the satellite are calculated by formulas (4.19-4.21). Because, x, y, z coordinates of the satellite are non-linear functions of the navigation parameters, range (ρ), azimuth angle (α), elevation angle (β) measured by single ground station antenna, by accepting that the navigation parameters' measurement errors are independent and errors of parameters local sidereal time, latitude and radius of the Earth θ, λ, R_E are negligible, the variances of coordinates' calculation errors are determined as [22];

$$\sigma_x^2 = \left(\frac{\partial x}{\partial \rho}\right)^2 \sigma_\rho^2 + \left(\frac{\partial x}{\partial \alpha}\right)^2 \sigma_\alpha^2 + \left(\frac{\partial x}{\partial \beta}\right)^2 \sigma_\beta^2 \quad \textbf{(4.22)}$$

$$\sigma_y^2 = \left(\frac{\partial x}{\partial \rho}\right)^2 \sigma_\rho^2 + \left(\frac{\partial x}{\partial \alpha}\right)^2 \sigma_\alpha^2 + \left(\frac{\partial x}{\partial \beta}\right)^2 \sigma_\beta^2 \quad \textbf{(4.23)}$$

$$\sigma_z^2 = \left(\frac{\partial x}{\partial \rho}\right)^2 \sigma_\rho^2 + \left(\frac{\partial x}{\partial \alpha}\right)^2 \sigma_\alpha^2 + \left(\frac{\partial x}{\partial \beta}\right)^2 \sigma_\beta^2 \quad \textbf{(4.24)}$$

where σ_x^2, σ_y^2, σ_z^2 are the variances of the calculated x, y, z coordinates' errors, respectively, σ_ρ^2, σ_α^2, σ_β^2 are the variances of the measurement errors of navigation parameters ρ, α, β respectively. The expressions for the partial derivatives in (4.22-4.24) are presented in Appendix A.

4.2.4 UKF based estimation of satellite position and velocity on linear position measurements

In this approach, the measurement vector can be presented as,

$$\mathrm{Y} = [\mathrm{x}\ \ \mathrm{y}\ \ \mathrm{z}]^{\mathrm{T}} \tag{4.25}$$

This new approach aims to simplify the measurement matrix as;

$$\mathrm{H} = \begin{bmatrix} 1 & 0 & 0 & 0 & 0 & 0 \\ 0 & 1 & 0 & 0 & 0 & 0 \\ 0 & 0 & 1 & 0 & 0 & 0 \end{bmatrix} \tag{4.26}$$

by deriving the components of the discrete measurement vector $\mathrm{Y(k)}$ from the directly measured range, azimuth, and elevation.

The UKF algorithm (3.21-3.35) is implemented for estimation procedure. The structural scheme of the proposed UKF for estimation of satellite's position and velocity on indirect linear x-y-z measurements is given in Figure 4.1.

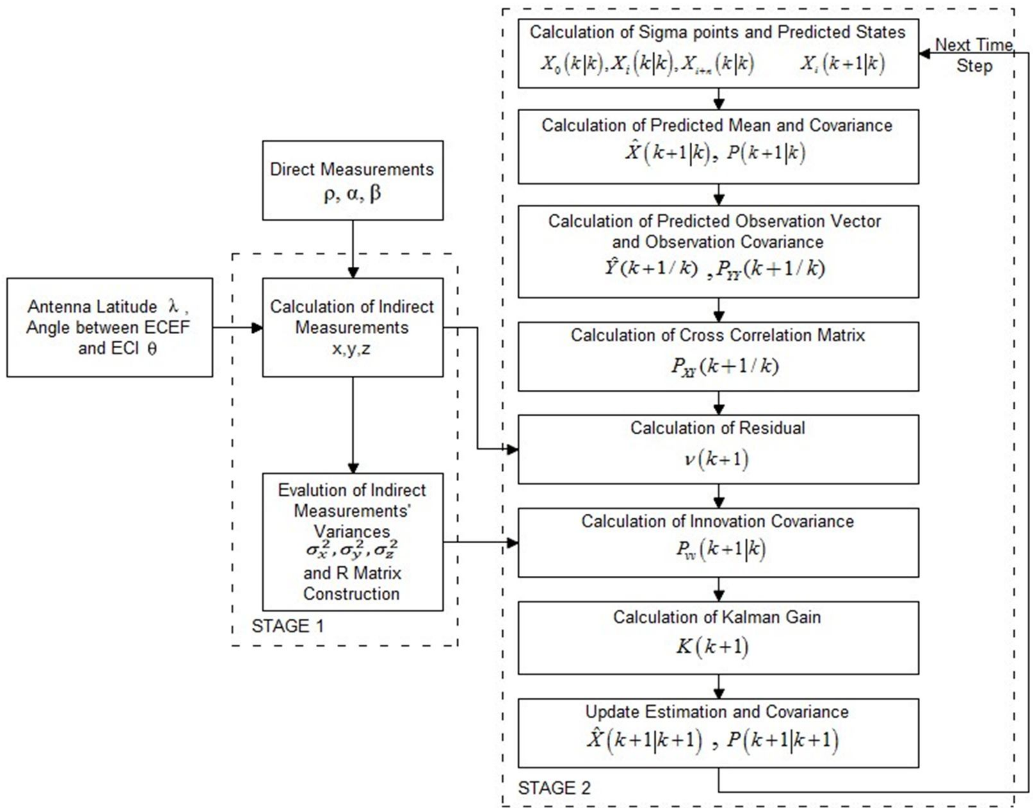

Figure 4.1: The structural scheme of the UKF based two-stage satellite's position and velocity estimation procedure via antenna.

4.3 UKF For Estimation Of Satellite Position and Velocity Based on Direct Position and Velocity Measurements via GPS

In the previous section which has the purpose of the calculation of indirect antenna measurements, inputting the position components of the satellite in ECI reference frame calculated from the real range measurements in ENU reference frame to the filter leads to a linear measurement function. The conventional approach of inputting directly the real range-azimuth-elevation measurements to the filter results in a highly nonlinear measurement function, which increases the computational load significantly. In conclusion, two-stage estimation of satellite's position and velocity by single station antenna tracking data, where the measurement nonlinearities are eliminated, is proposed. However, in this section which aims to measure direct GPS measurements, there is no need to imply a two-stage mechanism.

Mathematical model of the satellite motion and the state vector is the same with ground station in GPS. However, while two-stage estimation of satellite's position and velocity is used in antenna, GPS directly measures the positions and velocities. Therefore, it is not required to use a transformation between angles and positions as done in the antenna system. GPS obtains the needed linear x,y,z position and velocity measurements in the ECEF coordinate system. In this approach, the measurement vector can be presented as,

$$Y = [x \; y \; z \; u \; v \; w]^T \qquad \textbf{(4.27)}$$

In this case, the transition matrix;

$$H = \begin{bmatrix} 1 & 0 & 0 & 0 & 0 & 0 \\ 0 & 1 & 0 & 0 & 0 & 0 \\ 0 & 0 & 1 & 0 & 0 & 0 \\ 0 & 0 & 0 & 1 & 0 & 0 \\ 0 & 0 & 0 & 0 & 1 & 0 \\ 0 & 0 & 0 & 0 & 0 & 1 \end{bmatrix} \qquad \textbf{(4.28)}$$

The components of the measurement vector Y(k) are obtained directly via GPS measurements. The UKF algorithm (3.21-3.35) is implemented for estimation procedure. The structural scheme of the proposed UKF for estimation of satellite's position and velocity on linear position and velocity measurements is given in Figure 4.2.

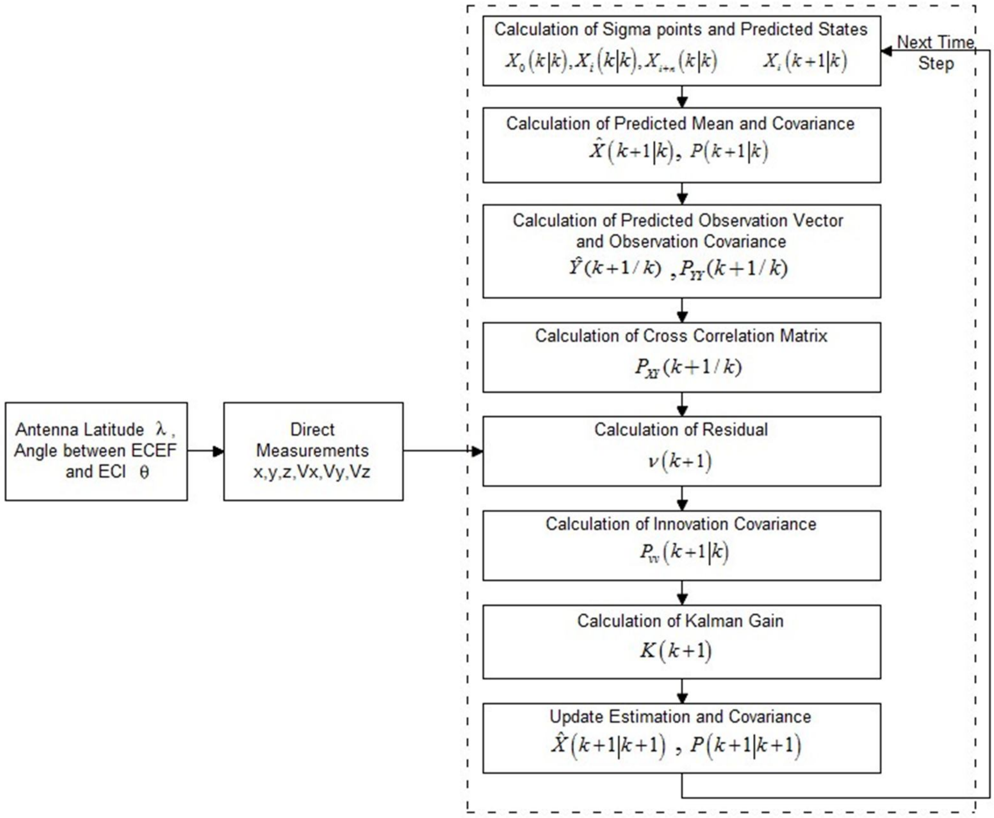

Figure 4.2 : The structural scheme of the UKF based satellite's position and velocity estimation procedure via GPS.

4.4 Simulation Results for Unscented Kalman Filter Application to Orbit Determination with Single Station Antenna

This subsection will give the steps to be followed to simulate the estimation of the position and velocity of a geostationary satellite by using its range, azimuth angle, and elevation angle with respect to a ground antenna.

The ground antenna is assumed to be located in the Daejeon, South Korea, so its latitude angle is taken as $\lambda = 36.4^o$. The standard deviation values of the range, azimuth and elevation measurements are accepted to be $\sigma_\rho = 10$ m, $\sigma_\alpha = 0.01^o$, $\sigma_\beta = 0.01^o$ respectively.

The Range-Azimuth-Elevation are measured in the East-North- Up (Zenith)- (ENU) coordinate system. Because the position and velocity components of the spacecraft, which are the states of the estimation problem, are defined in the Earth-Centered Inertial (ECI) coordinate system. The measured variables has to be expressed as function of the states. The range vector's components can be written in ECI coordinate frame as follows;

$$\begin{bmatrix} \rho_x \\ \rho_y \\ \rho_z \end{bmatrix} = \begin{bmatrix} x - R_E\cos\lambda\cos\theta \\ y - R_E\cos\lambda\sin\theta \\ z - R_E\sin\lambda \end{bmatrix} \quad \textbf{(4.29)}$$

Here, x, y, z are the inertial position components of the spacecraft, Re is the Earth's radius at equator, and θ is the rotation angle of the Earth-Centered Earth-Fixed (ECEF) reference system around the Earth's rotation axis with respect to the ECI coordinate systems. It is calculated according to;

$$\theta = 280.46061837 + 360.9854736628 d_{2000} \quad \textbf{(4.30)}$$

in degrees. d_{2000} is the duration from the epoch at the beginning of the year 2000 till the starting moment of the estimation process and calculated by the formula,

$$d_{2000} = 367y - \mathrm{INT}\left\{\frac{7\{y + \mathrm{INT}[(m+9)/12]\}}{4}\right\}$$

$$+\mathrm{INT}\left\{\frac{275m}{9}\right\} + \frac{h + \frac{min}{60} + s/3600}{24} + d - 730531.5 \quad \textbf{(4.31)}$$

in days [34]. The starting moment for the work is input to the simulation as year (y=2006), month (m=1), day (d=1), hour (h=0), minute (m=0), second (s=0).

The transformation matrix from the ECI system to the ECEF system is;

$$T^{ECI-ECEF} = \begin{bmatrix} -\sin\theta & \cos\theta & 0 \\ \cos\theta & \sin\theta & 0 \\ 0 & 0 & 1 \end{bmatrix} \quad \textbf{(4.32)}$$

whereas the transformation matrix from the ECEF system to the ENU system is as follows;

$$T^{ECEF-ENU} = \begin{bmatrix} 1 & 0 & 0 \\ 0 & -\sin\lambda & \cos\lambda \\ 0 & \cos\lambda & \sin\lambda \end{bmatrix} \quad \textbf{(4.33)}$$

Therefore, the quantities measured in the ENU system can be related to the position components defined in the ECI system through the following transformation;

$$\begin{bmatrix} \rho_E \\ \rho_N \\ \rho_U \end{bmatrix} = (T^{ECEF-ENU})(T^{ECI-ECEF}) \begin{bmatrix} \rho_x \\ \rho_y \\ \rho_z \end{bmatrix} \quad \textbf{(4.34)}$$

The following relation between the inertial position components of the satellite and $[\rho_x \;\; \rho_y \;\; \rho_z]^T$ is obvious from (4.29);

$$\begin{bmatrix} x \\ y \\ z \end{bmatrix} = \begin{bmatrix} \rho_x \\ \rho_y \\ \rho_z \end{bmatrix} + R_E \begin{bmatrix} \cos\lambda\cos\theta \\ \cos\lambda\sin\theta \\ \sin\lambda \end{bmatrix} \qquad \textbf{(4.35)}$$

By performing the inverse of the transformation given in (4.34), $[\rho_x \;\; \rho_y \;\; \rho_z]^T$ can be expressed in terms of the variables measured in the ENU coordinate system. Because the related transformation matrices defined in (4.32) and (4.33) are orthogonal, their inverses are equal to their transposes, so;

$$\begin{bmatrix} \rho_x \\ \rho_y \\ \rho_z \end{bmatrix} = (\, T^{ECI-ECEF})^T (T^{ECEF-ENU})^T \begin{bmatrix} \rho_E \\ \rho_N \\ \rho_U \end{bmatrix} \qquad \textbf{(4.36)}$$

holds. By substituting (4.36) in (4.35), the elements of the measurement vector (4.25) that will be input to the UKF can be obtained as in (4.19-4.21).

Because the measurement vector of the UKF consists the indirect x-y-z measurements $Y = [x \;\; y \;\; z]^T$ the measurement covariance matrix resulting from (4.22-4.24), can be written as follows,

$$R = \begin{bmatrix} \sigma_x^2 & 0 & 0 \\ 0 & \sigma_y^2 & 0 \\ 0 & 0 & \sigma_z^2 \end{bmatrix} \qquad \textbf{(4.37)}$$

The initial state vector is input to filter as,

$$X_0 = [-20000000 \text{ m} \; -25000000 \text{ m} \;\; 3400 \text{ m}$$
$$1800 \text{ m/s} \;\; -1700 \text{ m/s} \;\; -1.5 \text{ m/s}]^T \qquad \textbf{(4.38)}$$

The system noise covariance matrix is selected as,

$$Q = \begin{bmatrix} 1 & 0 & 0 & 0 & 0 & 0 \\ 0 & 1 & 0 & 0 & 0 & 0 \\ 0 & 0 & 1 & 0 & 0 & 0 \\ 0 & 0 & 0 & 1 & 0 & 0 \\ 0 & 0 & 0 & 0 & 1 & 0 \\ 0 & 0 & 0 & 0 & 0 & 1 \end{bmatrix} \qquad \textbf{(4.39)}$$

with $\Delta t = 10$ s simulation step interval in 5000 steps.

Simulation results are given in figure 4.3, figures C.1-C.8 in appendix C and in tables 4.1 and 4.2. First part of figures gives UKF state estimation results and the actual values in a comparing way. Second part of the figures shows the error of estimation process as the difference between the actual and estimated values of satellite states. The last part indicates the variance of the estimation. In graphics, dashed line refers to the actual value and solid line refers to estimation value. The results for the x component of the position is given in figure 4.3. For y, z position, x, y, z velocities and range, azimuth and elevation results are into appendix C (figures C.1-C.8). The method based on indirect measurements provides an unnoticeably short transient duration.

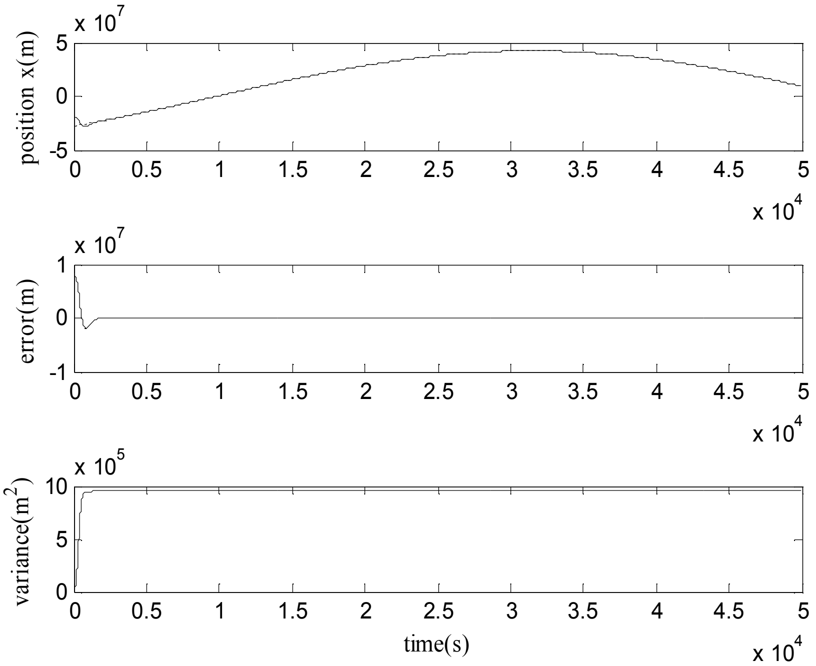

Figure 4.3 : X position est. of satellite by indirect measurements via antenna.

In the conventional method, calculation of predicted observation vector, observation covariance matrix and cross correlation matrix consists of complex terms which increase the computational load significantly.

In the proposed method, predicted observation vector, observation covariance matrix and cross correlation matrix are calculated via expressions (3.27), (3.28) and (3.29) respectively. This process is very simple and it does not increase the computational load significantly, which is an important advantage of the designed method.

The estimation accuracy of the proposed indirect method, which can be clearly observed from the figures 4.3, C.1-C.8 and tables 4.1 and 4.2, is good. Furthermore, the indirect method is able to make the filter output to converge. Error and variance values are adequate for a geostationary satellite tracked by ground station antenna.

Table 4.1 : Absolute estimation errors, SSA.

Parameter	1000	2000	3000	4000	5000
x position(m)	123.5995	207.0492	1.1165	120.2725	628.2238
y position(m)	117.5316	136.7559	147.9225	74.3314	281.952
z position(m)	1.13E+03	2.23E+03	63.4589	1.28E+03	1.47E+03
x velocity(m/s)	2.0479	0.9526	0.4429	0.8161	2.6127
y velocity(m/s)	0.064	0.0679	0.7506	0.7972	0.6712
z velocity(m/s)	6.84E-04	6.4693	2.8559	1.2426	1.0577
Range (m)	10.0502	7.8612	14.5074	41.6537	14.7946
Azimuth (rad)	2.58E-04	1.18E-05	1.51E-04	7.16E-05	1.47E-04
Elevation (rad)	4.32E-04	2.72E-04	1.40E-04	6.90E-05	3.34E-04

Table 4.2 : Variances of estimation errors, SSA.

Parameter	1000	2000	3000	4000	5000
x position(m)	9.58E+05	9.59E+05	9.61E+05	9.62E+05	9.64E+05
y position(m)	1.11E+06	1.11E+06	1.11E+06	1.11E+06	1.12E+06
z position(m)	9.58E+05	9.59E+05	9.60E+05	9.62E+05	9.64E+05
x velocity(m/s)	12.6414	12.6511	12.6611	12.6657	12.6692
y velocity(m/s)	13.2838	13.2833	13.2895	13.3086	13.3319
z velocity(m/s)	12.641	12.6475	12.6538	12.6609	12.6688
Range (m)	2.01E+04	2.02E+04	2.18E+04	2.59E+04	3.26E+04
Azimuth (rad)	9.26E-04	8.99E-04	8.11E-04	6.16E-04	2.78E-04
Elevation (rad)	0.0388	0.0388	0.0389	0.039	0.0393

4.5 Simulation Results for Unscented Kalman Filter Application to Orbit Determination with GPS

This subsection will give the steps to be followed to simulate the estimation of the position and velocity of a low earth orbit satellite by GPS mesurements. The GPS receiver is assumed to be located in the Daejeon, South Korea, so its latitude angle is taken as $\lambda = 36.4^{o}$. The standard deviation values of the position and velocity components are accepted to be 25 m for σ_x, σ_y, σ_z and 0.3 m/s for $\sigma_{Vx}, \sigma_{Vy}, \sigma_{Vz}$ respectively.

The positions and velocities are measured in the Earth-Centered Earth-Fixed (ECEF) coordinate system in GPS. Transformation between ECI and ECEF coordinates can be done as presented in (4.32). The rotation angle θ of the Earth-Centered Earth-Fixed (ECEF) reference system around the Earth's rotation axis with respect to the ECI coordinate systems can also be calculated via (4.30) and (4.31). The starting moment for the work is input to the simulation as year (y=2012), month (m=1), day (d=3), hour (h=23), minute (m=05), second (s=28) for the LEO satellite to be used with GPS.

The measurement vector of the UKF consists the position and velocity measurements including six parameters as $Y = [x\ y\ z\ Vx\ Vy\ Vz]^T$. The measurement covariance matrix, can be written as follows,

$$R = \begin{bmatrix} \sigma_x^2 & 0 & 0 & 0 & 0 & 0 \\ 0 & \sigma_y^2 & 0 & 0 & 0 & 0 \\ 0 & 0 & \sigma_z^2 & 0 & 0 & 0 \\ 0 & 0 & 0 & \sigma_{Vx}^2 & 0 & 0 \\ 0 & 0 & 0 & 0 & \sigma_{Vy}^2 & 0 \\ 0 & 0 & 0 & 0 & 0 & \sigma_{Vz}^2 \end{bmatrix}$$

$$R = \begin{bmatrix} 25^2 & 0 & 0 & 0 & 0 & 0 \\ 0 & 25^2 & 0 & 0 & 0 & 0 \\ 0 & 0 & 25^2 & 0 & 0 & 0 \\ 0 & 0 & 0 & 0.3^2 & 0 & 0 \\ 0 & 0 & 0 & 0 & 0.3^2 & 0 \\ 0 & 0 & 0 & 0 & 0 & 0.3^2 \end{bmatrix} \tag{4.40}$$

The initial state vector is input to filter as,

$$X_0 = [1000000\text{m}\ 100000\text{m}\ 1000000\text{m}$$

$$1000\text{m/s}\ \ 1000\text{m/s}\ \ -1000\ \text{m/s}]^T \tag{4.41}$$

The system noise covariance matrix is selected as,

$$Q = 0.1\text{x}\begin{bmatrix} 1 & 0 & 0 & 0 & 0 & 0 \\ 0 & 1 & 0 & 0 & 0 & 0 \\ 0 & 0 & 1 & 0 & 0 & 0 \\ 0 & 0 & 0 & 1 & 0 & 0 \\ 0 & 0 & 0 & 0 & 1 & 0 \\ 0 & 0 & 0 & 0 & 0 & 1 \end{bmatrix} \tag{4.42}$$

with $\Delta t = 1$ s simulation step interval in 5000 steps.

Simulation results are given in figure 4.4, figures C.81-C.85 and tables 4.3 and 4.4. First part of figures gives UKF state estimation results and the actual values in a comparing way. Second part of the figures shows the error of estimation process as the difference between the actual and estimated values of satellite states. The last part indicates the variance of the estimation. In graphics, dashed line refers to the actual value and solid line refers to estimation value. The result for x position is given in figure 4.4 and the other positions and velocities are given in appendix C (C.81-C.85).

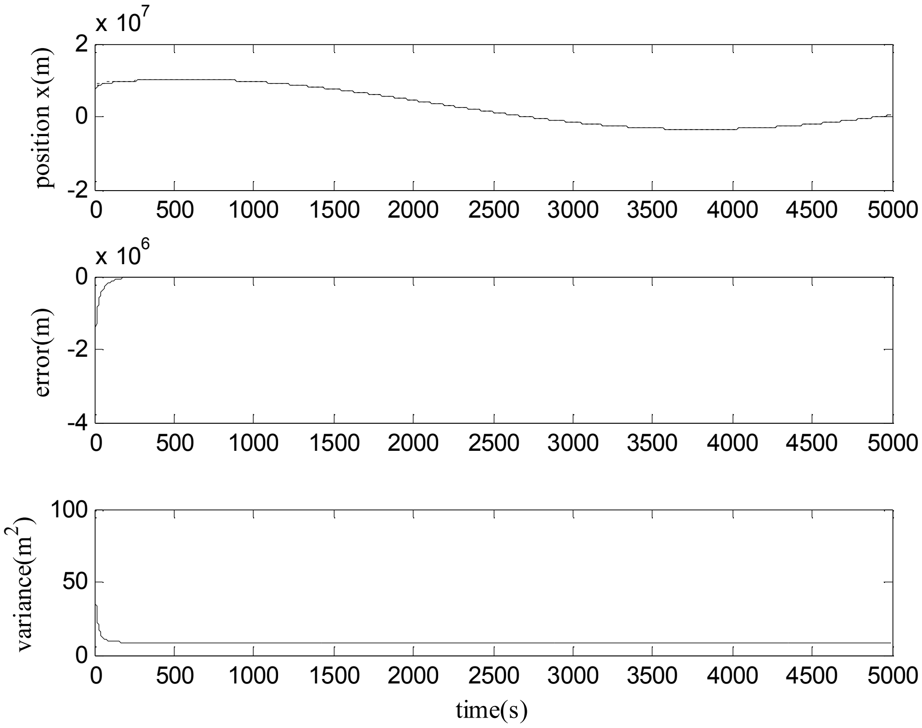

Figure 4.4 : X position estimation of satellite by measurements via GPS.

The estimation accuracy of the proposed method, which can be clearly observed from the figures 4.4, C.81-C.85 and tables 4.3 and 4.4, is very good. Estimation accuracy is better than the accuracy of estimations by indirect measurements of ground station. Estimation of parameters with GPS measurements are more accurate than the antenna. Estimation of low earth orbit satellite parameters is easier and more accurate when compared with geostationary satellites. Consequently, this method is able to make the filter output to converge, too. Error and variance values are reliable for estimations with GPS measurements of a low earth orbit satellite.

When both of the study results with antenna and GPS are compared with the previous study results in the literature, both of the application done via indirect antenna measurements and direct GPS measurements provide reliable results. For the application with indirect antenna measurements, standard deviation between 1000-1500 meters is normal for position components. GPS results are also in dependable interval.

Table 4.3 : Absolute estimation errors, GPS.

Parameter	1000	2000	3000	4000	5000
x position(m)	9.23E+00	8.72E+00	8.7344	8.7186	8.72E+00
y position(m)	8.8377	8.72E+00	8.7289	8.72E+00	8.7173
z position(m)	9.24E+00	8.75E+00	8.74E+00	8.73E+00	8.74E+00
x velocity(m/s)	0.0556	5.55E-02	0.0553	0.0556	0.0555
y velocity(m/s)	0.0556	5.56E-02	0.0554	0.0555	0.0556
z velocity(m/s)	5.52E-02	0.055	0.0553	0.0554	0.0551

Table 4.4 : Variances of estimation errors, GPS.

Parameter	1000	2000	3000	4000	5000
x position(m)	8.72E+00	8.72E+00	8.72E+00	8.72E+00	8.72E+00
y position(m)	8.72E+00	8.72E+00	8.72E+00	8.72E+00	8.72E+00
z position(m)	8.72E+00	8.72E+00	8.72E+00	8.72E+00	8.72E+00
x velocity(m/s)	0.0406	0.0406	0.0406	0.0406	0.0406
y velocity(m/s)	0.0406	0.0406	0.0406	0.0406	0.0406
z velocity(m/s)	0.0406	0.0406	0.0406	0.0406	0.0406

4.6 Application of Adaptive Robust Unscented Kalman Filters to Orbit Determination via Single Station Antenna

In order to understand the efficiency of the proposed robust unscented Kalman filter algorithms and examine the advantages of each algorithm, Robust Unscented Kalman Filter (RUKF) with single measurement noise scale factor (SMNSF) (3.36, 3.37) and RUKF with multiple measurement noise scale factors (MMNSF) (3.45, 3.48), various estimation scenarios are performed. Simulations are realized for 50000 seconds with a sampling time $\Delta t = 10\text{sec}$. Simulations are also done with regular UKF (3.21-3.35) so as to compare results with both RUKF algorithms. For robust Kalman filters $\chi^2_{\alpha,s}$ is taken as 7.8 and this value comes from chi-square distribution when the degree of freedom is 3 (three measurement parameters for antenna, x, y and z).

First part of figures gives UKF or RUKF state estimation results and the actual values in a comparing way. Dashed line refers to actual values and solid line symbolizes the estimations. Second part of the figures shows the error of estimation process based on the actual values of the satellite. The last part indicates the variance of the estimation.

4.6.1 Continuous bias at measurements

For the first scenario, continuous bias term is formed by adding a constant term to the azimuth angle in between 15000^{th} and 25000^{th} seconds (between 1500^{th} and 2500^{th} steps). Normally, the variances which form the covariance matrix (R) are related to azimuth, elevation angles and range. So, when continuous bias is added to azimuth angle, variances are affected from continuous bias and they are automatically changed in case of faults. Therefore, there is no need to implement RUKF with SMNSF and MMNSF in this case. Because, the aim of the application of RUKF with SMNSF and MMNSF is tuning the covariance matrix of innovation sequence. Automatic adaptation of R matrix makes the filter adaptive. Changes of variances forming the R matrix can be seen in figure 4.5 in case of continuous bias in azimuth. To apply the RUKF with SMNSF and MMNSF, covariance matrix R must be formed by constant values. To do this, variances of mean values of x, y and z position differences between actual and indirect measurement values are obtained and located in R matrix. After that, RUKF with SMNSF and MMNSF can be applied. As figure 4.6 for x parameter and figures C.9- C.16 for other parameters in appendix C and tables B.1, B.2 show that the regular UKF fails about estimating the parameters of geostationary satellite accurately. Continuous bias is added to the azimuth angle. However, after transformation from topocentric to ECI coordinates, cont bias added to azimuth, affects all of the position and velocity parameters. Therefore, RUKF fails for estimation.

Figures 4.7 for x position, C.17-C.24 for others are the graphics for RUKF with SMNSF and figures 4.8 for x position, C.25-C.32 for others are the graphics for RUKF with MMNSF for other parameters in appendix C. Results are summarized at tables B.1-B.6. Tables B.1 and B.2 present the errors of estimations and variances of estimation errors for Regular UKF in case of continuous bias. Tables B.3 and B.4 present the errors of estimations and variances of estimation errors for RUKF with SMNSF in case of continuous bias. Tables B.5 and B.6 present the errors of estimations and variances of estimation errors for RUKF with MMNSF in case of continuous bias. 2000th step can be examined to compare the filters in faulty interval. As seen from obtained results, some of the parameters are estimated better in RUKF with SMNSF and the others are estimated in RUKF with MMNSF. For example, x, y positions and velocities are better in RUKF with SMNSF where z position and velocities are better in RUKF with MMNSF. It can be said that Regular UKF obtains better results for x, y parameters in faulty interval. However, RUKF with SMNSF and MMNSF results are close to each other. As a consequence, RUKF with SMNSF and MMNSF reduce the fault in small amounts for some parameters and they obtain close results for this case. Moreover, Regular UKF can sometimes give better results, too. Normally, it is expected that the RUKF with MMNSF gives better results when compared with RUKF with SMNSF in general. This is not valid in this state. The reason is effect of azimuth angles on all indirect measurements. All position and velocity parameters are affected via azimuth with continuous bias. Bias is implemented to real measurement, but the measurement noise scale factors try to correct the indirect measurements.

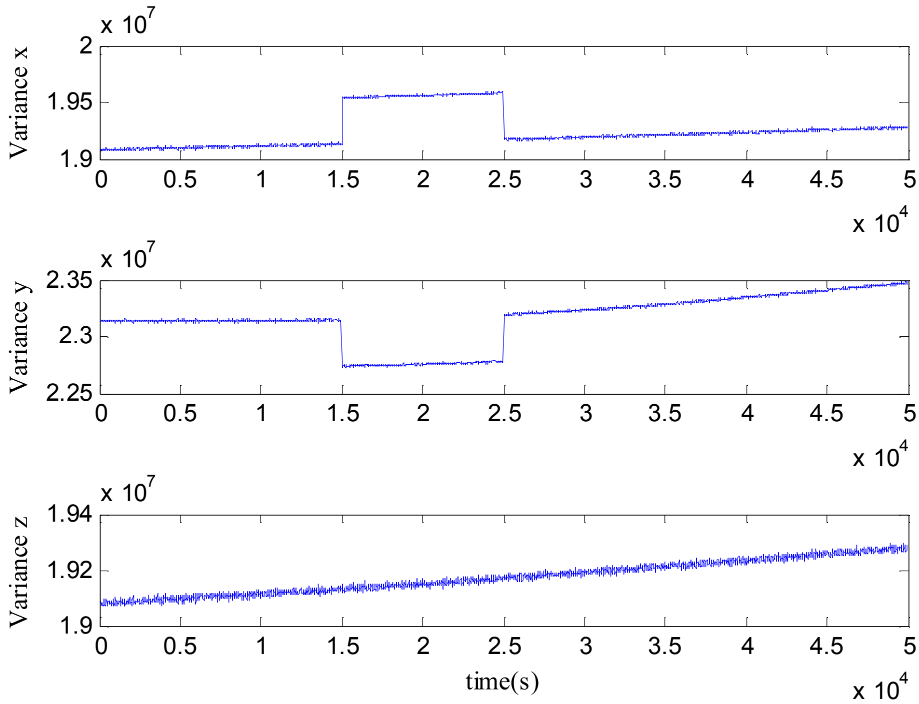

Figure 4.5: Variance changes in three dimension in case of cont. bias.

As seen in the figure 4.5, continuous bias is added to azimuth angle measurement between 15000th and 25000th seconds. Variances are also changed with respect to azimuth bias. For the variance x, variance increases in the 15000th and 25000th interval. For the variance y, variance decreases in the 15000th and 25000th interval. For the variance z, variance is nearly constant in the 15000th and 25000th interval. Because, azimuth angle affects the x and y variances.

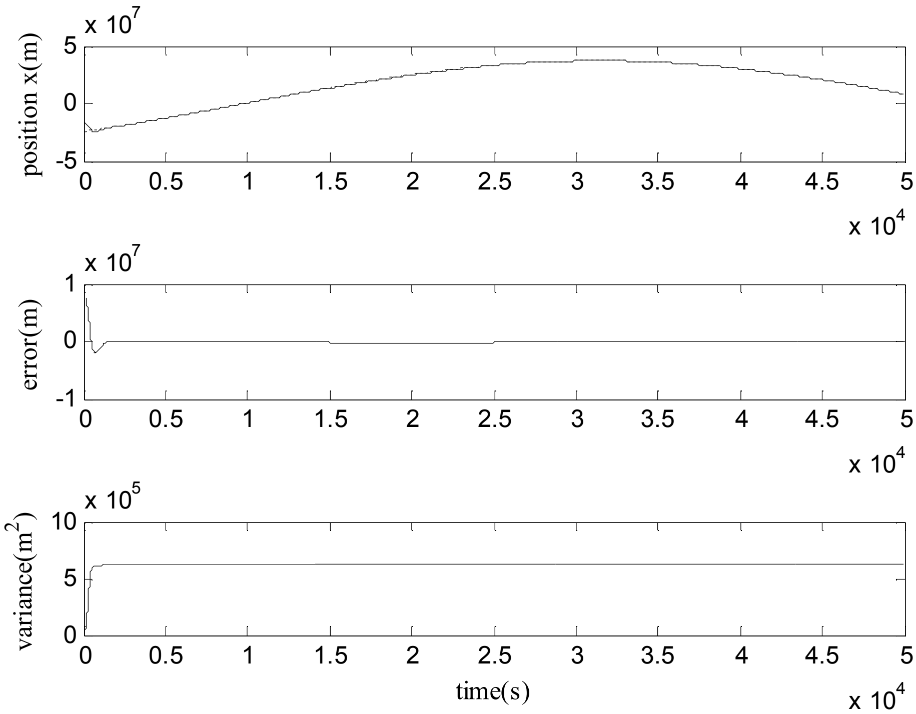

Figure 4.6: X position est. via Regular UKF in case of cont. bias, SSA.

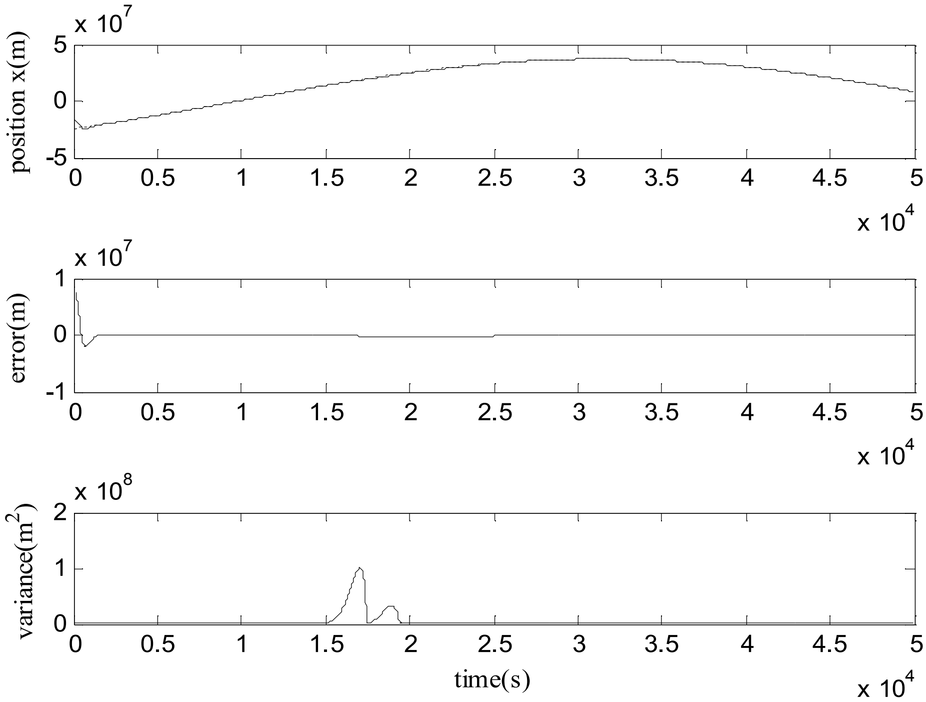

Figure 4.7: X position est. via RUKF with SMNSF in case of cont.bias, SSA.

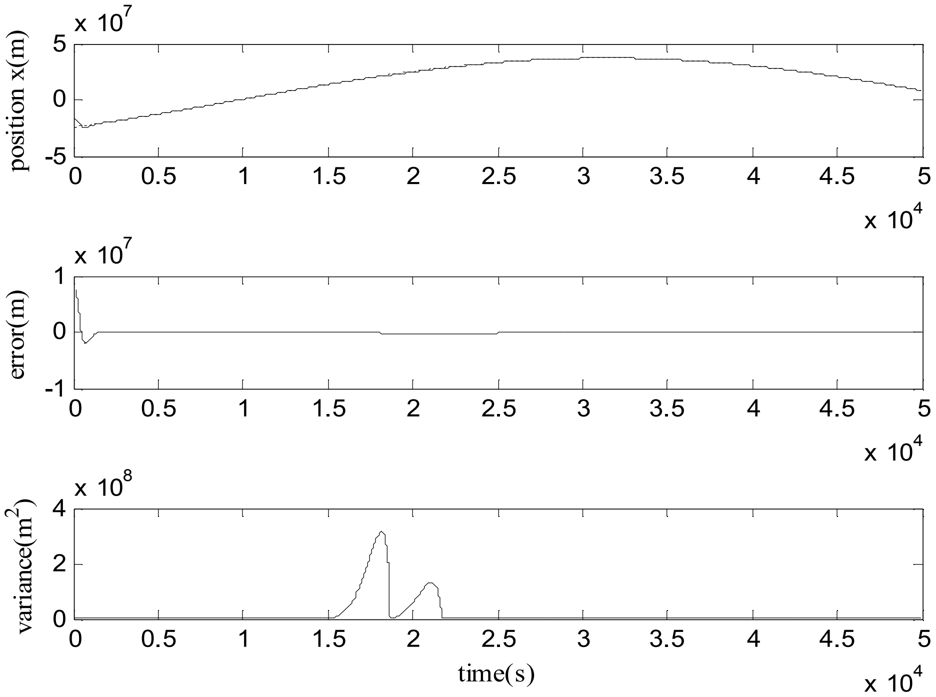

Figure 4.8: X position est. via RUKF with MMNSF in case of cont.bias, SSA.

4.6.2 Measurement noise increment

In that second measurement malfunction scenario, measurement fault is characterized by multiplying the variance of the measurement noise of the azimuth angle in between 15000th and 25000th seconds (between 1500th and 2500th steps). As in the first scenario, multiplying the variance of the measurement noise of the azimuth angle affects the variances. Therefore, there is no need to implement RUKF with SMNSF and MMNSF in this case. Changes of variances forming the R matrix can be seen in figure 4.9 in case of noise increment in azimuth. After constructing the constant R matrix, RUKF with SMNSF and MMNSF can be applied. As figure 4.10 for x parameter and figures C.33- C.40 for other parameters in appendix C and tables B.7, B.8 show that the regular UKF fails about estimating the parameters of geostationary satellite accurately.

Figures 4.11 for x position and C.41-C.48 are the graphics for RUKF with SMNSF and figures 4.12 for x position and C.49-C.56 are the graphics for RUKF with MMNSF for other parameters in appendix C. Results are summarized at tables B.7-B.12. Tables B.7 and B.8 present the errors of estimations and variances of estimation errors for Regular UKF in case of noise increment. Tables B.9 and B.10 present the errors of estimations and variances of estimation errors for RUKF with

SMNSF in case of noise increment. Tables B.11 and B.12 present the errors of estimations and variances of estimation errors for RUKF with MMNSF in case of noise increment. 2000th step can be examined to compare the filters in faulty interval. As seen from obtained results, x, y position estimations are better in Regular UKF. For velocities, RUKF with MMNSF is the best. Z position is better in RUKF with SMNSF. However, both of the robust algorithms reduce amount of fault a little in faulty interval for parameters which they give better results. Estimation results of RUKF with SMNSF and MMNSF are close to each other. Effect of azimuth angle on all indirect measurements impresses estimation characteristics badly.

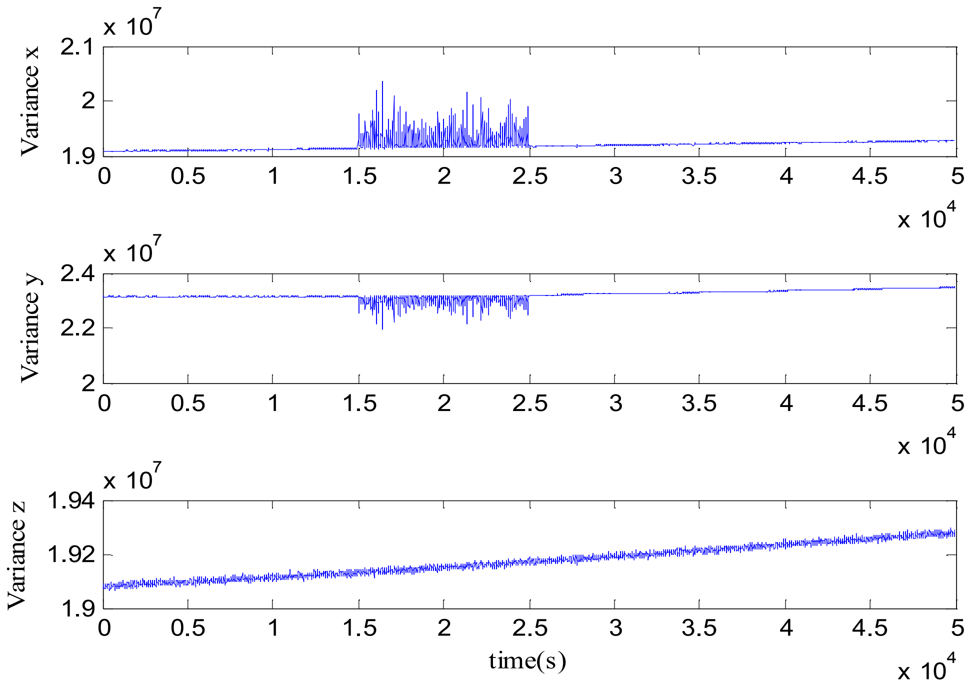

Figure 4.9: Variance changes in three dimension in case of noise inc.

As seen in the figure 4.9, noise increment is implemented to azimuth angle measurement between 15000th and 25000th seconds by multiplying the azimuth measurement noise value. Variances are also changed with respect to azimuth bias. For the variance x, variance increases in the 15000th and 25000th interval. For the variance y, variance decreases in the 15000th and 25000th interval. For the variance z, variance is nearly constant in the 15000th and 25000th interval. Because, azimuth angle affects the x and y variances.

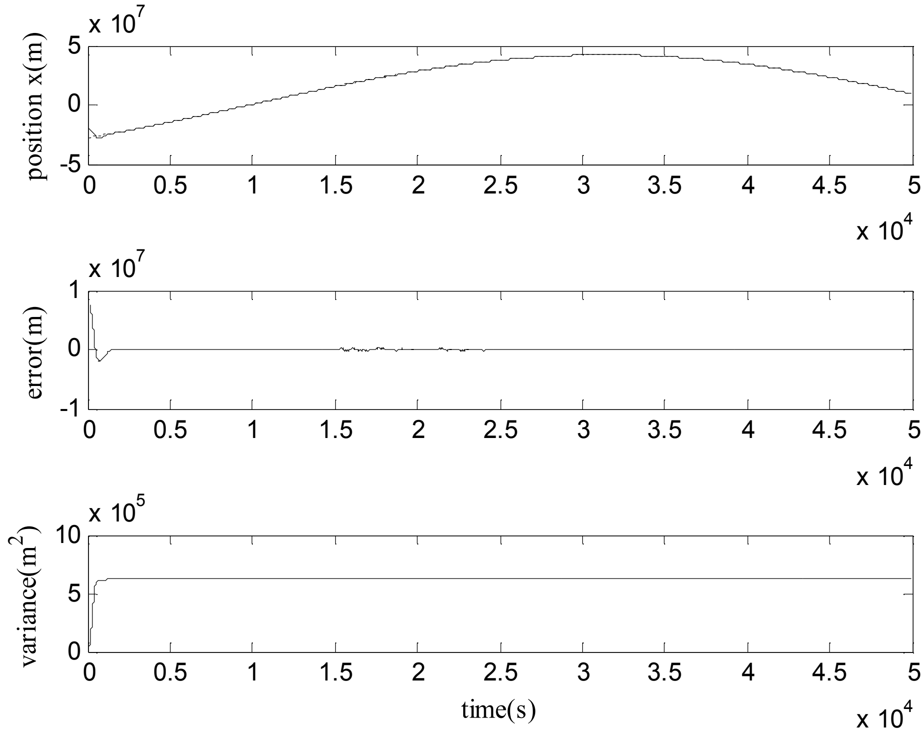

Figure 4.10: X position est. via Regular UKF in case of noise inc, SSA.

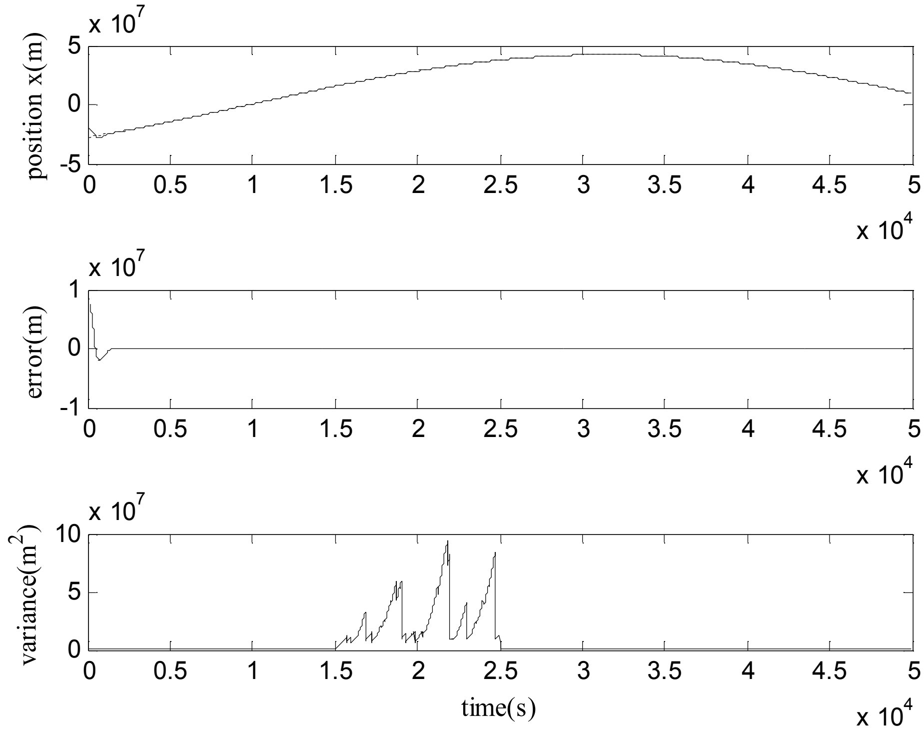

Figure 4.11: X position est. via RUKF with SMNSF in case of noise inc, SSA.

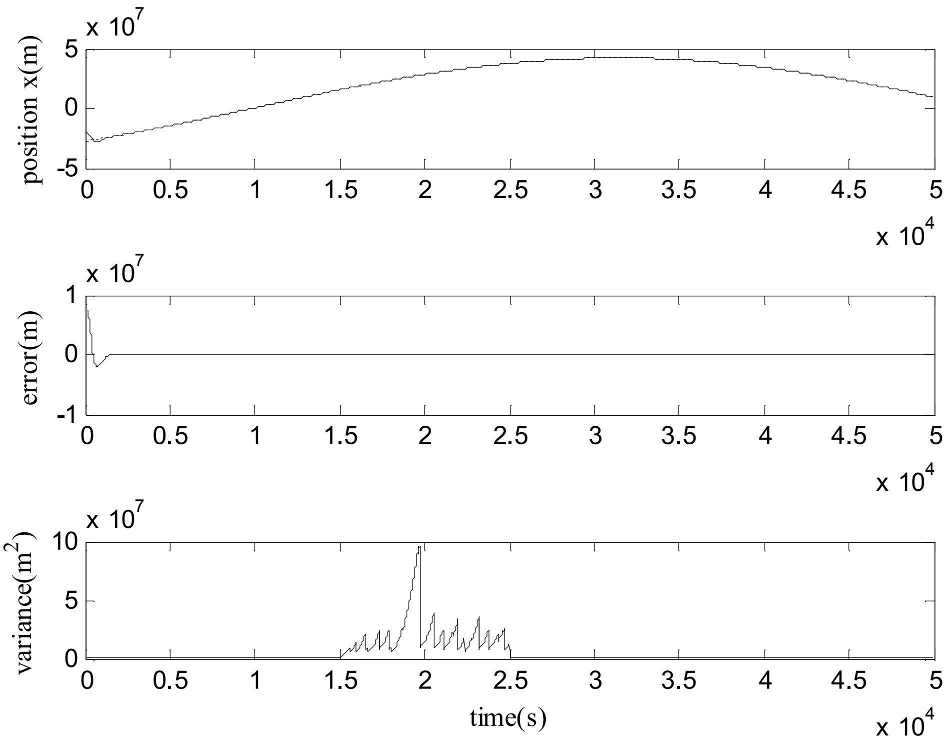

Figure 4.12: X position est. via RUKF with MMNSF in case of noise inc, SSA.

4.6.3 Zero output

In that third measurement malfunction scenario, there is not any azimuth angle measurement between 15000th and 25000th seconds (between 1500th and 2500th steps). Changes of variances forming the R matrix can be seen in figure 4.13 in case of zero output in azimuth. After constructing the constant R matrix, RUKF with SMNSF and MMNSF can be applied. As figure 4.14 for x parameter and figures C.57- C.64 for other parameters in appendix C and tables B.13, B.14 show that the regular UKF fails about estimating the parameters of geostationary satellite accurately.

Figures 4.15 for x position and C.65-C.72 are the graphics for RUKF with SMNSF and figures 4.16 for x position and C.73-C.80 are the graphics for RUKF with MMNSF for other parameters in appendix C. Results are summarized at tables B.13-B.18. Tables B.13 and B.14 present the errors of estimations and variances of estimation errors for Regular UKF in case of noise increment. Tables B.15 and B.16 present the errors of estimations and variances of estimation errors for RUKF with SMNSF in case of zero output. Tables B.17 and B.18 present the errors of estimations and variances of estimation errors for RUKF with MMNSF in case of zero output. 2000th step can be examined to compare the filters in faulty interval. As seen from obtained results, RUKF algorithms with SMNSF and MMNSF reduce the effect of the innovation sequence and decrease the estimation error. Generally, estimation results of RUKF with SMNSF and MMNSF are close to each other and better than the normal RUKF. Effect of azimuth angles on all indirect measurements impresses estimation characteristics badly.

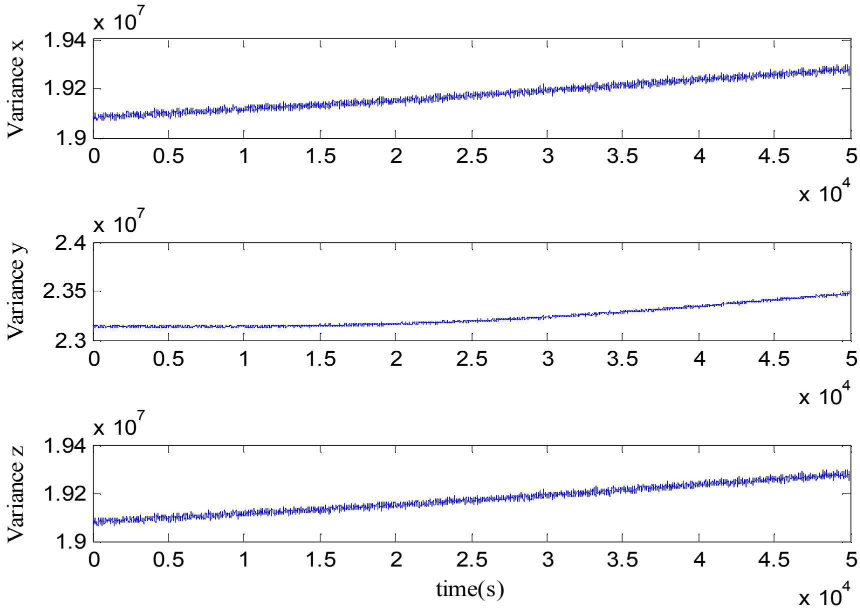

Figure 4.13: Variance changes in three dimension in case of zero output.

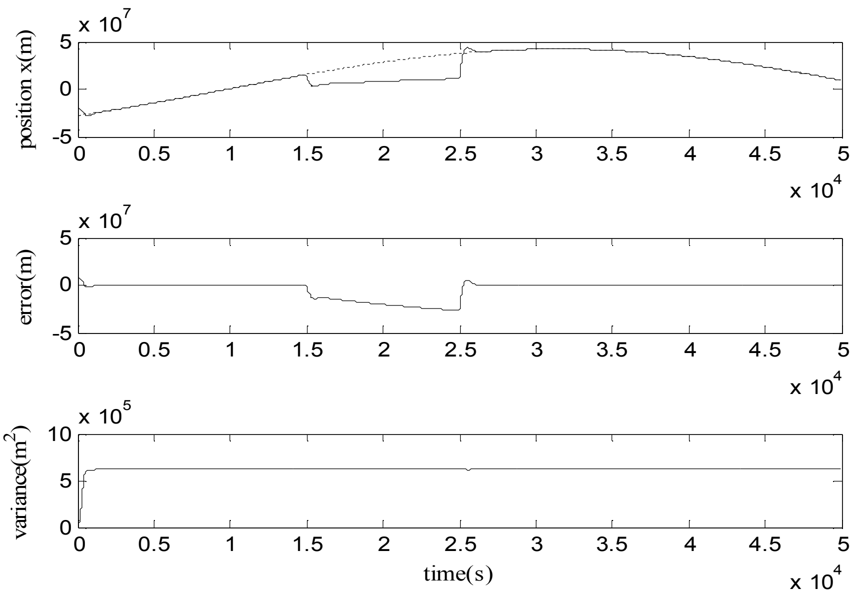

Figure 4.14: X position est. via Regular UKF in case of zero out, SSA.

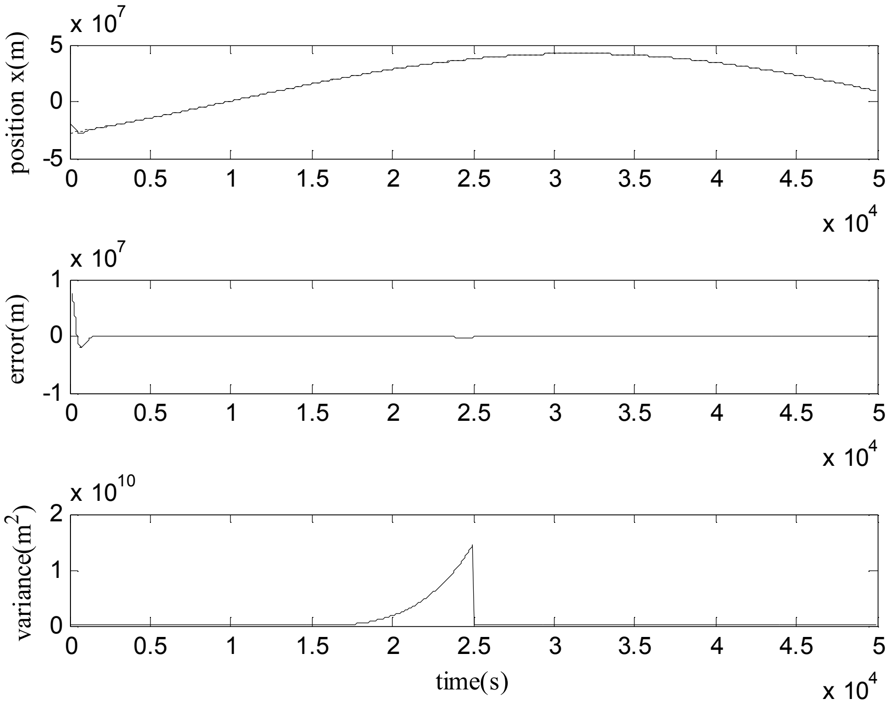

Figure 4.15: X position est. via RUKF with SMNSF in case of zero out, SSA.

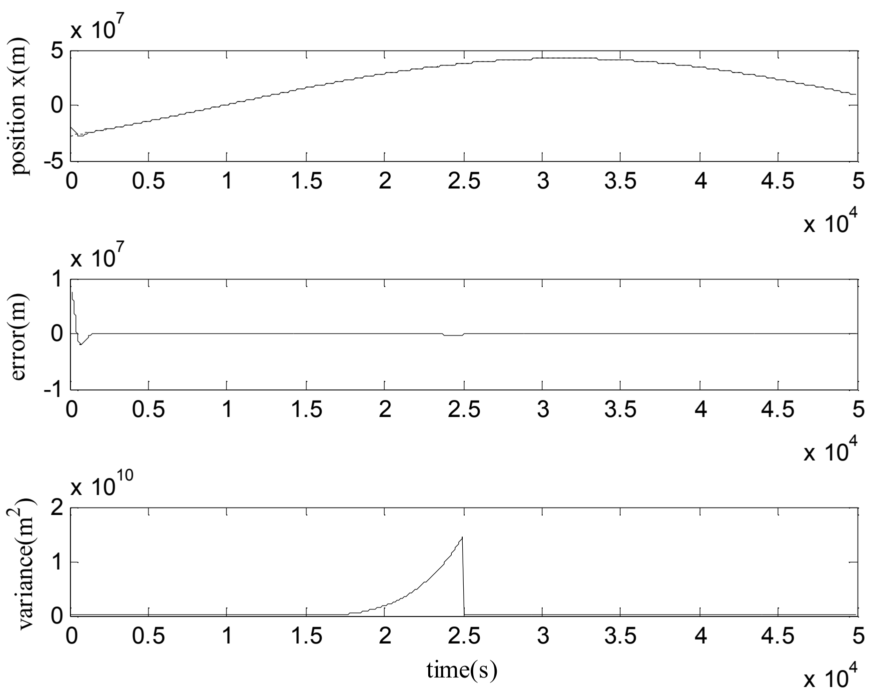

Figure 4.16: X position est. via RUKF with MMNSF in case of zero out, SSA.

In general, when the measurements are faulty, RUKF with SMNSF compensates that by increasing its single scale factor. As a result, all of the measurements for these time steps are scaled. That is not a healthy procedure as long as the filter performance differs for each state for the complex systems with multivariable. On the other hand RUKF with MMNSF secures the robustness of the filter by increasing related factors of the scale matrix individually. Increment of the related scale factors brings out a decrement in the related components of the Kalman gain, so as to reduce the corrective effect of the innovation sequences of the faulty measurements on the state estimation process (3.33). That makes RUKF with MMNSF more advantageous. However, this rule is not valid in this case. Because, measurement faults are implemented to direct measurement azimuth and adaptive algorithms are applied for indirect measurement estimations. Due to effect of azimuth on all indirect measurements, results of RUKF with SMNSF and RUKF with MMNSF are close. Both of them reduce the errors but, advantage of MMNSF can not be seen in here. To realise the advantage of RUKF with MMNSF to RUKF with SMNSF, both of the faults and adaptive algorithms must be applied to indirect measurements. In the next section, this type of implementation will be done via GPS.

4.7 Application of Adaptive Robust Unscented Kalman Filters to Orbit Determination via GPS

In order to understand the efficiency of the proposed robust unscented Kalman filter algorithms and examine the advantages of each algorithm, Robust Unscented Kalman Filter (RUKF) with single measurement noise scale factor (SMNSF) and RUKF with multiple measurement noise scale factors (MMNSF), various estimation scenarios are performed for orbit deternination via GPS, too. Simulations are realized for 5000 seconds with a sampling time $\Delta t = 1\text{sec}$. Simulations are also done with regular UKF so as to compare results with both RUKF algorithms. For robust Kalman filters $\chi^2_{\alpha,s}$ is taken as 12.6 and this value comes from chi-square distribution when the degree of freedom is 6 (six measurement parameters for GPS, position and velocities in three dimension).

First part of figures gives UKF or RUKF state estimation results and the actual values in a comparing way. Dashed line refers to actual values and solid line symbolizes the estimations. Second part of the figures shows the error of estimation process based on the actual values of the satellite. The last part indicates the variance of the estimation.

4.7.1 Continuous bias at measurements

For the first scenario, continuous bias term is formed by adding a constant term to the x position measurement of the GPS in between 1750th and 2250th seconds and the x velocity measurement of the GPS in between 3750th and 4250th seconds. As Figure 4.17 for x position and for the other paramaters Figures C.86-C.90 and Tables B.19-B.20 show, regular UKF fails about estimating the x position and x velocity accurately in the faulty intervals. Per contra, RUKF algorithms with SMNSF (Figures. 4.18, C.91-C.95) and MMNSF (Figures 4.19, C.96-C.100) reduce the effect of the innovation sequence and eliminate the estimation error which is caused by the biased measurements of GPS.

Figures 4.18 for x position and C.91-C.95 are the graphics for RUKF with SMNSF and figure 4.19 for x position figures C.96-C.100 are the graphics for RUKF with MMNSF in appendix C. Results are summarized at tables B.19-B.24. Tables B.19 and B.20 present the errors of estimations and variances of estimation errors for Regular UKF in case of continuous bias. Tables B.21 and B.22 present the errors of estimations and variances of estimation errors for RUKF with SMNSF in case of continuous bias. Tables B.23 and B.24 present the errors of estimations and variances of estimation errors for RUKF with MMNSF in case of continuous bias. 2000th and 4000th points can be examined in faulty intervals. As seen from obtained results, RUKF with MMNSF generally has a better estimation accuracy, where absolute errors are significantly smaller than Regular UKF and RUKF with SMNSF. The regular UKF gives better estimation results for parameters apart from x position in first faulty interval and x velocity in the second faulty interval which the faults are direcly applied, than the RUKF with SMNSF. RUKF with SMNSF only reduces errors for the bias implemented parameters in the faulty intervals. RUKF with SMNSF is not a healthy procedure as long as the filter performance differs for each state measurement for the complex systems with multivariable. RUKF with MMNSF gives the best results in the faulty intervals for bias implemented parameters. RUKF with MMNSF has smaller variance values than SMNSF. RUKF algorithm with MMNSF reduces the effect of the innovation sequence and decreases the estimation error. The similar results are obtained when the continuous bias is implemented to the other measurement channels.

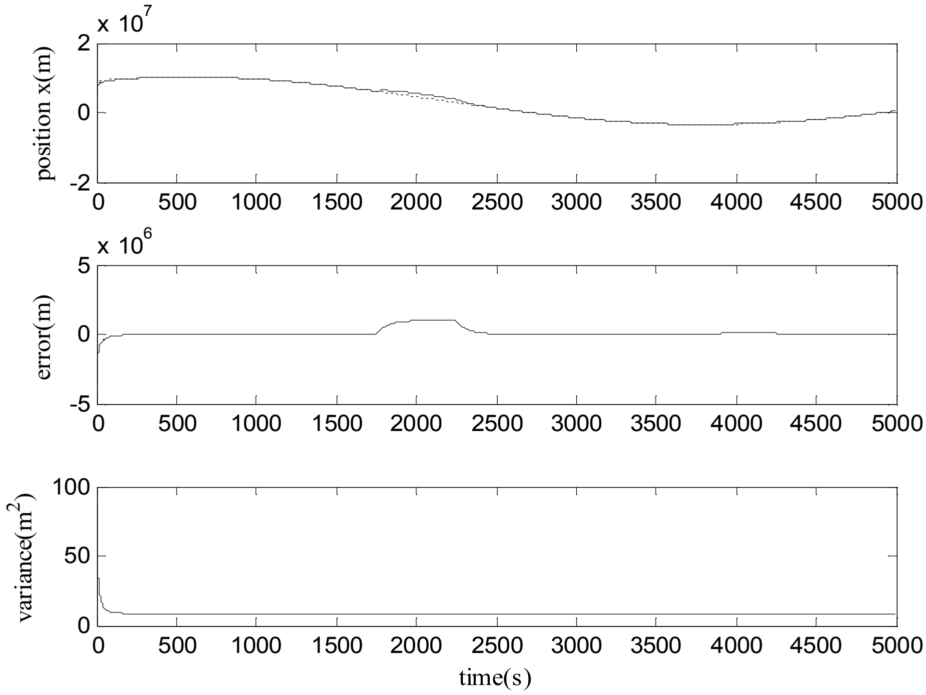

Figure 4.17: X position est. via Regular UKF in case of cont. bias, GPS.

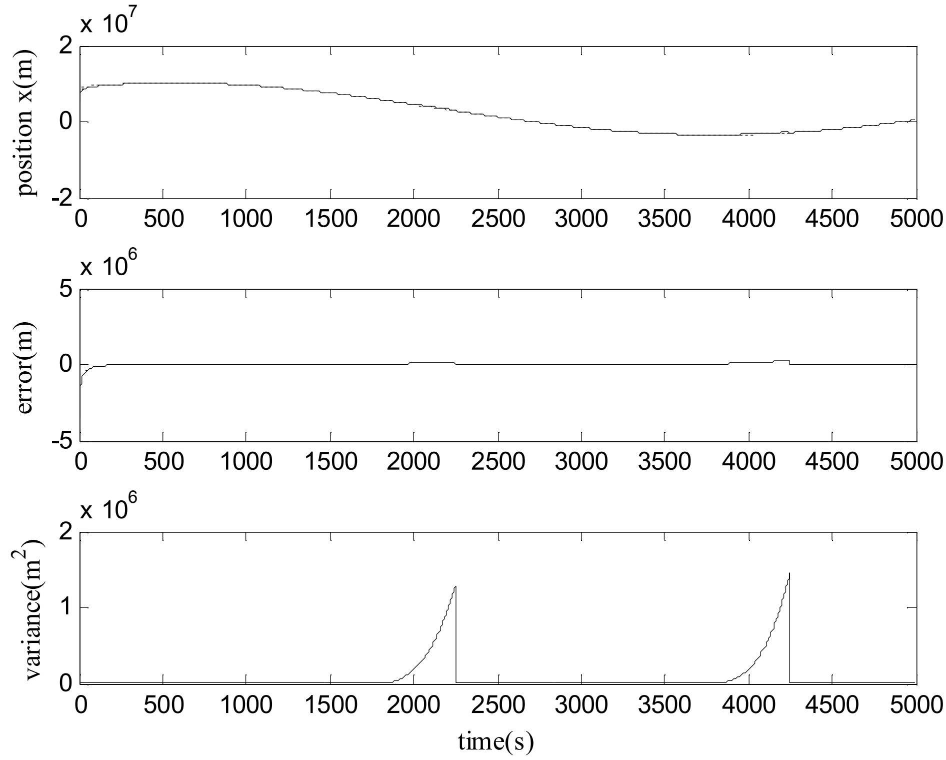

Figure 4.18: X position est. via RUKF with SMNSF in case of cont. bias, GPS.

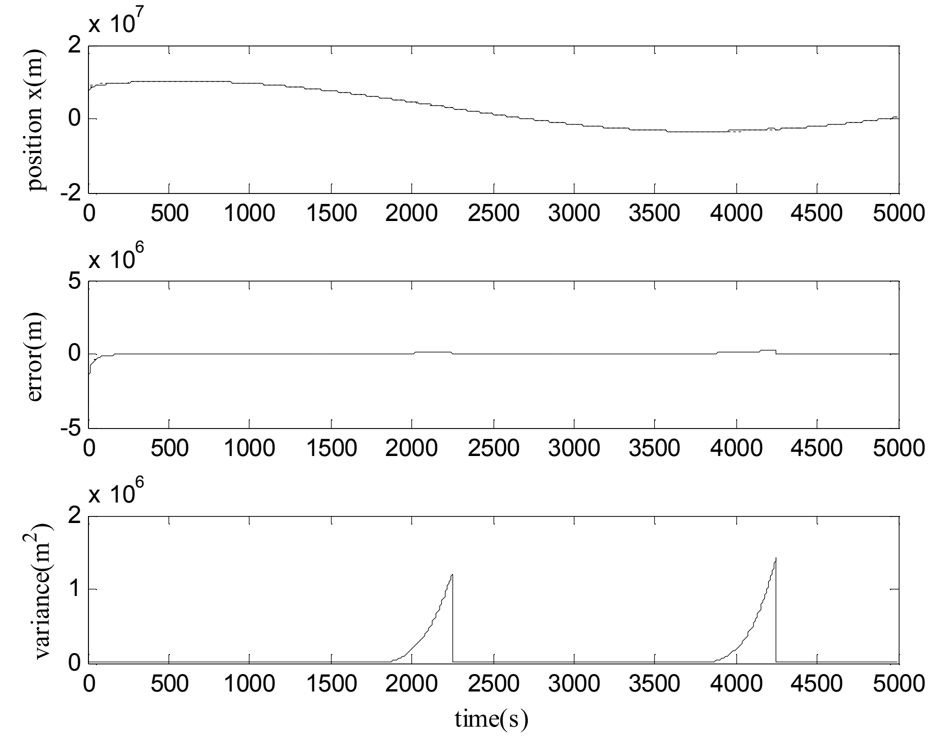

Figure 4.19: X position est. via RUKF with MMNSF in case of cont. bias, GPS.

4.7.2 Measurement noise increment

In that second measurement malfunction scenario, measurement fault is characterized by multiplying the variance of the measurement noise of the x position with a constant term in between 1750^{th} and 2250^{th} seconds and the x velocity with a constant term in between 3750^{th} and 4250^{th} seconds. As it is seen from Figs. (4.20-4.21-4.22, C.101-C.115), the both RUKF algorithms (with SMNSF and MMNSF) give more accurate estimation results than Regular UKF about estimating the x position and x velocity in case of the measurement noise increment in the faulty intervals. RUKF algorithms with SMNSF and MMNSF reduce the effect of the innovation sequence and decrease the estimation error.

Results are summarized at tables B.25-B.30. Tables B.25 and B.26 present the errors of estimations and variances of estimation errors for Regular UKF in case of noise increment. Tables B.27 and B.28 present the errors of estimations and variances of estimation errors for RUKF with SMNSF in case of noise increment. Tables B.29 and B.30 present the errors of estimations and variances of estimation errors for RUKF with MMNSF in case of noise increment. 2000th and 4000th points can be examined in faulty intervals. As seen from obtained results, the RUKF with MMNSF provides the most accurate estimation results. RUKF with MMNSF has smaller variance values than SMNSF. Simulations give similar results when the noise increment is implemented to other measurement channels.

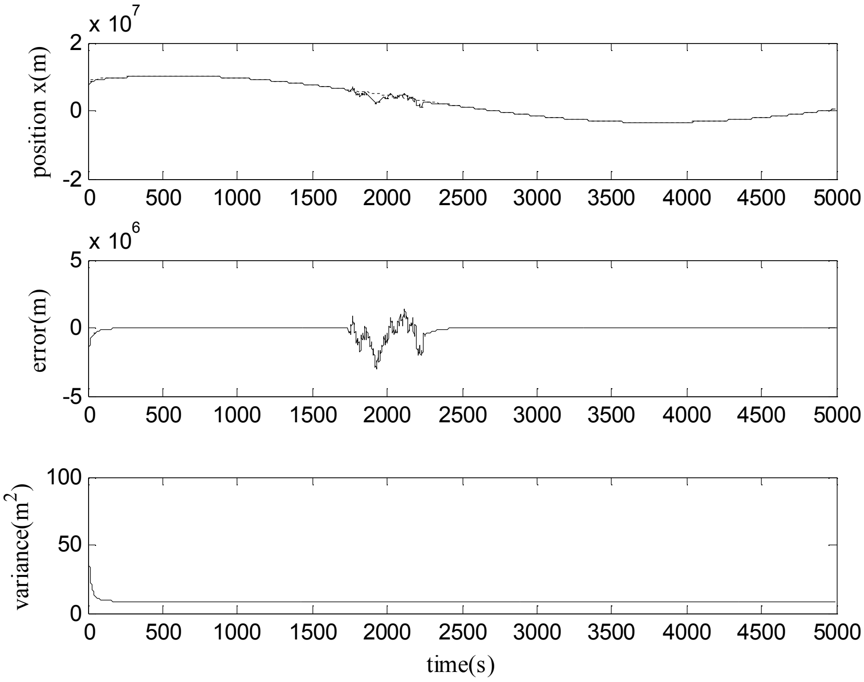

Figure 4.20: X position est. via Regular UKF in case of noise inc, GPS.

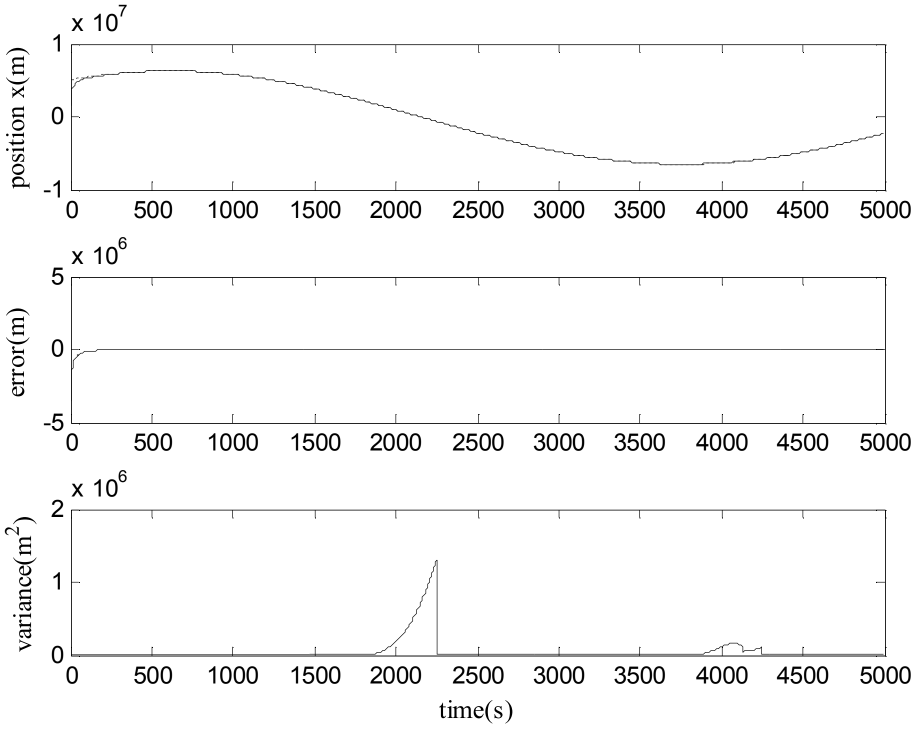

Figure 4.21: X position est. via RUKF with SMNSF in case of noise inc, GPS.

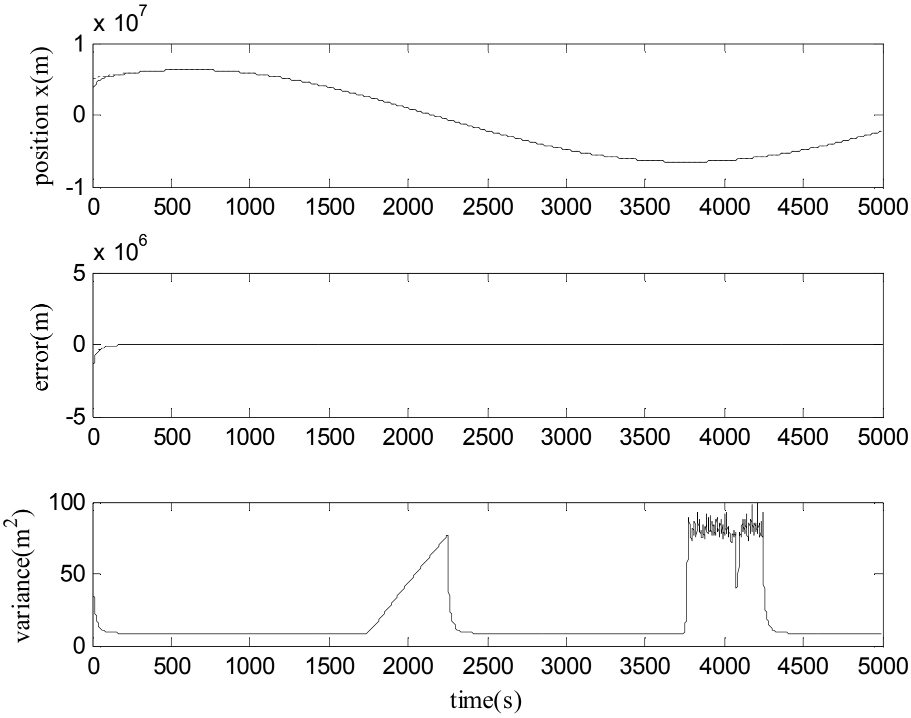

Figure 4.22: X position est. via RUKF with MMNSF in case of noise inc, GPS.

4.7.3 Zero output

In that third measurement malfunction scenario, there is not any x position measurement between 1750th and 2250th seconds and any x velocity measurement between 3750th and 4250th seconds. As it is seen from Figures (4.23-4.24-4.25, C.115-C.130), the both RUKF algorithms (with SMNSF and MMNSF) give more accurate estimation results than Regular UKF about estimating the x position and x velocity in case of the zero output in the faulty intervals.

Results are summarized at tables B.31-B.36. Tables B.31 and B.32 present the errors of estimations and variances of estimation errors for Regular UKF in case of zero output. Tables B.33 and B.34 present the errors of estimations and variances of estimation errors for RUKF with SMNSF in case of zero output. Tables B.35 and B.36 present the errors of estimations and variances of estimation errors for RUKF with MMNSF in case of zero output. 2000th and 4000th points can be examined in faulty intervals. As seen from obtained results, the RUKF with MMNSF provides the most accurate estimation results. RUKF with MMNSF has smaller variance values than SMNSF. Regular UKF is better than RUKF with SMNSF for the parameters which faults are not added to in the faulty interval. Simulations give similar results when the zero output is implemented to other measurement channels.

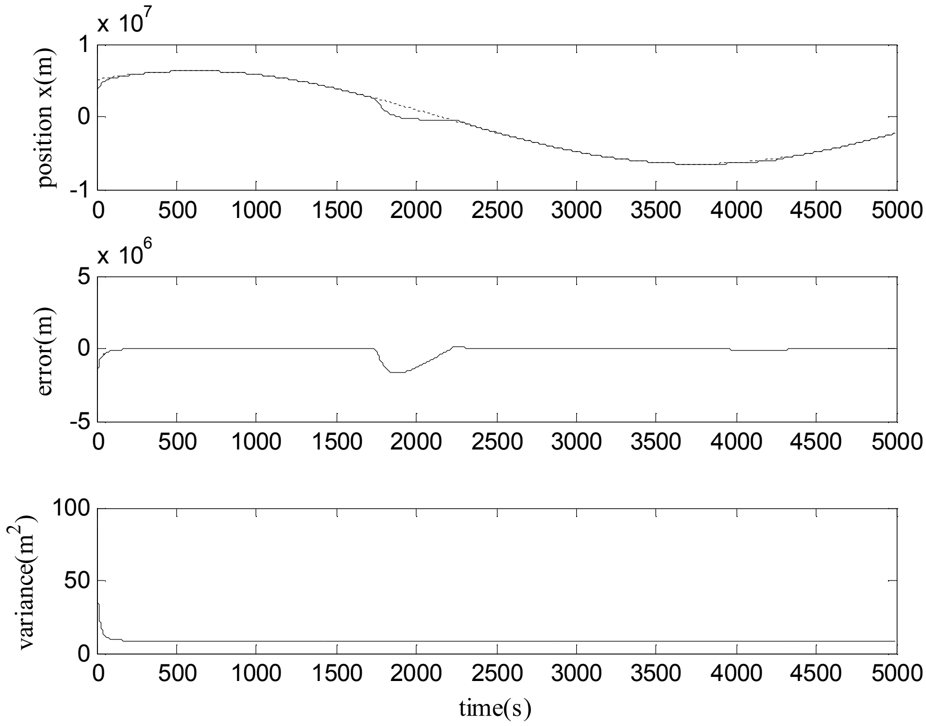

Figure 4.23: X position est.via Regular UKF in case of zero out, GPS.

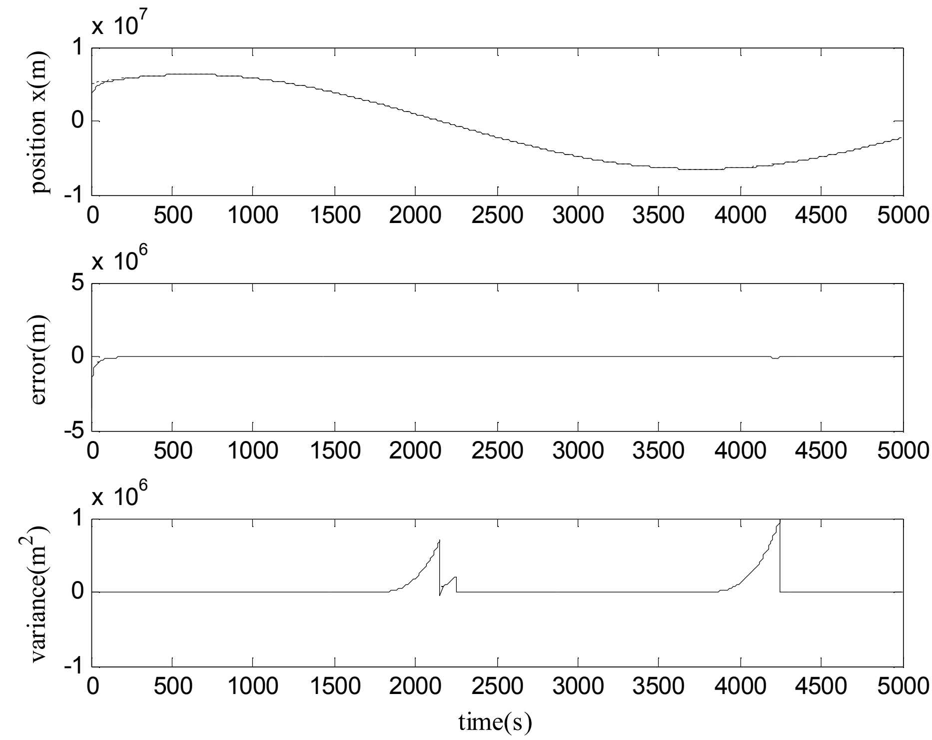

Figure 4.24: X position est. via RUKF with SMNSF in case of zero out, GPS.

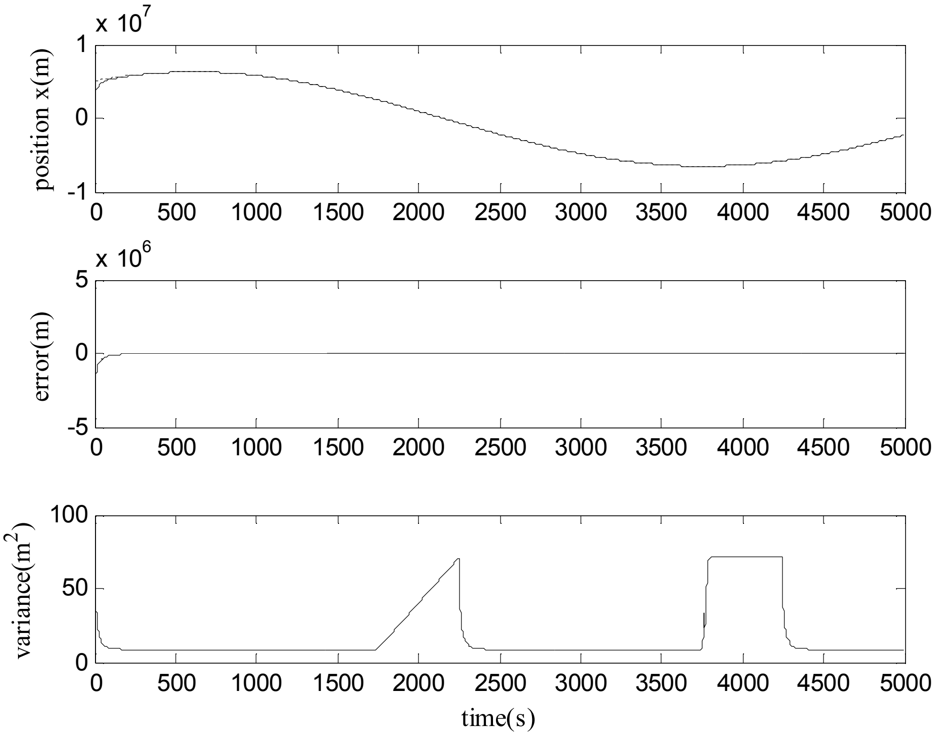

Figure 4.25: X position est. via RUKF with MMNSF in case of zero out, GPS.

When the measurements are faulty, RUKF with SMNSF compensates that by increasing its single scale factor. As a result, all of the measurements for these time steps are scaled. That is not a healthy procedure as long as the filter performance differs for each state for the complex systems with multivariable. On the other hand RUKF with MMNSF secures the robustness of the filter by increasing related factors of the scale matrix individually. Increment of the related scale factors brings out a decrement in the related components of the Kalman gain, so as to reduce the corrective effect of the innovation sequences of the faulty measurements on the state estimation process (3.33). That makes RUKF with MMNSF more advantageous. For all three scenarios estimation characteristic of the RUKF with SMNSF is worse than RUKF with MMNSF in faulty interval. Hence, utilizing RUKF with MMNSF may be more meaningful despite the increased computational demands.

5. COMPLEMENTARY KALMAN FILTER TO INTEGRATE ANTENNA AND GPS FOR BIAS ESTIMATION

The purpose of this study is to integrate two navigation sources in the base of a Linear Kalman Filter (3.1-3.14) [22]. Instead of system state variable estimates, the system's error estimates will be obtained by the Kalman Filter. The single station antenna and the GPS are summed together in the integrated navigation system shown in figure (5.1).

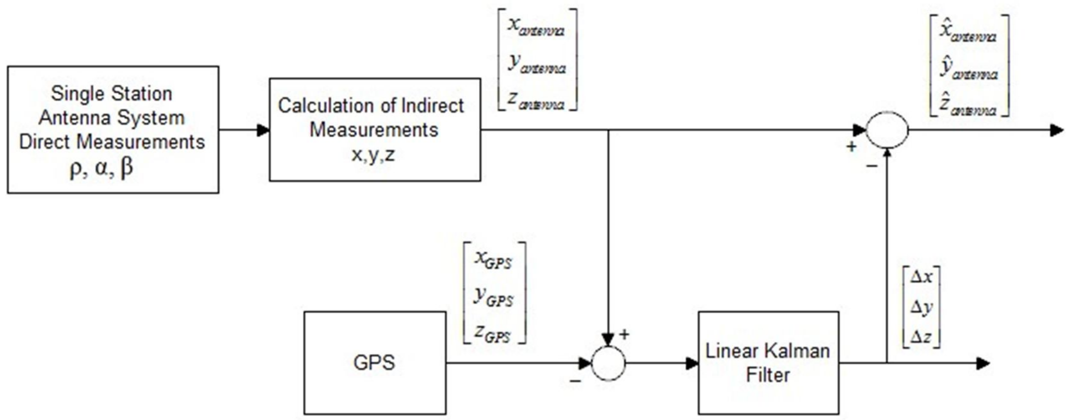

Figure 5.1: Integration of GPS and single station antenna schematics.

As seen in Figure (5.1), the difference of positions obtained from antenna and GPS is introduced into the Linear Kalman Filter. Kalman Filter estimates the position biases which are the indirect measurements. A bias is added to the one of the direct antenna measurements such as azimuth angle. After reverse transformation from topocentric coordinates to ECI coordinates to calculate indirect measurements, azimuth angle bias affects the x, y and z position values. Linear Kalman Filter is used to determine these indirect measurement biases.

The information we need for this filtering process are the system error models and the measurement error model.

The system error vector with required parameters is as follows,

$$X = [\Delta x \quad \Delta y \quad \Delta z]^T \tag{5.1}$$

In here, the $\Delta x, \Delta y, \Delta z$ are the position errors of antenna system.

The bias model used with Linear Kalman Filter to estimate position errors caused by azimuth angle bias, presented below;

$$X(k) = AX(k-1) + W(k-1) \tag{5.2}$$

$$\begin{bmatrix} \Delta x(k) \\ \Delta y(k) \\ \Delta z(k) \end{bmatrix} = \begin{bmatrix} 1 & 0 & 0 \\ 0 & 1 & 0 \\ 0 & 0 & 1 \end{bmatrix} \begin{bmatrix} \Delta x(k-1) \\ \Delta y(k-1) \\ \Delta z(k-1) \end{bmatrix} + \begin{bmatrix} \Delta t W_x(k-1) \\ \Delta t W_y(k-1) \\ \Delta t W_z(k-1) \end{bmatrix} \tag{5.3}$$

$$X(k) = \begin{bmatrix} \Delta x(k) \\ \Delta y(k) \\ \Delta z(k) \end{bmatrix} \tag{5.4}$$

$$A = \begin{bmatrix} 1 & 0 & 0 \\ 0 & 1 & 0 \\ 0 & 0 & 1 \end{bmatrix} \tag{5.5}$$

$$W(k-1) = \begin{bmatrix} \Delta t W_x(k-1) \\ \Delta t W_y(k-1) \\ \Delta t W_z(k-1) \end{bmatrix} \tag{5.6}$$

In (5.3), W_x, W_y, W_z are the Gauss distributed noises with standard deviations 1000m in three position dimension. Δt is sampling time interval taken as 1 second. Initial values for state matrix as input to filter; $X(0) = [0.1 \;\; 0.1 \;\; 0.1]^T$.

Using the indirect antenna position and GPS position measurement differences as measurements observation vector in the Kalman Filter, the observation vector can be stated as;

$$Z = [Z_{\Delta x} \;\; Z_{\Delta y} \;\; Z_{\Delta z}]^T \tag{5.7}$$

$$Z_{\Delta x} = x_{GPS} - x_{antenna} \tag{5.8}$$

$$Z_{\Delta y} = y_{GPS} - y_{antenna} \tag{5.9}$$

$$Z_{\Delta z} = z_{GPS} - z_{antenna} \tag{5.10}$$

In (5.8, 5.9, 5.10), $x_{GPS}, y_{GPS}, z_{GPS}$ are the direct GPS position mesurements and $x_{antenna}, y_{antenna}, z_{antenna}$ indirect antenna measurements. The difference between the GPS position measurement and the antenna position measurement gives us the antenna position error. Standard deviations for antenna position components are taken as 100m to calculate random noises. For GPS, they are taken as 25m. If measurement statements of (5.8, 5.9, 5.10) are written in matrix form;

$$Z(k)=\begin{bmatrix}Z_{\Delta x}\\ Z_{\Delta y}\\ Z_{\Delta z}\end{bmatrix}=\begin{bmatrix}1&0&0\\0&1&0\\0&0&1\end{bmatrix}\begin{bmatrix}x_{GPS}-x_{antenna}\\ y_{GPS}-y_{antenna}\\ z_{GPS}-z_{antenna}\end{bmatrix} \quad \textbf{(5.11)}$$

$$H(k)=\begin{bmatrix}1&0&0\\0&1&0\\0&0&1\end{bmatrix} \quad \textbf{(5.12)}$$

$Z_{\Delta x}, Z_{\Delta y}, Z_{\Delta z}$ are error measurement vector components in three dimension and H is the transition matrix. To obtain the antenna true error values that will be used in the simulation, the system error model is used. The system's error vector for the error values;

$$X_m = [\Delta x_m \;\; \Delta y_m \;\; \Delta z_m]^T \quad \textbf{(5.13)}$$

The system error values;

$$\Delta x_m = x - x_{antenna} \quad \textbf{(5.14)}$$

$$\Delta y_m = y - y_{antenna} \quad \textbf{(5.15)}$$

$$\Delta z_m = z - z_{antenna} \quad \textbf{(5.16)}$$

In here, the $\Delta x_m, \Delta y_m, \Delta z_m$ are the system errors in terms of position components. x, y, z are the position values calculated by equations of motion of satellite and $x_{antenna}, y_{antenna}, z_{antenna}$ indirect antenna measurements.

As seen on figure(5.1), the output of the Kalman Filter gives antenna position error estimates. Subtracting these error values from the measured position values of the antenna, the estimated positions $\hat{x}_{antenna}, \hat{y}_{antenna}, \hat{z}_{antenna}$ obtained. After obtaining these values, antenna angles can be calculated via using ECI to topocentric transformation and the difference between true azimuth and azimuth with bias can be realized. And the position estimates can be written as:

$$\hat{x}_{antenna} = x_{antenna} - \Delta x \quad \textbf{(5.17)}$$

$$\hat{y}_{antenna} = y_{antenna} - \Delta y \quad \textbf{(5.18)}$$

$$\hat{z}_{antenna} = z_{antenna} - \Delta z \quad \textbf{(5.19)}$$

Standard deviations $(\sigma^2_{W_x}, \sigma^2_{W_y}, \sigma^2_{W_z})$ of Gauss distributed noises W_x, W_y, W_z are taken as 1000m and Δt is sampling time interval taken as 1 second. Then, the noise correlation matrix Q(k) and measurement error correlation matrix R(k) can be taken as;

$$Q(k) = \begin{bmatrix} \Delta t^2 \sigma_{W_x}^2 & 0 & 0 \\ 0 & \Delta t^2 \sigma_{W_y}^2 & 0 \\ 0 & 0 & \Delta t^2 \sigma_{W_z}^2 \end{bmatrix} \quad \textbf{(5.20)}$$

$$R(k) = \begin{bmatrix} \sigma_{x_{antenna}}^2 + \sigma_{x_{GPS}}^2 & 0 & 0 \\ 0 & \sigma_{y_{antenna}}^2 + \sigma_{y_{GPS}}^2 & 0 \\ 0 & 0 & \sigma_{z_{antenna}}^2 + \sigma_{z_{GPS}}^2 \end{bmatrix} \quad \textbf{(5.21)}$$

As seen in (5.21) measurement error correlation matrix is a diagonal matrix, with; the sum of the random measurement variants of antenna and those of GPS composing the diagonal elements.

Bias estimations for indirect measurements of antenna, x, y and z positions are presented below in figures 5.2, 5.3 and 5.4 respectively. Simulations are done for 500 seconds with 500 steps. First part of figures gives state estimation results and the actual values in a comparing way. Blue line refers to actual values and red line symbolizes the bias estimations. Second part of the figures shows the error of estimation process based on the actual values of the bias. The last part indicates the variance of the estimation. Figure 5.5 presents the comparison of azimuth angles. First part of the Figure 5.5 shows biased azimuth (black line), actual azimuth (blue line) and the azimuth (red line) which is calculated after substracting the estimated bias values from x, y and z positions. Second part of the figure 5.5, introduces the difference between actual azimuth (blue line) and the azimuth (red line) which is calculated after substracting the estimated bias values from x, y and z positions.

Firstly, 0.1 degree bias is added to the antenna azimuth measurement. After transformation to ECI coordinates, azimuth bias affects the x, y and z positions which are indirect antenna measurements. The actual bias values are calculated by using the difference between real position values and faulty positions. Estimations are done by using Linear Kalman Filter with the model given in (5.3). As seen from the results (figures 5.2-5.3-5.4), bias estimation values converge to the actual values. They reduce and fluctuate around zero. Second, estimated bias values are substracted from the position values affected by faulty azimuth angle. Thus, positions in three dimension are cleared from the bias. After that, new position values are again transformed to topocentric coordinates to compute new azimuth angle.

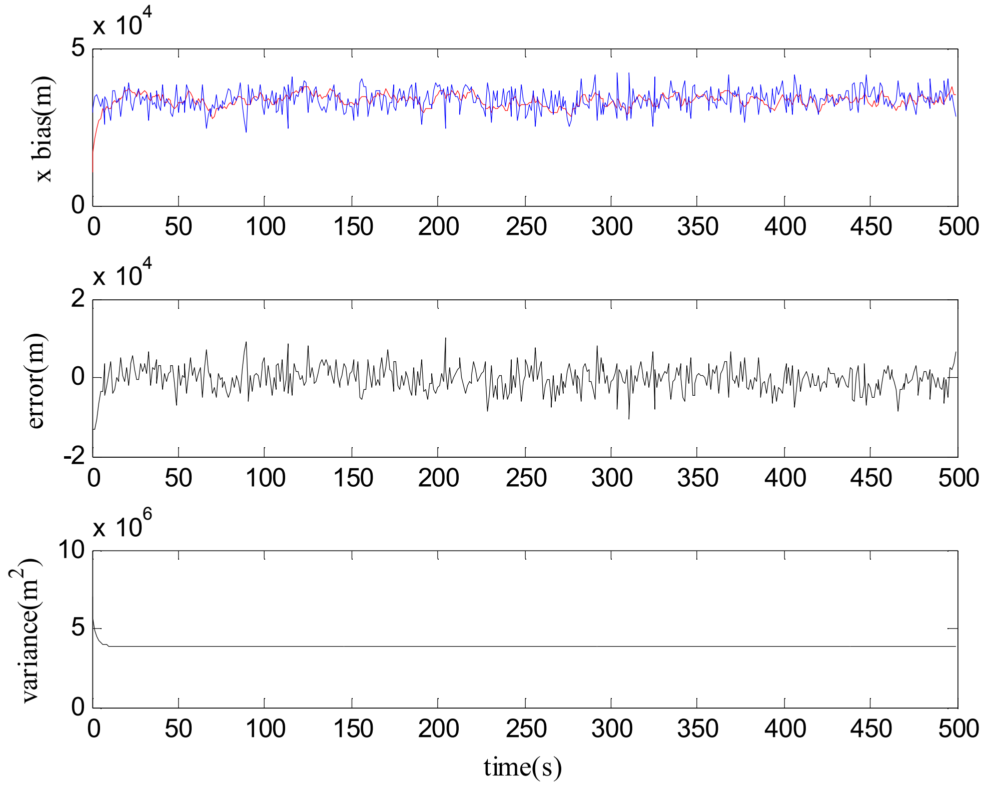

Figure 5.2: X position bias estimation with Linear Kalman Filter.

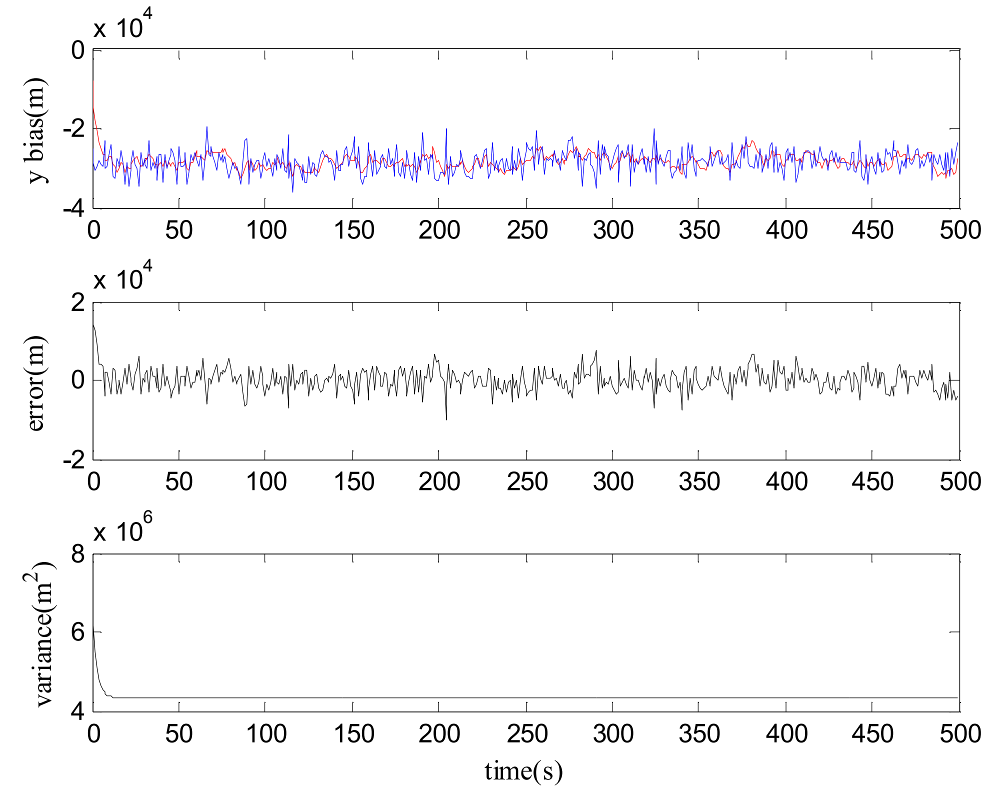

Figure 5.3: Y position bias estimation with Linear Kalman Filter.

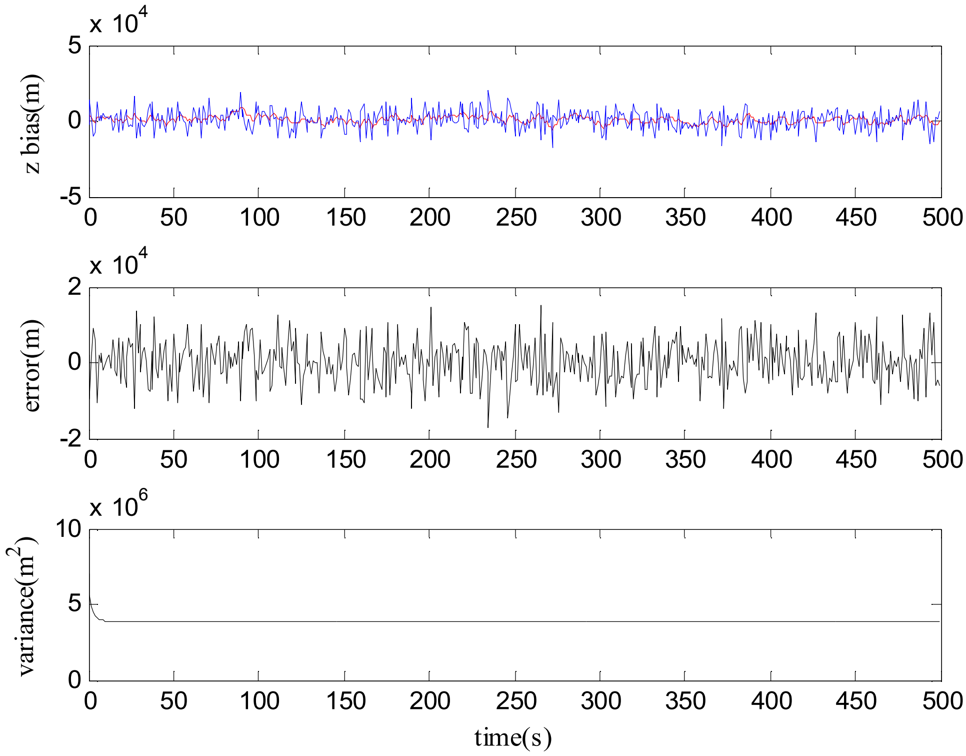

Figure 5.4: Z position bias estimation with Linear Kalman Filter.

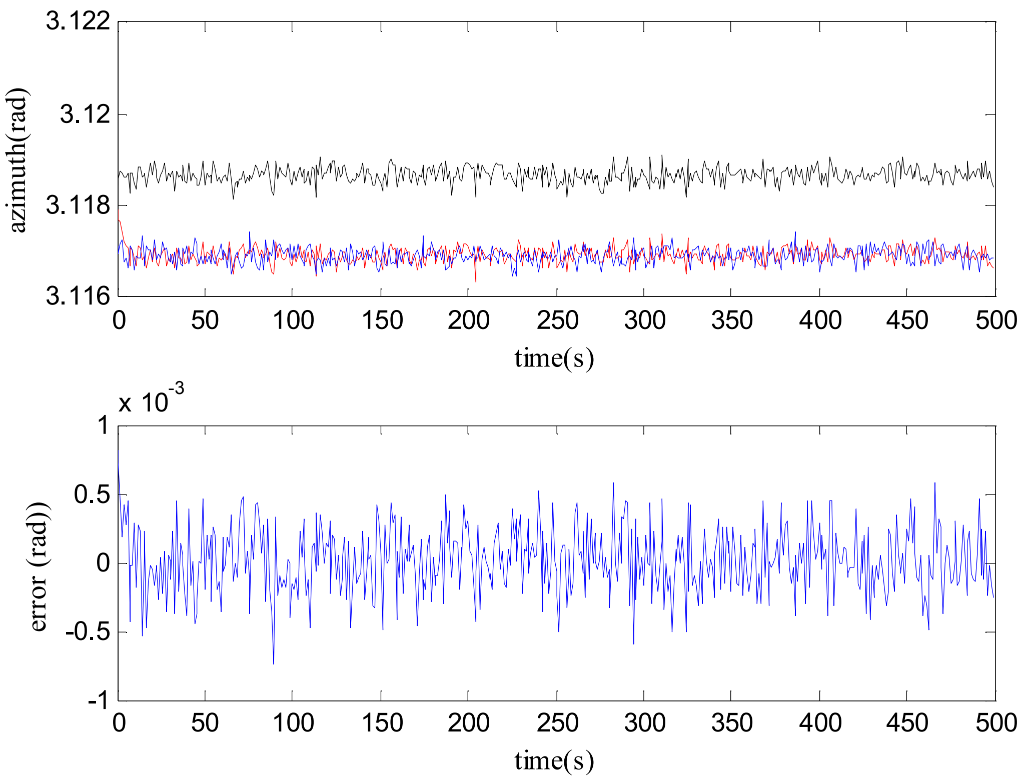

Figure 5.5: Comparison of azimuth angles.

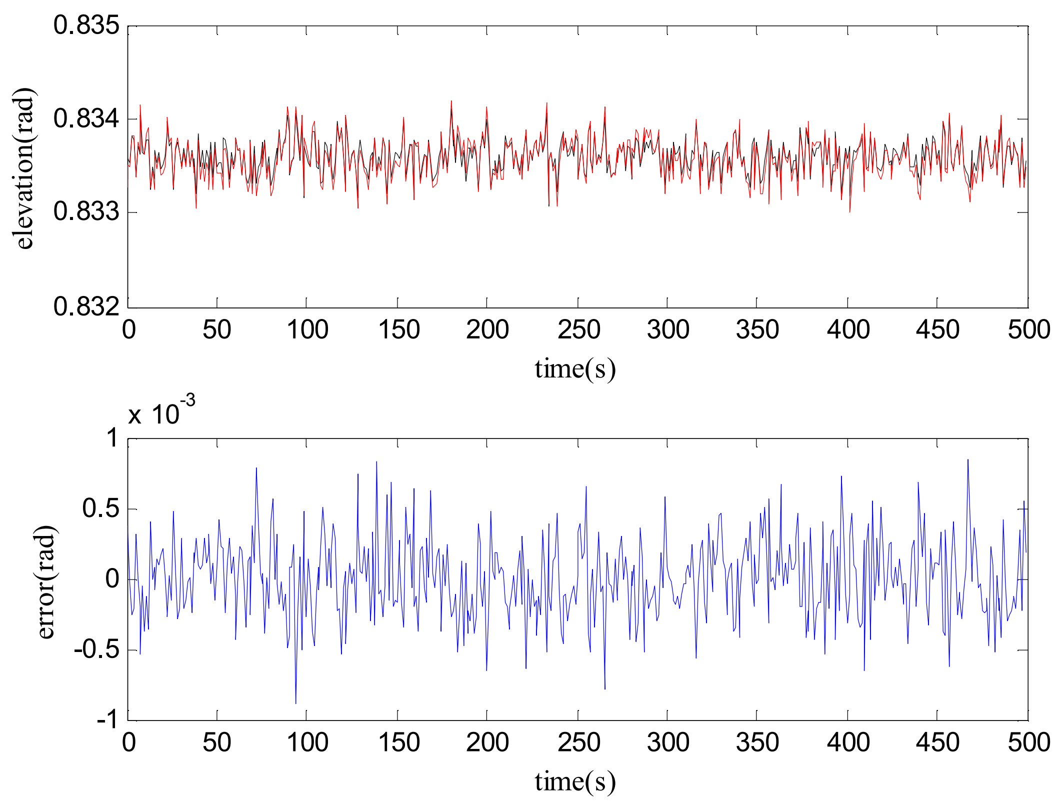

Figure 5.6: Comparison of elevation angles.

As seen from (figure 5.5), new azimuth calculated with unbiased positions converge to the actual azimuth value. Difference between biased and unbiased azimuths can also be realized.

As seen from (figure 5.6), elevation calculated with unbiased positions converge to the actual elevation angle value, too. Difference between elevation calculated by unbiased positions and actual elevation angle can also be realized.

Third, unbiased x, y and z positions after estimated bias values are substracted, and actual position values are compared in figures 5.7, 5.8 and 5.9 respectively. First part of figures gives biased position results and the actual values in a comparing way. Black line refers to actual values and red line symbolizes the unbiased values. Second part of the figures shows the error between unbiased and actual values of positions. The last part indicates the total variances. They are calculated by sum of measurement covariance matrix of antenna and correlation matrix of filtering error of estimated biases (total of diagonal elements of R(k)(4.37) and P(k|k)). As seen from the results, unbiased position values converge to actual values. Errors converge to zero.

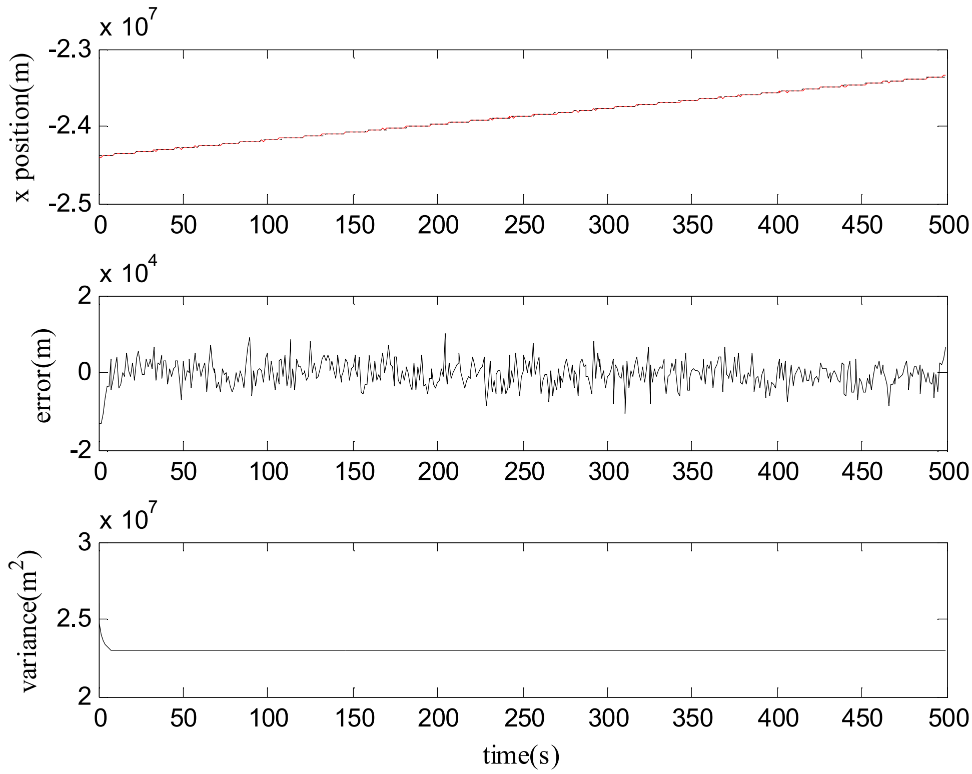

Figure 5.7: Comparison of unbiased and actual x positions.

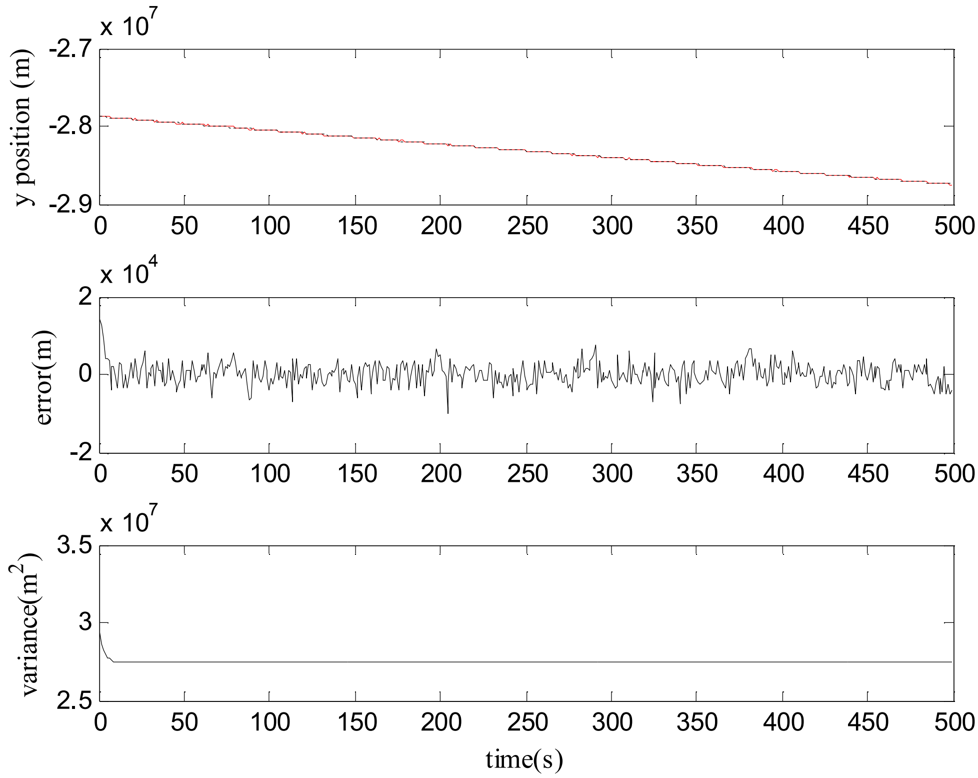

Figure 5.8: Comparison of unbiased and actual y positions.

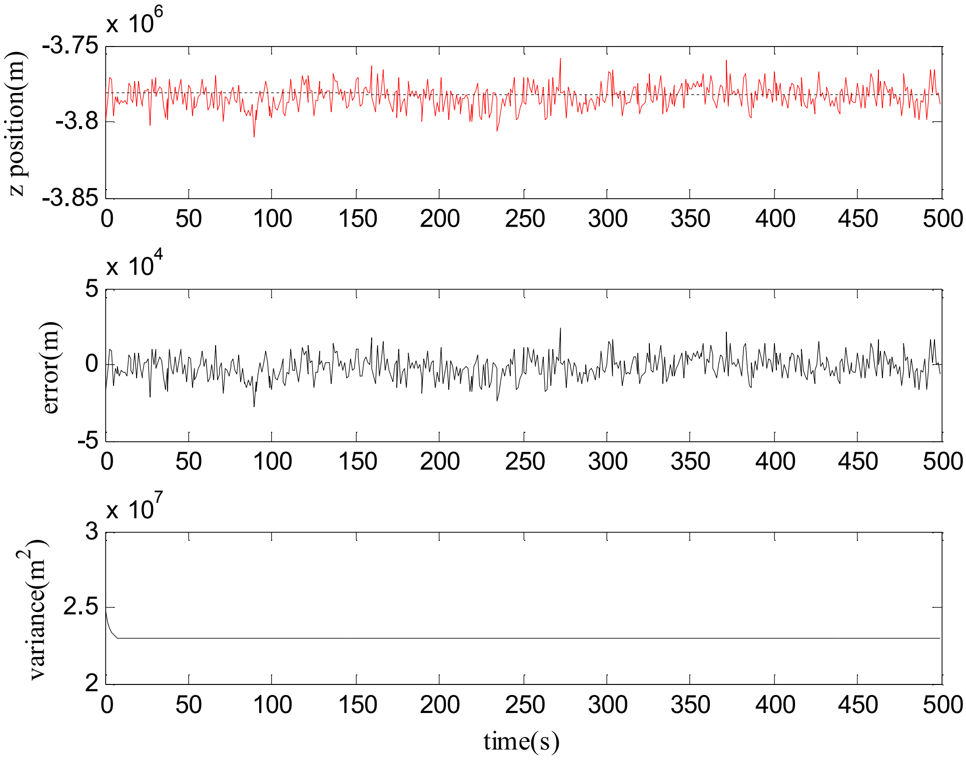

Figure 5.9: Comparison of unbiased and actual z positions.

6. CONCLUSION

A new Unscented Kalman filter that uses indirect position measurements to estimate the position and velocity components of GEO satellite is developed. Inputting the position components of the satellite in ECI reference frame calculated from real range measurements in ENU reference frame to the filter leads to a linear measurement function. The conventional approach of inputting directly the real range-azimuth-elevation measurements results in a highly nonlinear measurement function. The corresponding calculation of predicted observation vector, observation covariance matrix and cross correlation matrix consists of complex terms which increases the computational load significantly.

UKF based two-stage estimation of satellite's position and velocity by single station antenna tracking data, where the measurement nonlinearities are eliminated, is proposed. In the first stage, the direct nonlinear antenna measurements are transformed to the linear x-y-z coordinate measurements of satellite's position, and their errors' variances are evaluated. In the second stage, the solutions of the first stage are improved by UKF for estimation of the satellite position and velocity on indirect linear x-y-z measurements.

The simulation results show that the proposed UKF based two-stage procedure performs good estimation accuracy and good convergence characteristics. Furthermore, the method based on indirect measurements provides an unnoticeably short transient duration.

Unscented Kalman Filter which uses position and velocity measurements of GPS for LEO satellite in three dimension is also proposed. The difference of this application from UKF for single station antenna implementation, is using the direct measurements. GPS directly measures the position and velocities of the satellite. Therefore, UKF uses the directly obtained measurements and it does not require hard transformations to obtain indirect measurements from real antenna measurements.

The simulation results show that the proposed UKF based orbit determination on GPS measurements has better estimation accuracy and convergence characteristics than the UKF based two-stage estimation procedure.

Robust Unscented Kalman Filter algorithms with single and multiple measurement noise scale factors for the case of measurement malfunctions are developed. By the use of defined variables named as scale factor, faulty measurements are taken into consideration with small weight and the estimations are corrected without affecting the characteristic of the accurate ones. In the presented RUKFs, the filter gain correction is performed only in the case of malfunctions in the measurement system.

RUKF algorithms with single (SMNSF) and multiple measurement noise scale factors (MMNSF) are proposed. In the first case filter is adapted by using single scale factor as a corrective term on the filter gain, and in the second one, a scale matrix built of multiple factors is used to fix the relevant term of the Kalman gain matrix, individually.

Proposed RUKF algorithms with single and multiple MNSF are applied for the parameters of GEO satellite estimations by indirect measurements of ground station and parameters of LEO satellite estimations by measurements of GPS. Algorithms are tested for three types of measurement faults such as continuous bias, noise increment, zero output and results are compared with the outputs of UKF for the same cases. As seen from the results, RUKF with SMNSF and MMNSF results are close to each other for two stage estimation procedure with antenna measurements. For GPS measurements, simulation results show that RUKF with MMNSF is better than RUKF with SMNSF.

For the purpose of antenna bias estimation the Complementary Kalman Filter which integrates single station antenna system and GPS is developed. GEO satellite's position measurement biases caused by constant bias addition to azimuth angle are estimated via proposed Kalman Filter algorithm. The simulation results show that the bias estimation values converge to the actual values for all three x, y and z position biases and the Complementary Kalman Filter can successfully be able to estimate antenna measurement biases.

REFERENCES

[1] **Pardal, P. C. P. M., Kuga, H. K., and de Moraes, R. V.** (2009). A discussion related to orbit determination using nonlinear sigma point Kalman filter, *Mathematical Problems in Engineering*, Article ID 140963, 12 p, doi:10.1155/2009/.

[2] **Curti, F., and Longo, F.** (2002). Iterative filtering of antenna pointing angles for orbit determination*, Advances in the Astronautical Sciences*, 109, Part I, pp. 519-528.

[3] **Hwang, Y., et al.** (2008). Orbit determination accuracy improvement for geostationary satellite with single station antenna tracking data*, ETRI Journal*, Vol. 30, No. 6, pp. 774-782.

[4] **Hwang, Y., et al.** (2006). Communication, ocean, and meteorological satellite orbit determination analysis considering maneuver scheme*, AIAA/AAS Astrodynamics Specialist Conference and Exhibit*, Keystone, Colorado, August, AAS Paper 2006-6668.

[5] **Upadhyay, T., Cotterill, S., and Deaton., A. W.** (1993). Auto- nomous GPS/INS Navigation Experiment for Space Trans- fer Vehicle, *IEEE Transactions on Aerospace and Electronic Systems*, Vol. 3, No. 29, pp. 782-785.

[6] **Ceccarelli, N., et al.** (2007). Spacecraft Localization via Angle Measurements for Autonomous Navigation in Deep Space, *Proceedings of the 17th IFAC Symposium on Automatic Control in Aerospace*, Toulouse.

[7] **Giannatrapani, A., et al.** (2011). Comparison of EKF and UKF for Spacecraft Localization via Angle Measurements, *IEEE Transactions on Aerospace and Electronic Systems*, Vol. 1, No. 47, pp. 75-84.

[8] **Matusewicz, J., Subbarao, K., and Frisbee, J.** (2008). Uncertainty characterization of orbital debris using the extended Kalman filter, *Advances in the Astronautical Sciences*, 129, Part III, 2163-2188.

[9] **Park, E. S., Park, S. Y., Roh, K. M., and Choi, K. H.** (2010). Satellite orbit determination using a batch filter based on the unscented transformation, *Aerospace Science and Technology*, 14, pp. 387–396.

[10] **Xu, T., et al.** (2010). A Maneuvered GEO Satellite Orbit Determination using Robustly Adaptive Kalman Filter, *2010 International Conference on Intelligent System Design and Engineering Application*, IEEE DOI 10.1109/ISDEA.2010.82.

[11] **Psiaki, M. L.** (n.d.). ***S****atellite Orbit Determination Using a Single-Channel Global Positioning System Receiver*, Cornell University, Ithaca, N.Y. 14853-7501.

[12] **Choi, E. J., et al.** (2010). Onboard orbit determination using GPS observations based on the unscented Kalman filter, *Advances in Space Research* , 46, 1440–1450.

[13] **Ruiz, J. L., and Frey, C. H.** (2005). Geosynchronous Satellite Use of GPS, *ION GNSS 18th International Technical Meeting of the Satellite Division*, 13-16 September 2005, Long Beach, CA.

[14] **Pardal, P. C. P. M., Kuga, H. K., and de Moraes, R. V.** (2009). Non Linear Sigma Point Kalman Filter Applied to Orbit Determination Using GPS Measurements, *22nd International Meeting of the Satellite Division of The Institute of Navigation*, Savannah, GA, September 22-25 2009.

[15] **Hua, S., Hong, Y., and Juntao, M.** (2008). Signal Simulation and positioning mechanisms for Single Antenna GPS receiver used in fuse, *Asia Simulation Conference — 7th Intl. Conf. on Sys. Simulation and Scientific Computing.*

[16] **Kolawole, M. O.** (2002). *Satellite Communication Engineering*, Signal Processing and Communication Series, Marcel Dekker Inc.

[17] **Bostian, C. W., et al.** (1993). Review Assessment of Satellite Communications Technologies, *WTEC Hyper-Librarian*, Retrieved from http://www.wtec.org/loyola/satcom/c2_s1a.htm.

[18] **Satellite Acquisition and Tracking.** (n.d.), 4-13, Date retrieved: 20.03.2013, Address:http://electriciantraining.tpub.com/14189/css/14189_133.htm.

[19] **Irish, K. J.** (1996). *Precision Orbit Determination for the GEOSAT Follow-on Satellites Using GPS* (Doctoral dissertation),Faculty of Graduate School, University of Colorado, Department of Aerospace Engineering Sciences, Bell&Howell Information and Learning, pp. 21-25.

[20] **Nagel, P. B.** (1999). *Multiprocessor Implementation of Algorithms for Multisatellite Orbit Determination* (Doctoral dissertation), Faculty of Graduate School of the University of Texas at Austin, Bell&Howell Information and Learning, Pp. 2-3.

[21] **Parkinson, B. W., and Spilker Jr., J. J.** (1996). *Global Positioning System: Theory and Applications Volume I*, American Institute of Aeronautics and Astronautics, Pp. 3-13.

[22] **Hacıyev, C.** (1999). *Radyo Navigasyon*, Istanbul Technical University Press, Ayazağa.

[23] **Welch, G., and Bishop, G.** (2001). *An Introduction to the Kalman Filter*, SIGGRAPH 2001, Pp. 19-24.

[24] **Julier, J., and Uhlmann, K.** (1997). A New Extension of the Kalman Filter to Nonlinear Systems, *The 11th International Symposium on Aerospace/Defence Sensing, Simulation and Controls*, Orlando, pp. 182-193.

[25] **Julier, J., and Uhlmann, K.** (2004). Unscented Filtering and Nonlinear Estimation, *PROCEEDINGS OF THE IEEE*, Vol. 92 No. 3, pp. 401-422.

[26] **Merwe, R. V. D., and Wan, E. A.** (2001). The Square-Root Unscented Kalman Filter For State And Parameter Estimation, *Proc of.IEEE*.

[27] **Julier, S. J., Uhlmann, J. K., and Durrant-Whyte, H. F.** (1995). A new approach for filtering nonlinear system. *Proc. of American Control Conference*, Seattle, USA, 3, 1628-1632.

[28] **Julier, S. J., Uhlmann, J. K., and Durrant-Whyte, H. F.** (2000). A new method for the nonlinear transformation of means and covariances in filters and estimator. *IEEE Trans. Autom. Control*, 45, 477-482. doi: 10.1109/9.847726.

[29] **Crassidis, J. L., and Markley, F. L.** (2003). Unscented filtering for spacecraft attitude estimation. *J. Guid. Cont. Dyn.,* 26, pp. 536-542.

[30] **Hajiyev, Ch.** (2007). Adaptive filtration algorithm with the filter gain correction applied to integrated INS/Radar altimeter. *Proc. IMechE*, Part G: J. Aerosp. Eng., 221, pp. 847-885. doi: 10.1243/09544100JAERO173.

[31] **Geng, Y., and Wang, J.** (2008). Adaptive estimation of multiple fading factors in Kalman filter for navigation applications. *GPS Solut.*, 12, pp. 273-279. doi: 10.1007/s10291-007-0084-6.

[32] **Soken, H. E., and Hajiyev, C.** (2010). Pico Satellite Attitude Estimation via Robust Unscented Kalman Filter in the Presence of Measurement Faults. *ISA Trans.,* Vol.49, No.3, pp. 249-256.

[33] **Vallado, D. A.** (2007). *Fundamentals of Astrodynamics and Applications*, third ed., Published jointly by Microcosm Press, Hawthorne, CA, and Springer, New York.

[34] **Crassidis, J. L., and Junkins, J. L.** (2004). *Optimal Estimation of Dynamic Systems*, Chapman & Hall/CRC applied mathematics and nonlinear science series, CRC Press LLC, USA.

[35] **Curtis, H. D.** (2005). *Orbital Mechanics for Engineering Students*, Elsevier Butterworth- Heinemann.

[36] **Hajiyev, C., and Ata, M.** (2011). Error analysis of orbit determination for the geostationary satellite with single station antenna tracking data, *Positioning*, 2, 135-144, doi:10.4236/pos.2011.24013.

APPENDICES

APPENDIX A: Partial derivatives required to calculate x-y-z position errors' variances

APPENDIX B: Tables

APPENDIX C: Figures

APPENDIX A

$$\frac{\partial x}{\partial \rho} = -\cos\beta\sin\alpha\sin\theta - \cos\beta\cos\alpha\sin\lambda\cos\theta + \sin\beta\cos\lambda\cos\theta \qquad \textbf{(A.1)}$$

$$\frac{\partial x}{\partial \alpha} = -\rho\cos\beta\cos\alpha\sin\theta + \rho\cos\beta\sin\alpha\sin\lambda\cos\theta \qquad \textbf{(A.2)}$$

$$\frac{\partial x}{\partial \beta} = \rho\sin\beta\sin\alpha\sin\theta + \rho\sin\beta\cos\alpha\sin\lambda\cos\theta + \rho\cos\beta\cos\lambda\cos\theta \qquad \textbf{(A.3)}$$

$$\frac{\partial y}{\partial \rho} = \cos\beta\sin\alpha\cos\theta - \cos\beta\cos\alpha\sin\lambda\sin\theta + \sin\beta\cos\lambda\sin\theta \qquad \textbf{(A.4)}$$

$$\frac{\partial y}{\partial \alpha} = \rho\cos\beta\cos\alpha\cos\theta + \rho\cos\beta\sin\alpha\sin\lambda\sin\theta \qquad \textbf{(A.5)}$$

$$\frac{\partial y}{\partial \beta} = -\rho\sin\beta\sin\alpha\cos\theta + \rho\sin\beta\cos\alpha\sin\lambda\sin\theta + \rho\cos\beta\cos\lambda\sin\theta \qquad \textbf{(A.6)}$$

$$\frac{\partial z}{\partial \rho} = \cos\beta\cos\alpha\cos\lambda + \sin\beta\sin\lambda \qquad \textbf{(A.7)}$$

$$\frac{\partial z}{\partial \alpha} = -\rho\cos\beta\sin\alpha\cos\lambda \qquad \textbf{(A.8)}$$

$$\frac{\partial z}{\partial \beta} = -\rho\sin\beta\cos\alpha\cos\lambda + \rho\cos\beta\sin\lambda \qquad \textbf{(A.9)}$$

APPENDIX B

Table B.1 : Abs. est. errors via Regular UKF in case of cont. bias, SSA.

Parameter	1000	2000	3000	4000	5000
x position(m)	693.4597	3.27E+05	142.1083	274.8157	306.0897
y position(m)	95.7669	2.93E+05	1.26E+03	141.5185	26.8624
z position(m)	5.96E+02	5.65E+03	208.4127	6.02E+02	8.25E+02
x velocity(m/s)	2.9474	19.0766	0.714	0.5754	0.3419
y velocity(m/s)	0.4587	25.8599	4.3259	0.3244	0.2164
z velocity(m/s)	2.80E+00	0.9341	0.5569	3.1966	1.2994
Range (m)	52.2141	14.1597	29.4756	69.8962	10.594
Azimuth (rad)	1.96E-04	1.76E-02	1.42E-04	1.04E-04	8.68E-05
Elevation (rad)	7.43E-05	5.09E-06	2.88E-05	3.94E-04	1.58E-04

Table B.2 : Variances via Regular UKF in case of cont. bias, SSA.

Parameter	1000	2000	3000	4000	5000
x position(m)	6.18E+05	6.18E+05	6.19E+05	6.18E+05	6.18E+05
y position(m)	5.32E+05	5.31E+05	5.31E+05	5.31E+05	5.31E+05
z position(m)	1.79E+06	1.79E+06	1.79E+06	1.79E+06	1.79E+06
x velocity(m/s)	10.8962	10.8982	10.9006	10.8991	10.8964
y velocity(m/s)	10.3521	10.3504	10.3483	10.3495	10.3518
z velocity(m/s)	15.6231	15.6231	15.6231	15.6231	15.6231
Range (m)	9.77E+05	9.69E+05	9.76E+05	9.75E+05	9.73E+05
Azimuth (rad)	6.00E-04	1.48E-04	5.21E-04	3.96E-04	1.78E-04
Elevation (rad)	0.0426	0.0428	0.0425	0.0425	0.0425

Table B.3 : Abs. est. errors via RUKF with SMNSF in case of cont. bias, SSA.

Parameter	1000	2000	3000	4000	5000
x position(m)	1.21E+03	3.24E+05	164.9988	296.8449	140.1359
y position(m)	118.9716	2.91E+05	2.28E+03	133.338	128.8219
z position(m)	7.39E+02	5.87E+03	631.911	1.23E+03	1.34E+03
x velocity(m/s)	5.1929	24.9672	0.4752	0.0099	0.084
y velocity(m/s)	0.4873	23.7322	6.4352	0.9116	0.1987
z velocity(m/s)	2.82E+00	2.0695	0.9081	3.8301	2.5237
Range (m)	54.4305	743.8875	10.125	38.3697	21.0621
Azimuth (rad)	4.89E-05	1.74E-02	9.07E-05	1.05E-05	3.96E-06
Elevation (rad)	1.95E-05	1.61E-05	1.81E-05	3.32E-05	3.61E-05

Table B.4 : Variances via RUKF with SMNSF in case of cont. bias, SSA.

Parameter	1000	2000	3000	4000	5000
x position(m)	6.18E+05	6.87E+05	6.19E+05	6.18E+05	6.18E+05
y position(m)	5.32E+05	5.85E+05	5.31E+05	5.31E+05	5.31E+05
z position(m)	1.79E+06	2.04E+06	1.79E+06	1.79E+06	1.79E+06
x velocity(m/s)	10.8962	11.7191	10.9006	10.8991	10.8964
y velocity(m/s)	10.3521	10.9406	10.3483	10.3495	10.3518
z velocity(m/s)	15.6231	19.5113	15.6231	15.6231	15.6231
Range (m)	9.77E+05	1.12E+06	9.76E+05	9.75E+05	9.72E+05
Azimuth (rad)	5.98E-04	1.68E-04	5.21E-04	3.96E-04	1.79E-04
Elevation (rad)	0.0426	0.0483	0.0425	0.0425	0.0425

Table B.5 : Abs. est. errors via RUKF with MMNSF in case of cont. bias, SSA.

Parameter	1000	2000	3000	4000	5000
x position(m)	2.33E+02	4.47E+05	36.3634	792.1788	86.3431
y position(m)	77.9961	2.92E+05	5.20E+02	1.17E+03	53.8812
z position(m)	1.37E+01	2.90E+03	128.3762	3.27E+01	5.51E+02
x velocity(m/s)	0.361	73.2929	0.214	0.7207	1.2482
y velocity(m/s)	0.5588	21.9763	1.7563	1.2236	0.6235
z velocity(m/s)	2.12E+00	3.0556	0.5482	0.5516	1.2441
Range (m)	81.1876	8.04E+04	5.1046	36.9604	16.0227
Azimuth (rad)	9.26E-06	2.10E-02	2.07E-05	5.61E-05	2.73E-06
Elevation (rad)	2.67E-07	1.52E-04	3.71E-06	1.27E-06	1.48E-05

Table B.6 : Variances via RUKF with MMNSF in case of cont. bias, SSA.

Parameter	1000	2000	3000	4000	5000
x position(m)	6.18E+05	5.63E+07	6.19E+05	6.18E+05	6.18E+05
y position(m)	5.32E+05	7.09E+05	5.31E+05	5.31E+05	5.31E+05
z position(m)	1.79E+06	1.98E+06	1.79E+06	1.79E+06	1.79E+06
x velocity(m/s)	10.8962	60.531	10.9006	10.8991	10.8964
y velocity(m/s)	10.3521	11.7248	10.3483	10.3495	10.3518
z velocity(m/s)	15.6231	16.2421	15.6231	15.6231	15.6231
Range (m)	9.77E+05	1.08E+06	9.76E+05	9.75E+05	9.72E+05
Azimuth (rad)	5.99E-04	5.50E-03	5.22E-04	3.95E-04	1.79E-04
Elevation (rad)	0.0426	0.0472	0.0425	0.0425	0.0425

Table B.7 : Abs. est. errors via Regular UKF in case of noise inc, SSA.

Parameter	1000	2000	3000	4000	5000
x position(m)	1.48E+03	2.72E+04	102.532	908.5613	921.6779
y position(m)	163.4444	1.82E+04	386.3203	1.65E+03	217.5169
z position(m)	1.43E+03	6.12E+03	5.89E+02	1.60E+03	3.15E+01
x velocity(m/s)	1.8218	19.9206	0.0352	0.5853	1.3615
y velocity(m/s)	0.1818	11.041	0.7735	1.6808	0.2946
z velocity(m/s)	1.04E+00	7.5745	0.2834	3.6158	0.1046
Range (m)	3.1015	5.45E+03	1.0609	58.1626	7.9354
Azimuth (rad)	5.79E-05	1.30E-03	1.61E-05	7.53E-05	3.76E-05
Elevation (rad)	3.93E-05	1.66E-04	1.57E-05	4.25E-05	9.72E-07

Table B.8 : Variances via Regular UKF in case of noise inc, SSA.

Parameter	1000	2000	3000	4000	5000
x position(m)	6.18E+05	6.18E+05	6.19E+05	6.18E+05	6.18E+05
y position(m)	5.32E+05	5.31E+05	5.31E+05	5.31E+05	5.31E+05
z position(m)	1.79E+06	1.79E+06	1.79E+06	1.79E+06	1.79E+06
x velocity(m/s)	10.8962	10.8982	10.9006	10.8991	10.8964
y velocity(m/s)	10.3521	10.3503	10.3483	10.3495	10.3518
z velocity(m/s)	15.6231	15.6231	15.6231	15.6231	15.6231
Range (m)	9.77E+05	9.77E+05	9.76E+05	9.75E+05	9.73E+05
Azimuth (rad)	6.01E-04	5.48E-04	5.22E-04	3.98E-04	1.80E-04
Elevation (rad)	0.0426	0.0426	0.0425	0.0425	0.0425

Table B.9 : Abs. est. errors via RUKF with SMNSF in case of noise inc, SSA.

Parameter	1000	2000	3000	4000	5000
x position(m)	582.0079	4.07E+04	346.0941	440.2823	6.78E+02
y position(m)	29.2638	3.61E+04	290.9508	1.06E+03	31.1554
z position(m)	2.52E+02	8.24E+02	2.69E+03	2.01E+03	1.24E+03
x velocity(m/s)	0.449	3.2337	0.2283	0.0495	1.2734
y velocity(m/s)	0.0967	6.6448	0.8007	0.8021	0.0434
z velocity(m/s)	1.08E+00	0.1316	2.2356	4.2663	2.2762
Range (m)	2.0696	7.02E+02	37.3881	53.198	3.5343
Azimuth (rad)	2.30E-05	2.20E-03	1.48E-05	4.56E-05	2.62E-05
Elevation (rad)	7.09E-06	4.67E-05	7.24E-05	5.39E-05	3.34E-05

Table B.10 : Variances via RUKF with SMNSF in case of noise inc, SSA.

Parameter	1000	2000	3000	4000	5000
x position(m)	6.18E+05	9.24E+06	6.19E+05	6.18E+05	6.18E+05
y position(m)	5.32E+05	7.95E+06	5.31E+05	5.31E+05	5.31E+05
z position(m)	1.79E+06	2.67E+07	1.79E+06	1.79E+06	1.79E+06
x velocity(m/s)	10.8962	28.9557	10.9006	10.8991	10.8964
y velocity(m/s)	10.3521	27.3774	10.3483	10.3495	10.3518
z velocity(m/s)	15.6231	41.329	15.6231	15.6231	15.6231
Range (m)	9.77E+05	1.46E+07	9.76E+05	9.75E+05	9.73E+05
Azimuth (rad)	5.99E-04	7.90E-03	5.22E-04	3.95E-04	1.78E-04
Elevation (rad)	0.0426	0.6364	0.0425	0.0425	0.0425

Table B.11 : Abs. est. errors via RUKF with MMNSF in case of noise inc, SSA.

Parameter	1000	2000	3000	4000	5000
x position(m)	7.79E+02	4.11E+04	75.1432	418.0522	2.86E+02
y position(m)	97.1167	3.60E+04	1.49E+03	476.0609	88.2118
z position(m)	8.39E+02	1.58E+03	7.12E+02	7.35E+02	2.64E+02
x velocity(m/s)	5.1797	0.721	0.009	0.054	1.3756
y velocity(m/s)	0.0879	4.9805	2.7919	0.1248	0.4996
z velocity(m/s)	3.71E-02	0.1329	2.2755	0.2486	0.1896
Range (m)	3.6707	9.28E+02	8.3846	11.794	48.2429
Azimuth (rad)	3.05E-05	2.20E-03	5.89E-05	2.47E-05	1.18E-05
Elevation (rad)	2.31E-05	1.59E-05	1.99E-05	1.99E-05	7.00E-06

Table B.12 : Variances via RUKF with MMNSF in case of noise inc, SSA.

Parameter	1000	2000	3000	4000	5000
x position(m)	6.18E+05	1.43E+07	6.19E+05	6.18E+05	6.18E+05
y position(m)	5.32E+05	1.19E+07	5.31E+05	5.31E+05	5.31E+05
z position(m)	1.79E+06	3.15E+06	1.79E+06	1.79E+06	1.79E+06
x velocity(m/s)	10.8962	32.4771	10.9006	10.8991	10.8964
y velocity(m/s)	10.3521	31.1754	10.3483	10.3495	10.3518
z velocity(m/s)	15.6231	18.9184	15.6231	15.6231	15.6231
Range (m)	9.77E+05	5.39E+06	9.76E+05	9.75E+05	9.72E+05
Azimuth (rad)	5.99E-04	1.46E-02	5.24E-04	3.97E-04	1.78E-04
Elevation (rad)	0.0426	0.2849	0.0425	0.0425	0.0425

Table B.13 : Abs. est. errors via Regular UKF in case of zero out, SSA.

Parameter	1000	2000	3000	4000	5000
x position(m)	6.72E+02	2.01E+07	157.7604	198.5877	1.94E+03
y position(m)	150.7859	2.19E+07	1.35E+03	355.4185	624.4834
z position(m)	1.48E+03	4.03E+07	3.81E+02	3.28E+02	1.24E+03
x velocity(m/s)	4.0687	1.60E+03	0.179	0.0881	4.4484
y velocity(m/s)	0.2042	1.46E+03	1.0981	0.111	1.3893
z velocity(m/s)	1.08E+00	101.9057	4.2286	0.8918	1.3129
Range (m)	4.9677	2.40E+04	54.7299	11.715	45.9615
Azimuth (rad)	2.79E-05	3.12E+00	5.37E-05	1.63E-05	8.11E-05
Elevation (rad)	3.97E-05	9.10E-05	1.07E-05	8.70E-06	3.32E-05

Table B.14 : Variances via Regular UKF in case of zero out, SSA.

Parameter	1000	2000	3000	4000	5000
x position(m)	6.18E+05	6.18E+05	6.19E+05	6.18E+05	6.18E+05
y position(m)	5.32E+05	5.31E+05	5.31E+05	5.31E+05	5.31E+05
z position(m)	1.79E+06	1.79E+06	1.79E+06	1.79E+06	1.79E+06
x velocity(m/s)	10.8962	10.8964	10.9006	10.8991	10.8964
y velocity(m/s)	10.3521	10.3484	10.3483	10.3495	10.3518
z velocity(m/s)	15.6231	15.6354	15.6231	15.6231	15.6231
Range (m)	9.77E+05	1.68E+06	9.76E+05	9.75E+05	9.73E+05
Azimuth (rad)	6.00E-04	4.37E-07	5.21E-04	3.96E-04	1.81E-04
Elevation (rad)	0.0426	0.0218	0.0425	0.0425	0.0425

Table B.15 : Abs. est. errors via RUKF with SMNSF in case of zero out, SSA.

Parameter	1000	2000	3000	4000	5000
x position(m)	1.29E+03	6.37E+02	298.4114	39.6455	4.03E+02
y position(m)	85.6831	2.82E+04	772.5601	1.37E+01	83.5772
z position(m)	6.80E+02	1.07E+04	1.57E+03	2.53E+02	1.11E+03
x velocity(m/s)	0.9745	1.43E+00	0.8376	1.2112	0.7791
y velocity(m/s)	0.0126	6.98E+00	2.2702	1.4072	0.3643
z velocity(m/s)	7.48E-01	2.4914	3.2356	1.6972	2.6445
Range (m)	28.0505	2.23E+04	54.8835	14.3477	58.9535
Azimuth (rad)	5.19E-05	7.45E-04	3.29E-05	3.43E-07	1.46E-05
Elevation (rad)	1.77E-05	2.17E-04	4.20E-05	6.84E-06	3.01E-05

Table B.16 : Variances via RUKF with SMNSF in case of zero out, SSA.

Parameter	1000	2000	3000	4000	5000
x position(m)	6.18E+05	1.74E+09	6.19E+05	6.18E+05	6.18E+05
y position(m)	5.32E+05	1.79E+09	5.31E+05	5.31E+05	5.31E+05
z position(m)	1.79E+06	1.83E+09	1.79E+06	1.79E+06	1.79E+06
x velocity(m/s)	10.8962	188.2909	10.9006	10.8991	10.8964
y velocity(m/s)	10.3521	195.9924	10.3483	10.3495	10.3518
z velocity(m/s)	15.6231	182.6072	15.6231	15.6231	15.6231
Range (m)	9.77E+05	1.83E+08	9.76E+05	9.75E+05	9.72E+05
Azimuth (rad)	5.98E-04	1.68E+00	5.24E-04	3.96E-04	1.79E-04
Elevation (rad)	0.0426	67.7513	0.0425	0.0425	0.0425

Table B.17 : Abs. est. errors via RUKF with MMNSF in case of zero out, SSA.

Parameter	1000	2000	3000	4000	5000
x position(m)	1.74E+02	1.78E+04	103.5007	104.551	6.66E+02
y position(m)	97.4905	1.48E+04	312.4885	2.09E+02	422.0709
z position(m)	9.77E+02	1.72E+04	1.05E+03	4.08E+02	2.54E+03
x velocity(m/s)	0.3717	4.95E+00	0.4228	0.892	2.2321
y velocity(m/s)	0.0647	3.99E+00	1.6519	1.0886	0.9165
z velocity(m/s)	4.58E-01	3.4721	1.3193	0.3613	3.3109
Range (m)	4.3493	2.45E+04	27.769	5.0517	4.0894
Azimuth (rad)	6.21E-06	1.19E-04	1.12E-05	9.40E-06	3.02E-05
Elevation (rad)	2.64E-05	3.97E-04	2.85E-05	1.09E-05	6.81E-05

Table B.18 : Variances via RUKF with MMNSF in case of zero out, SSA.

Parameter	1000	2000	3000	4000	5000
x position(m)	6.18E+05	1.74E+09	6.19E+05	6.18E+05	6.18E+05
y position(m)	5.32E+05	1.79E+09	5.31E+05	5.31E+05	5.31E+05
z position(m)	1.79E+06	1.83E+09	1.79E+06	1.79E+06	1.79E+06
x velocity(m/s)	10.8962	188.267	10.9006	10.8991	10.8964
y velocity(m/s)	10.3521	196.0325	10.3483	10.3495	10.3518
z velocity(m/s)	15.6231	182.6062	15.6231	15.6231	15.6231
Range (m)	9.77E+05	1.82E+08	9.76E+05	9.75E+05	9.73E+05
Azimuth (rad)	5.99E-04	1.62E+00	5.23E-04	3.96E-04	1.79E-04
Elevation (rad)	0.0426	67.7937	0.0425	0.0425	0.0425

Table B.19 : Abs. est. errors via Regular UKF in case of cont. bias, GPS.

Parameter	1000	2000	3000	4000	5000
x position(m)	1.57E+01	9.71E+05	42.6835	6.86E+04	1.81E+01
y position(m)	16.0833	5.95E+00	16.1937	1.80E+01	16.2057
z position(m)	1.57E+01	5.69E+01	1.62E+01	1.67E+01	1.62E+01
x velocity(m/s)	0.1027	8.49E+00	0.0945	978.6551	0.1021
y velocity(m/s)	0.1026	4.04E-01	0.1028	0.2032	0.1026
z velocity(m/s)	1.03E-01	0.5039	0.103	0.0976	0.1031

Table B.20 : Variances via Regular UKF in case of cont. bias, GPS.

Parameter	1000	2000	3000	4000	5000
x position(m)	8.72E+00	8.72E+00	8.72E+00	8.72E+00	8.72E+00
y position(m)	8.72E+00	8.72E+00	8.72E+00	8.72E+00	8.72E+00
z position(m)	8.72E+00	8.72E+00	8.72E+00	8.72E+00	8.72E+00
x velocity(m/s)	0.0406	0.0406	0.0406	0.0406	0.0406
y velocity(m/s)	0.0406	0.0406	0.0406	0.0406	0.0406
z velocity(m/s)	0.0406	0.0406	0.0406	0.0406	0.0406

Table B.21 : Abs. est. errors via RUKF with SMNSF in case of cont. bias, GPS.

Parameter	1000	2000	3000	4000	5000
x position(m)	2.26E+01	7.17E+04	23.1031	1.16E+05	2.31E+01
y position(m)	23.0008	4.34E+02	23.1111	1.52E+03	23.1229
z position(m)	2.26E+01	5.75E+02	2.31E+01	3.17E+02	2.31E+01
x velocity(m/s)	0.1466	2.48E+02	0.1469	471.9688	0.1466
y velocity(m/s)	0.1466	3.38E+00	0.1467	18.2468	0.1465
z velocity(m/s)	1.47E-01	5.6157	0.1469	1.866	0.147

Table B.22 : Variances via RUKF with SMNSF in case of cont. bias, GPS.

Parameter	1000	2000	3000	4000	5000
x position(m)	8.72E+00	1.72E+05	8.72E+00	1.78E+05	8.72E+00
y position(m)	8.72E+00	1.73E+05	8.72E+00	1.75E+05	8.72E+00
z position(m)	8.72E+00	1.76E+05	8.72E+00	1.73E+05	8.72E+00
x velocity(m/s)	0.0406	8.1138	0.0406	8.538	0.0406
y velocity(m/s)	0.0406	8.2036	0.0406	8.2951	0.0406
z velocity(m/s)	0.0406	8.48	0.0406	8.1583	0.0406

Table B.23 : Abs. est. errors via RUKF with MMNSF in case of cont. bias, GPS.

Parameter	1000	2000	3000	4000	5000
x position(m)	1.13E+01	5.71E+04	11.7815	1.15E+05	1.18E+01
y position(m)	11.6787	1.10E+01	11.7888	4.54E+00	11.8003
z position(m)	1.13E+01	1.32E+01	1.18E+01	1.16E+01	1.18E+01
x velocity(m/s)	0.0747	1.76E+02	0.075	468.6794	0.0747
y velocity(m/s)	0.0747	8.75E-02	0.0749	0.2596	0.0746
z velocity(m/s)	7.51E-02	0.0493	0.075	0.0658	0.0751

Table B.24 : Variances via RUKF with MMNSF in case of cont. bias, GPS.

Parameter	1000	2000	3000	4000	5000
x position(m)	8.72E+00	1.69E+05	8.72E+00	1.79E+05	8.72E+00
y position(m)	8.72E+00	8.72E+00	8.72E+00	8.72E+00	8.72E+00
z position(m)	8.72E+00	8.72E+00	8.72E+00	8.72E+00	8.72E+00
x velocity(m/s)	0.0406	7.9887	0.0406	8.5445	0.0406
y velocity(m/s)	0.0406	0.0406	0.0406	0.0406	0.0406
z velocity(m/s)	0.0406	0.0406	0.0406	0.0406	0.0406

Table B.25 : Abs. est. errors via Regular UKF in case of noise inc, GPS.

Parameter	1000	2000	3000	4000	5000
x position(m)	2.42E+00	4.71E+05	12.5732	1.64E+04	2.81E+00
y position(m)	2.8137	3.63E+01	2.9799	6.35E+00	2.8974
z position(m)	2.41E+00	7.21E+01	2.97E+00	7.32E+00	2.92E+00
x velocity(m/s)	0.0642	1.17E+03	0.3259	52.4835	0.1333
y velocity(m/s)	0.0642	1.24E-02	0.3208	0.0193	0.1333
z velocity(m/s)	6.38E-02	0.2612	0.3209	0.0136	0.1328

Table B.26 : Variances via Regular UKF in case of noise inc, GPS.

Parameter	1000	2000	3000	4000	5000
x position(m)	8.72E+00	8.72E+00	8.72E+00	8.72E+00	8.72E+00
y position(m)	8.72E+00	8.72E+00	8.72E+00	8.72E+00	8.72E+00
z position(m)	8.72E+00	8.71E+00	8.72E+00	8.72E+00	8.72E+00
x velocity(m/s)	0.0406	0.0406	0.0406	0.0406	0.0406
y velocity(m/s)	0.0406	0.0406	0.0406	0.0406	0.0406
z velocity(m/s)	0.0406	0.0406	0.0406	0.0406	0.0406

Table B.27 : Abs. est. errors via RUKF with SMNSF in case of noise inc, GPS.

Parameter	1000	2000	3000	4000	5000
x position(m)	7.55E+00	1.70E+01	1.9518	1.22E+04	5.05E-01
y position(m)	7.1636	1.44E+01	1.958	1.02E+02	0.5082
z position(m)	7.57E+00	3.14E+01	1.95E+00	2.48E+01	4.81E-01
x velocity(m/s)	0.1326	3.70E-02	0.2615	46.2907	0.0444
y velocity(m/s)	0.1326	1.33E-02	0.2614	1.5569	0.0444
z velocity(m/s)	1.33E-01	0.1508	0.2615	0.1325	0.0439

Table B.28 : Variances via RUKF with SMNSF in case of noise inc, GPS.

Parameter	1000	2000	3000	4000	5000
x position(m)	8.72E+00	1.77E+05	8.72E+00	1.07E+05	8.72E+00
y position(m)	8.72E+00	1.79E+05	8.72E+00	1.06E+05	8.72E+00
z position(m)	8.72E+00	1.82E+05	8.72E+00	1.05E+05	8.72E+00
x velocity(m/s)	0.0406	8.2516	0.0406	6.4698	0.0406
y velocity(m/s)	0.0406	8.347	0.0406	6.3407	0.0406
z velocity(m/s)	0.0406	8.6363	0.0406	6.2691	0.0406

Table B.29 : Abs. est. errors via RUKF with MMNSF in case of noise inc, GPS.

Parameter	1000	2000	3000	4000	5000
x position(m)	1.53E+00	2.17E+00	4.698	1.07E+01	3.25E+00
y position(m)	1.1394	2.11E+00	4.7045	1.60E+00	3.2534
z position(m)	1.55E+00	2.12E+00	4.70E+00	1.60E+00	3.23E+00
x velocity(m/s)	0.1501	1.29E-01	0.1701	0.3527	0.2017
y velocity(m/s)	0.1501	1.31E-01	0.17	0.1444	0.2016
z velocity(m/s)	1.50E-01	0.1298	0.1702	0.1447	0.2021

Table B.30 : Variances via RUKF with MMNSF in case of noise inc, GPS.

Parameter	1000	2000	3000	4000	5000
x position(m)	8.72E+00	4.32E+01	8.72E+00	7.95E+01	8.72E+00
y position(m)	8.72E+00	9.88E+00	8.72E+00	1.00E+01	8.72E+00
z position(m)	8.72E+00	9.88E+00	8.72E+00	1.00E+01	8.72E+00
x velocity(m/s)	0.0406	0.0585	0.0406	0.5464	0.0406
y velocity(m/s)	0.0406	0.0585	0.0406	0.052	0.0406
z velocity(m/s)	0.0406	0.0586	0.0406	0.052	0.0406

Table B.31 : Abs. est. errors via Regular UKF in case of zero out, GPS.

Parameter	1000	2000	3000	4000	5000
x position(m)	3.41E+01	1.34E+06	29.5043	7.39E+04	3.83E+01
y position(m)	33.7145	1.72E+01	33.6072	3.49E+01	33.5965
z position(m)	3.41E+01	6.26E+01	3.36E+01	3.39E+01	3.36E+01
x velocity(m/s)	0.2136	1.11E+02	0.2146	1.43E+03	0.2119
y velocity(m/s)	0.2136	3.20E-01	0.2133	0.3141	0.2135
z velocity(m/s)	2.13E-01	0.0018	0.2133	0.2082	0.213

Table B.32 : Variances via Regular UKF in case of zero out, GPS.

Parameter	1000	2000	3000	4000	5000
x position(m)	8.72E+00	8.72E+00	8.72E+00	8.72E+00	8.72E+00
y position(m)	8.72E+00	8.72E+00	8.72E+00	8.72E+00	8.72E+00
z position(m)	8.72E+00	8.71E+00	8.72E+00	8.72E+00	8.72E+00
x velocity(m/s)	0.0406	0.0406	0.0406	0.0406	0.0406
y velocity(m/s)	0.0406	0.0406	0.0406	0.0406	0.0406
z velocity(m/s)	0.0406	0.0406	0.0406	0.0406	0.0406

Table B.33 : Abs. est. errors via RUKF with SMNSF in case of zero out, GPS.

Parameter	1000	2000	3000	4000	5000
x position(m)	3.19E+01	1.21E+02	31.3677	2.88E+04	3.14E+01
y position(m)	31.4722	8.62E+01	31.364	3.41E+02	31.3526
z position(m)	3.19E+01	6.93E+01	3.14E+01	1.07E+02	3.14E+01
x velocity(m/s)	0.1994	4.10E-01	0.1991	1.45E+02	0.1992
y velocity(m/s)	0.1994	2.33E-01	0.1991	3.9088	0.1993
z velocity(m/s)	1.99E-01	0.102	0.1991	0.4132	0.1988

Table B.34 : Variances via RUKF with SMNSF in case of zero out, GPS.

Parameter	1000	2000	3000	4000	5000
x position(m)	8.72E+00	1.77E+05	8.72E+00	1.13E+05	8.72E+00
y position(m)	8.72E+00	1.79E+05	8.72E+00	1.11E+05	8.72E+00
z position(m)	8.72E+00	1.82E+05	8.72E+00	1.10E+05	8.72E+00
x velocity(m/s)	0.0406	8.2514	0.0406	7.0523	0.0406
y velocity(m/s)	0.0406	8.3469	0.0406	6.9056	0.0406
z velocity(m/s)	0.0406	8.6362	0.0406	6.8256	0.0406

Table B.35 : Abs. est. errors via RUKF with MMNSF in case of zero out, GPS.

Parameter	1000	2000	3000	4000	5000
x position(m)	8.84E+00	2.46E+01	9.3377	4.99E+00	9.35E+00
y position(m)	9.2347	9.36E+00	9.3446	9.35E+00	9.3563
z position(m)	8.83E+00	9.32E+00	9.34E+00	9.35E+00	9.33E+00
x velocity(m/s)	0.0592	6.06E-02	0.0595	5.10E-03	0.0592
y velocity(m/s)	0.0591	5.91E-02	0.0593	0.0592	0.0591
z velocity(m/s)	5.96E-02	0.0597	0.0595	0.0593	0.0596

Table B.36 : Variances via RUKF with MMNSF in case of zero out, GPS.

Parameter	1000	2000	3000	4000	5000
x position(m)	8.72E+00	3.97E+01	8.72E+00	7.13E+01	8.72E+00
y position(m)	8.72E+00	8.72E+00	8.72E+00	8.72E+00	8.72E+00
z position(m)	8.72E+00	8.72E+00	8.72E+00	8.72E+00	8.72E+00
x velocity(m/s)	0.0406	0.0406	0.0406	0.5198	0.0406
y velocity(m/s)	0.0406	0.0406	0.0406	0.0406	0.0406
z velocity(m/s)	0.0406	0.0406	0.0406	0.0406	0.0406

APPENDIX C

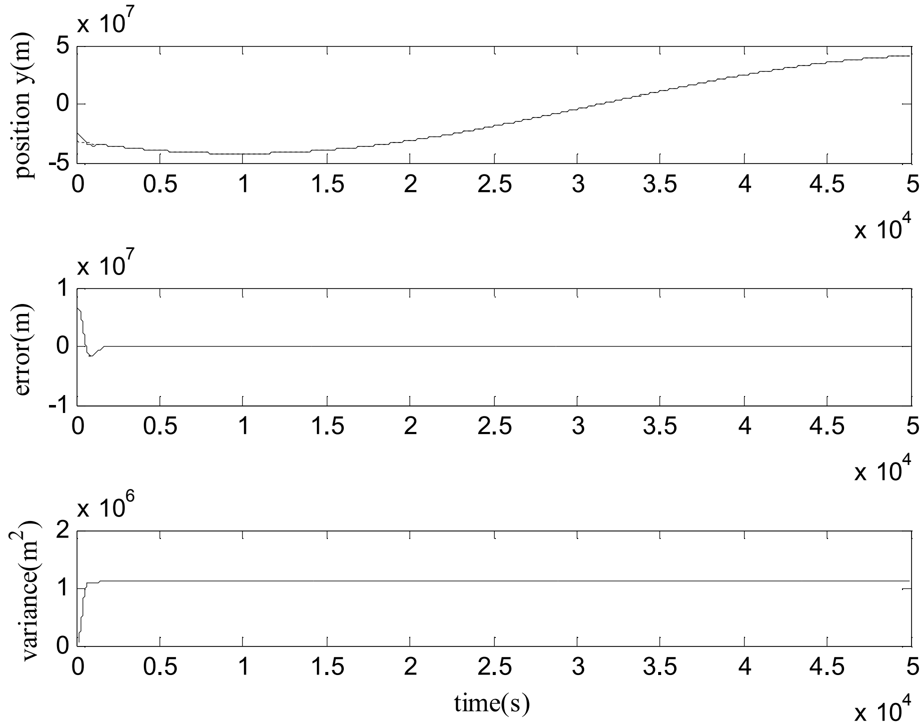

Figure C.1 : Y position est. of satellite by indirect measurements via antenna.

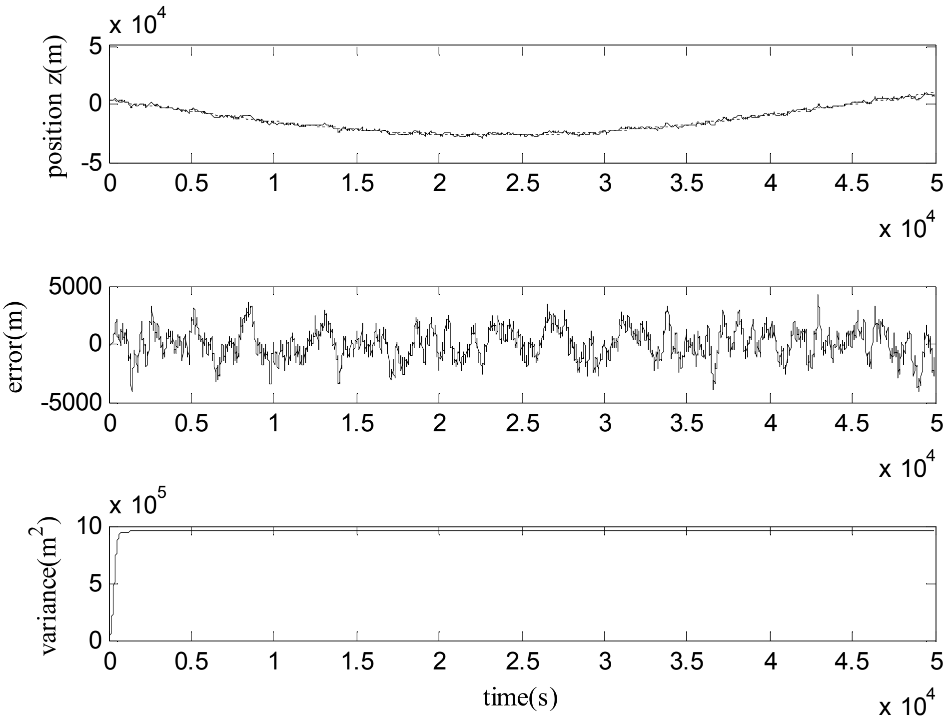

Figure C.2 : Z position est. of satellite by indirect measurements via antenna.

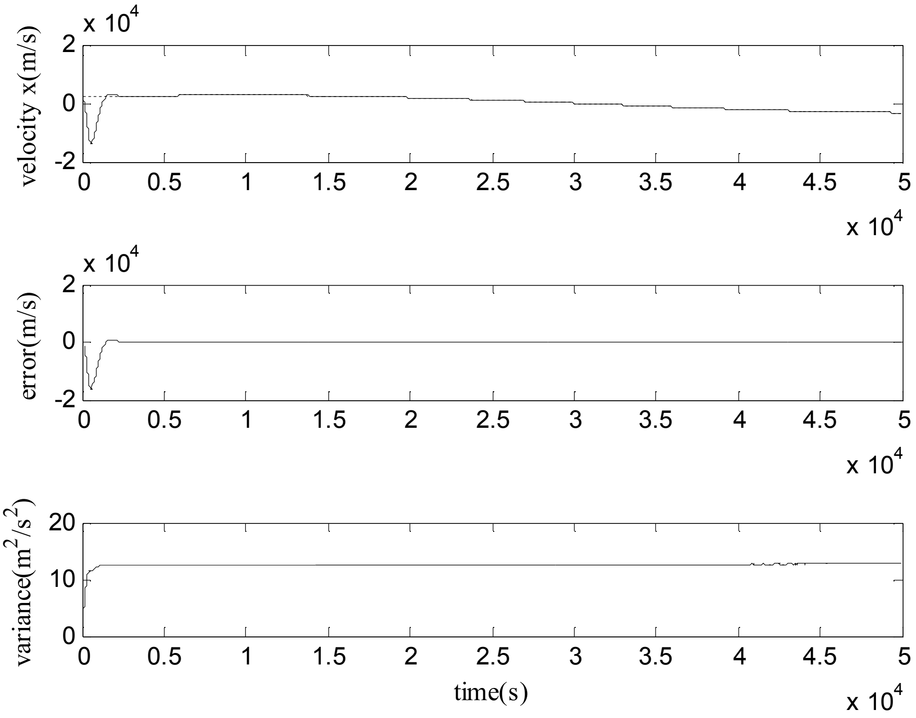

Figure C.3 : X velocity est. of satellite by indirect measurements via antenna.

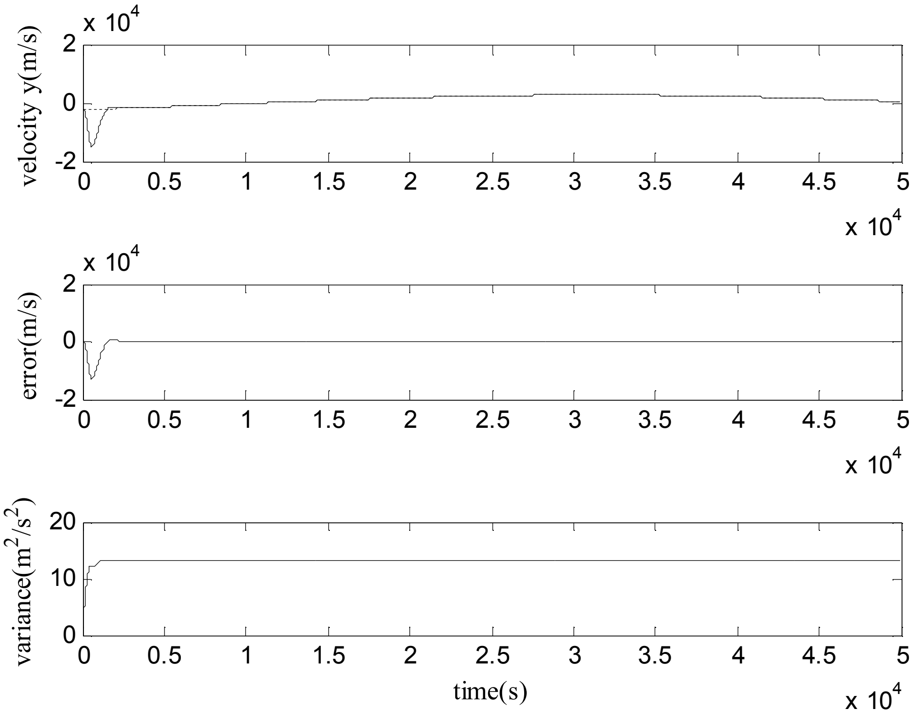

Figure C.4 : Y velocity est. of satellite by indirect measurements via antenna.

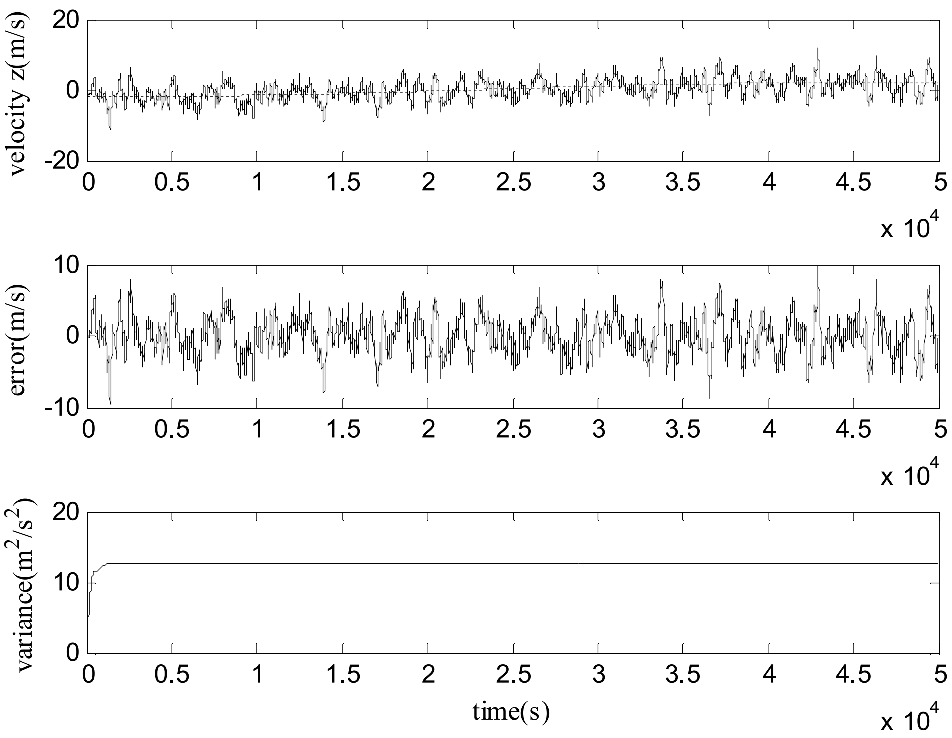

Figure C.5 : Z velocity est. of satellite by indirect measurements via antenna.

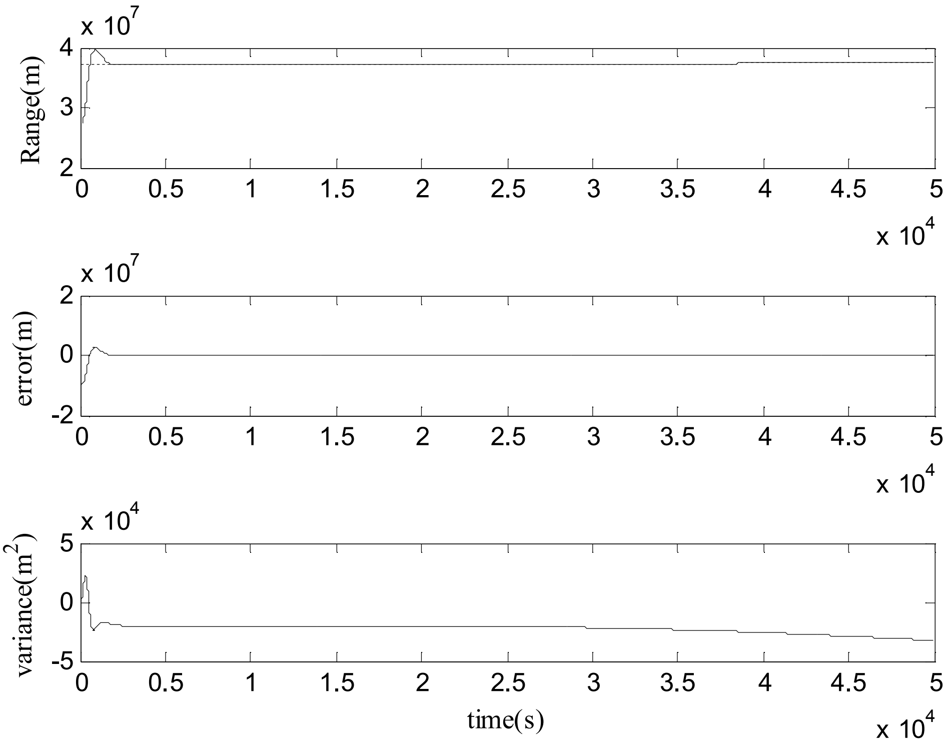

Figure C.6 : Range by using indirect x-y-z measurements via antenna.

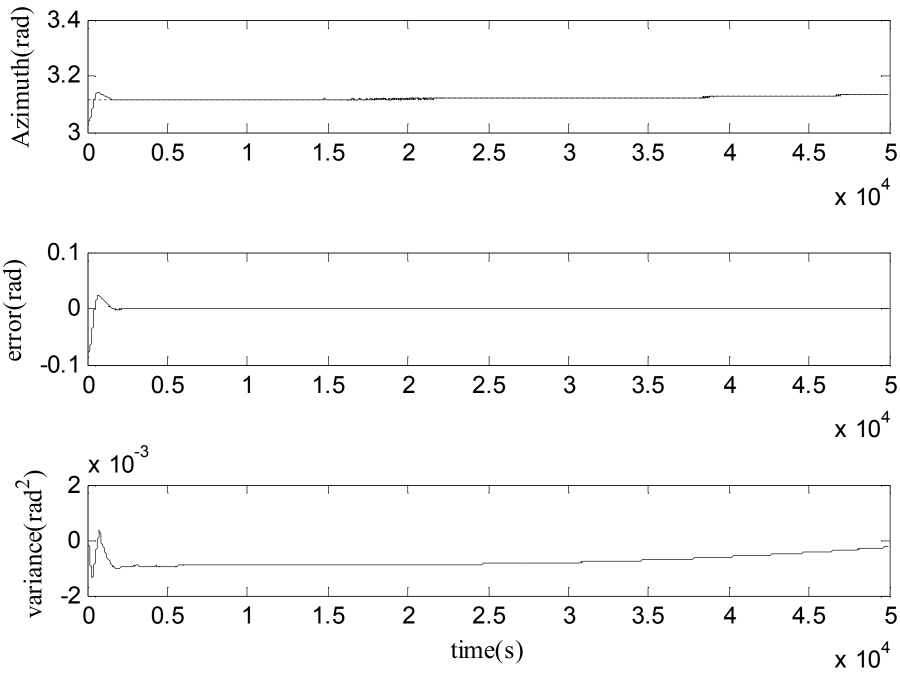

Figure C.7 : Azimuth by using indirect x-y-z measurements via antenna.

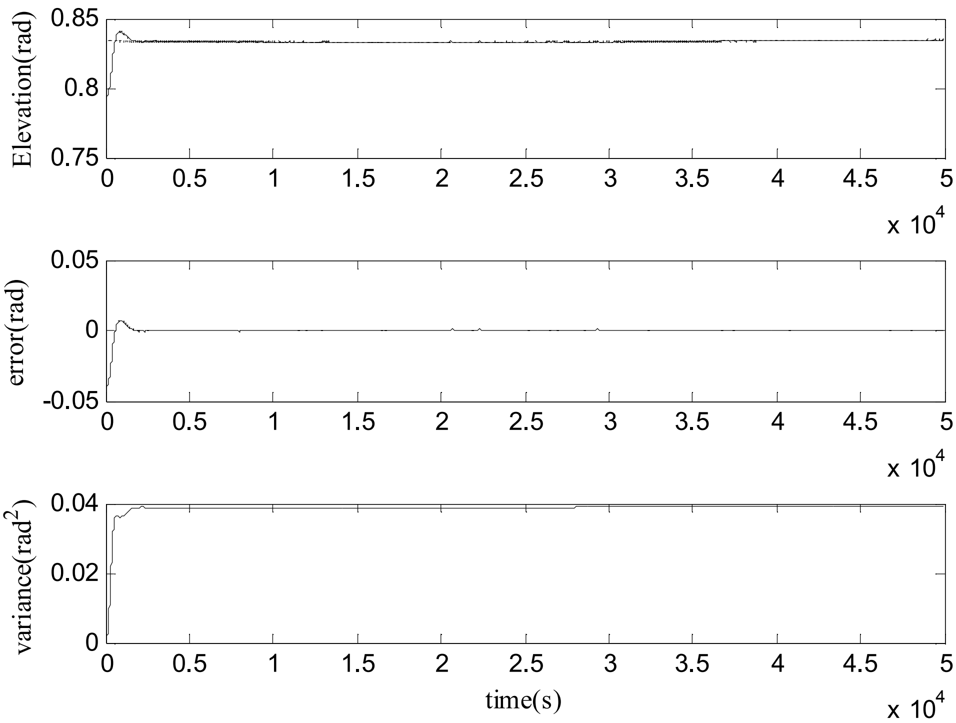

Figure C.8 : Elevation by using indirect x-y-z measurements via antenna.

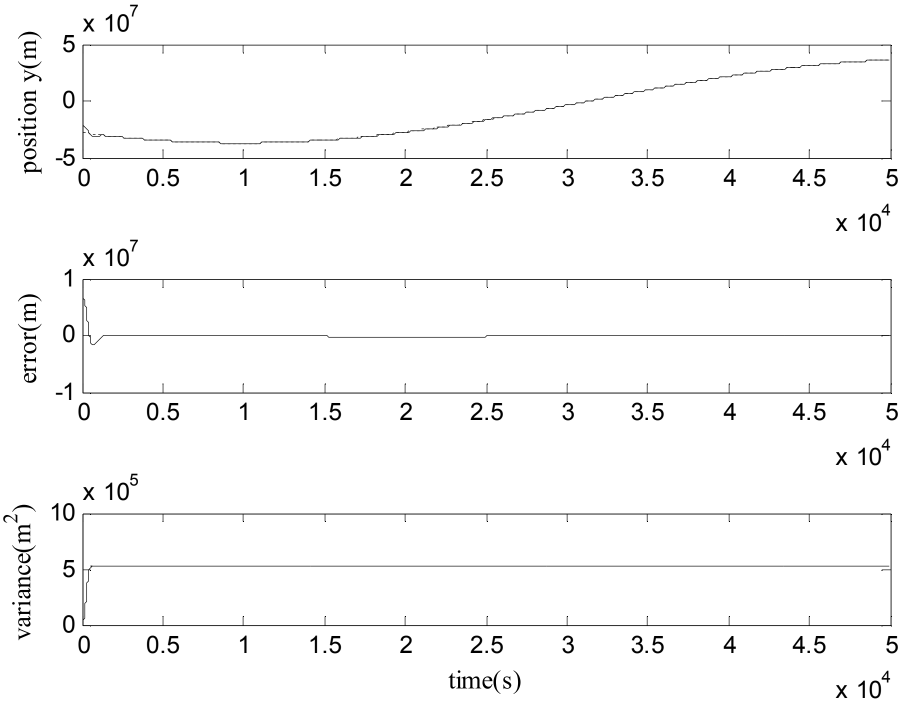

Figure C.9 : Y position est. via Regular UKF in case of cont. bias, SSA.

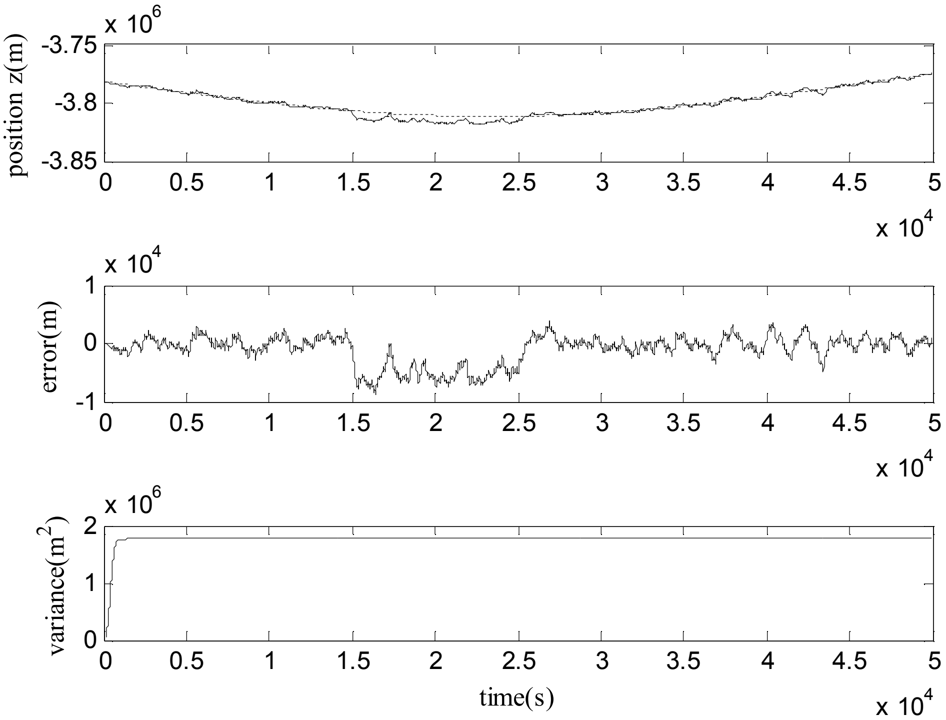

Figure C.10 : Z position est. via Regular UKF in case of cont. bias, SSA.

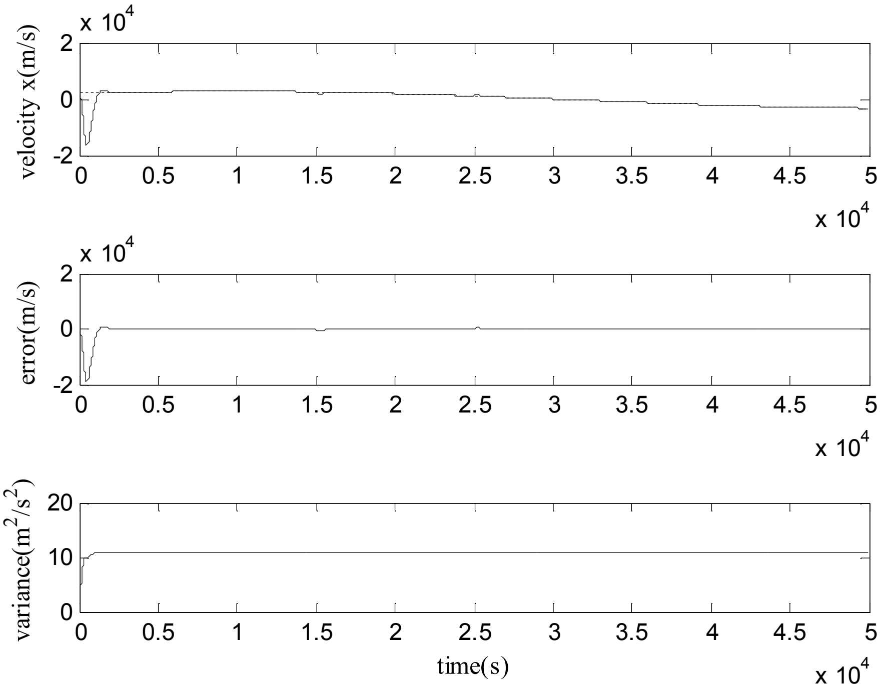

Figure C.11 : X velocity est. via Regular UKF in case of cont. bias, SSA.

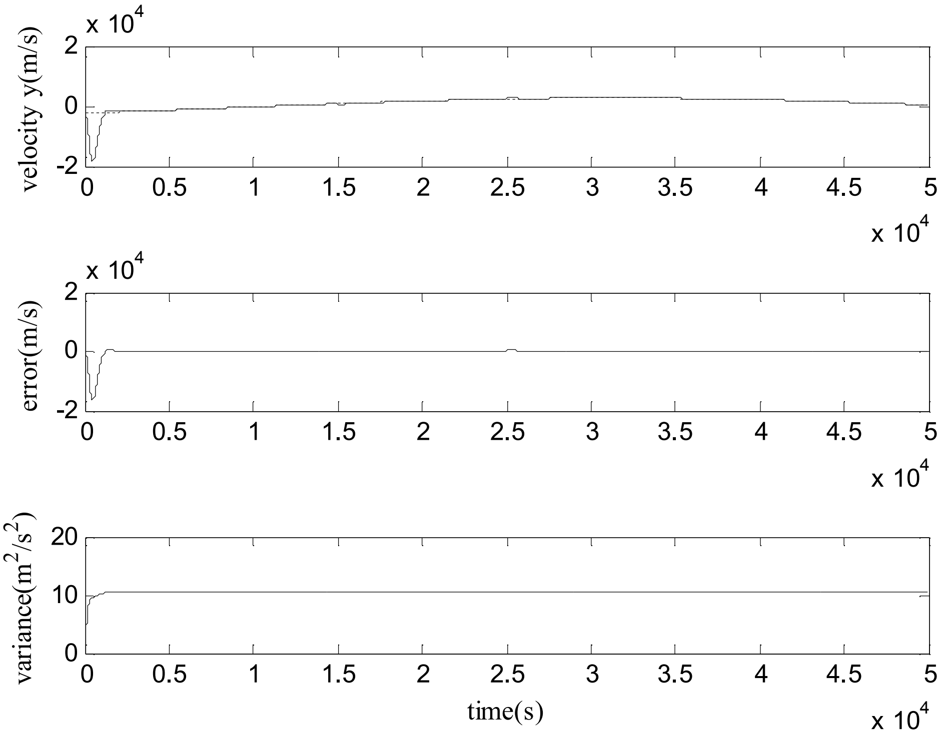

Figure C.12 : Y velocity est. via Regular UKF in case of cont. bias, SSA.

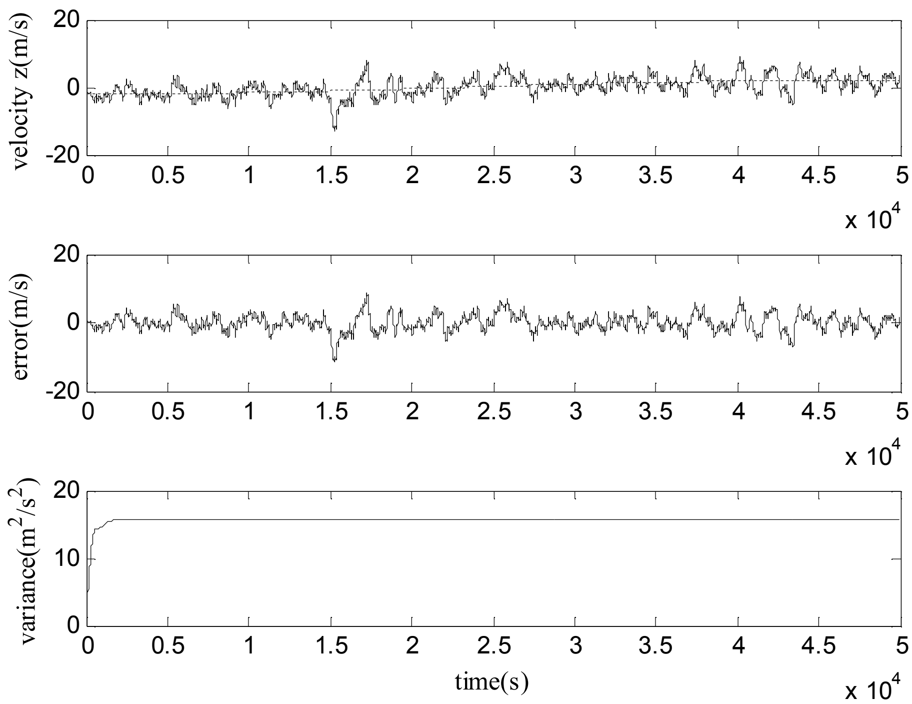

Figure C.13 : Z velocity est. via Regular UKF in case of cont. bias, SSA.

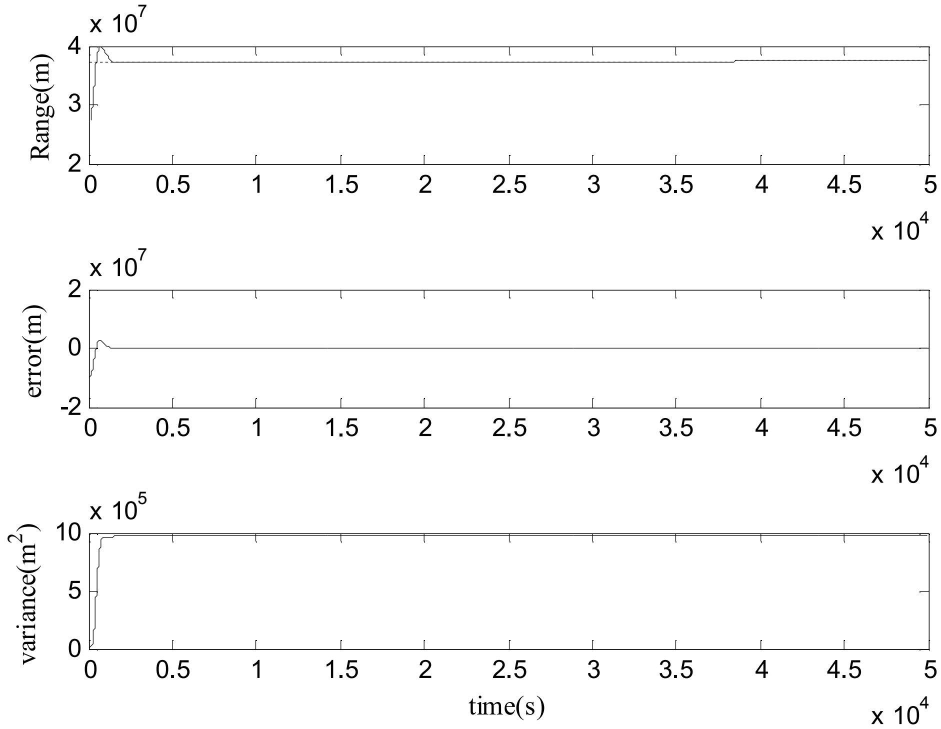

Figure C.14 : Range via Regular UKF in case of cont. bias, SSA.

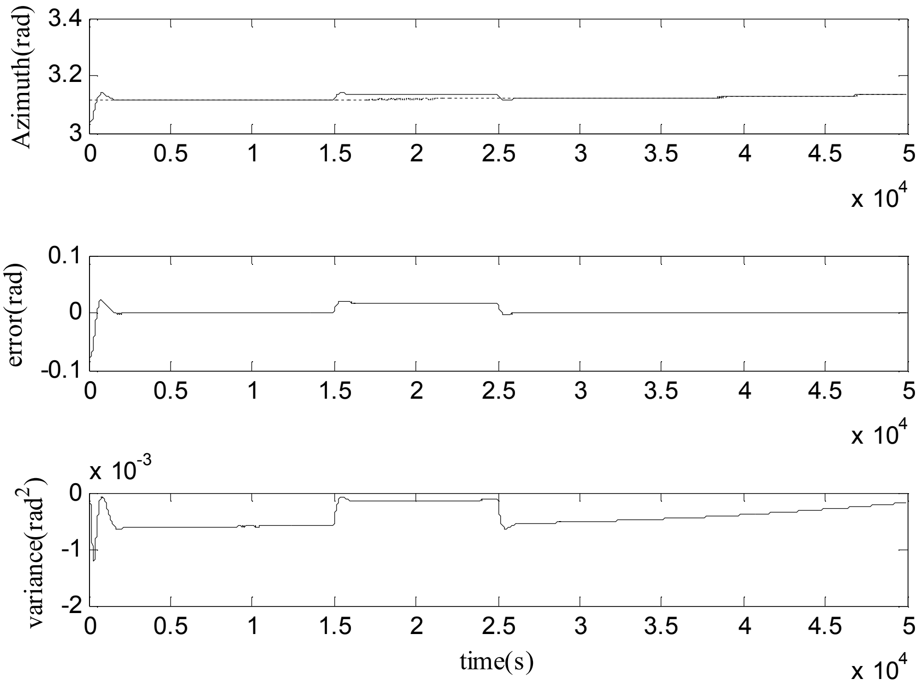

Figure C.15 : Azimuth via Regular UKF in case of cont. bias, SSA.

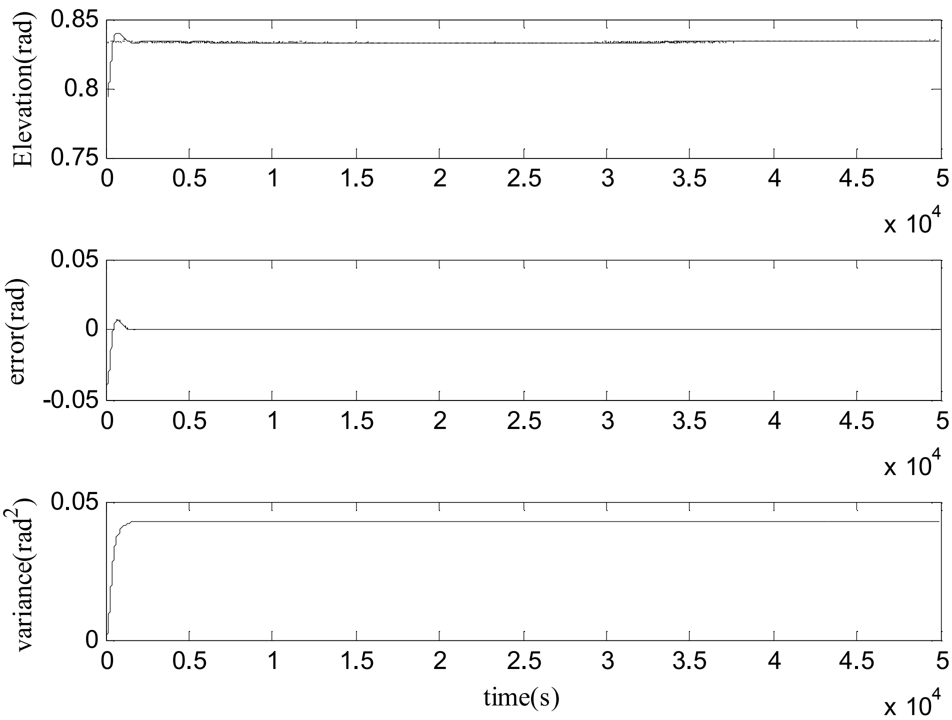

Figure C.16 : Elevation via Regular UKF in case of cont. bias, SSA.

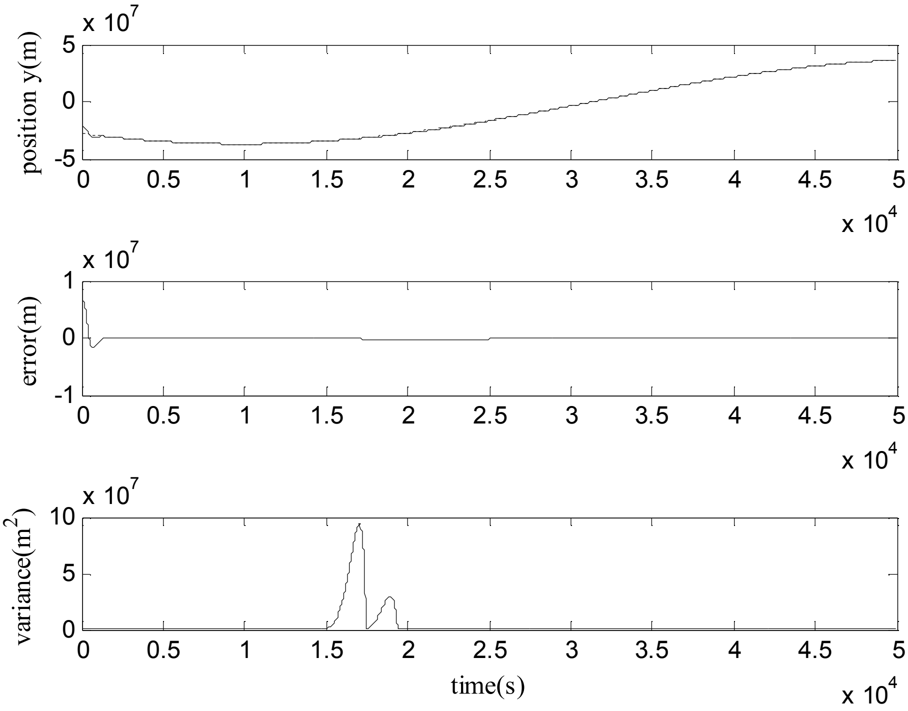

Figure C.17 : Y position est. via RUKF with SMNSF in case of cont bias, SSA.

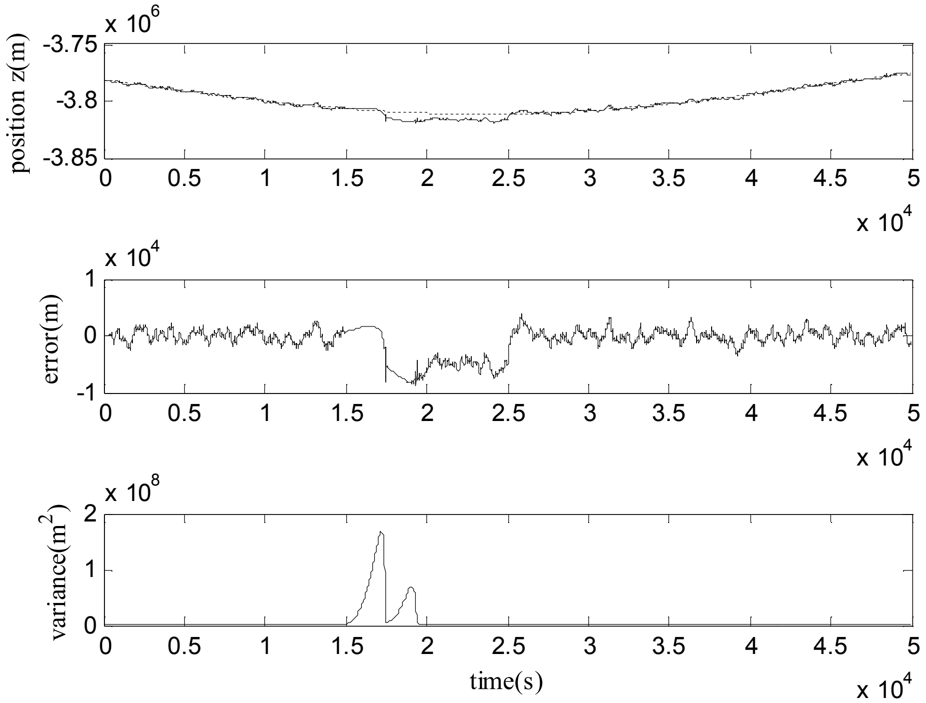

Figure C.18 : Z position est. via RUKF with SMNSF in case of cont bias, SSA.

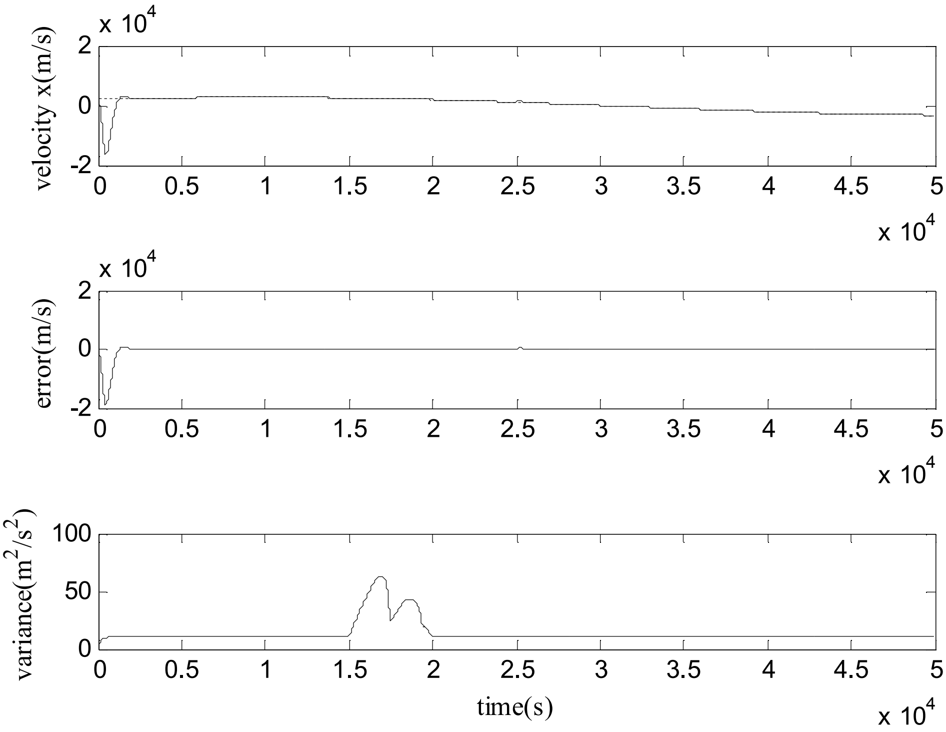

Figure C.19 : X velocity est. via RUKF with SMNSF in case of cont bias, SSA.

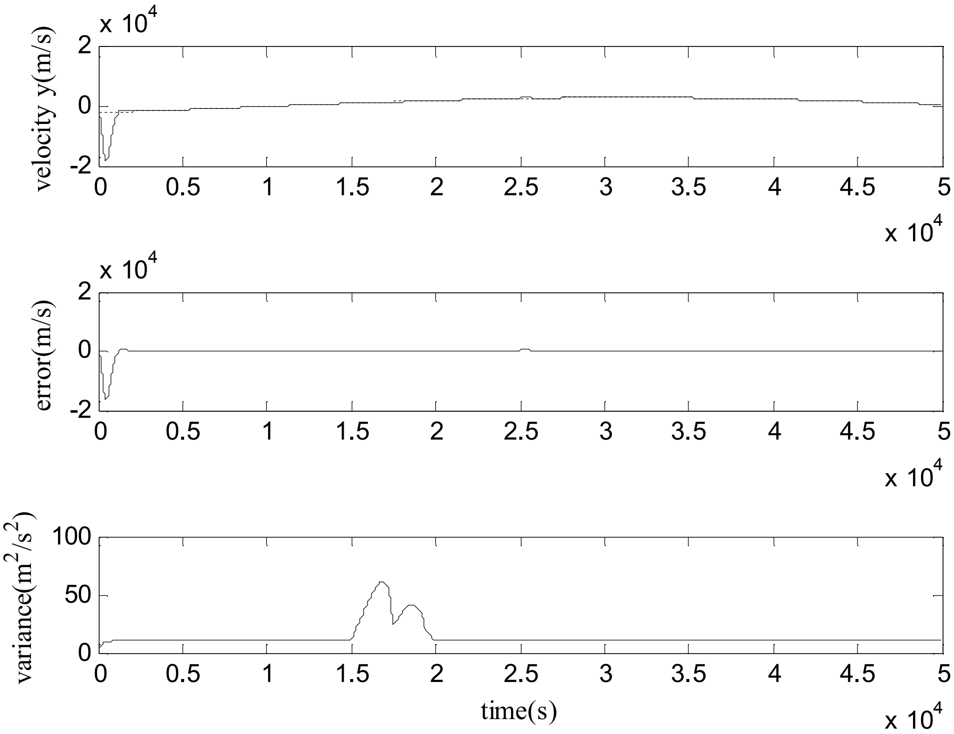

Figure C.20 : Y velocity est. via RUKF with SMNSF in case of cont bias, SSA.

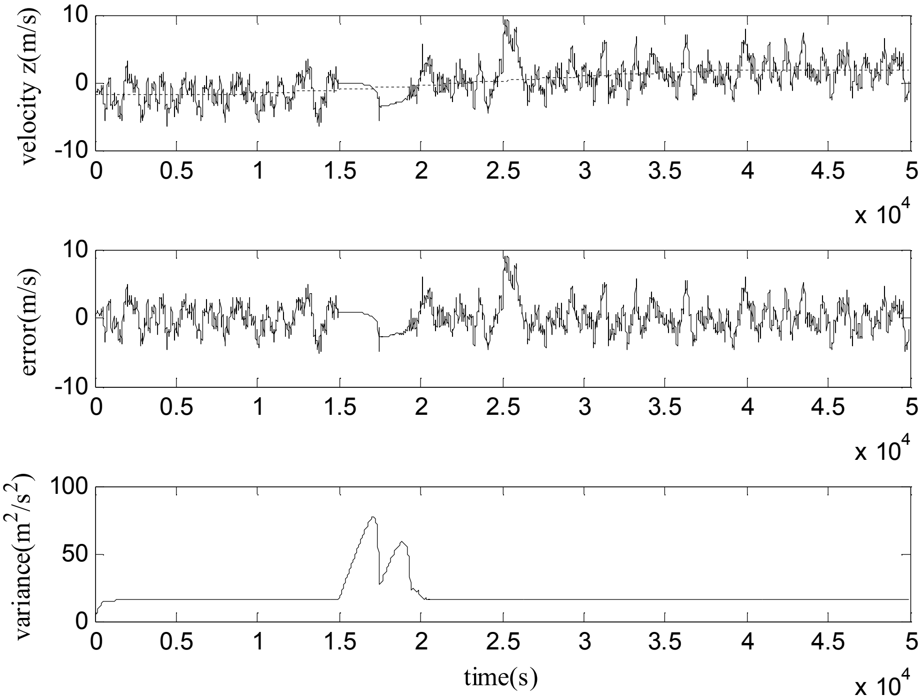

Figure C.21 : Z velocity est. via RUKF with SMNSF in case of cont bias, SSA.

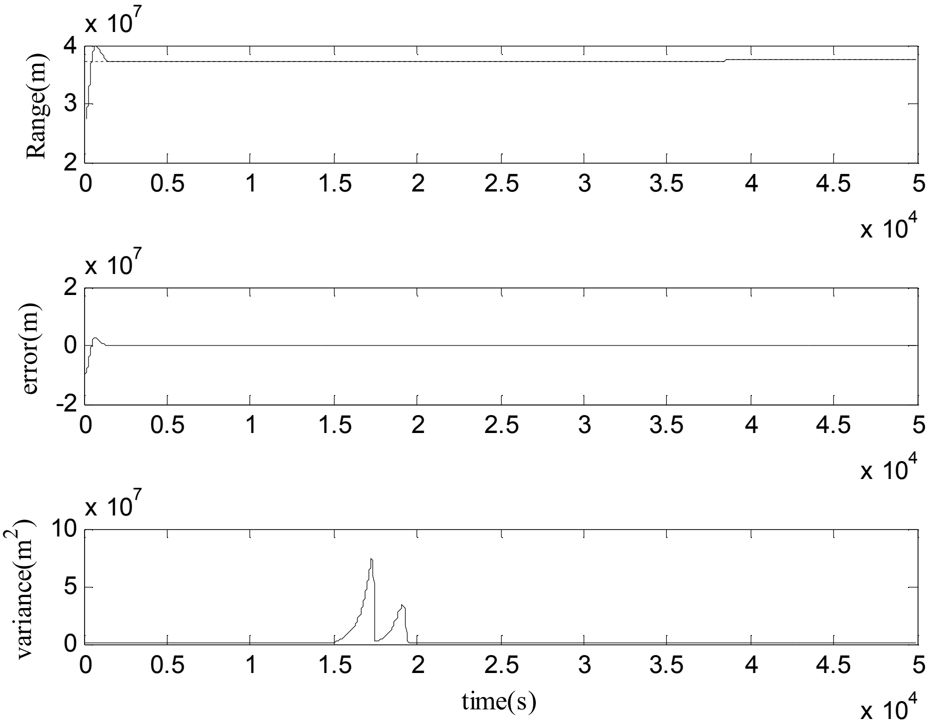

Figure C.22 : Range via RUKF with SMNSF in case of cont bias, SSA.

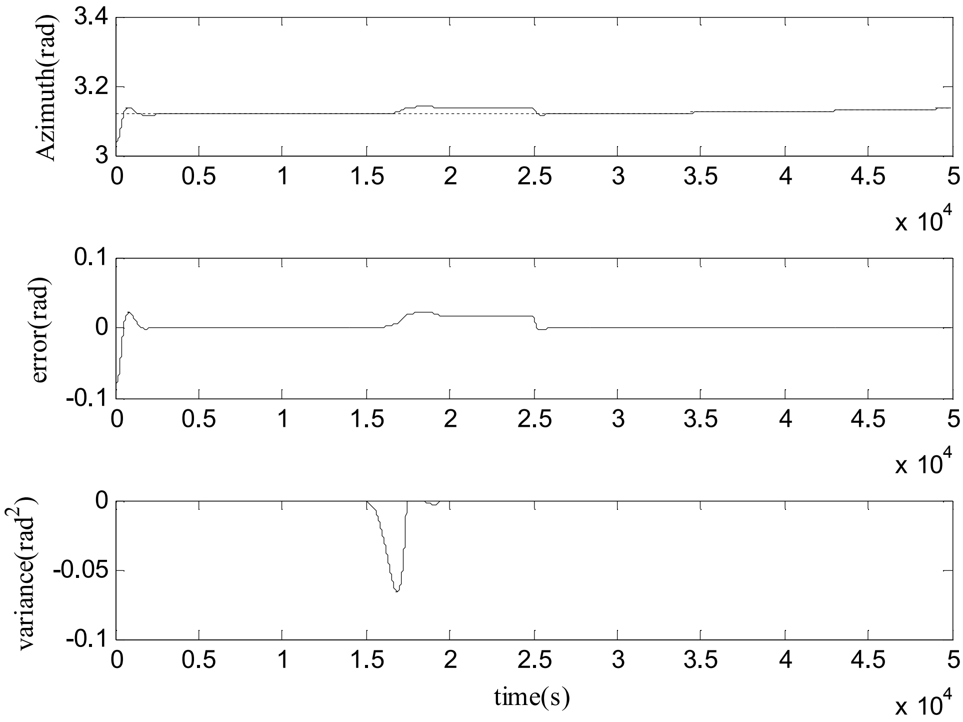

Figure C.23 : Azimuth via RUKF with SMNSF in case of cont bias, SSA.

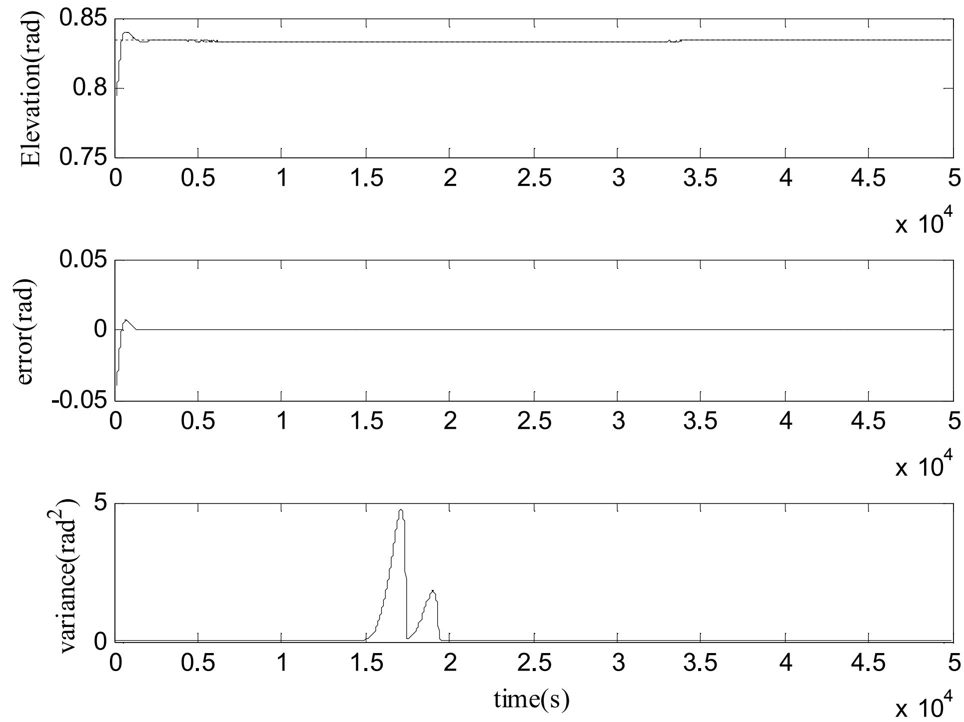

Figure C.24 : Elevation via RUKF with SMNSF in case of cont bias, SSA.

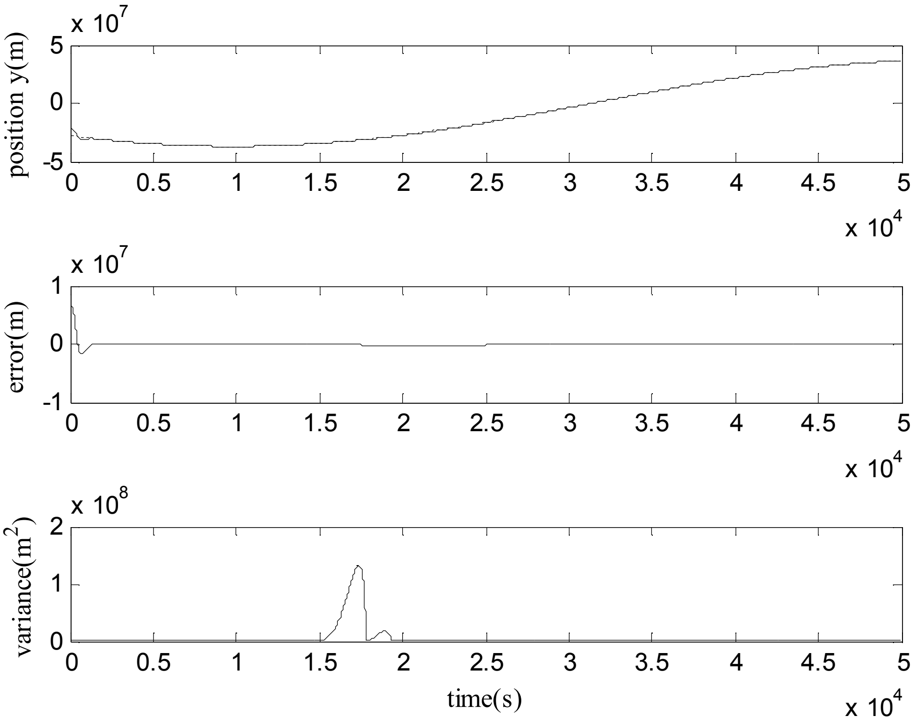

Figure C.25 : Y position est. via RUKF with MMNSF in case of cont bias, SSA.

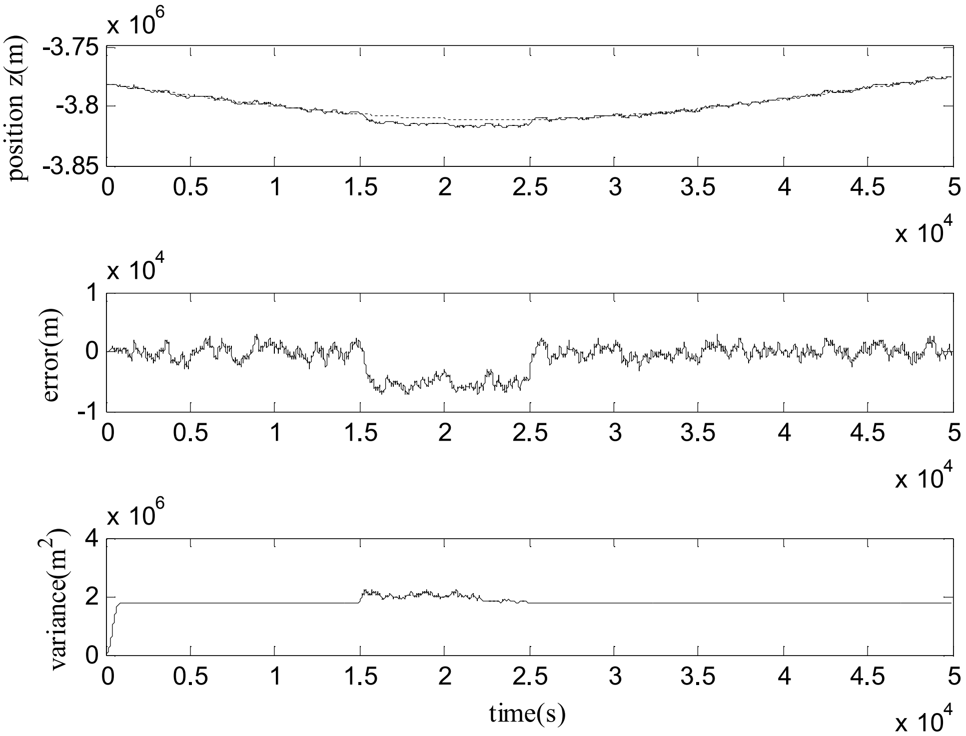

Figure C.26 : Z position est. via RUKF with MMNSF in case of cont bias, SSA.

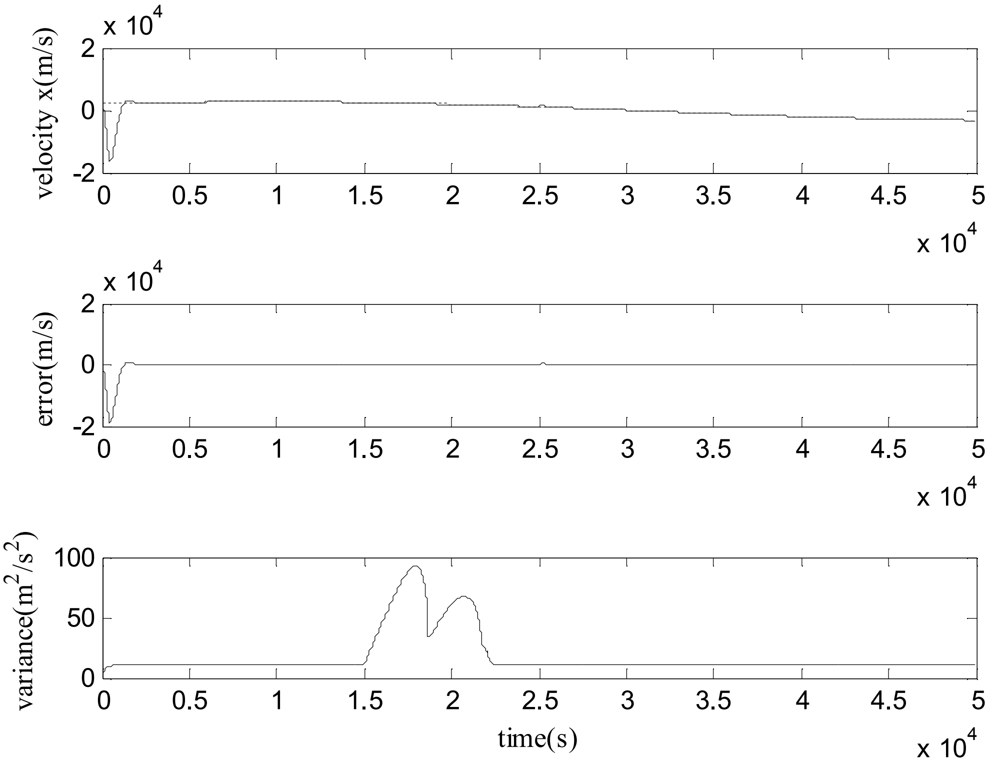

Figure C.27 : X velocity est. via RUKF with MMNSF in case of cont bias, SSA.

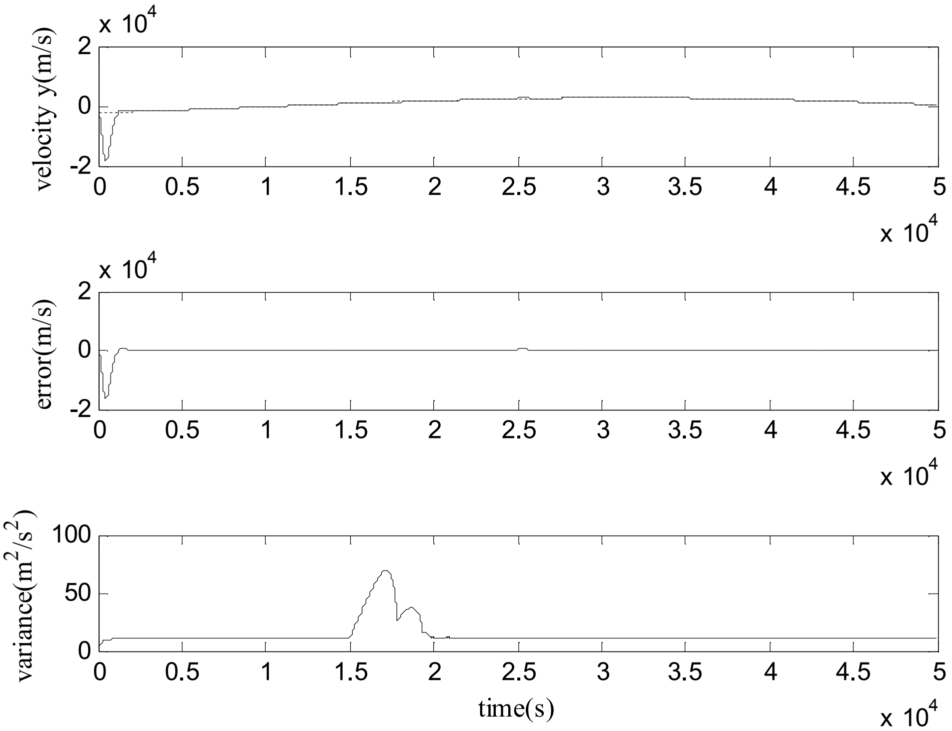

Figure C.28 : Y velocity est. via RUKF with MMNSF in case of cont bias, SSA.

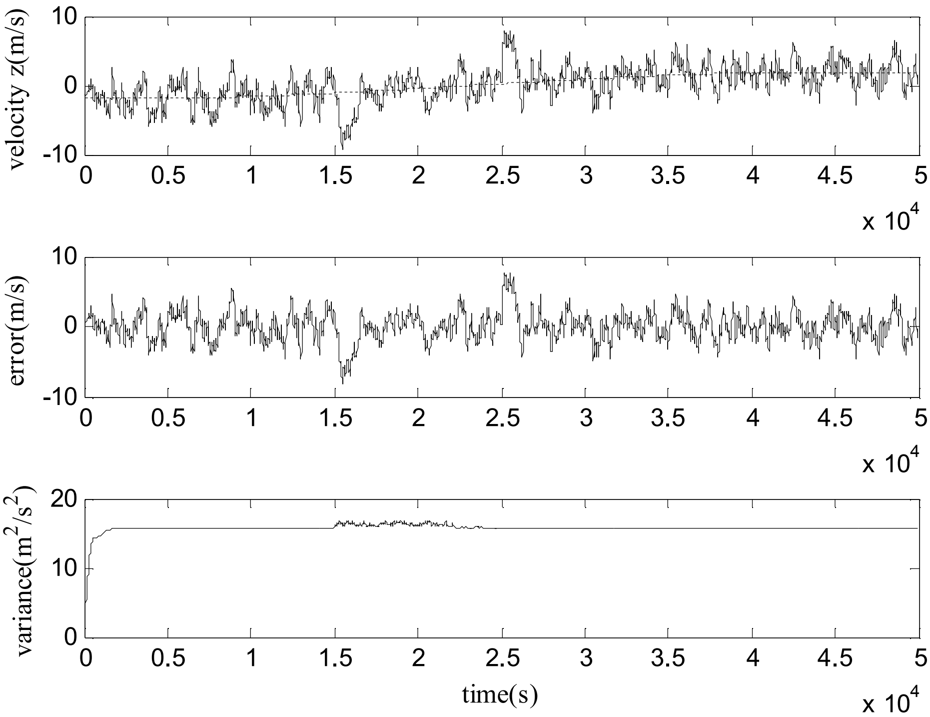

Figure C.29 : Z velocity est. via RUKF with MMNSF in case of cont bias, SSA.

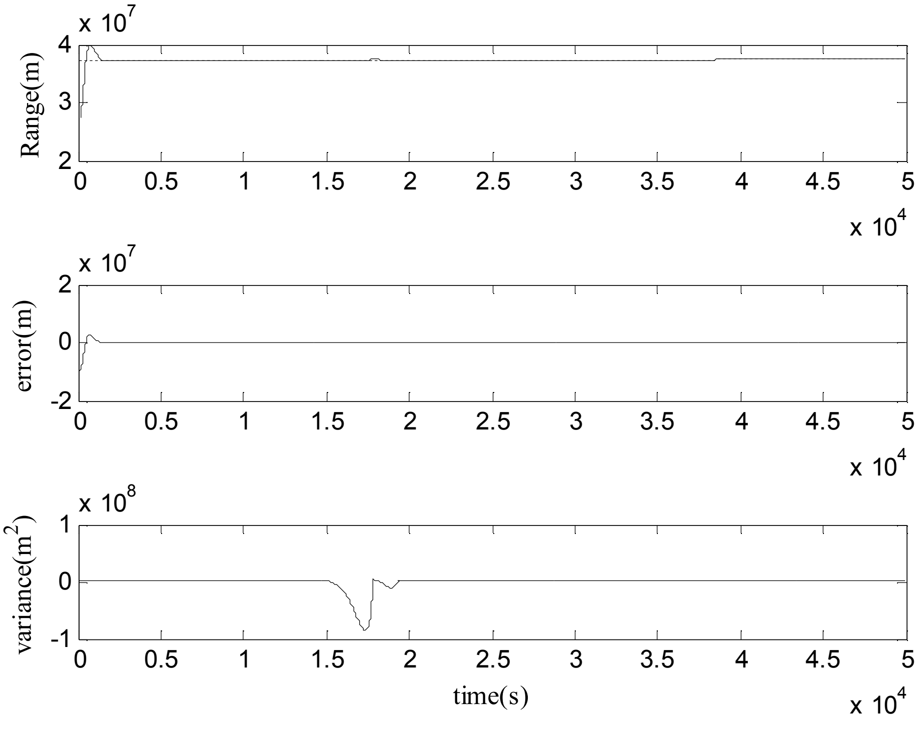

Figure C.30 : Range via RUKF with MMNSF in case of cont bias, SSA.

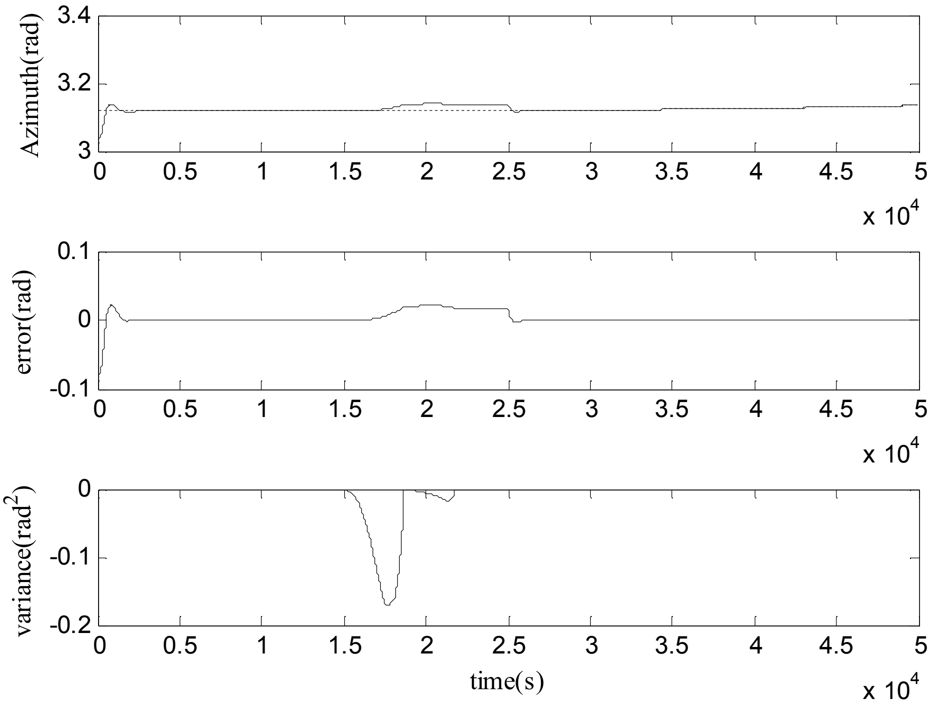

Figure C.31 : Azimuth via RUKF with MMNSF in case of cont bias, SSA.

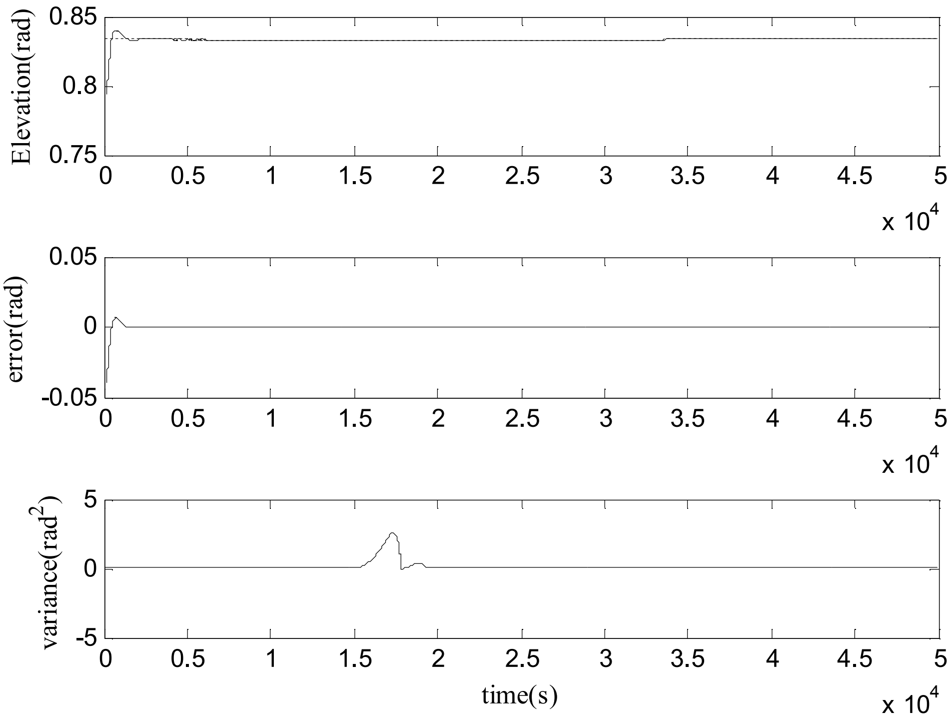

Figure C.32 : Elevation via RUKF with MMNSF in case of cont bias, SSA.

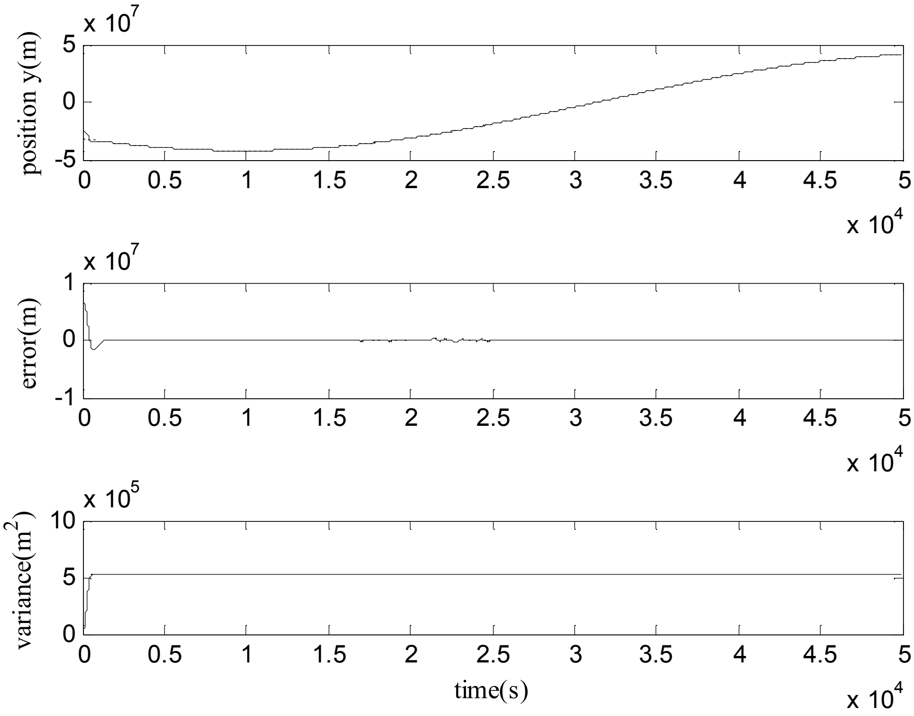

Figure C.33 : Y position est. via Regular UKF in case of noise inc, SSA.

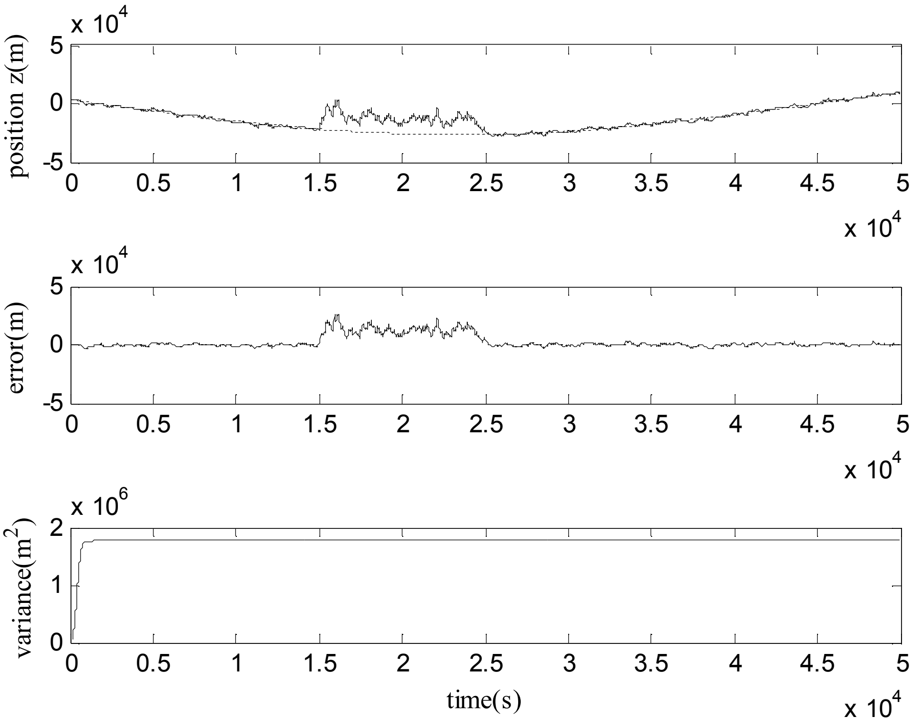

Figure C.34 : Z position est. via Regular UKF in case of noise inc, SSA.

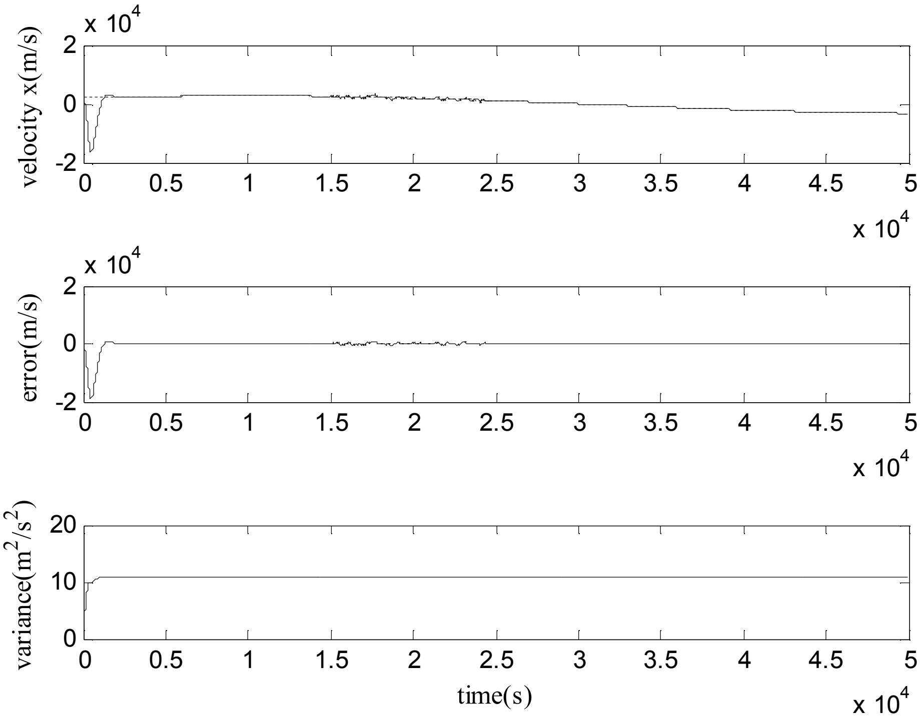

Figure C.35 : X velocity est. via Regular UKF in case of noise inc, SSA.

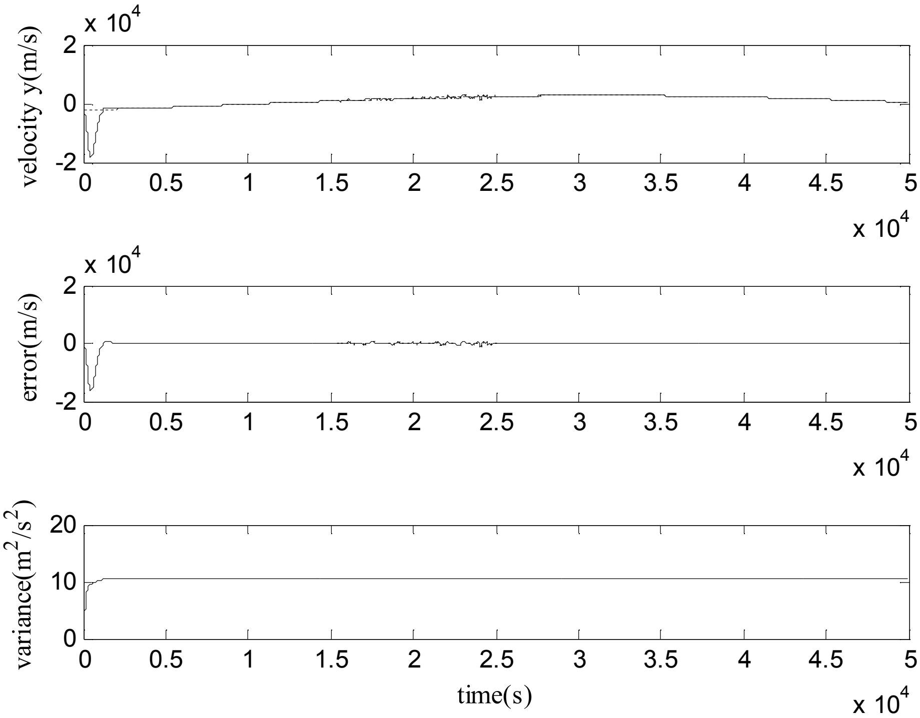

Figure C.36 : Y velocity est. via Regular UKF in case of noise inc, SSA.

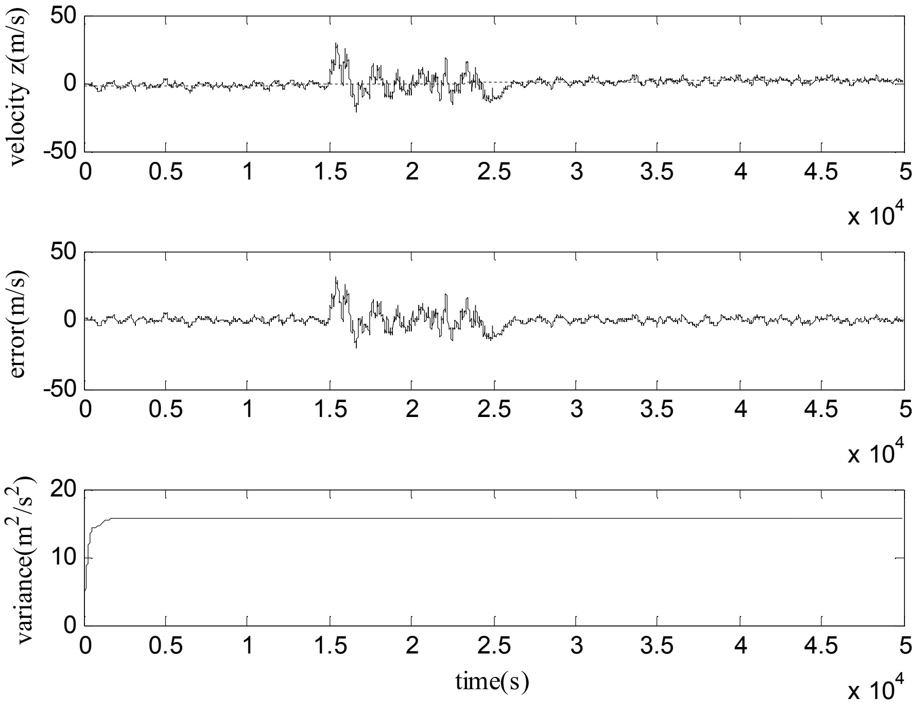

Figure C.37 : Z velocity est. via Regular UKF in case of noise inc, SSA.

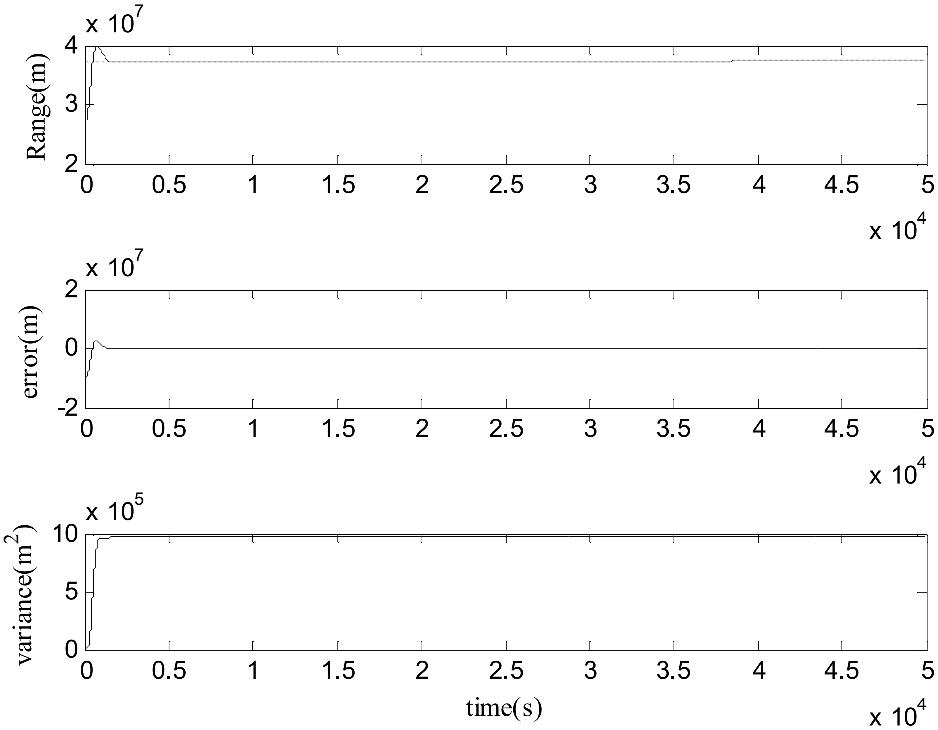

Figure C.38 : Range via Regular UKF in case of noise inc, SSA.

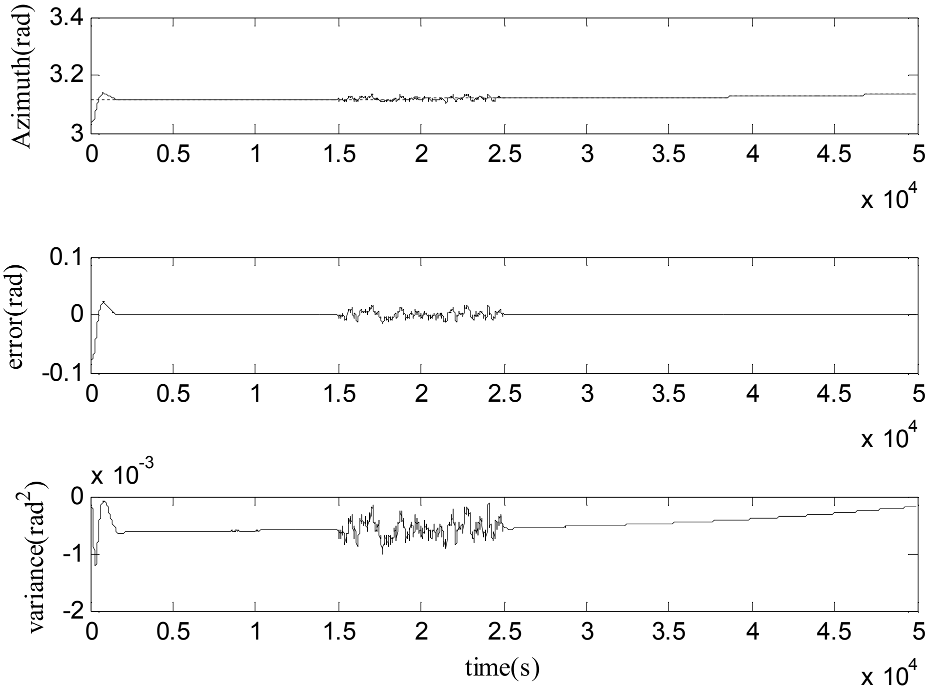

Figure C.39 : Azimuth via Regular UKF in case of noise inc, SSA.

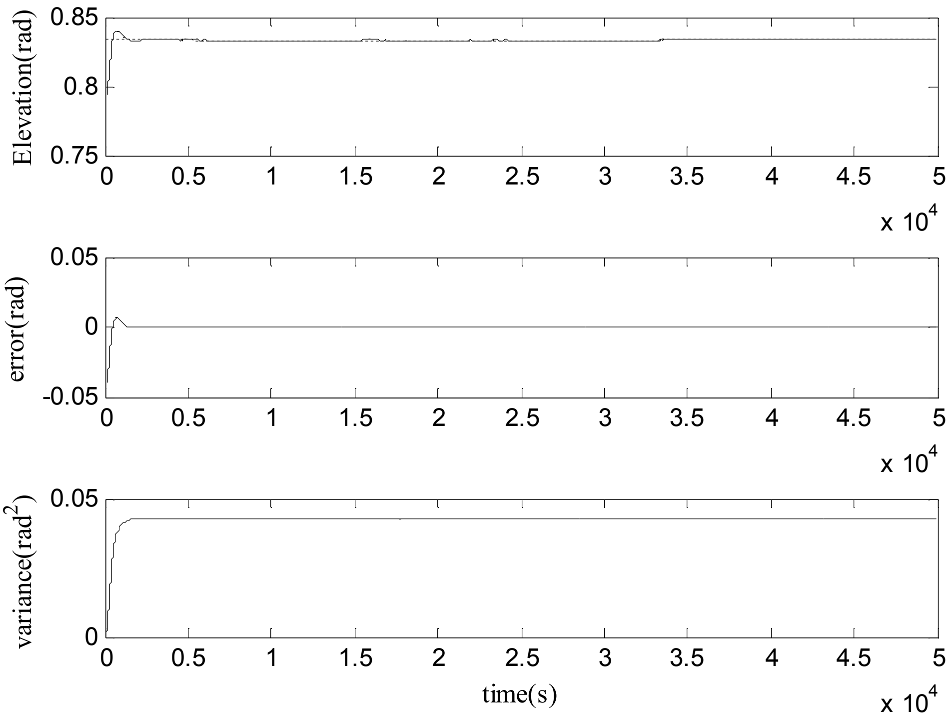

Figure C.40 : Elevation via Regular UKF in case of noise inc, SSA.

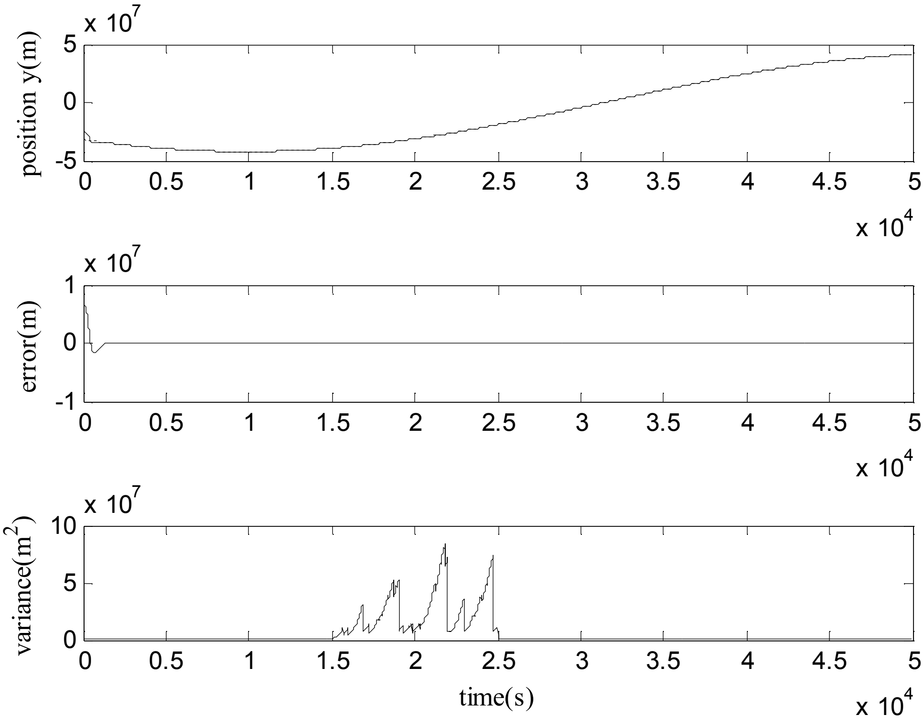

Figure C.41 : Y position est. via RUKF with SMNSF in case of noise inc, SSA.

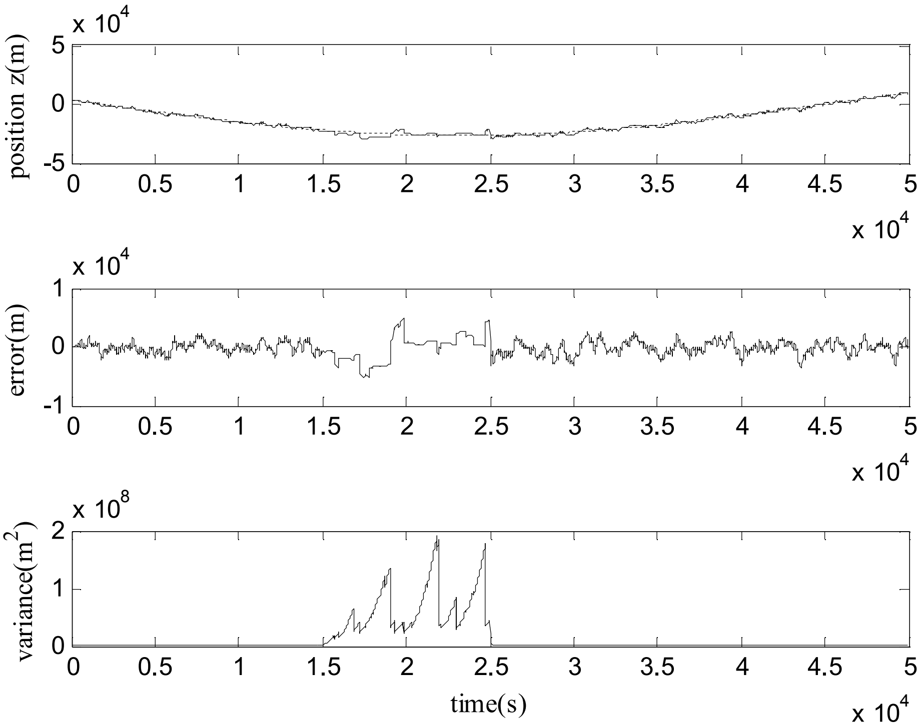

Figure C.42 : Z position est. via RUKF with SMNSF in case of noise inc, SSA.

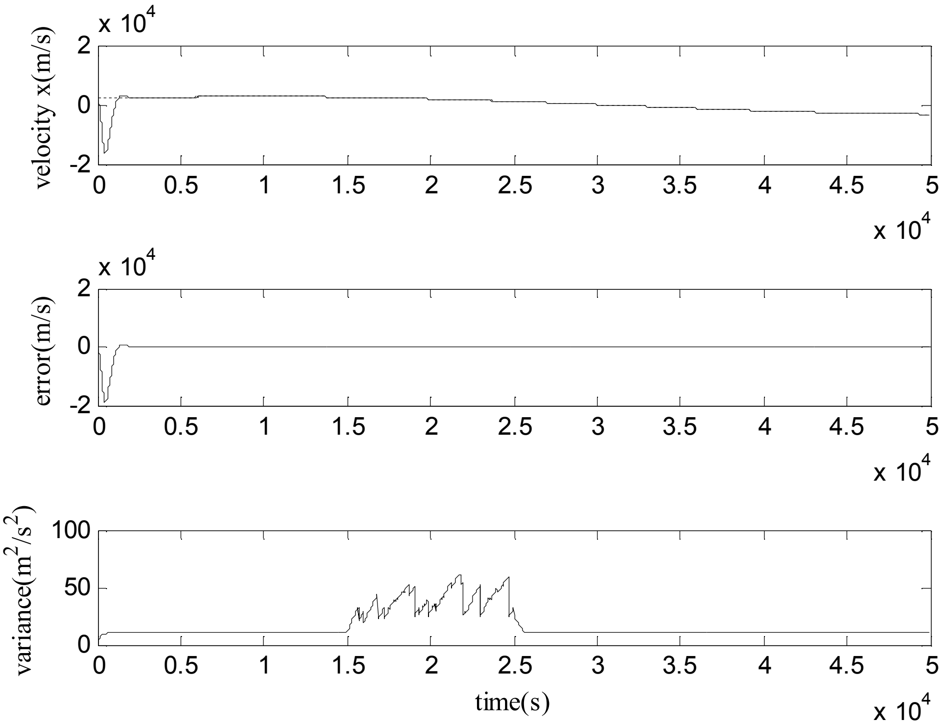

Figure C.43 : X velocity est. via RUKF with SMNSF in case of noise inc, SSA.

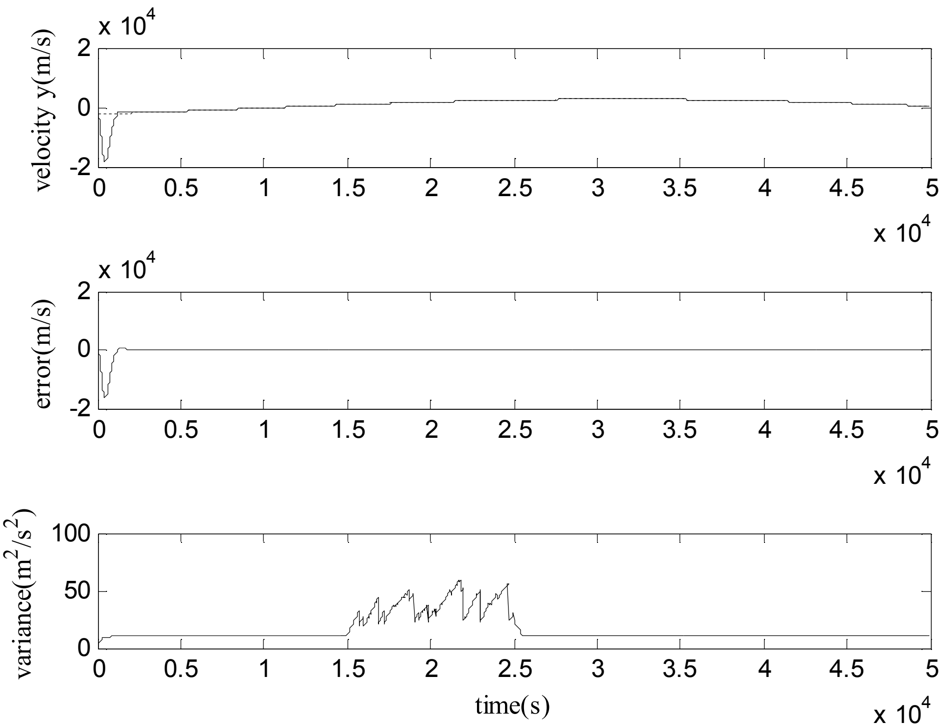

Figure C.44 : Y velocity est. via RUKF with SMNSF in case of noise inc, SSA.

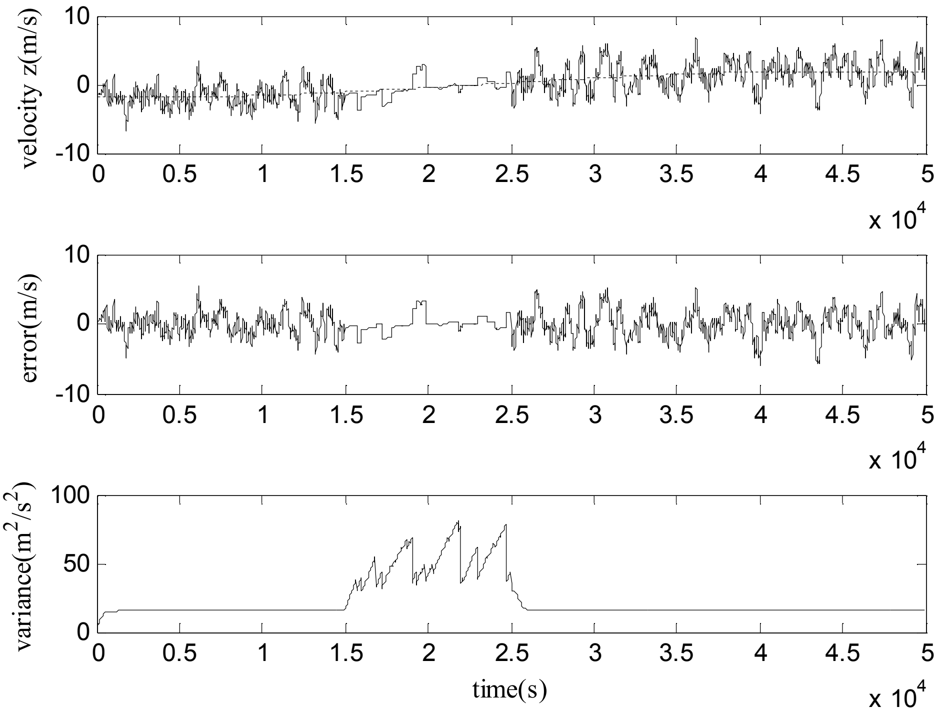

Figure C.45 : Z velocity est. via RUKF with SMNSF in case of noise inc, SSA.

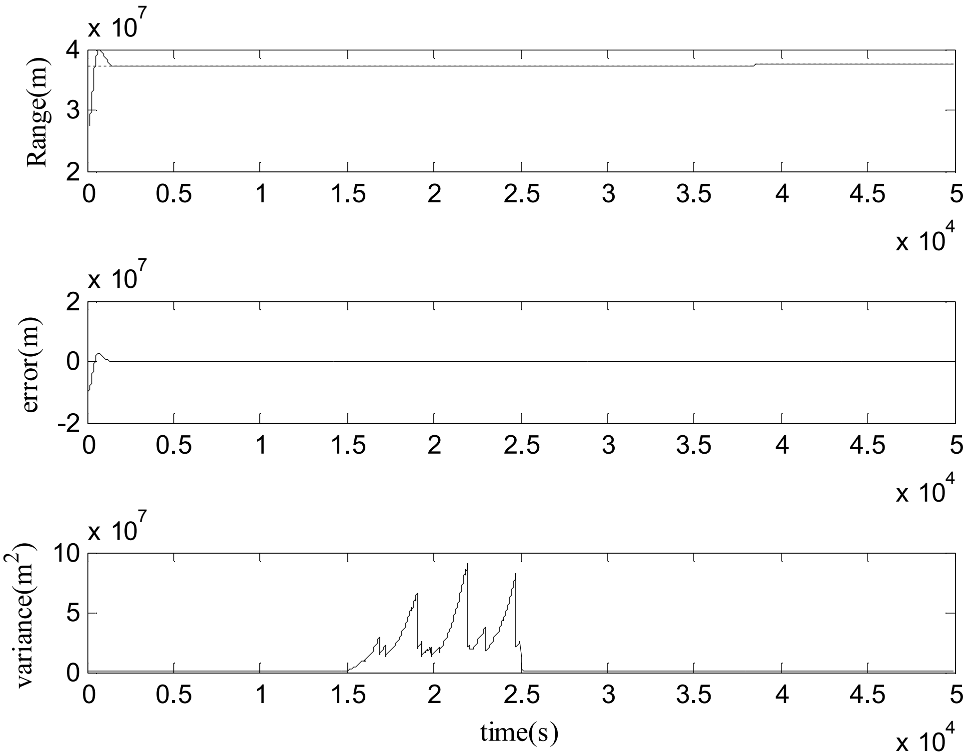

Figure C.46 : Range via RUKF with SMNSF in case of noise inc, SSA.

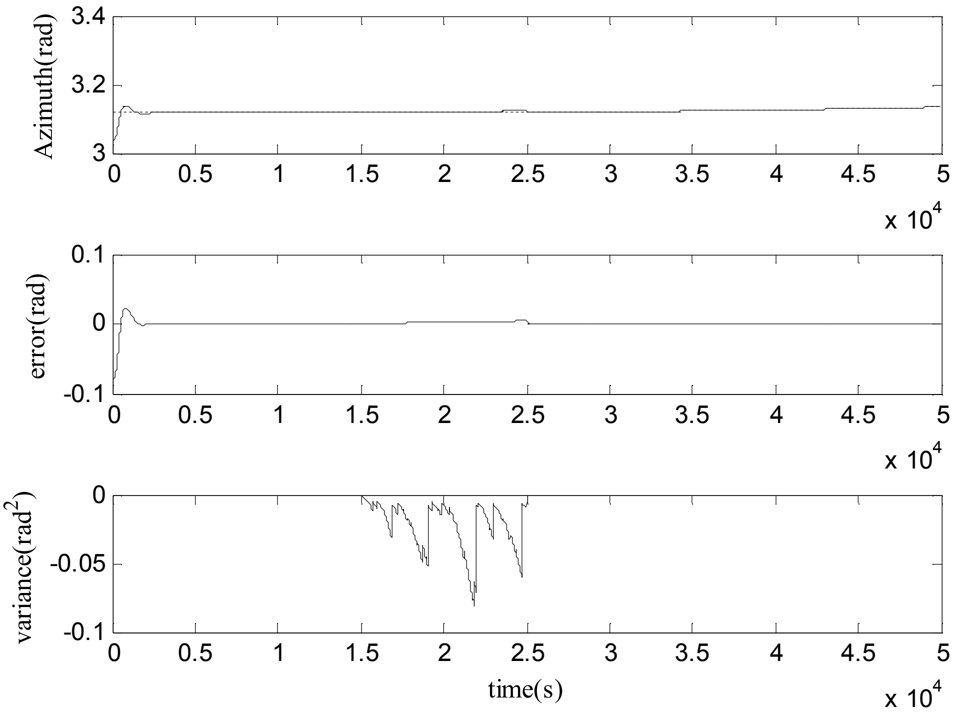

Figure C.47 : Azimuth via RUKF with SMNSF in case of noise inc, SSA.

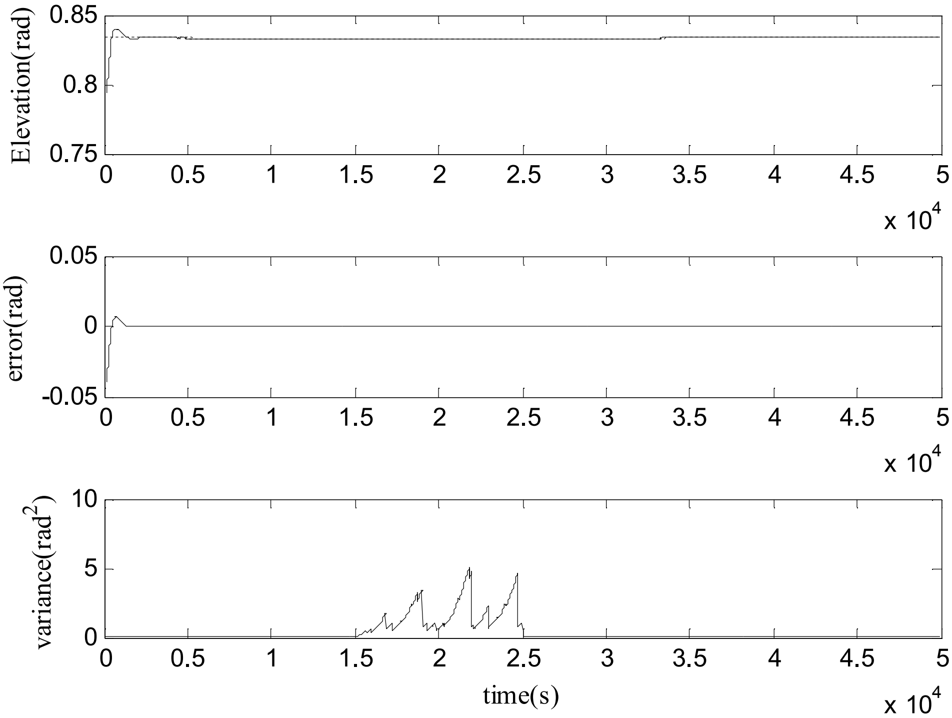

Figure C.48 : Elevation via RUKF with SMNSF in case of noise inc, SSA.

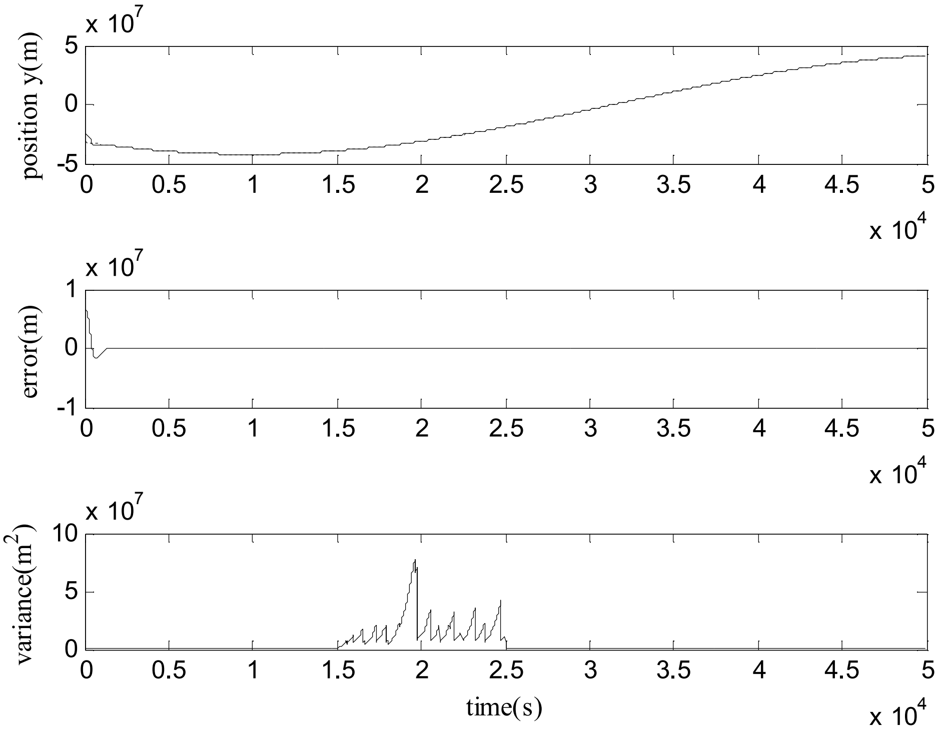

Figure C.49 : Y position est. via RUKF with MMNSF in case of noise inc, SSA.

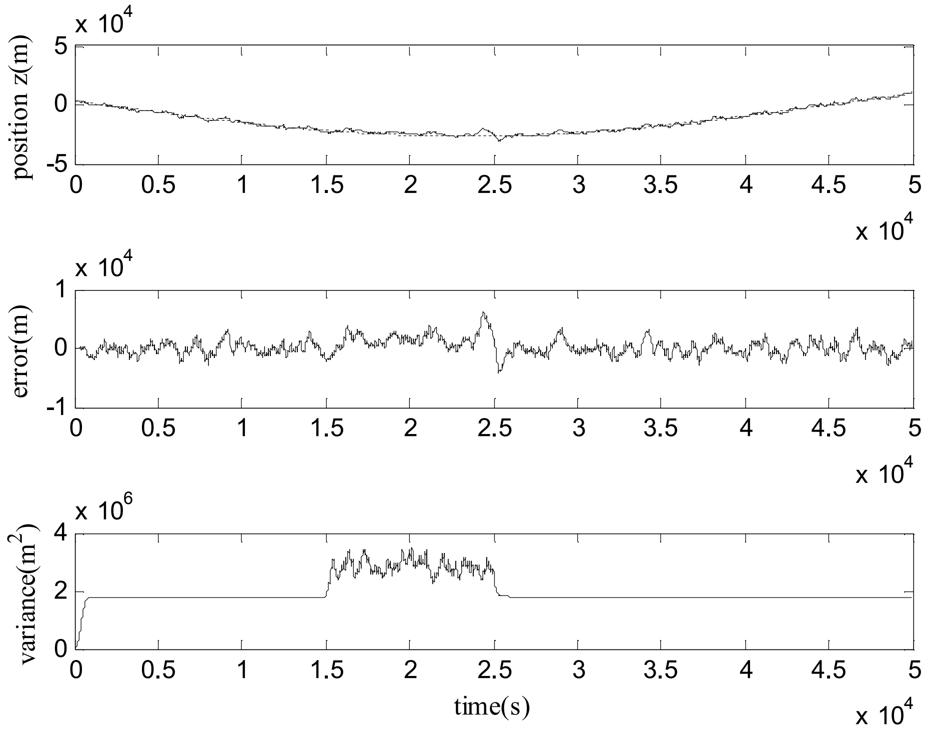

Figure C.50 : Z position est. via RUKF with MMNSF in case of noise inc, SSA.

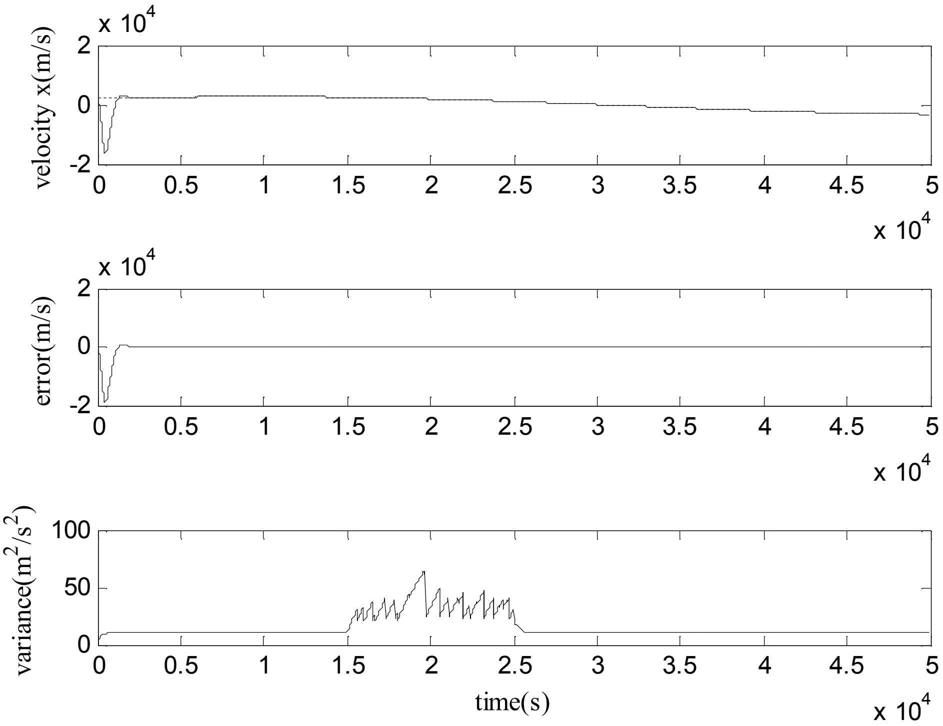

Figure C.51 : X velocity est. via RUKF with MMNSF in case of noise inc, SSA.

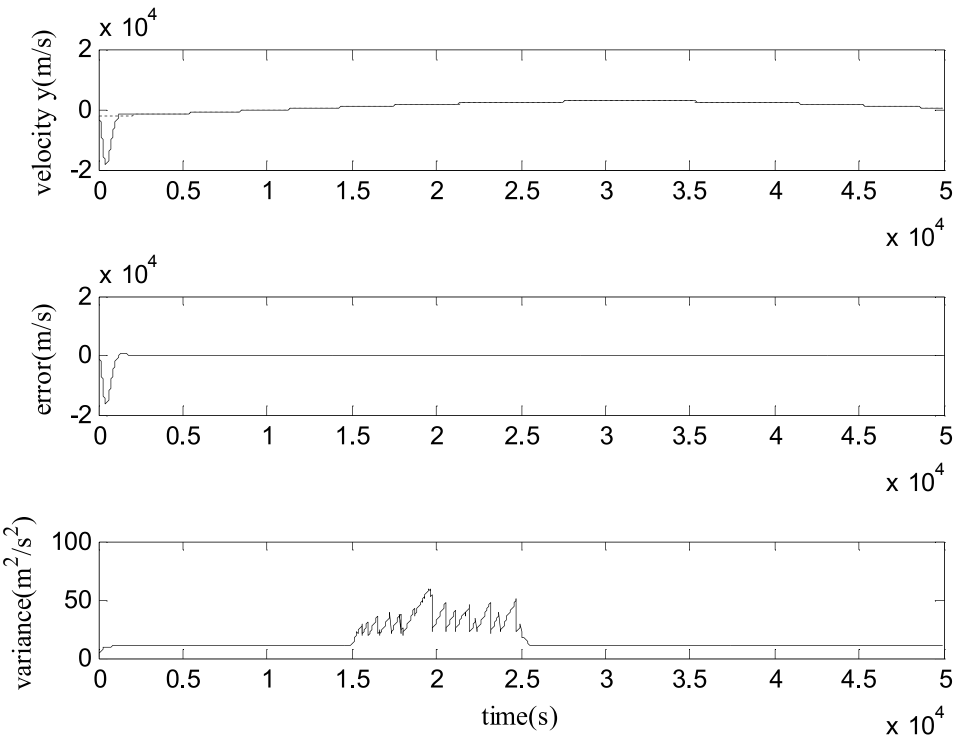

Figure C.52 : Y velocity est. via RUKF with MMNSF in case of noise inc, SSA.

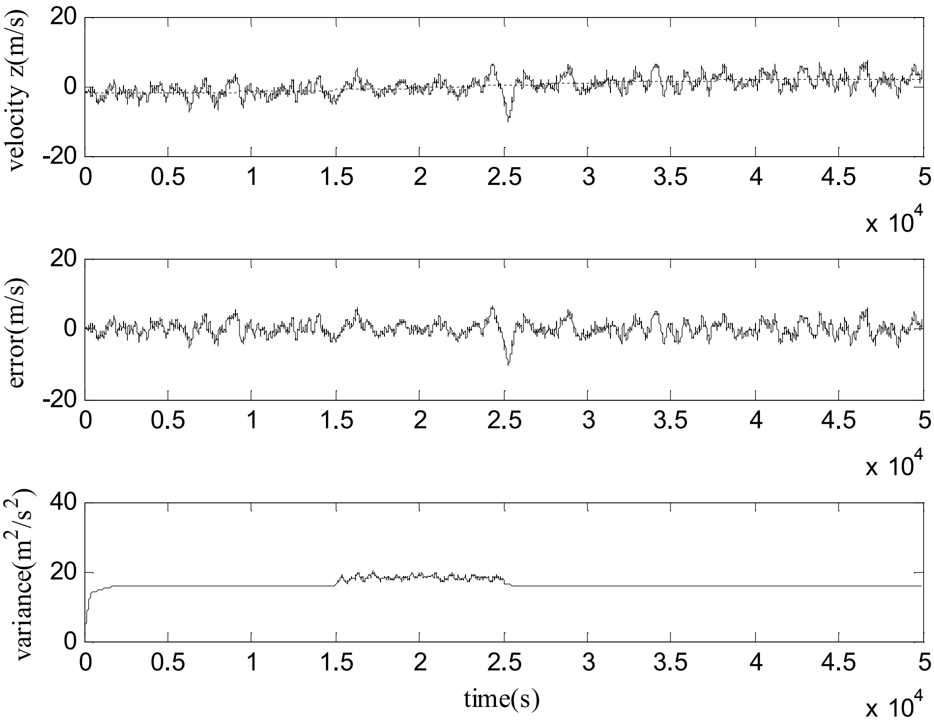

Figure C.53 : Z velocity est. via RUKF with MMNSF in case of noise inc, SSA.

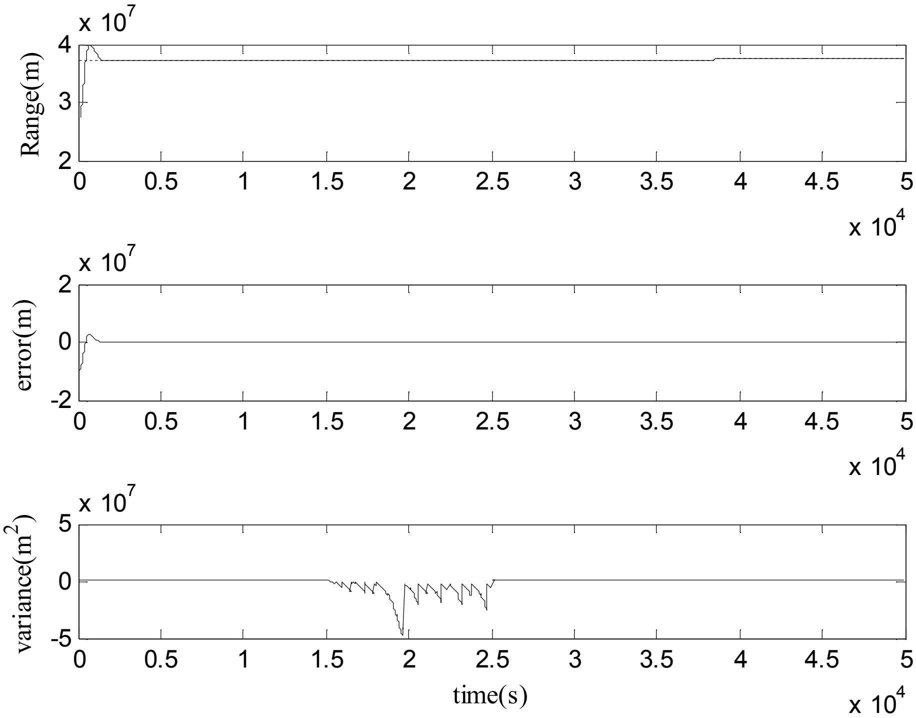

Figure C.54 : Range via RUKF with MMNSF in case of noise inc, SSA.

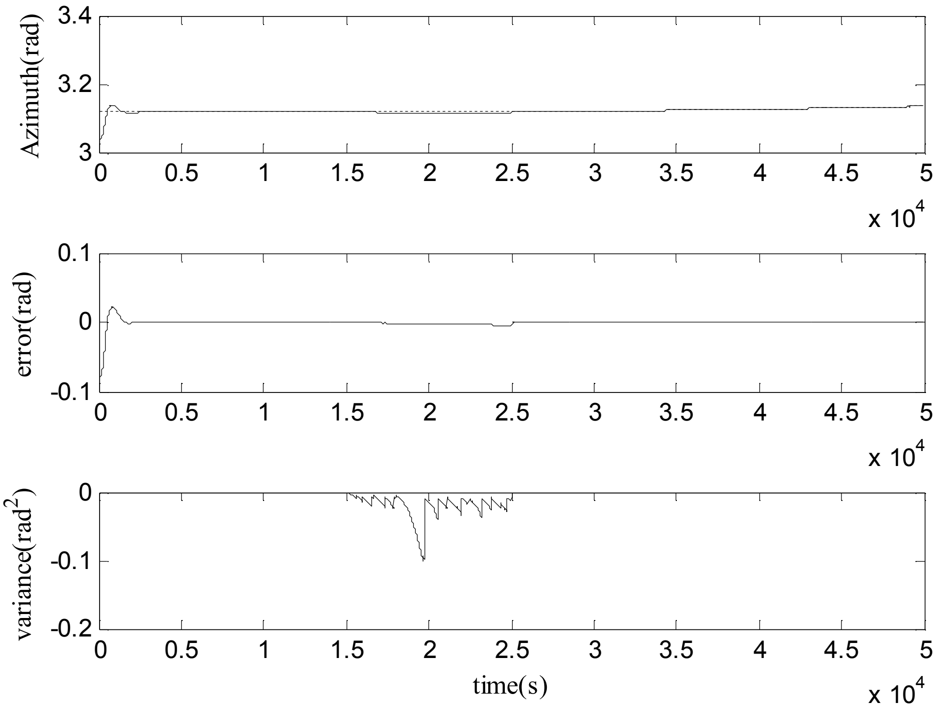

Figure C.55 : Azimuth via RUKF with MMNSF in case of noise inc, SSA.

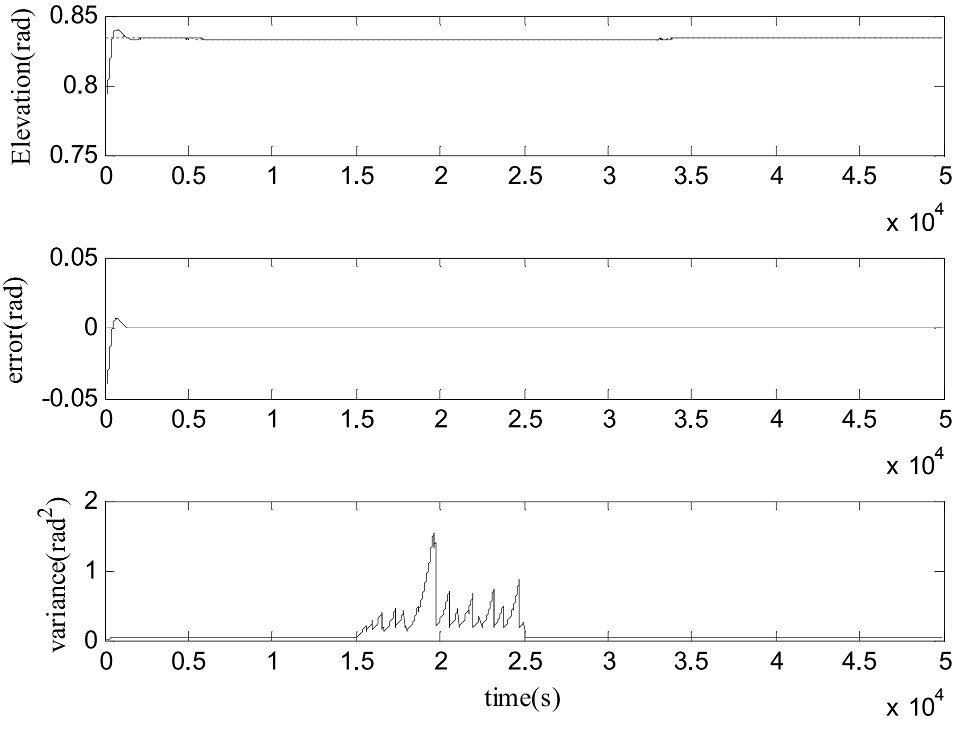

Figure C.56 : Elevation via RUKF with MMNSF in case of noise inc, SSA.

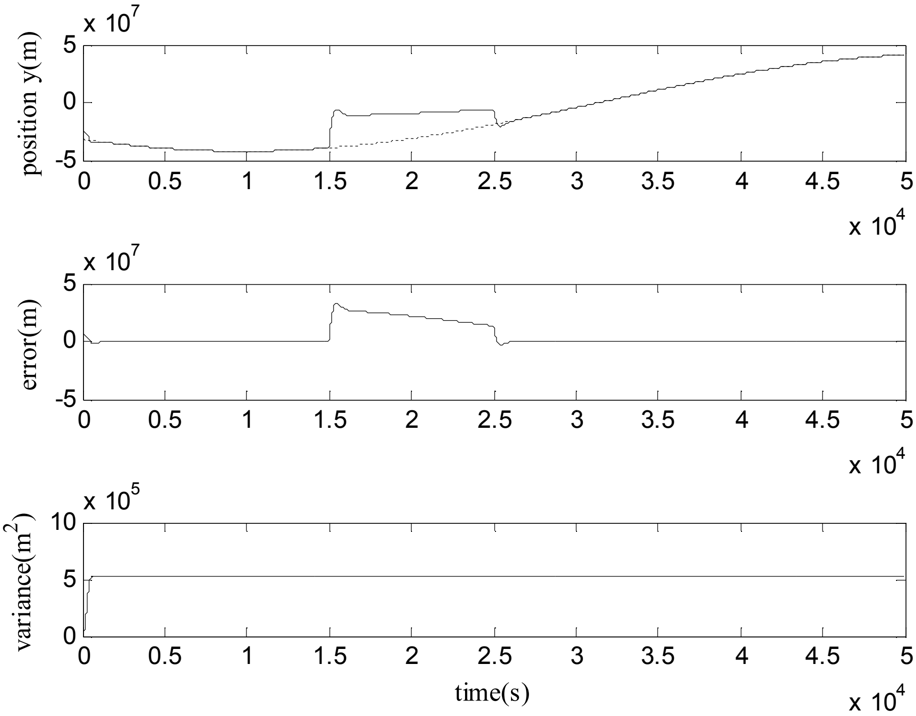

Figure C.57 : Y position est. via Regular UKF in case of zero out, SSA.

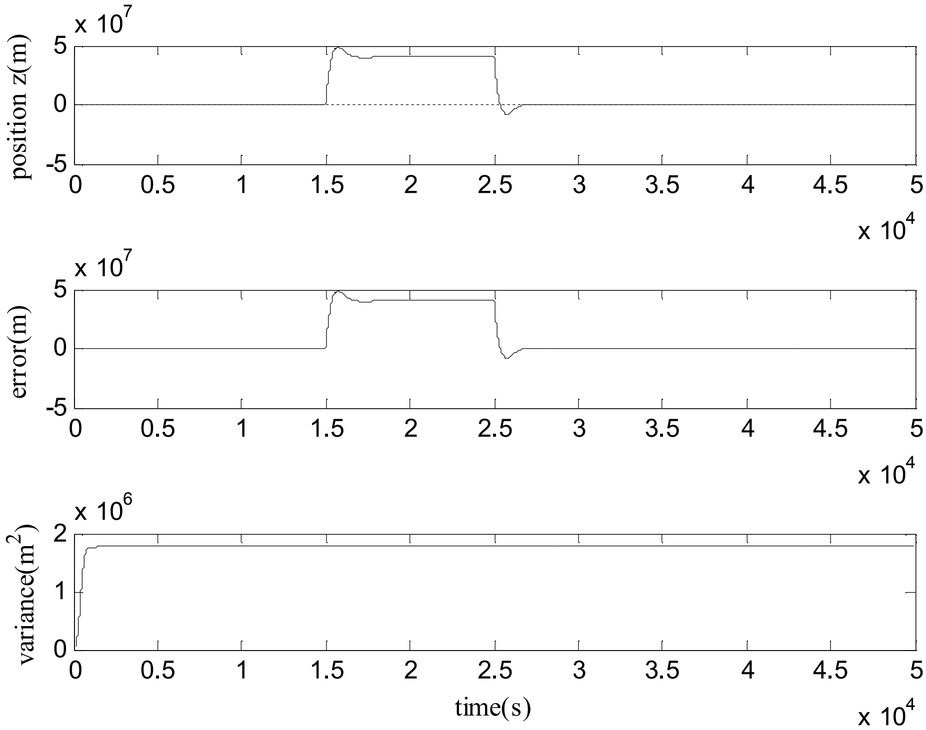

Figure C.58 : Z position est. via Regular UKF in case of zero out, SSA.

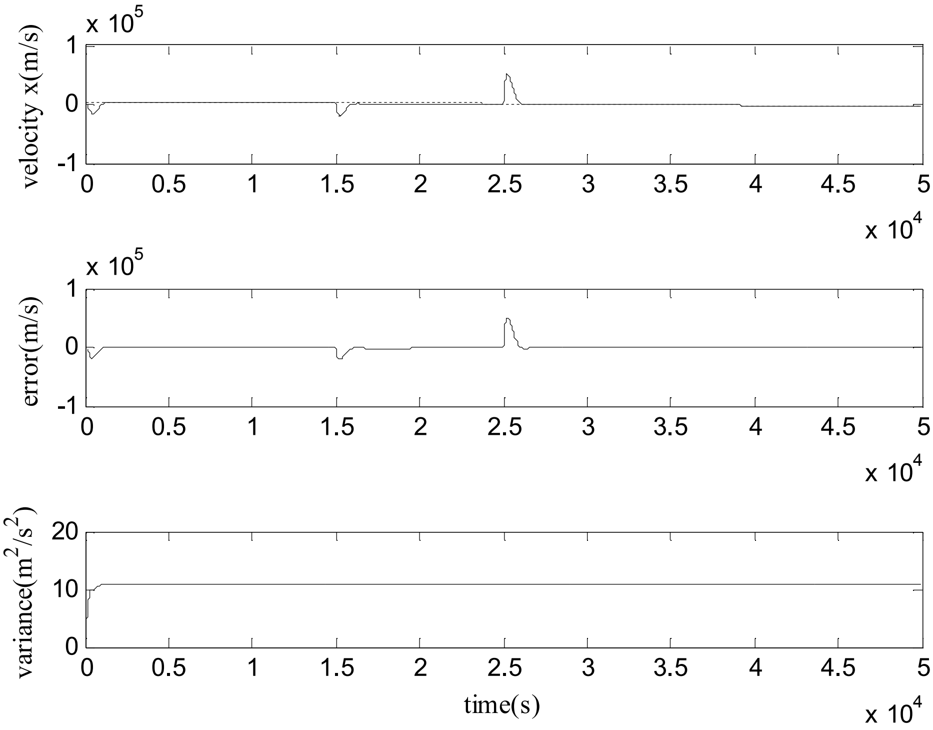

Figure C.59 : X velocity est. via Regular UKF in case of zero out, SSA.

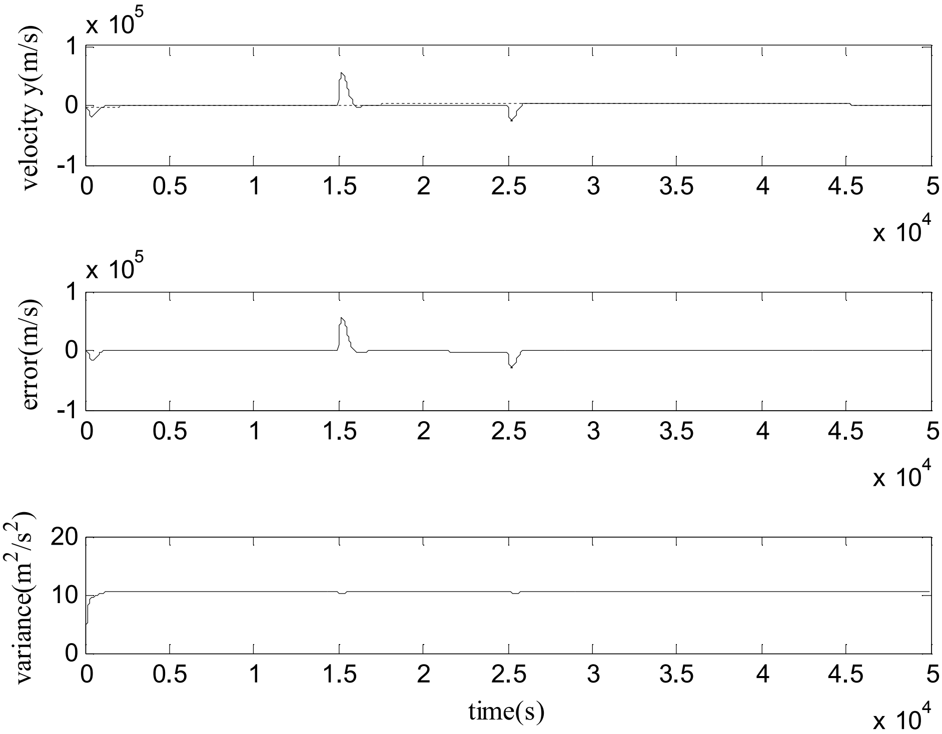

Figure C.60 : Y velocity est. via Regular UKF in case of zero out, SSA.

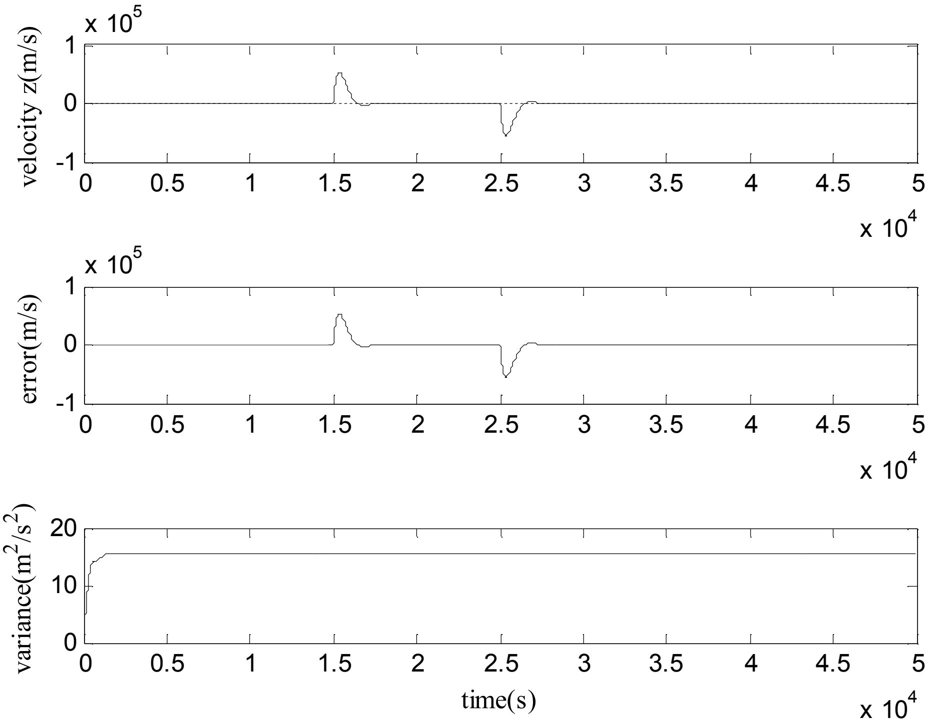

Figure C.61 : Z velocity est. via Regular UKF in case of zero out, SSA.

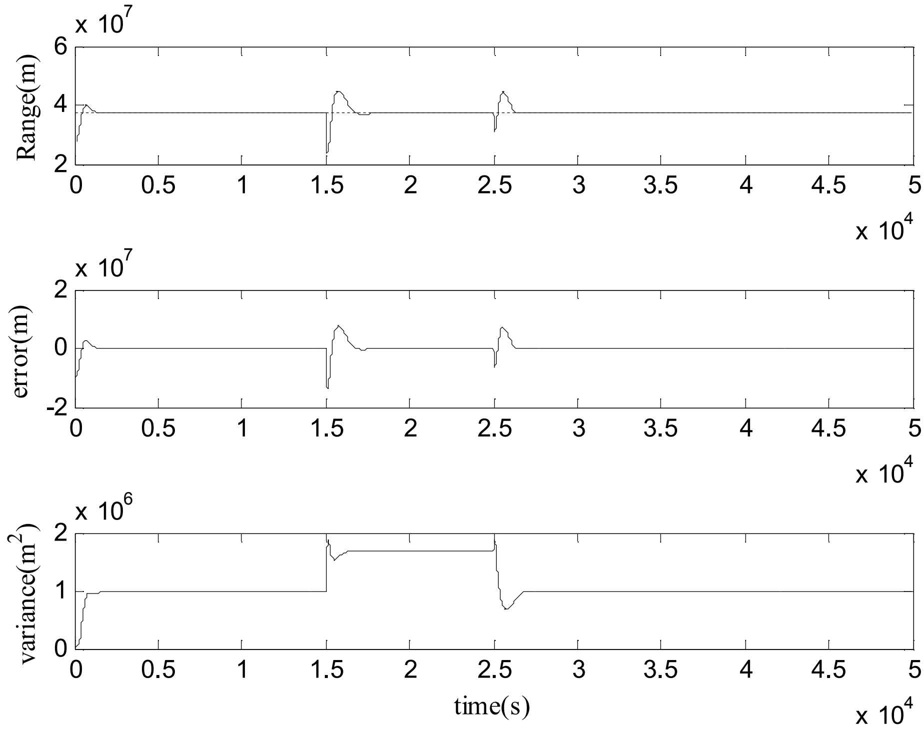

Figure C.62 : Range via Regular UKF in case of zero out, SSA.

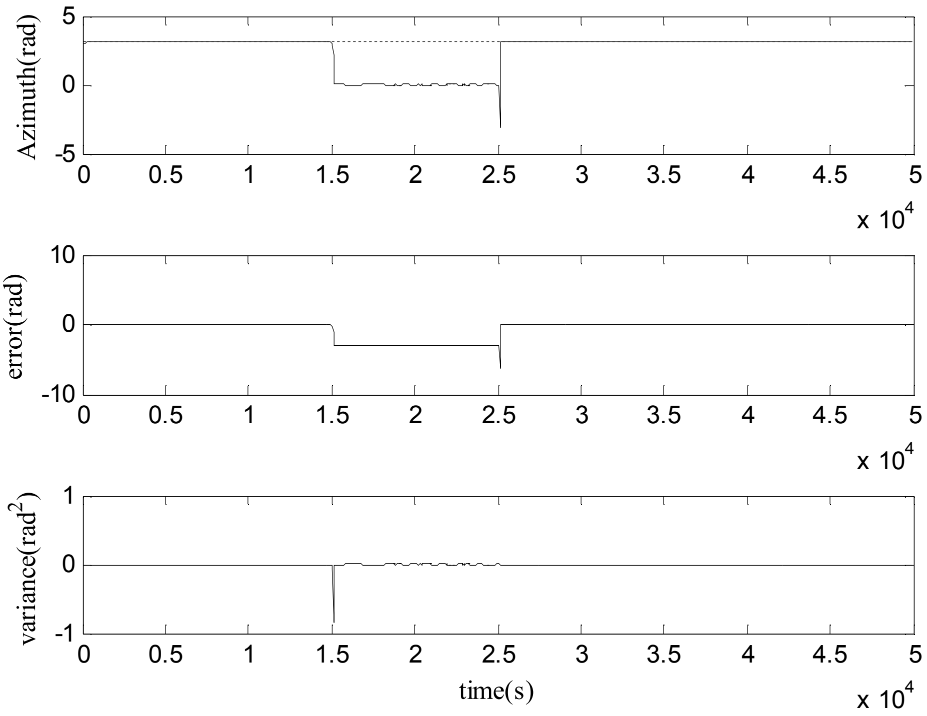

Figure C.63 : Azimuth via Regular UKF in case of zero out, SSA.

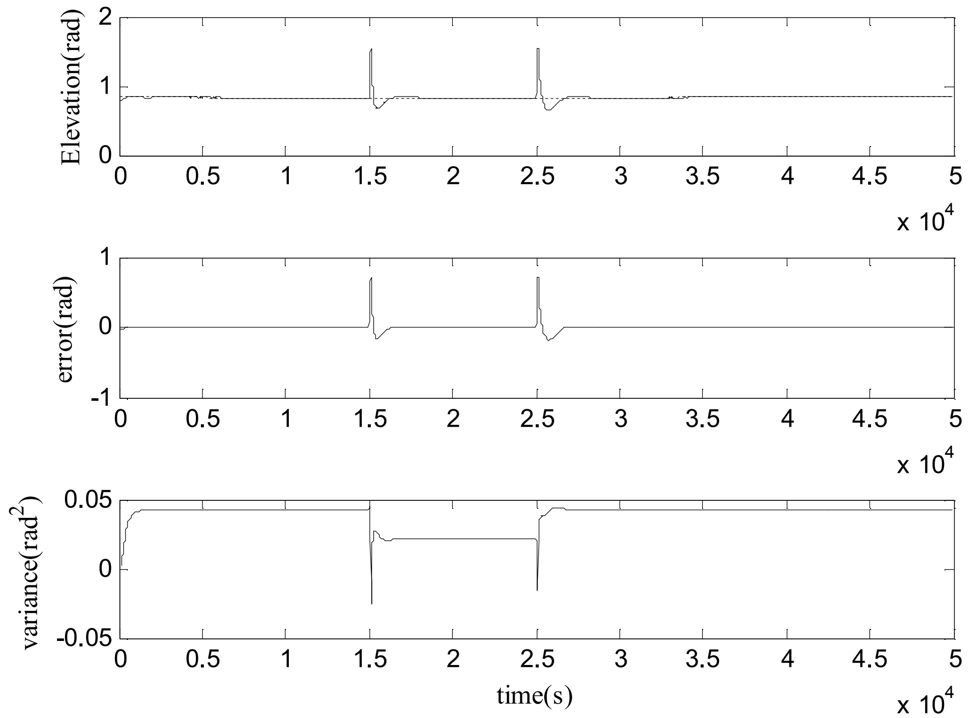

Figure C.64 : Elevation via Regular UKF in case of zero out, SSA.

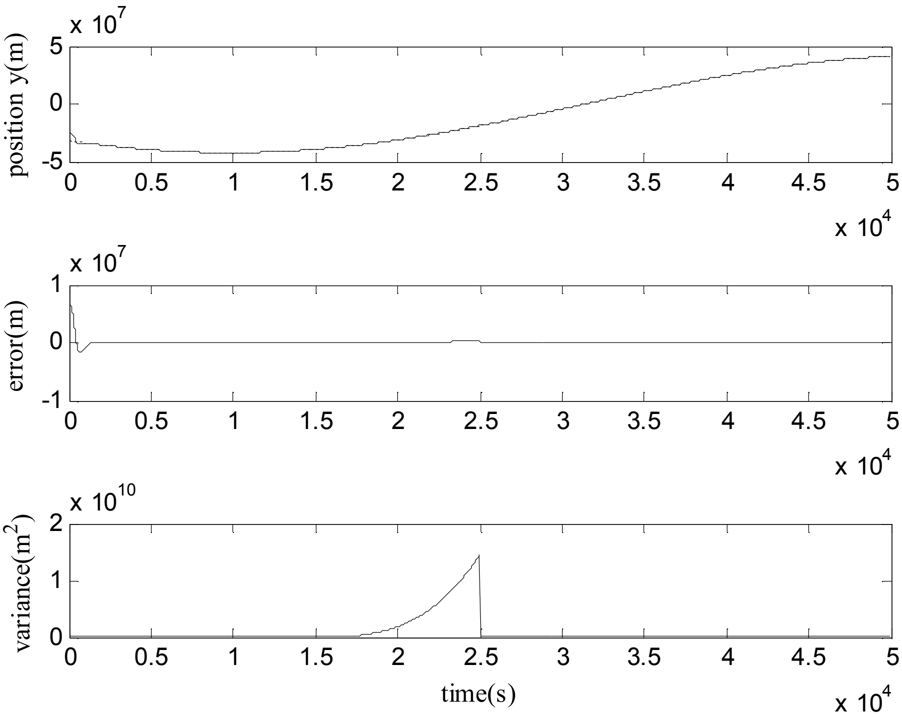

Figure C.65 : Y position est. via RUKF with SMNSF in case of zero out, SSA.

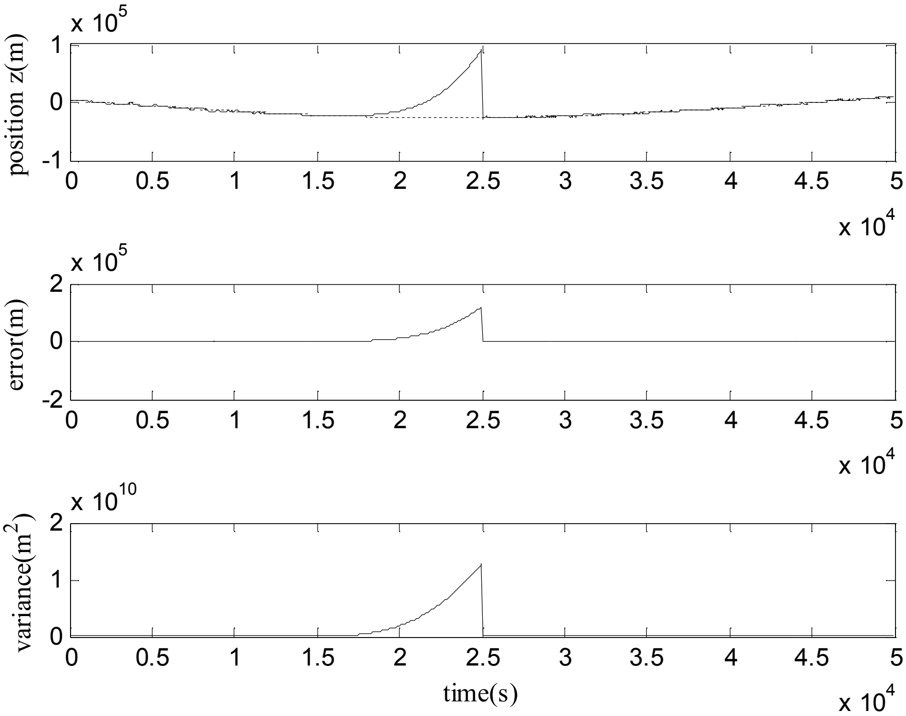

Figure C.66 : Z position est. via RUKF with SMNSF in case of zero out, SSA.

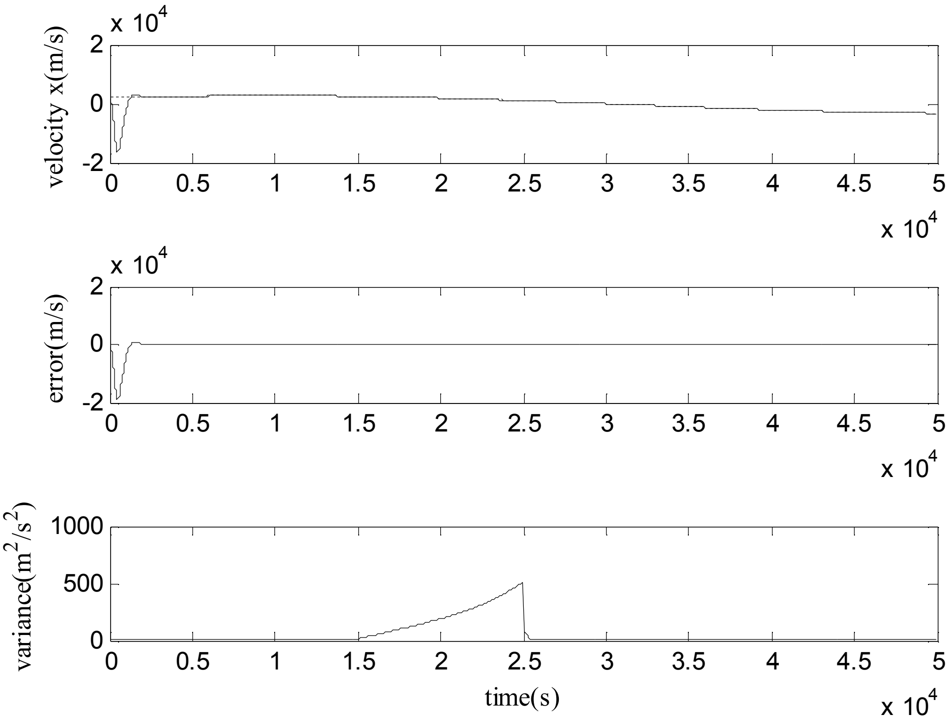

Figure C.67 : X velocity est. via RUKF with SMNSF in case of zero out, SSA.

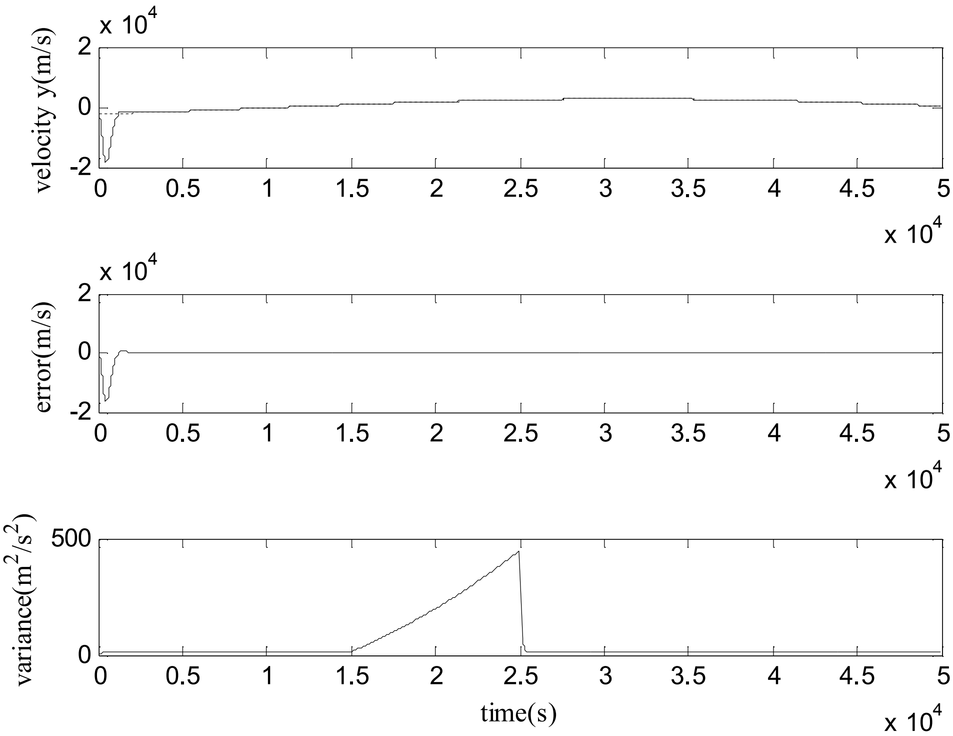

Figure C.68 : Y velocity est. via RUKF with SMNSF in case of zero out, SSA.

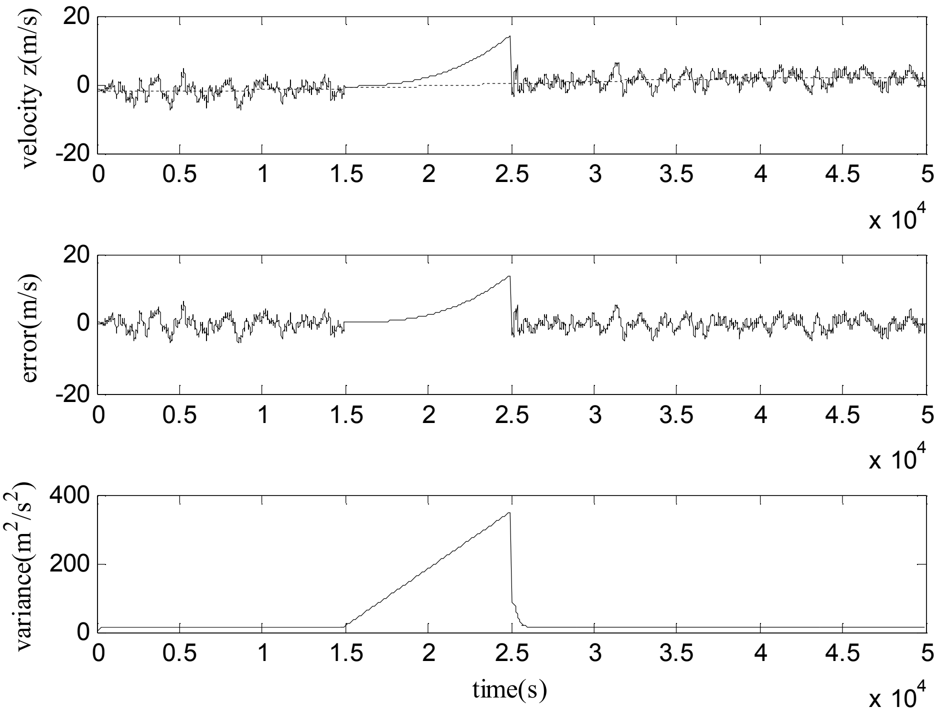

Figure C.69 : Z velocity est. via RUKF with SMNSF in case of zero out, SSA.

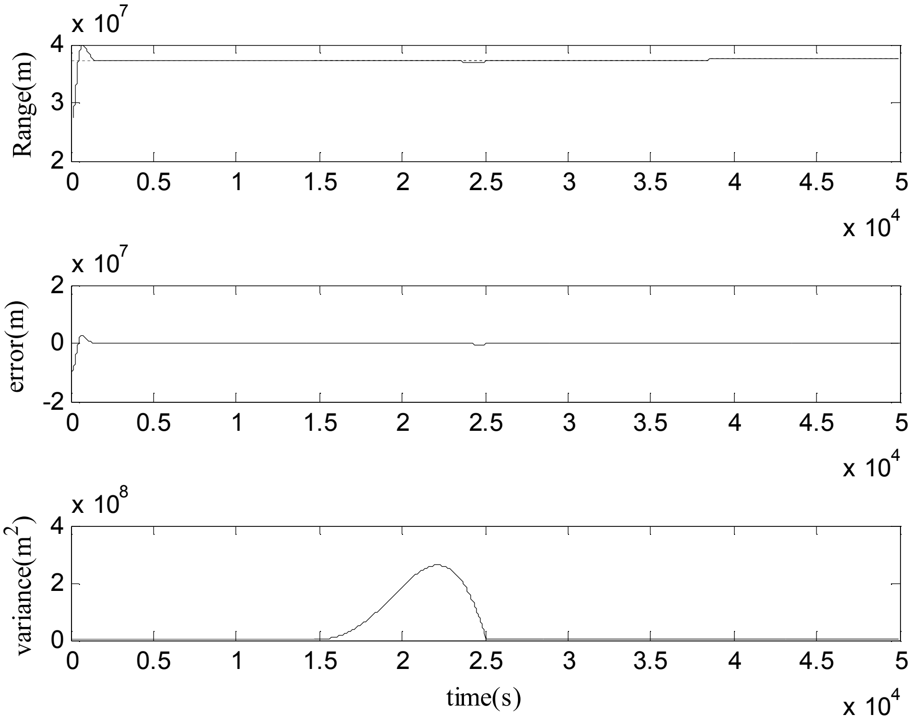

Figure C.70 : Range via RUKF with SMNSF in case of zero out, SSA.

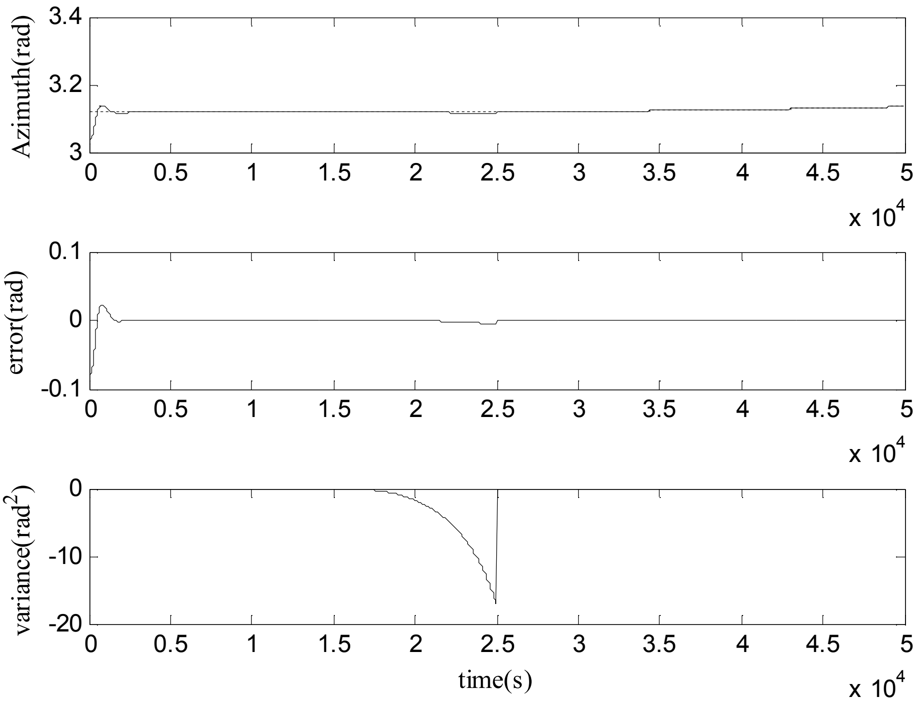

Figure C.71 : Azimuth via RUKF with SMNSF in case of zero out, SSA.

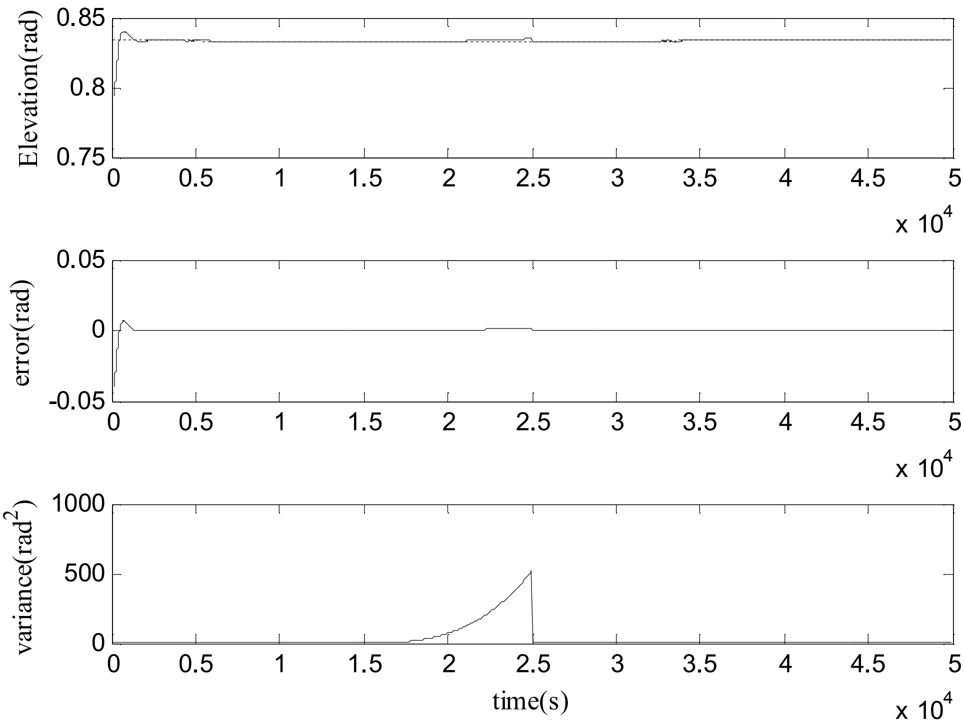

Figure C.72 : Elevation via RUKF with SMNSF in case of zero out, SSA.

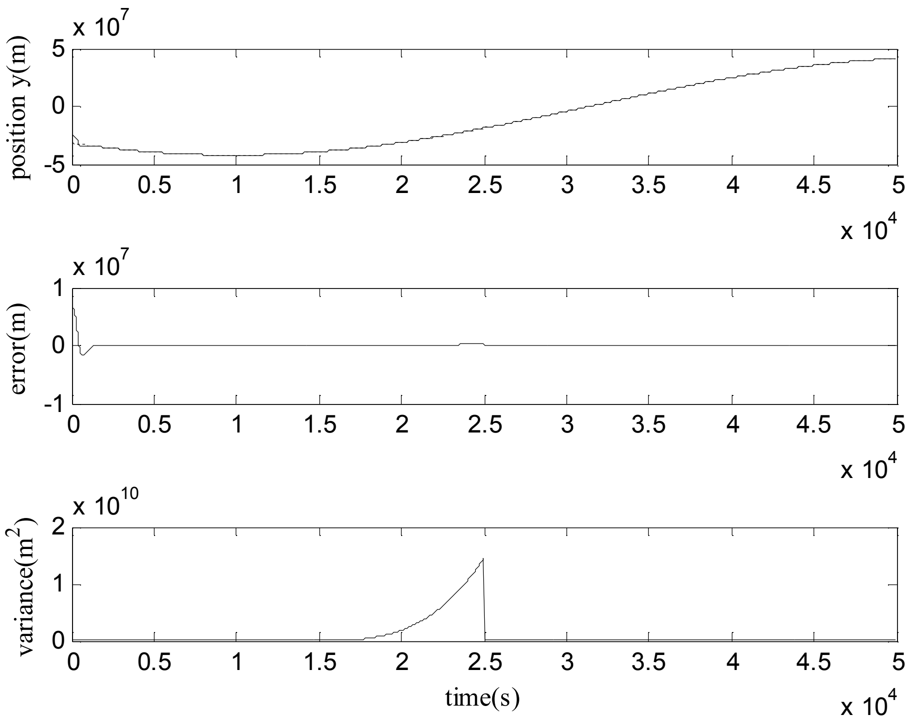

Figure C.73 : Y position est. via RUKF with MMNSF in case of zero out, SSA.

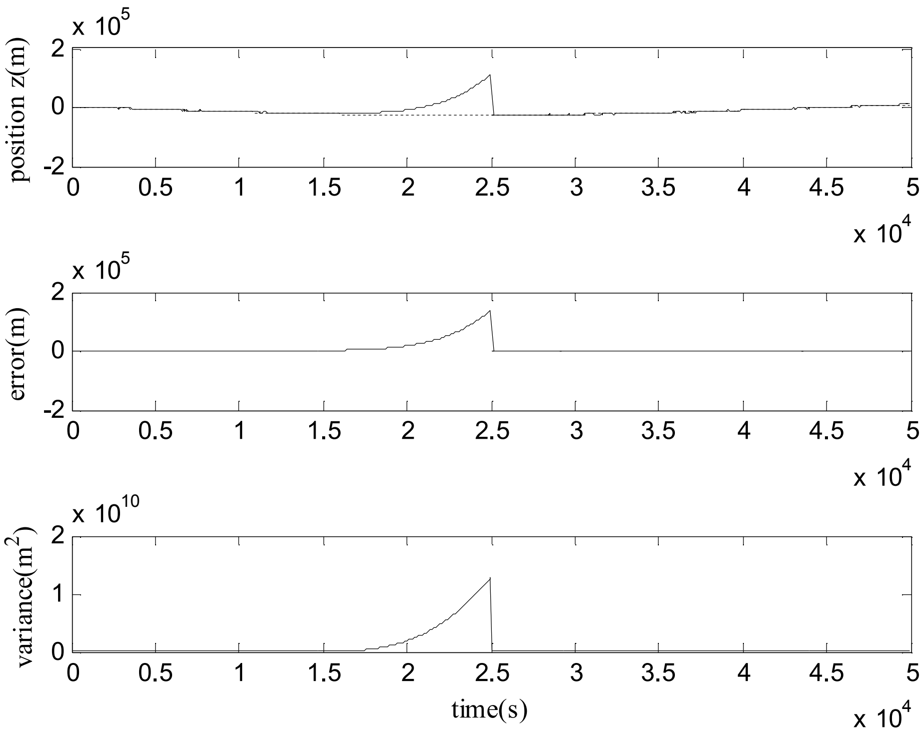

Figure C.74 : Z position est. via RUKF with MMNSF in case of zero out, SSA.

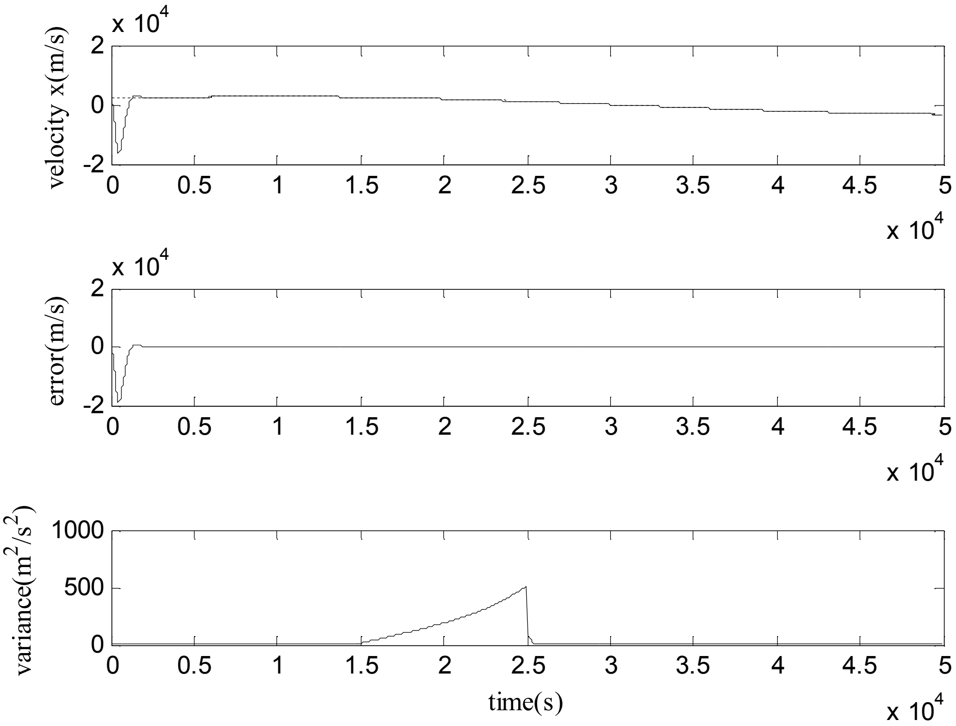

Figure C.75 : X velocity est. via RUKF with MMNSF in case of zero out, SSA.

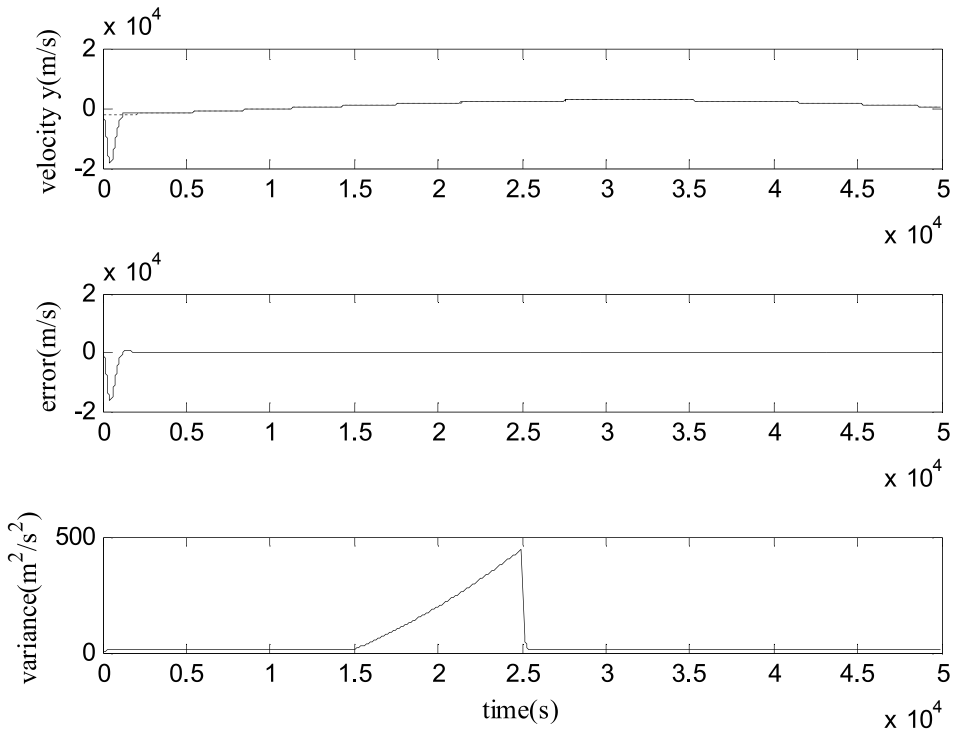

Figure C.76 : Y velocity est. via RUKF with MMNSF in case of zero out, SSA.

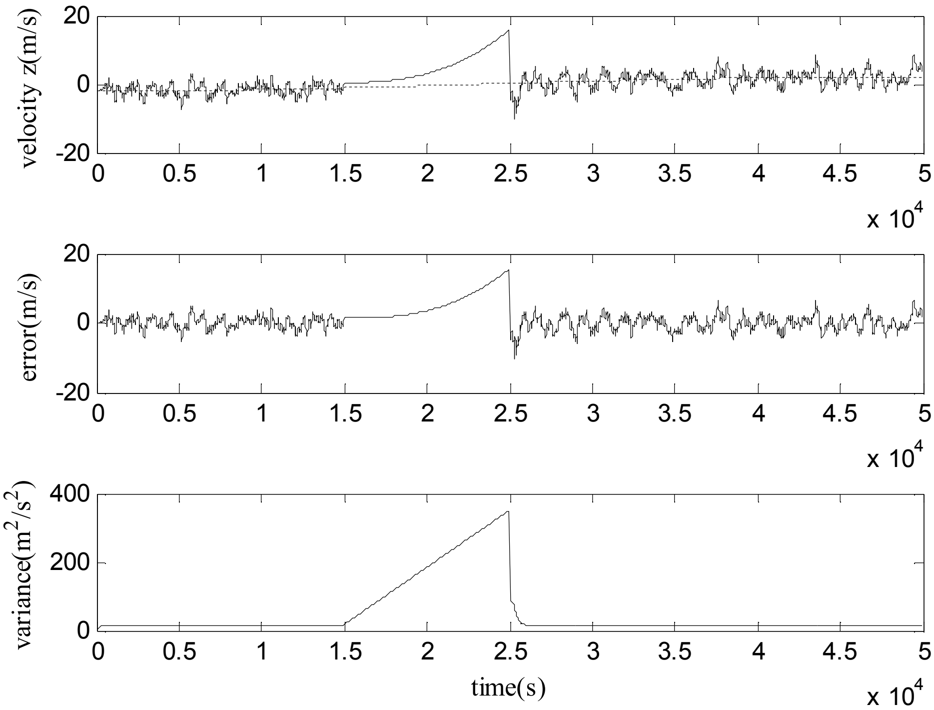

Figure C.77 : Z velocity est. via RUKF with MMNSF in case of zero out, SSA.

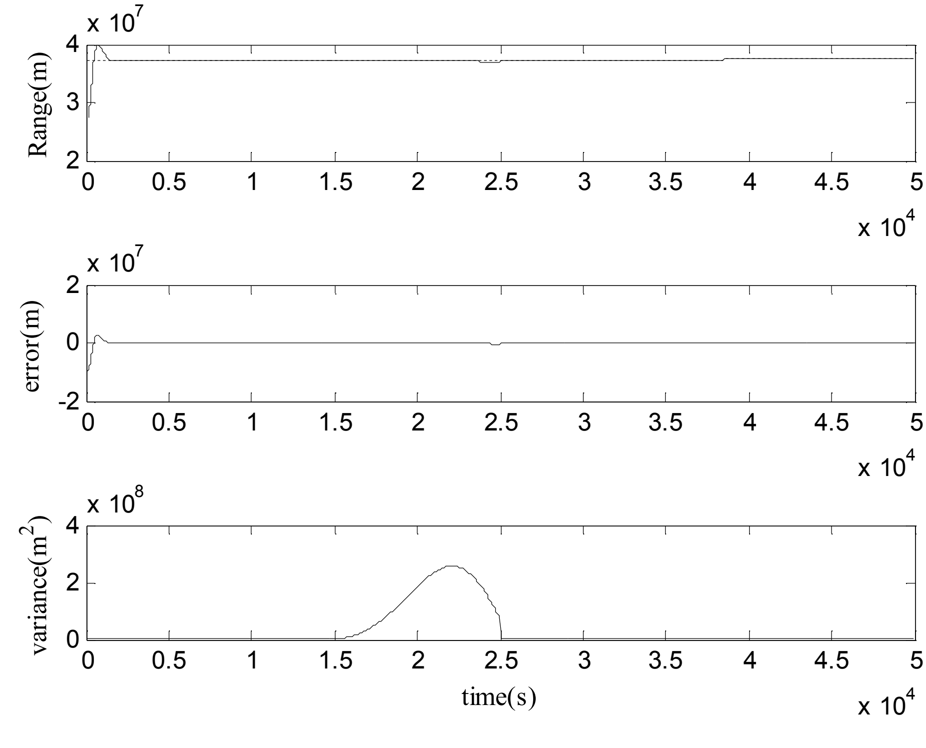

Figure C.78 : Range via RUKF with MMNSF in case of zero out, SSA.

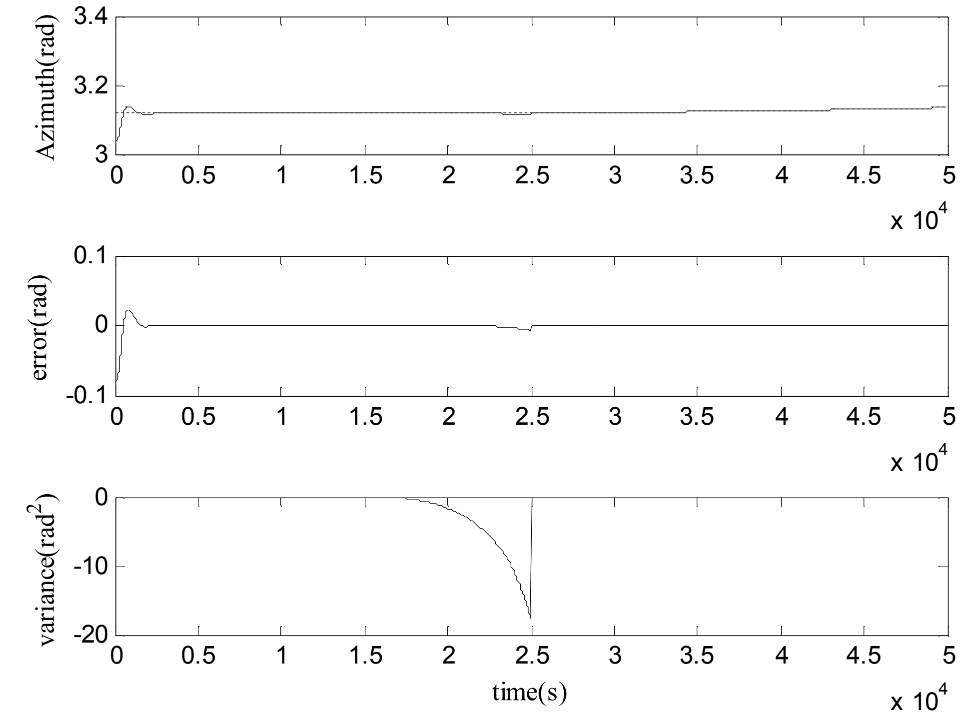

Figure C.79 : Azimuth via RUKF with MMNSF in case of zero out, SSA.

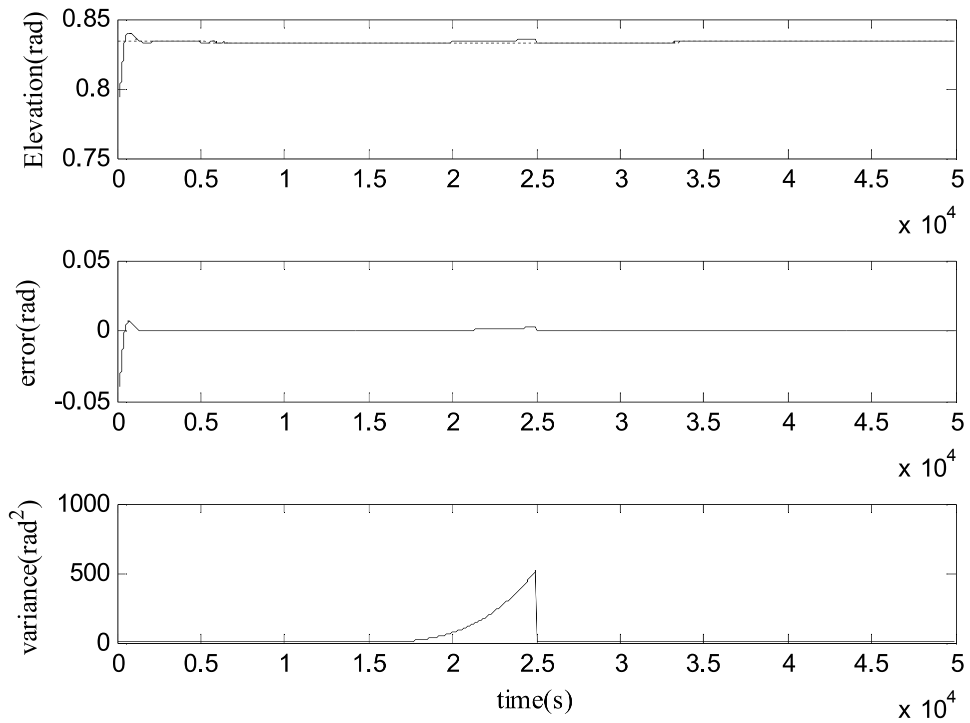

Figure C.80 : Elevation via RUKF with MMNSF in case of zero out, SSA.

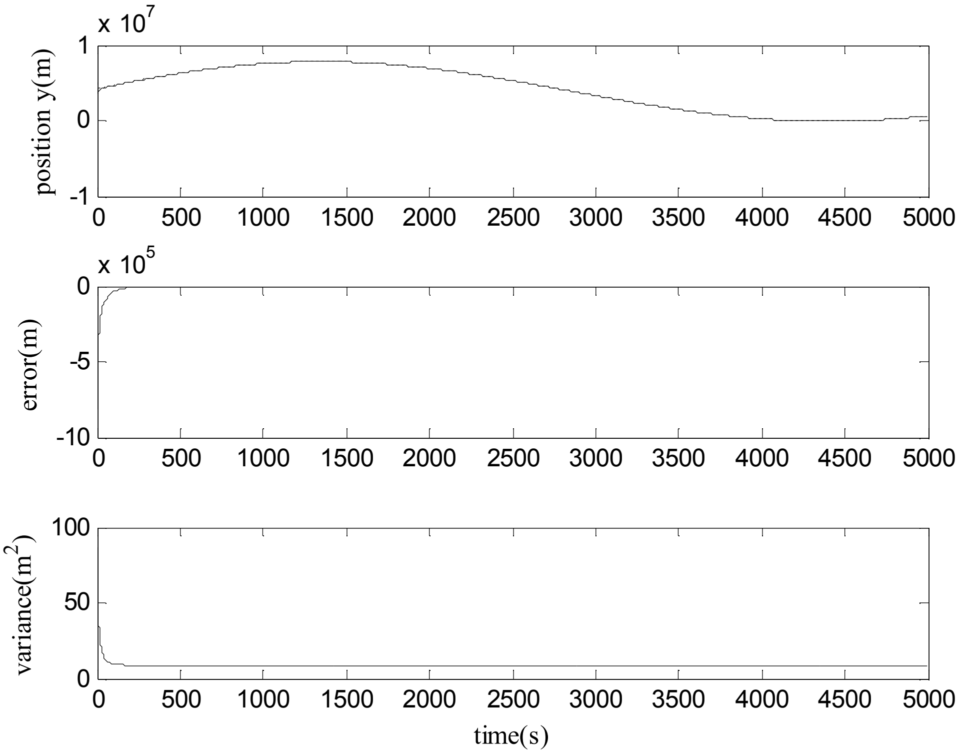

Figure C.81 : Y position estimation of spacecraft by measurements via GPS.

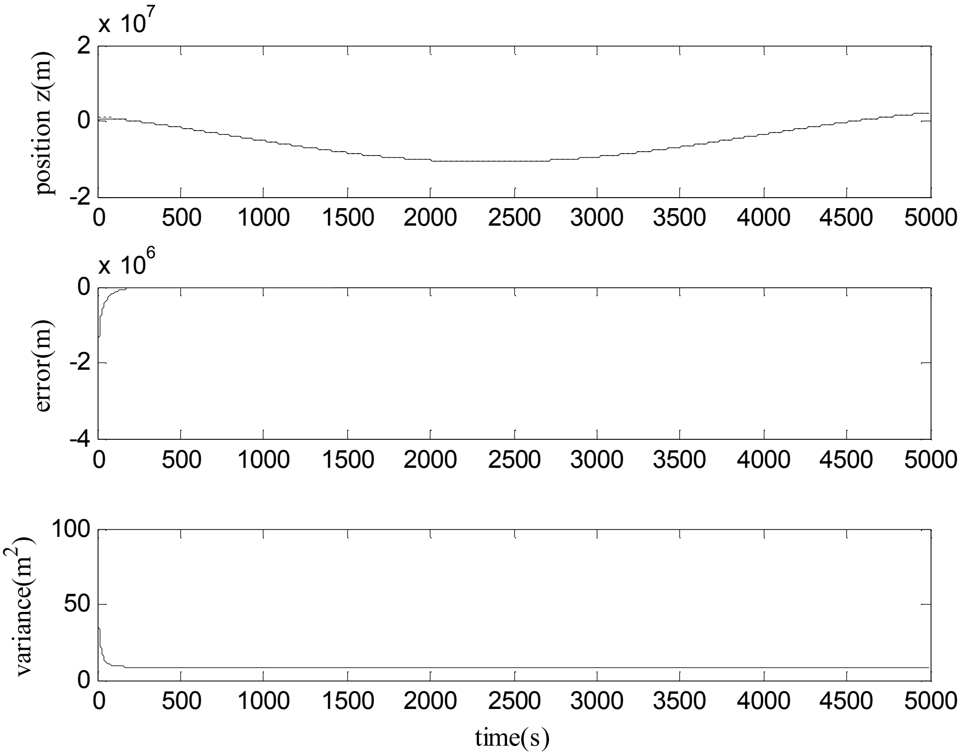

Figure C.82 : Z position estimation of spacecraft by measurements via GPS.

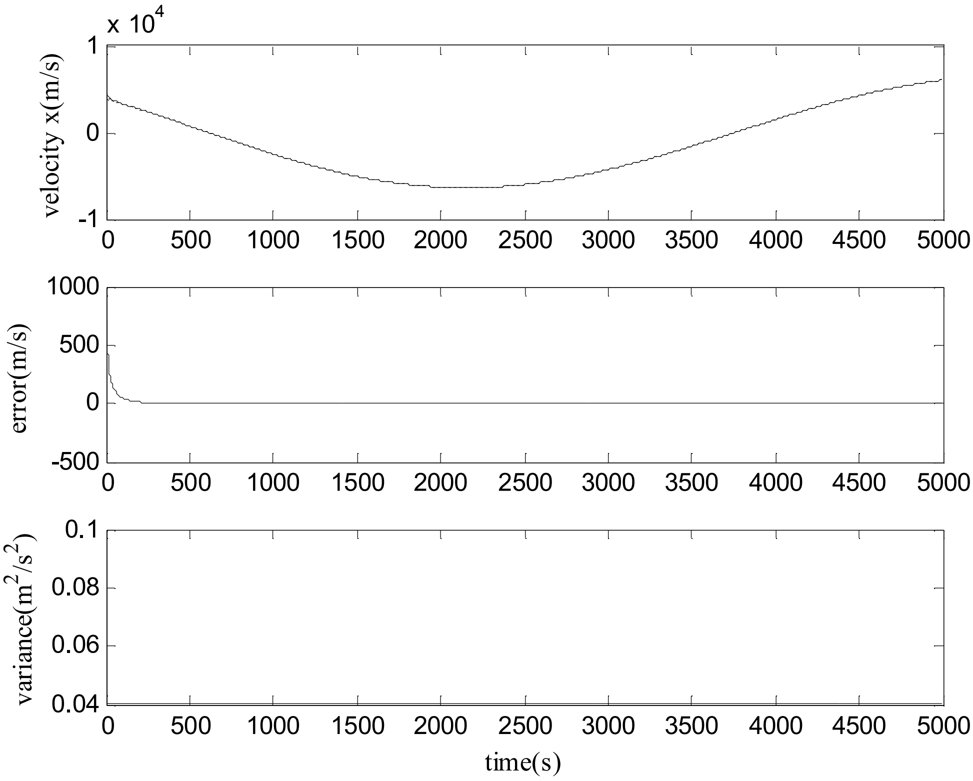

Figure C.83 : X velocity estimation of spacecraft by measurements via GPS.

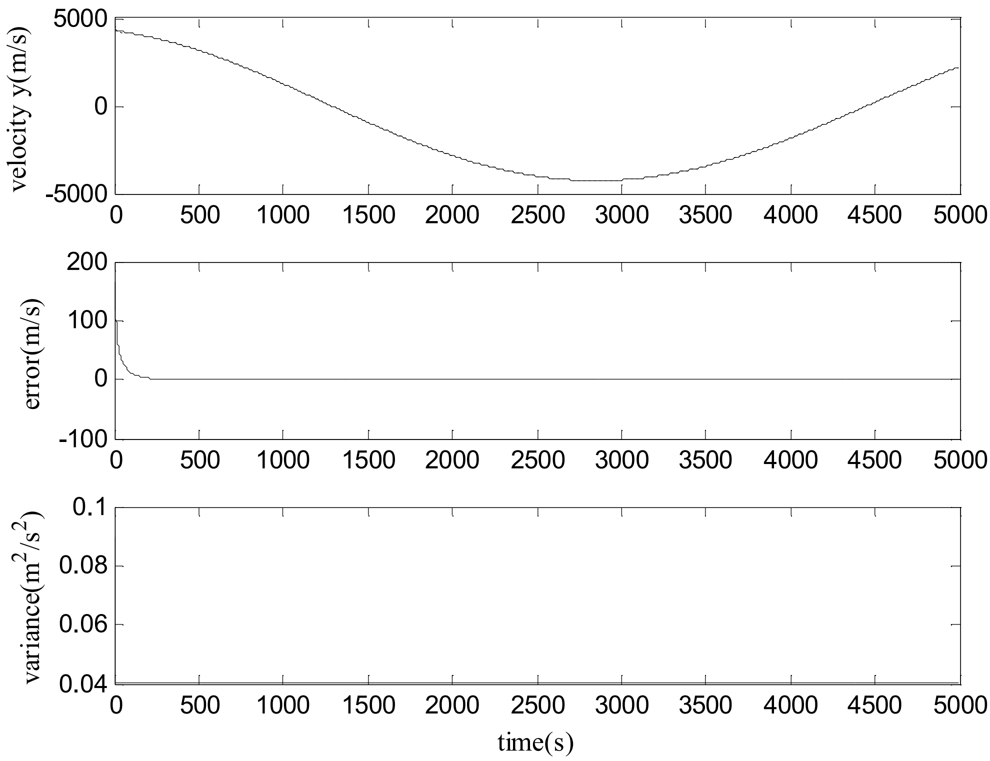

Figure C.84 : Y velocity estimation of spacecraft by measurements via GPS.

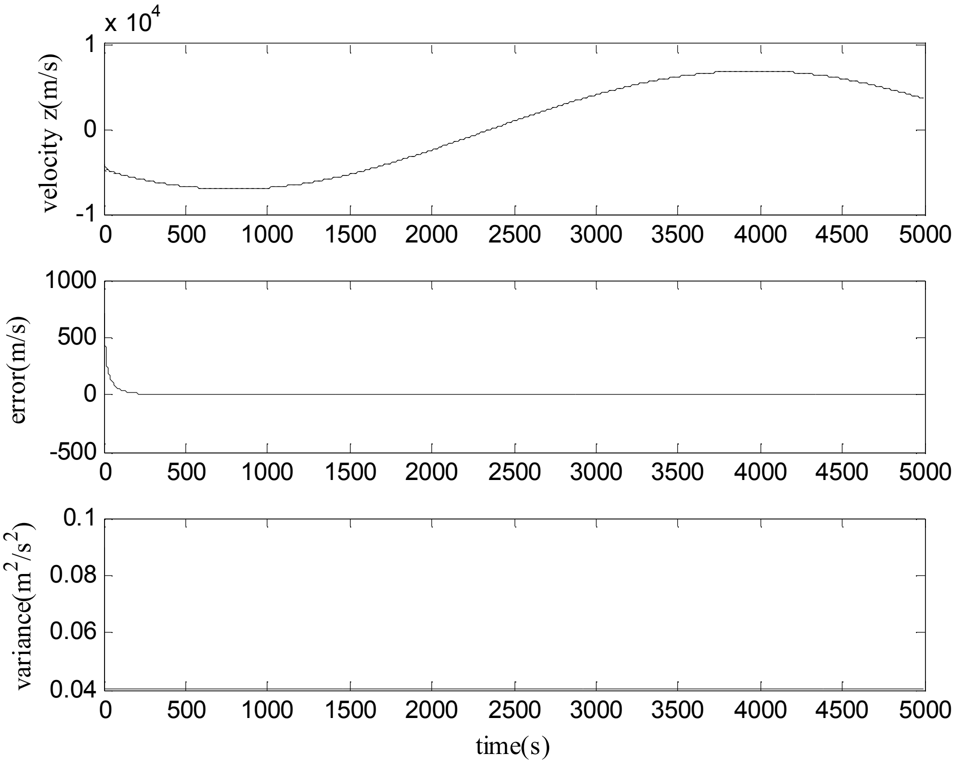

Figure C.85 : Z velocity estimation of spacecraft by measurements via GPS.

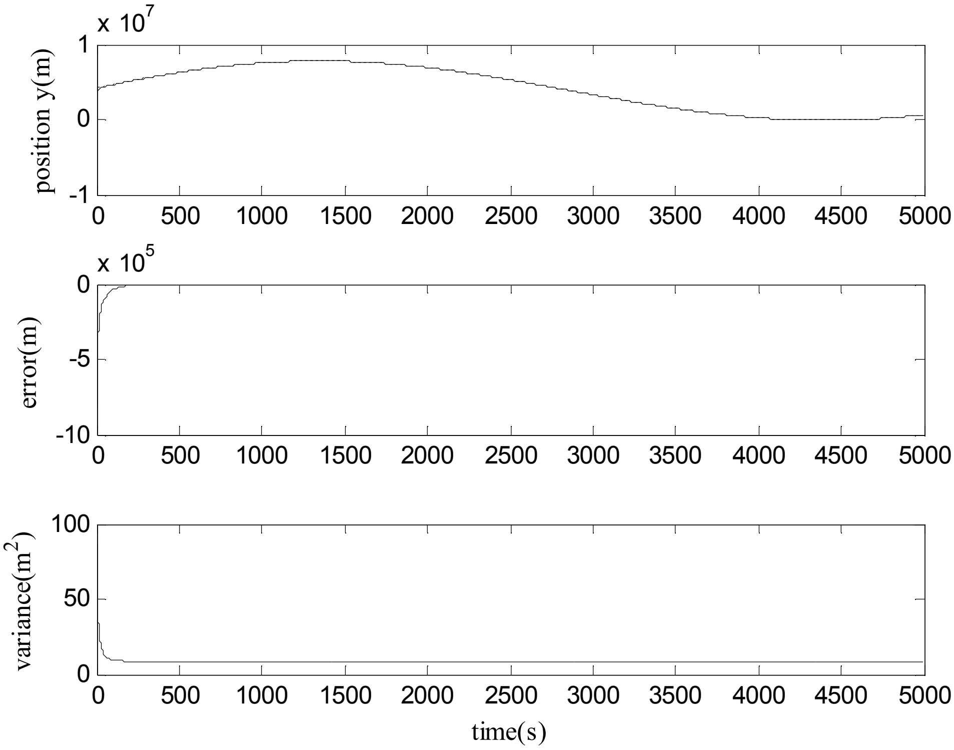

Figure C.86 : Y position est. via Regular UKF in case of cont. bias, GPS.

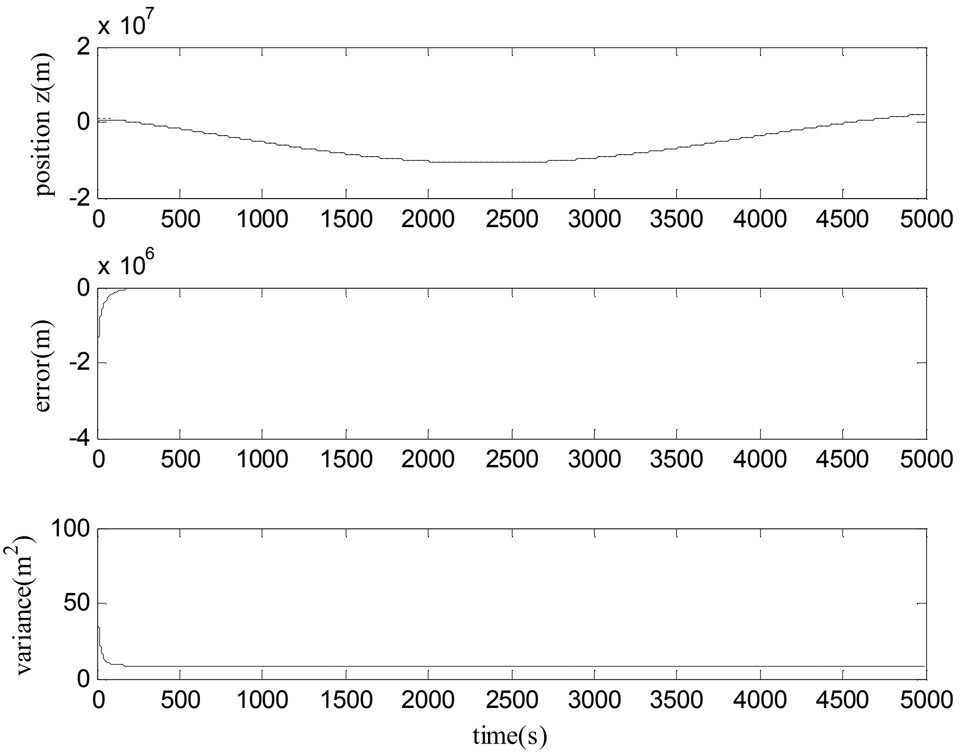

Figure C.87 : Z position est. via Regular UKF in case of cont. bias, GPS.

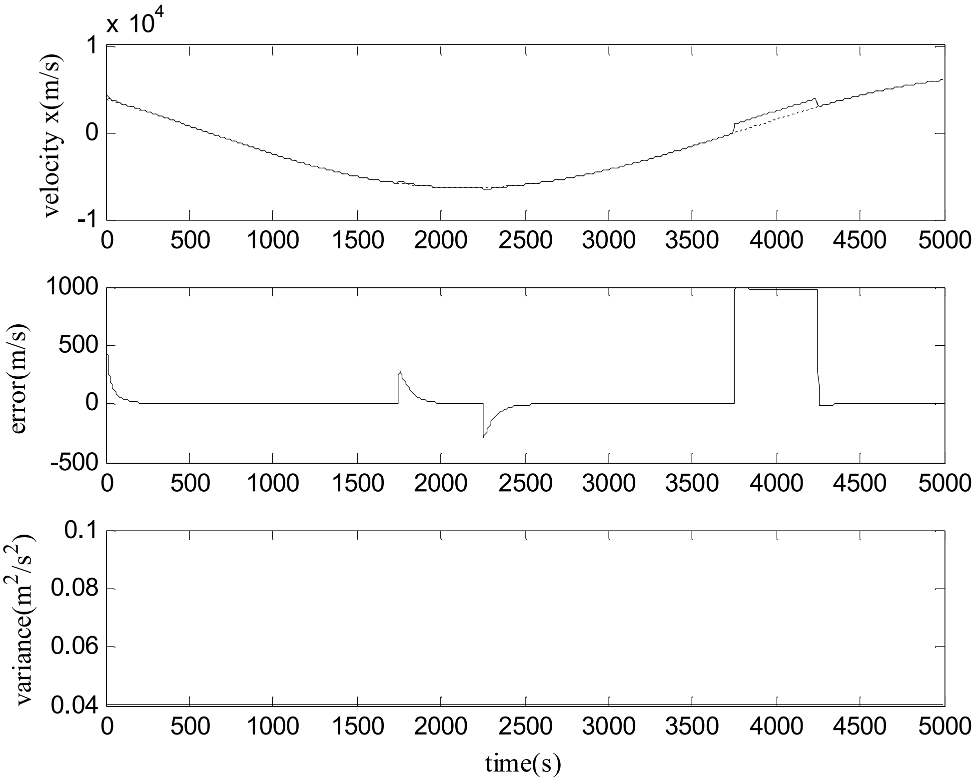

Figure C.88 : X velocity est. via Regular UKF in case of cont. bias, GPS.

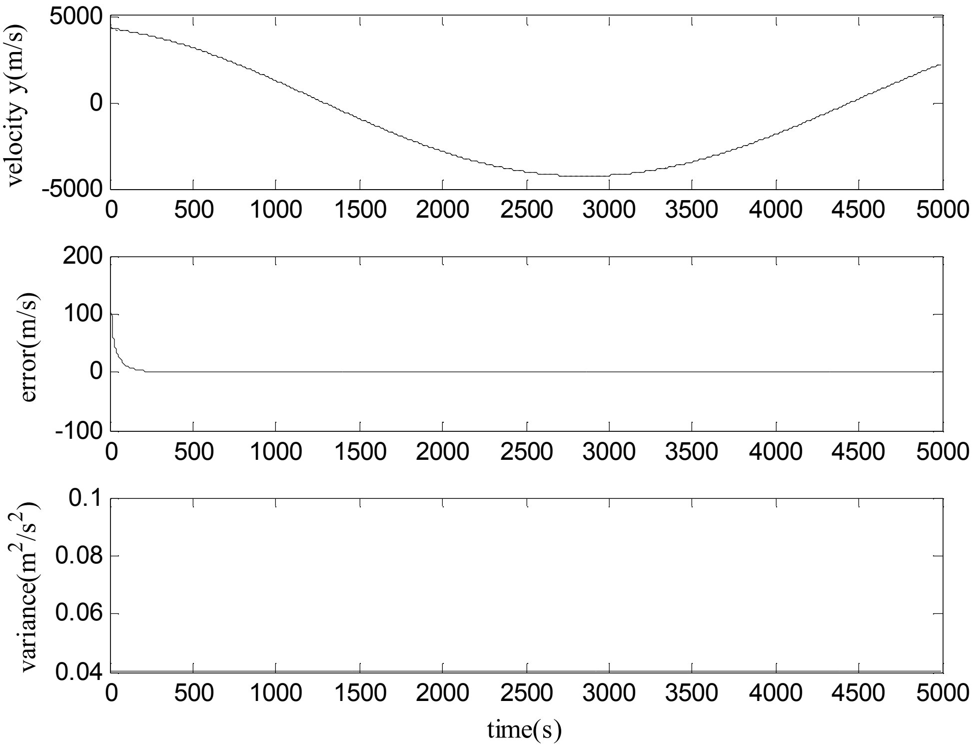

Figure C.89 : Y velocity est. via Regular UKF in case of cont. bias, GPS.

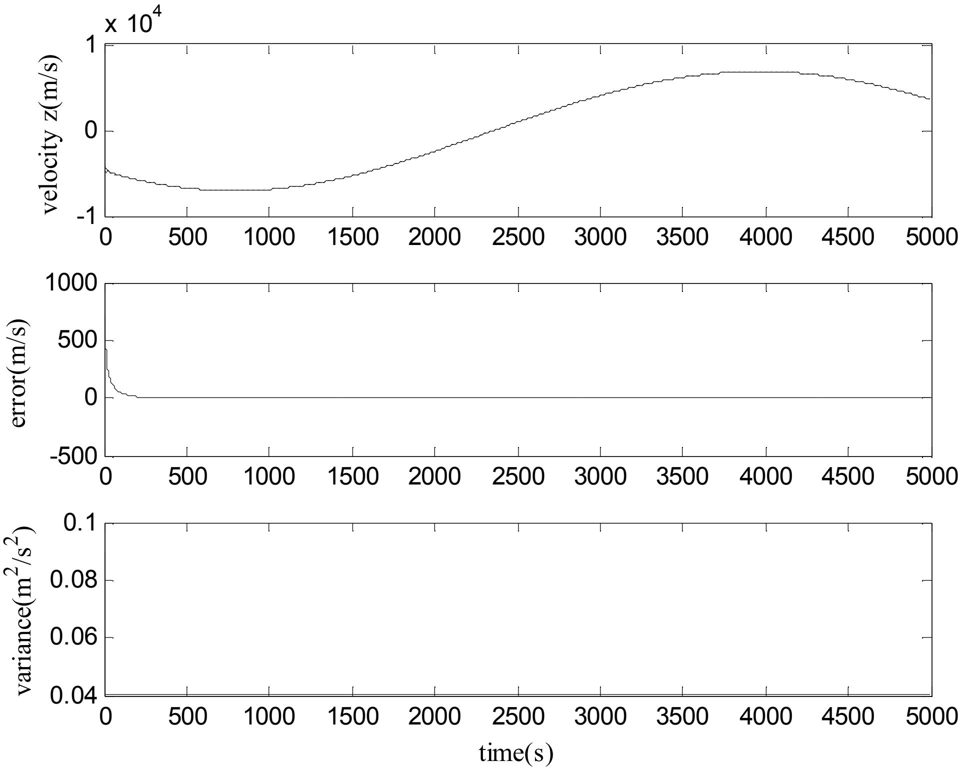

Figure C.90 : Z velocity est. via Regular UKF in case of cont. bias, GPS.

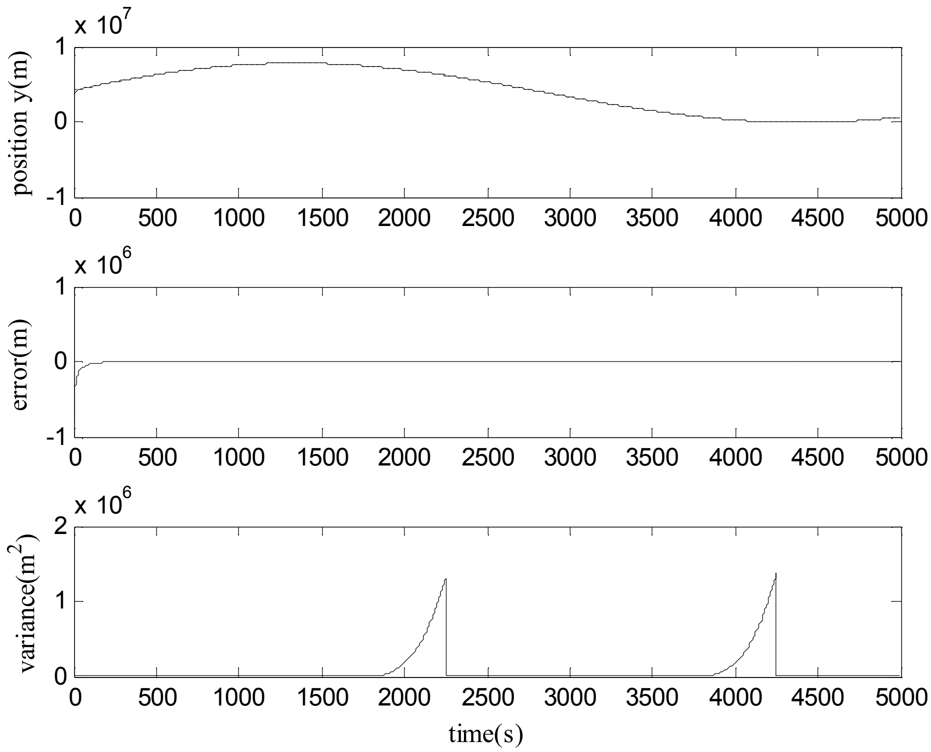

Figure C.91 : Y position est. via RUKF with SMNSF in case of cont. bias, GPS.

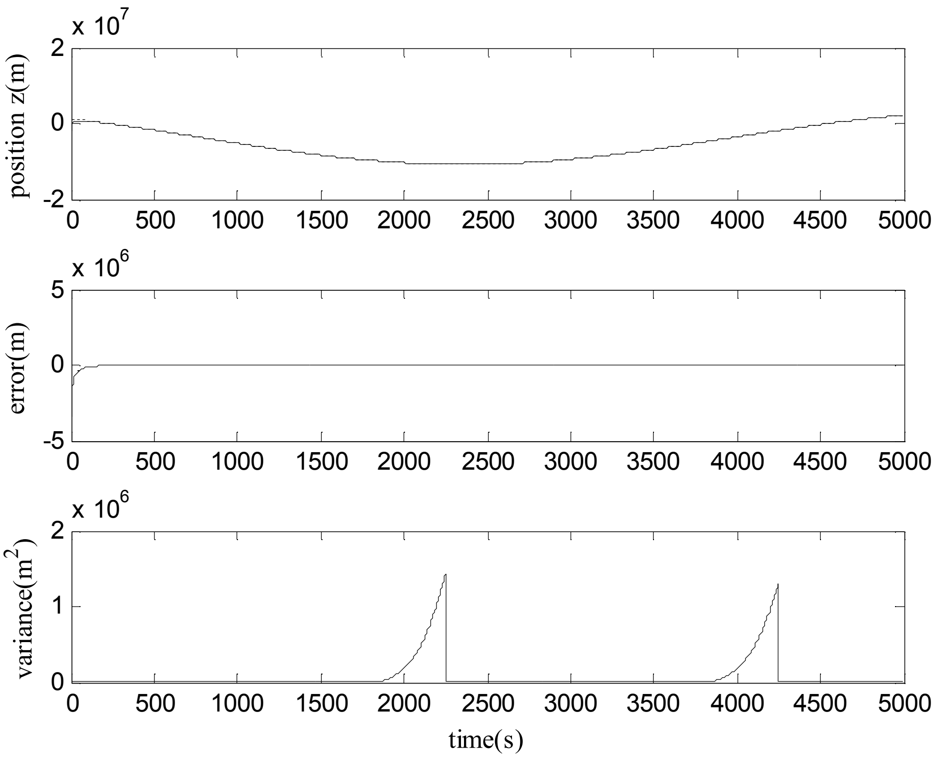

Figure C.92 : Z position est. via RUKF with SMNSF in case of cont. bias, GPS.

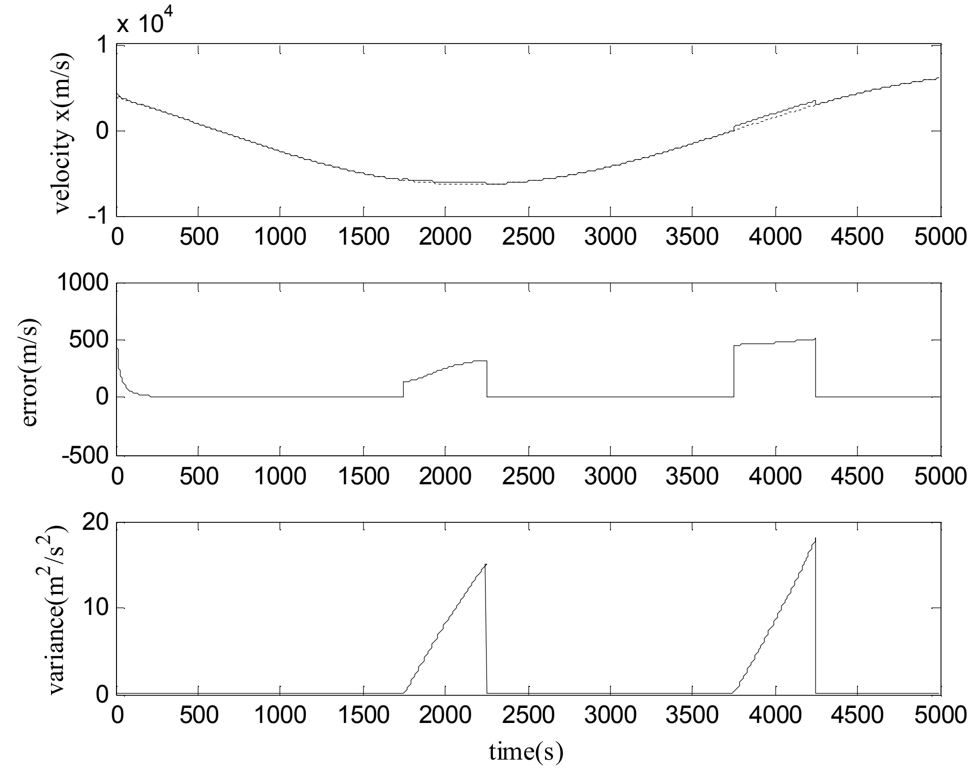

Figure C.93 : X velocity est. via RUKF with SMNSF in case of cont. bias, GPS.

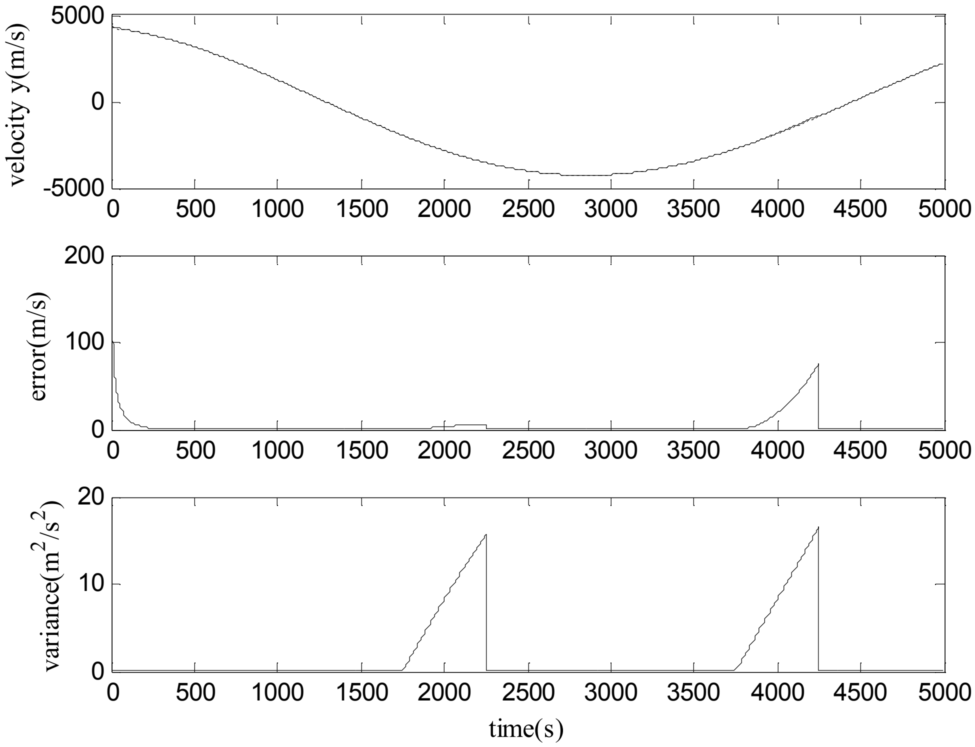

Figure C.94 : Y velocity est. via RUKF with SMNSF in case of cont. bias, GPS.

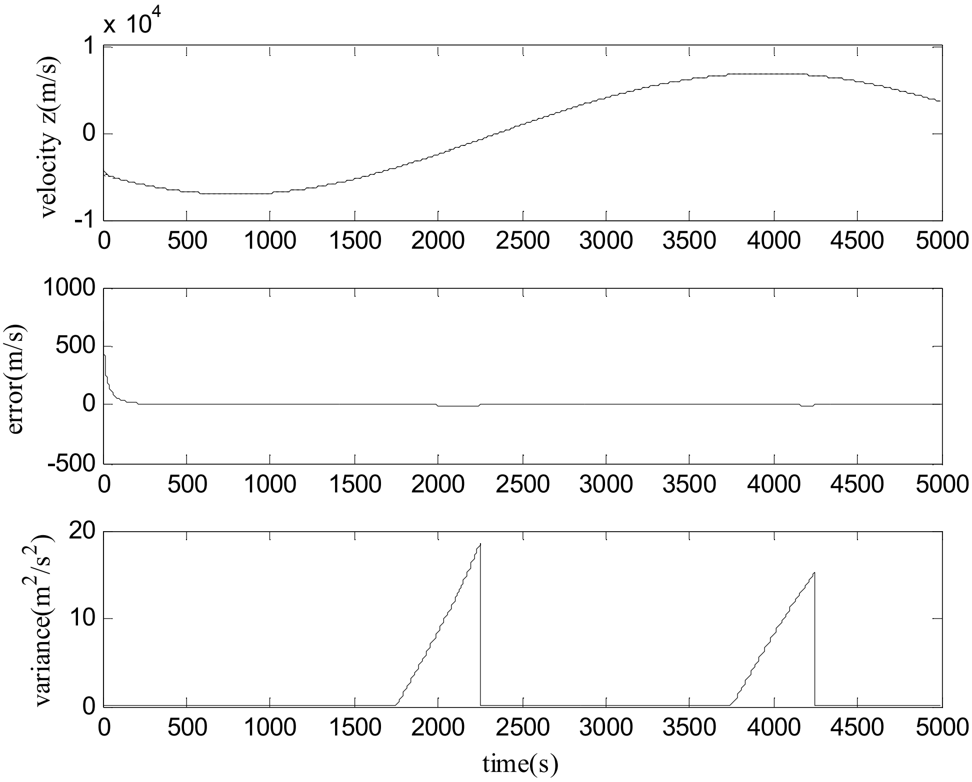

Figure C.95 : Z velocity est. via RUKF with SMNSF in case of cont. bias, GPS.

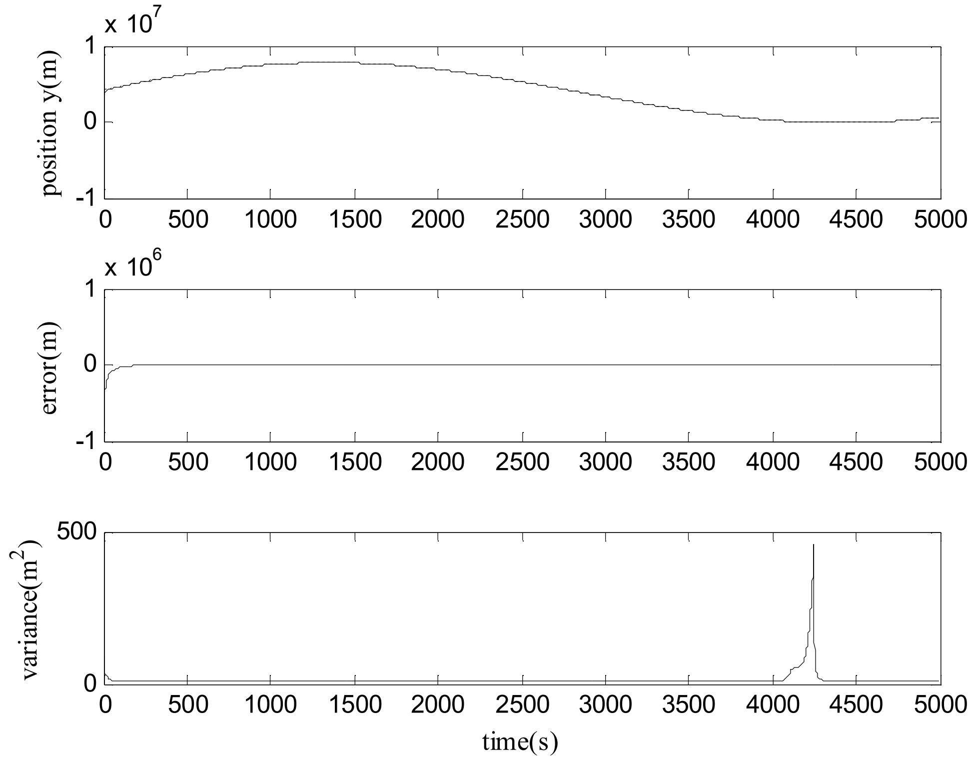

Figure C.96 : Y position est. via RUKF with MMNSF in case of cont. bias, GPS.

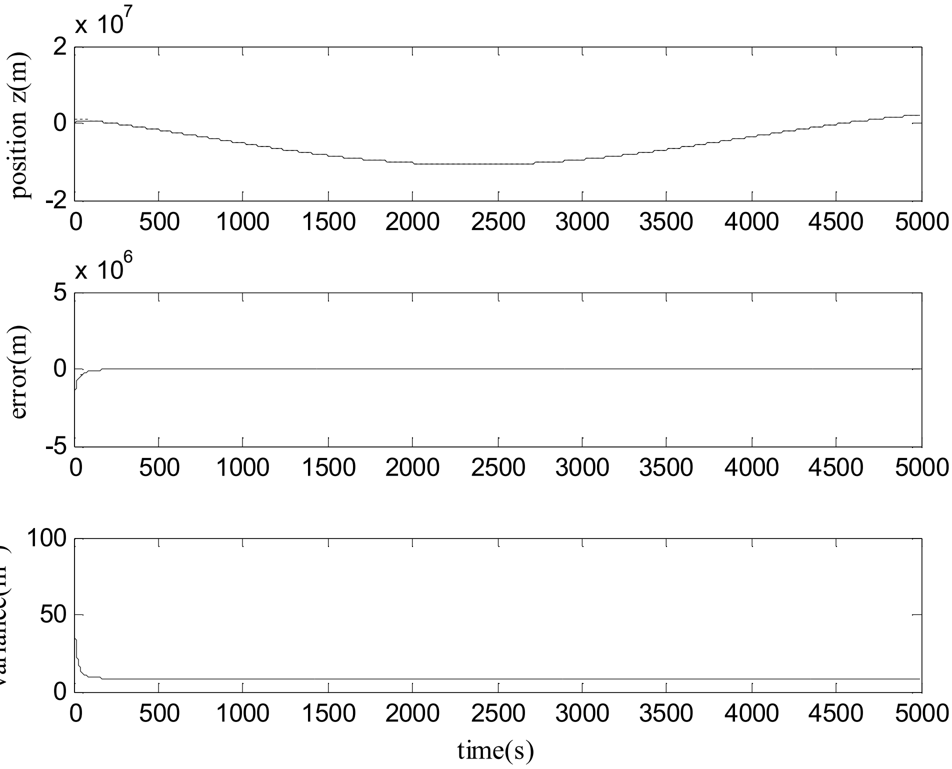

Figure C.97 : Z position est. via RUKF with MMNSF in case of cont. bias, GPS.

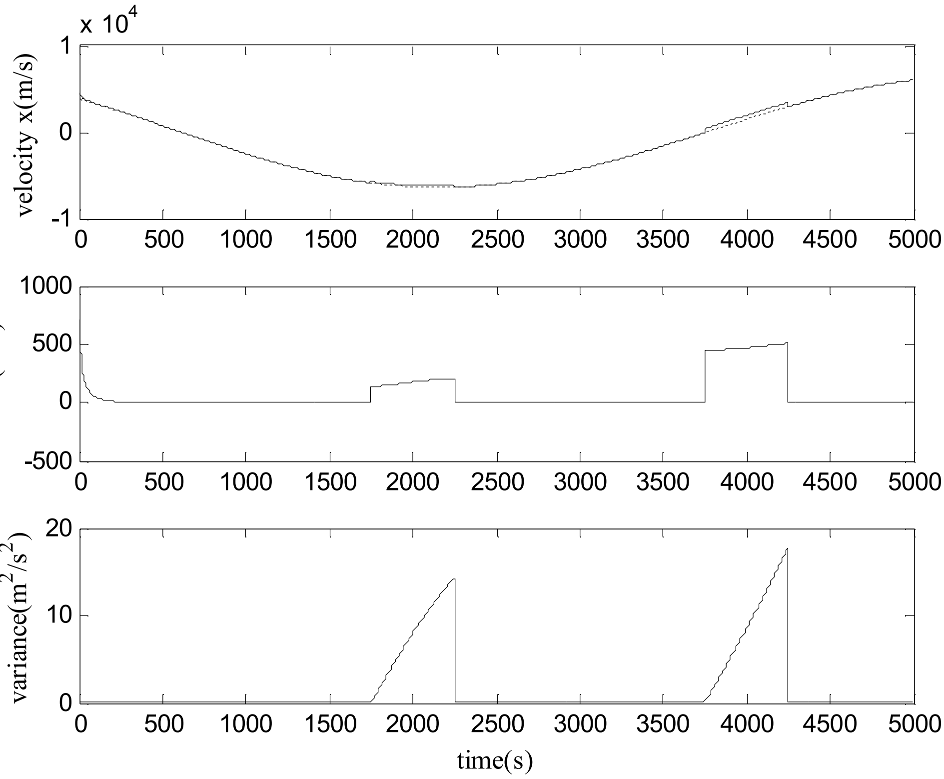

Figure C.98 : X velocity est. via RUKF with MMNSF in case of cont. bias, GPS.

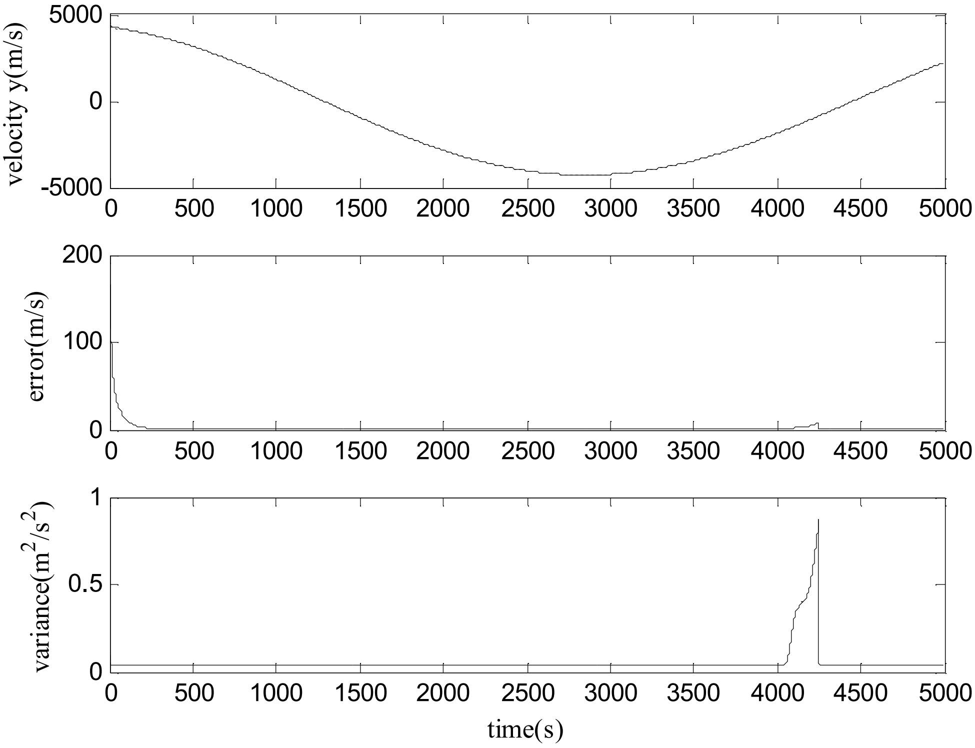

Figure C.99 : Y velocity est. via RUKF with MMNSF in case of cont. bias, GPS.

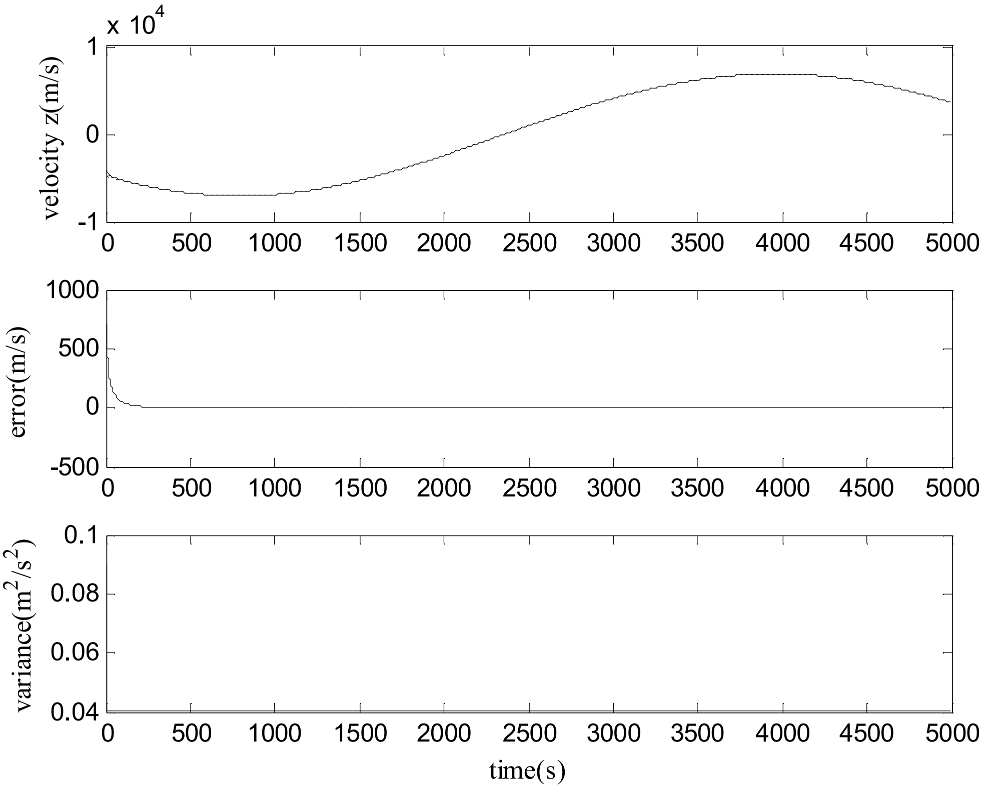

Figure C.100 : Z velocity est. via RUKF with MMNSF in case of cont. bias, GPS.

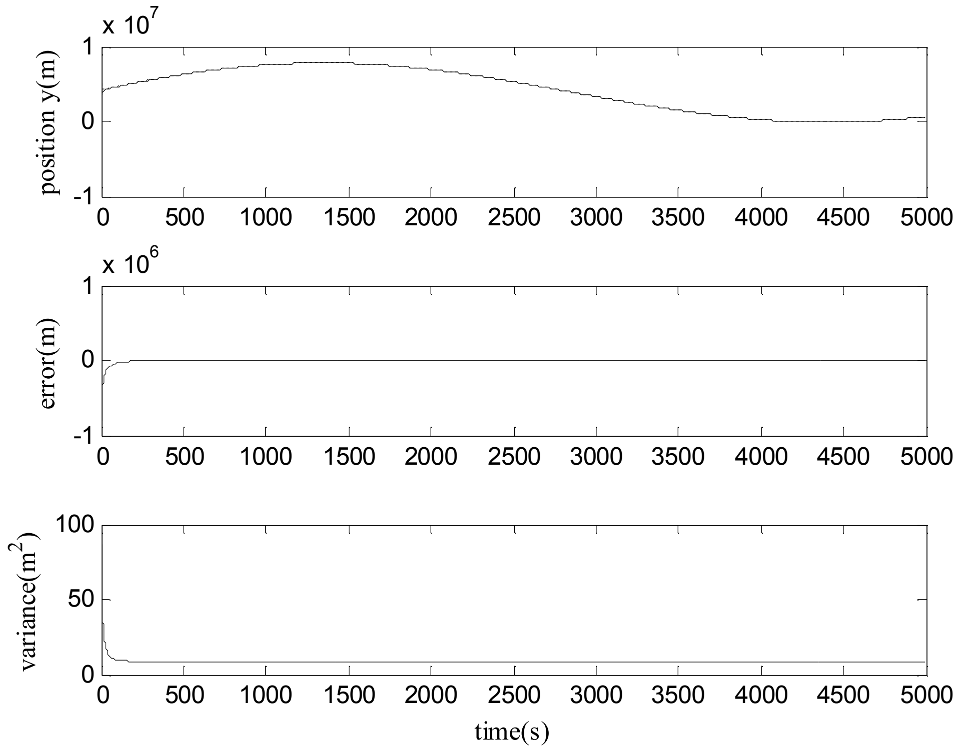

Figure C.101 : Y position est. via Regular UKF in case of noise inc, GPS.

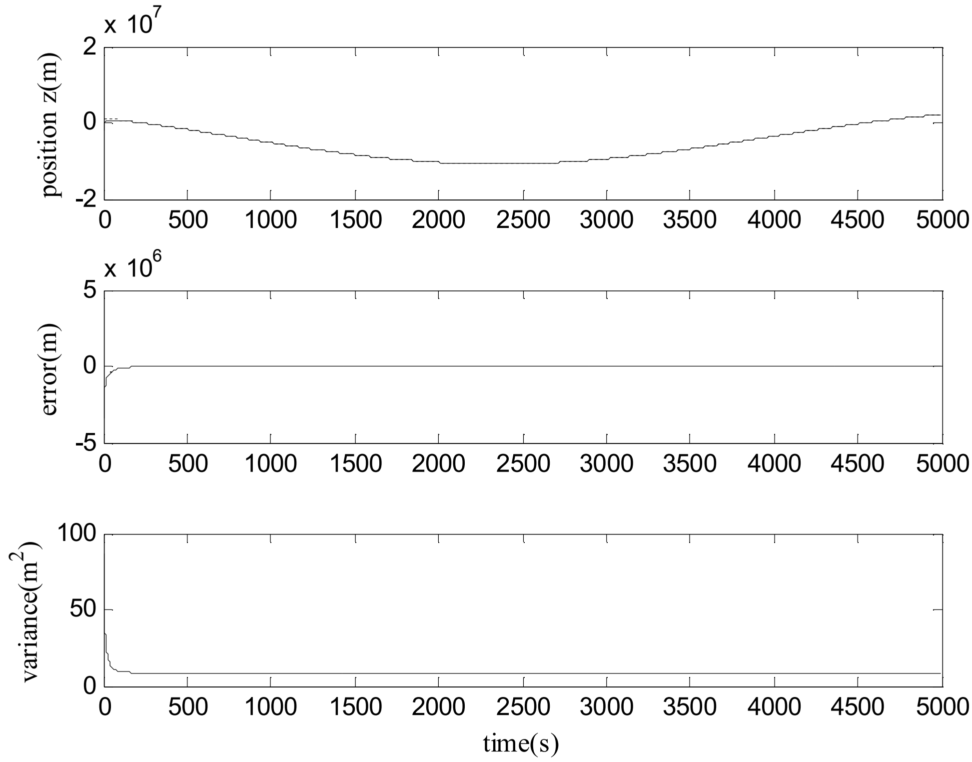

Figure C.102 : Z position est. via Regular UKF in case of noise inc, GPS.

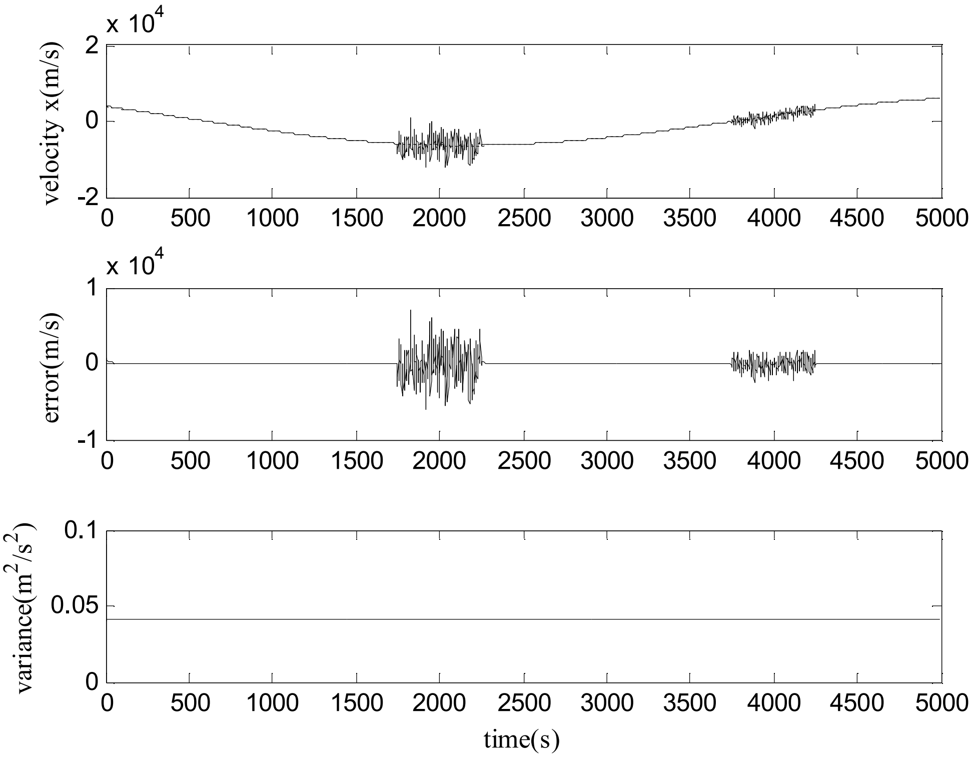

Figure C.103 : X velocity est. via Regular UKF in case of noise inc, GPS.

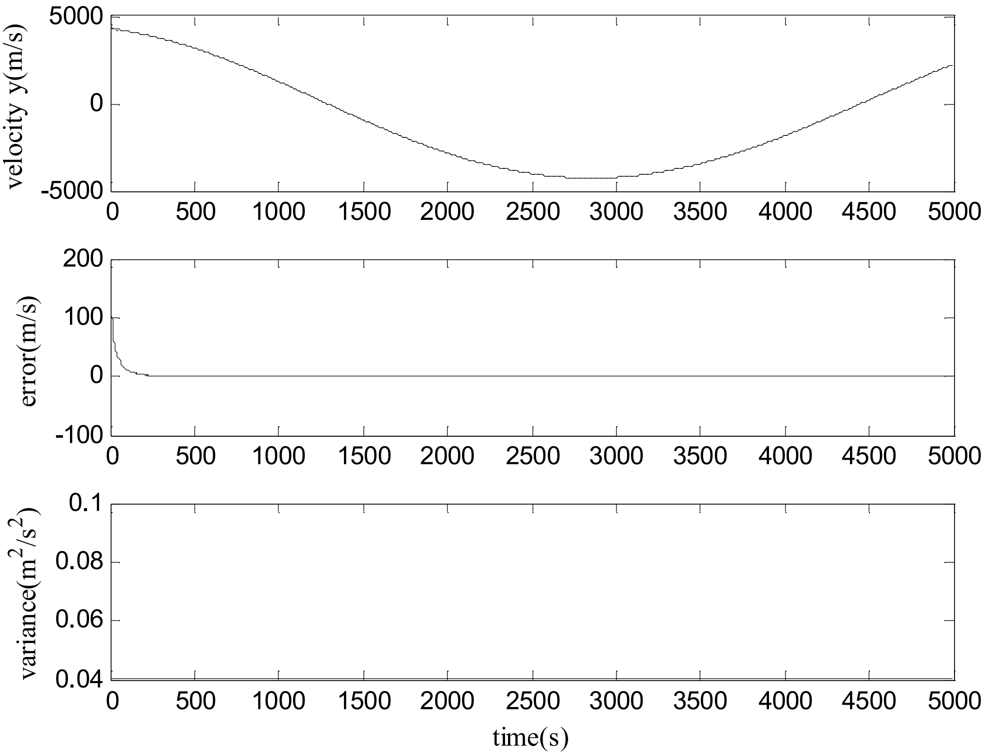

Figure C.104 : Y velocity est. via Regular UKF in case of noise inc, GPS.

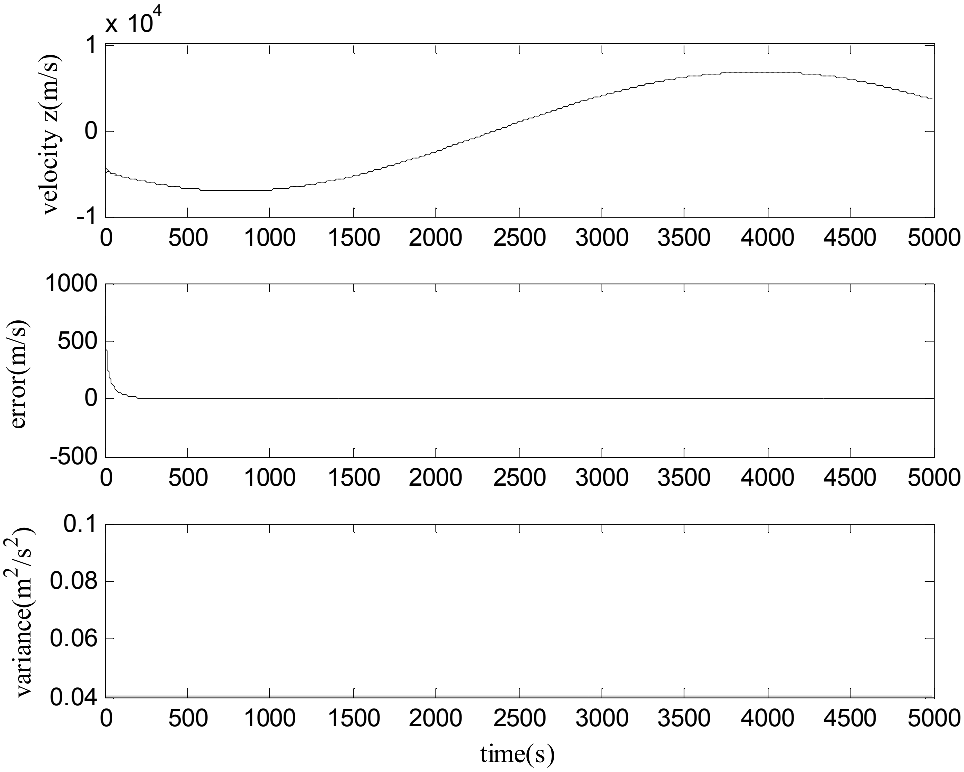

Figure C.105 : Z velocity est. via Regular UKF in case of noise inc, GPS.

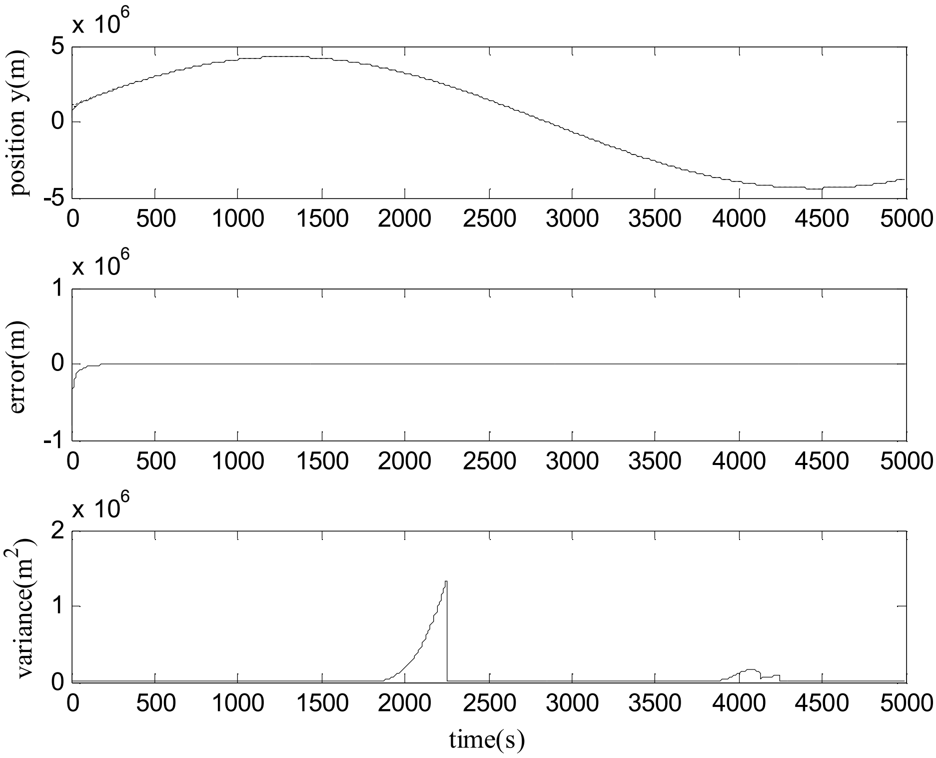

Figure C.106 : Y position est. via RUKF with SMNSF in case of noise inc, GPS.

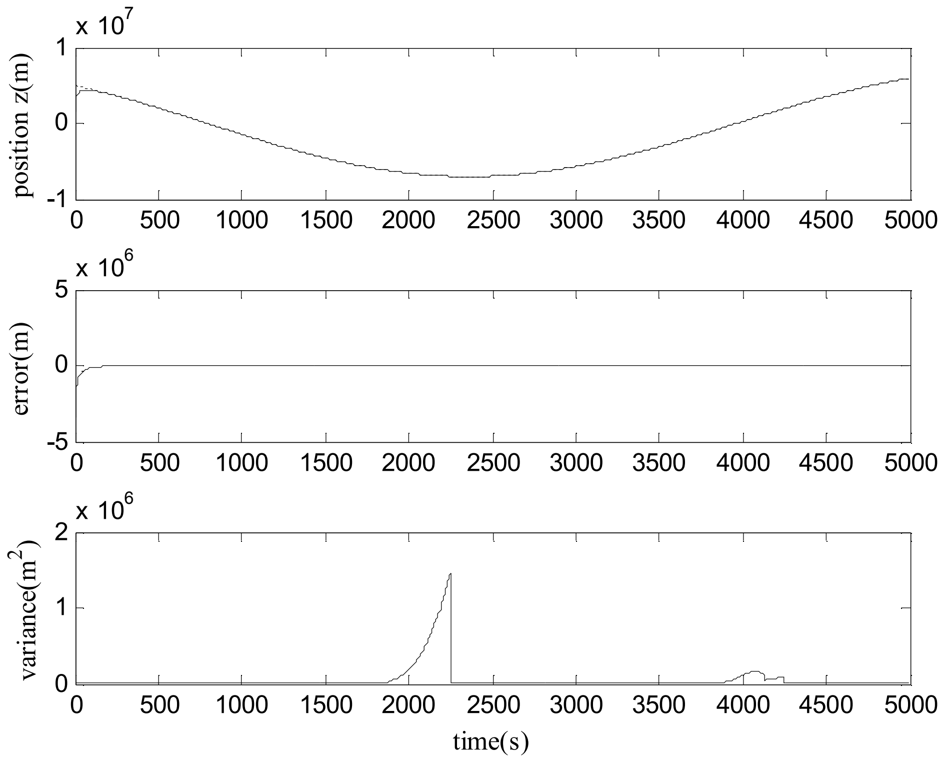

Figure C.107 : Z position est. via RUKF with SMNSF in case of noise inc, GPS.

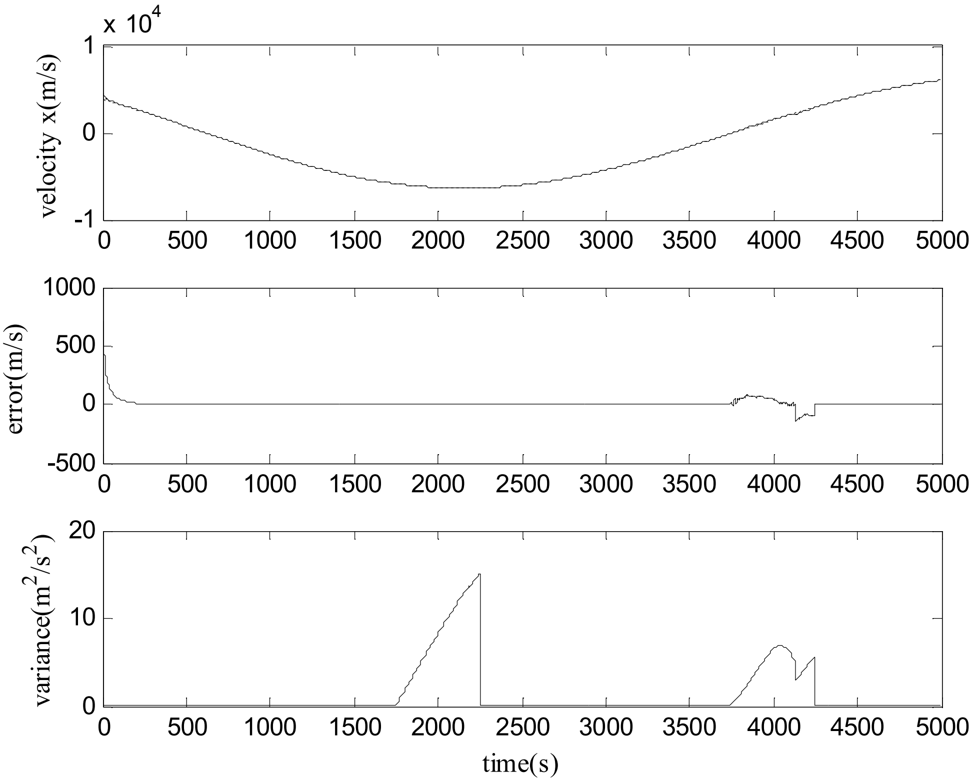

Figure C.108 : X velocity est. via RUKF with SMNSF in case of noise inc, GPS.

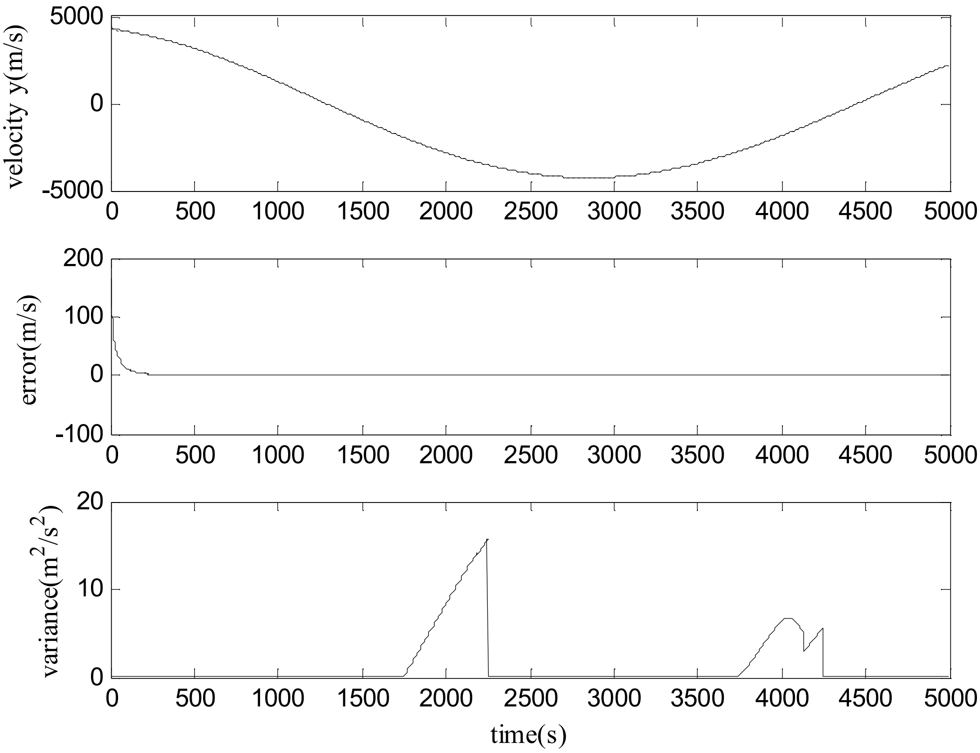

Figure C.109 : Y velocity est. via RUKF with SMNSF in case of noise inc, GPS.

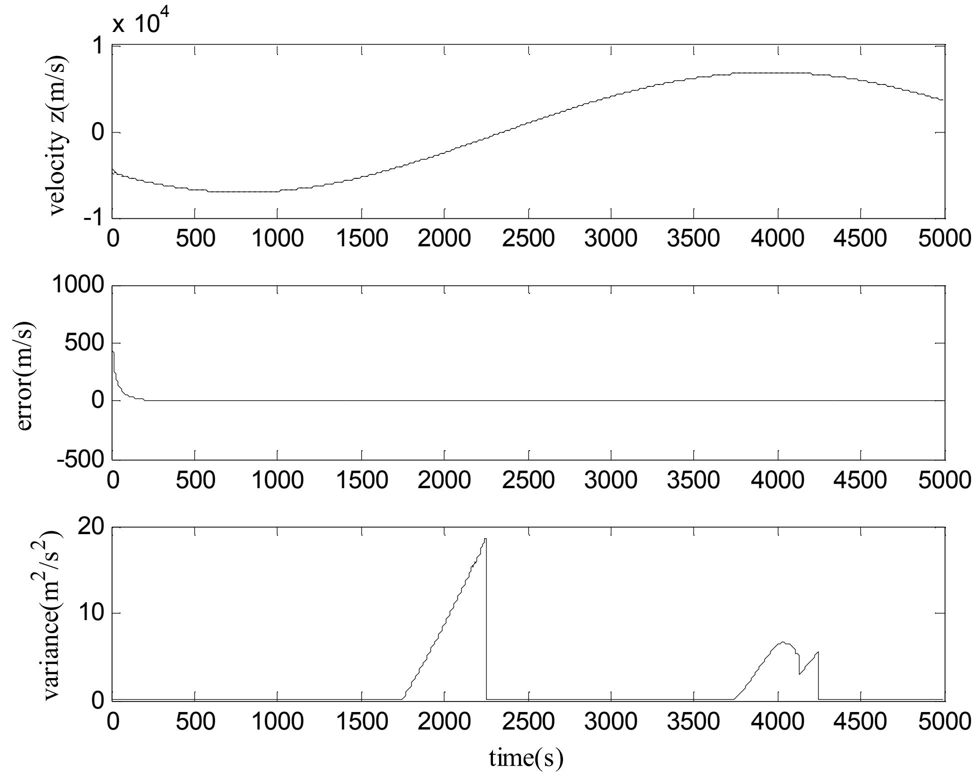

Figure C.110 : Z velocity est. via RUKF with SMNSF in case of noise inc, GPS.

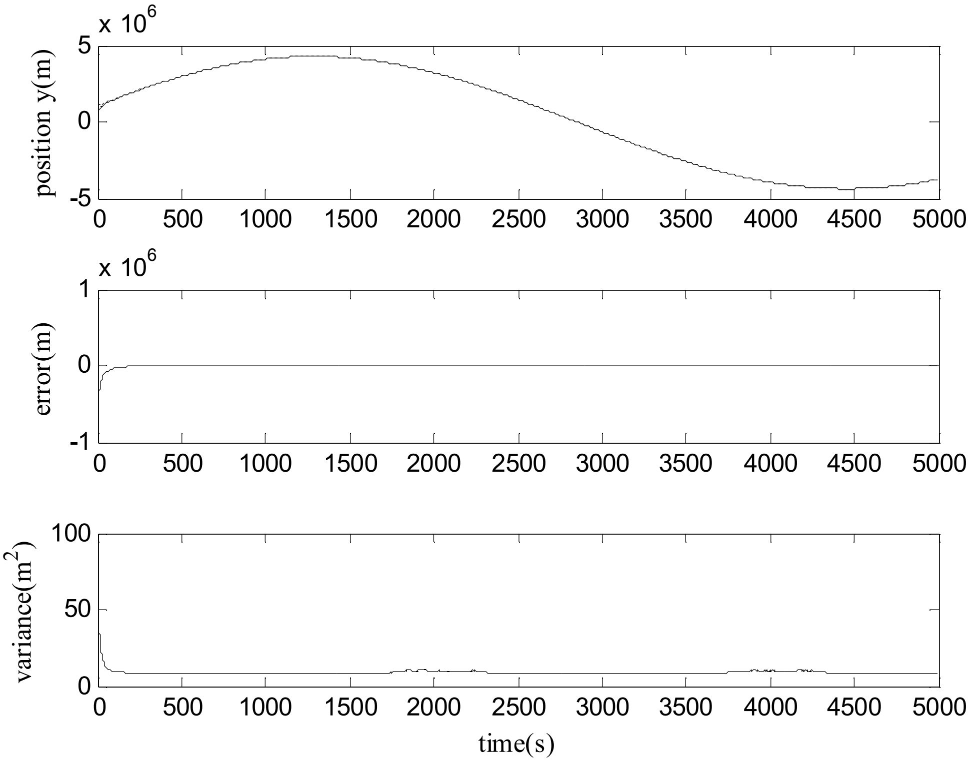

Figure C.111 : Y position est. via RUKF with MMNSF in case of noise inc, GPS.

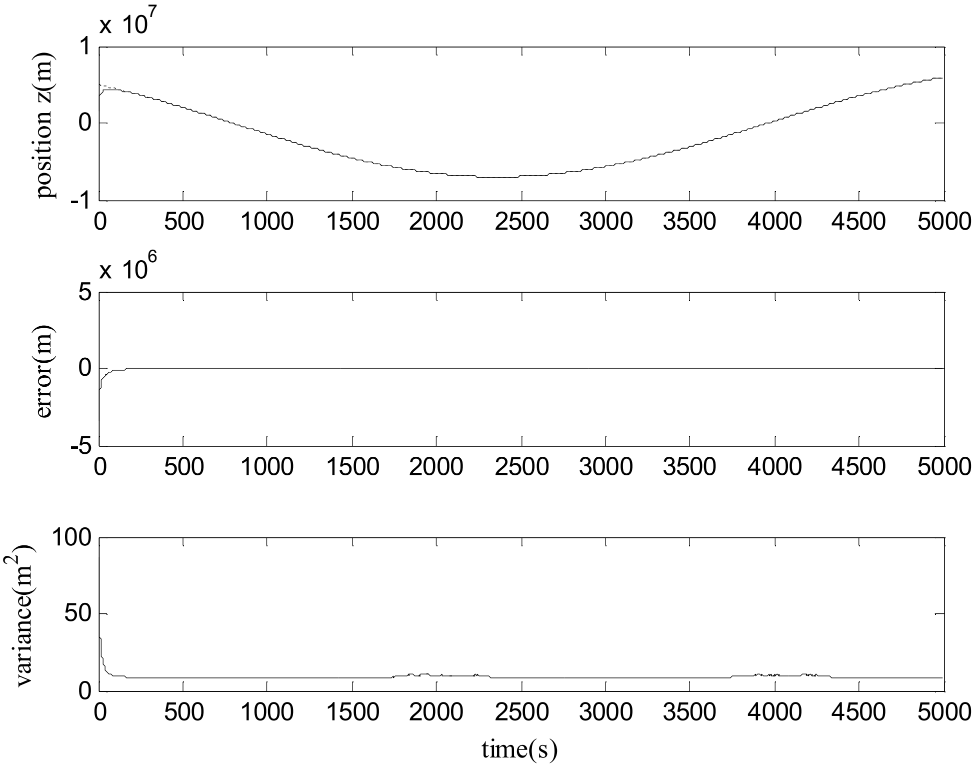

Figure C.112 : Z position est. via RUKF with MMNSF in case of noise inc, GPS.

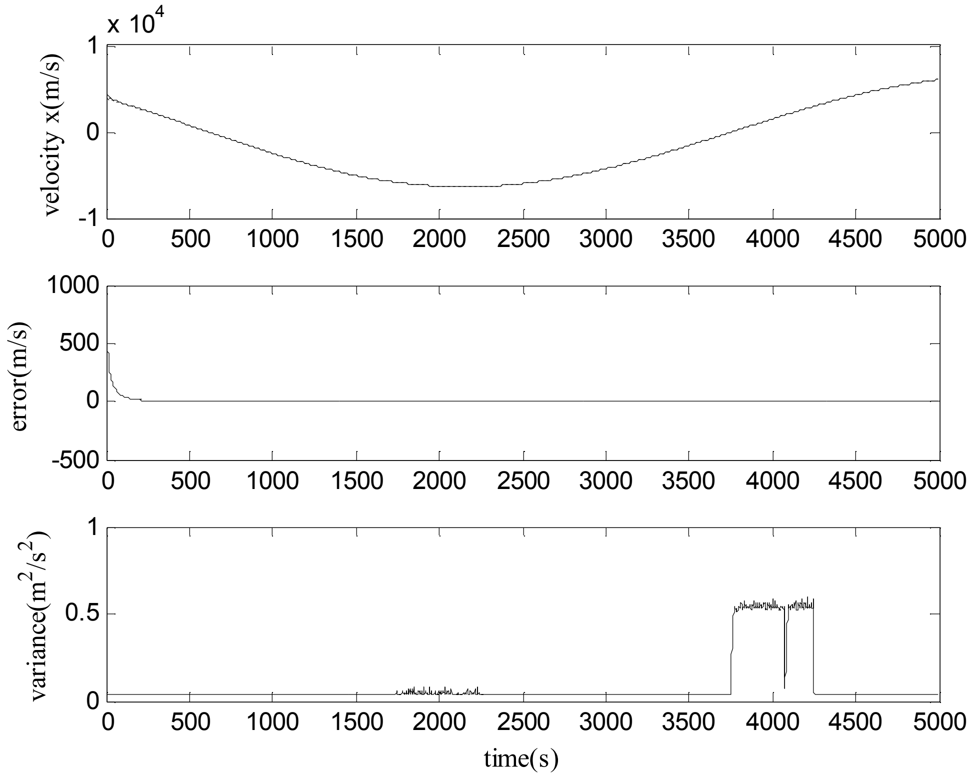

Figure C.113 : X velocity est. via RUKF with MMNSF in case of noise inc, GPS.

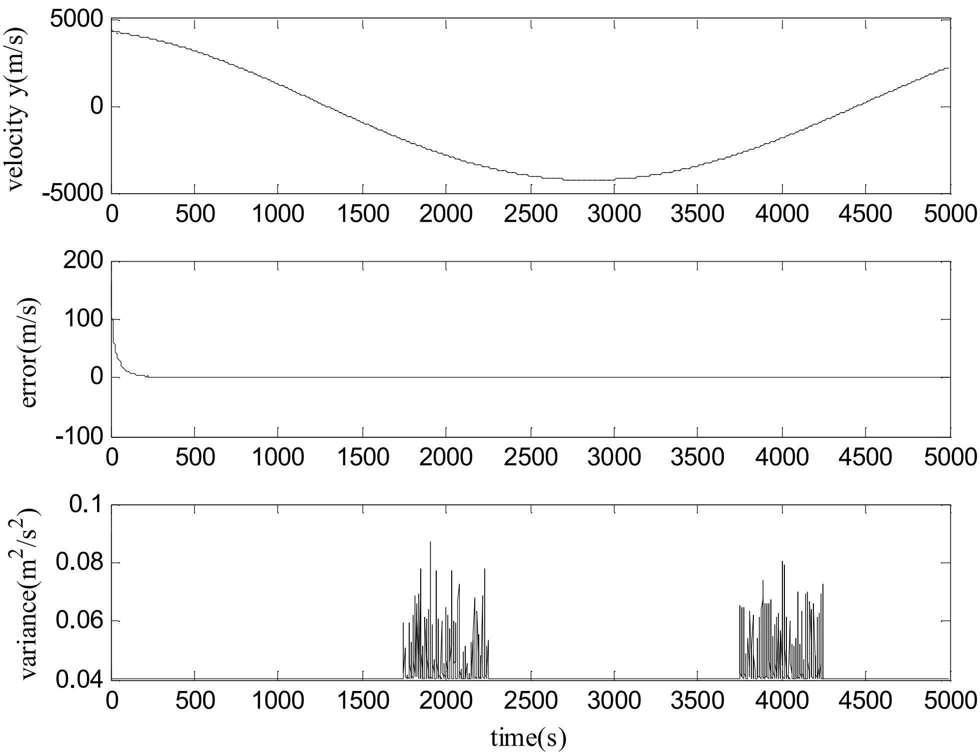

Figure C.114 : Y velocity est. via RUKF with MMNSF in case of noise inc, GPS.

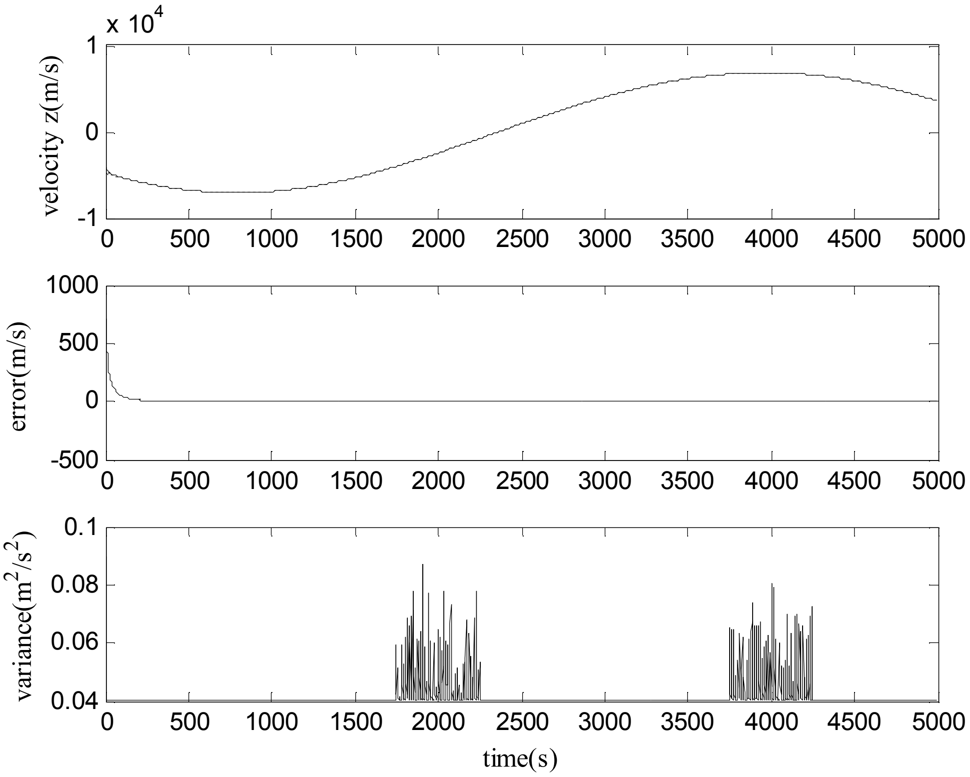

Figure C.115 : Z velocity est. via RUKF with MMNSF in case of noise inc, GPS.

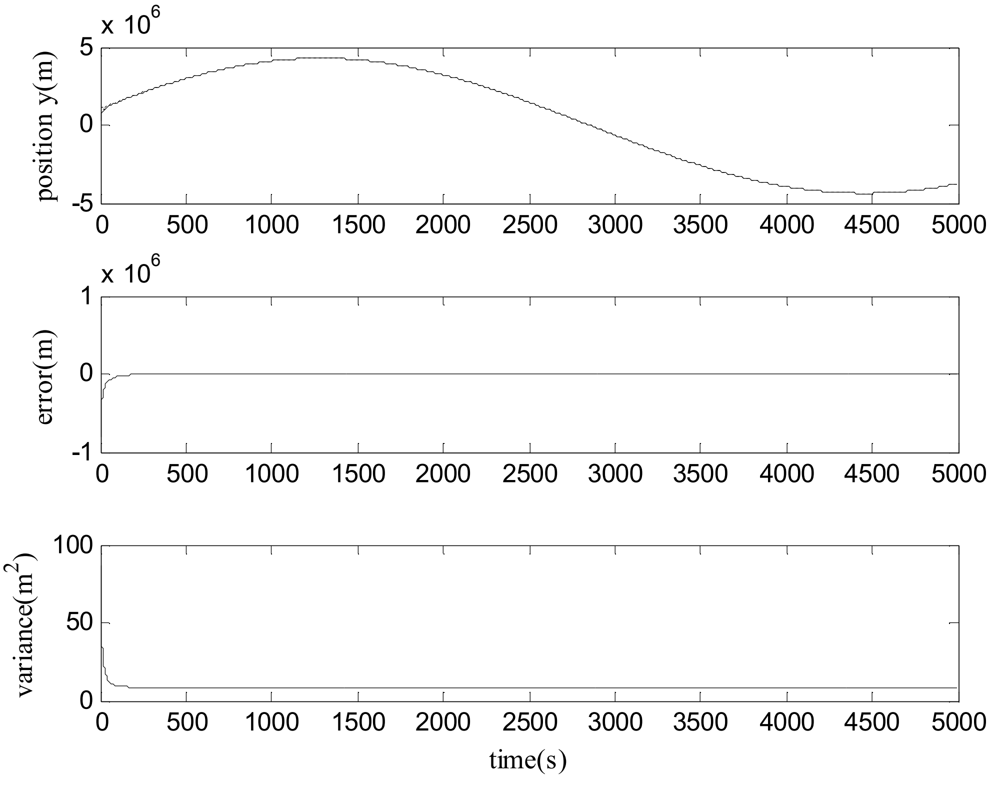

Figure C.116 : Y position est. via Regular UKF in case of zero out, GPS.

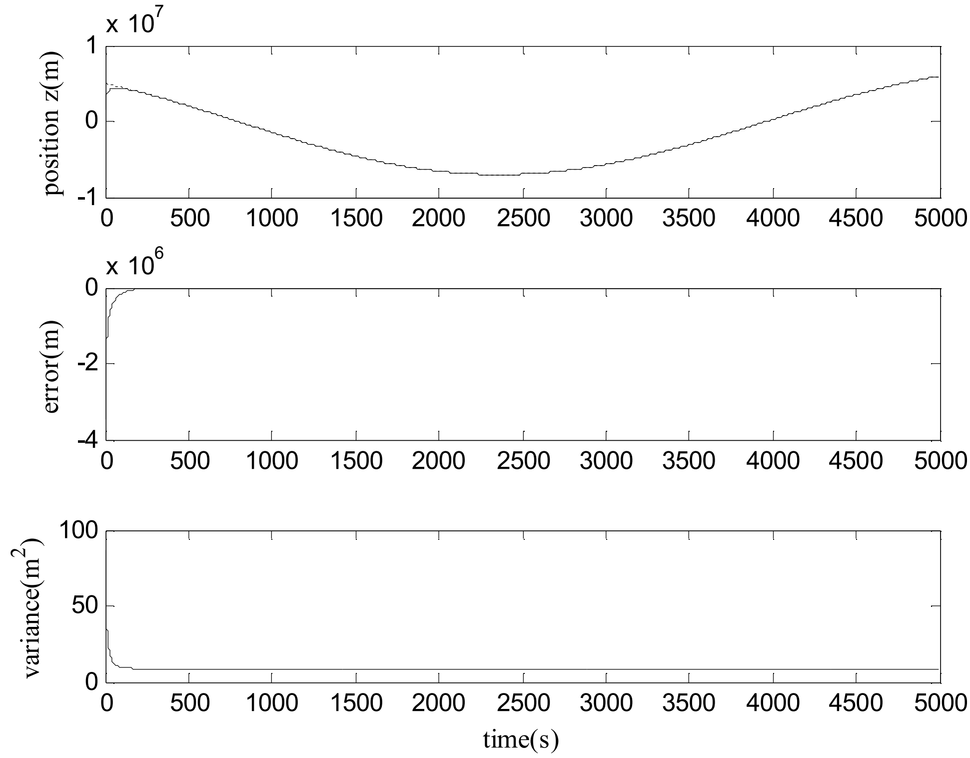

Figure C.117 : Z position est. via Regular UKF in case of zero out, GPS.

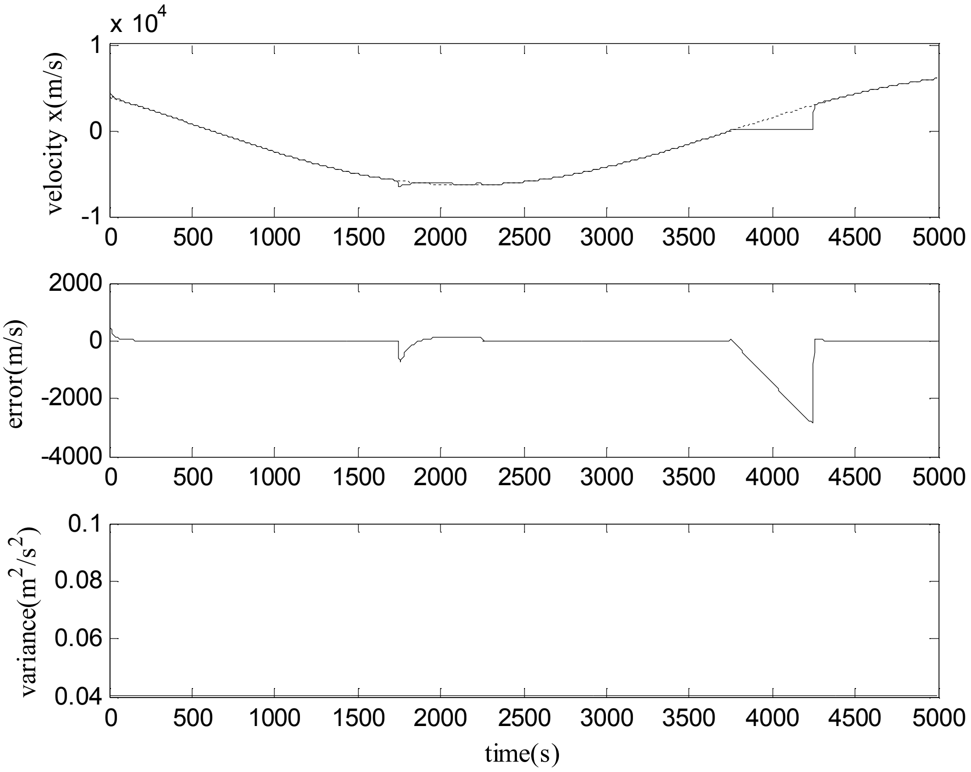

Figure C.118 : X velocity est. via Regular UKF in case of zero out, GPS.

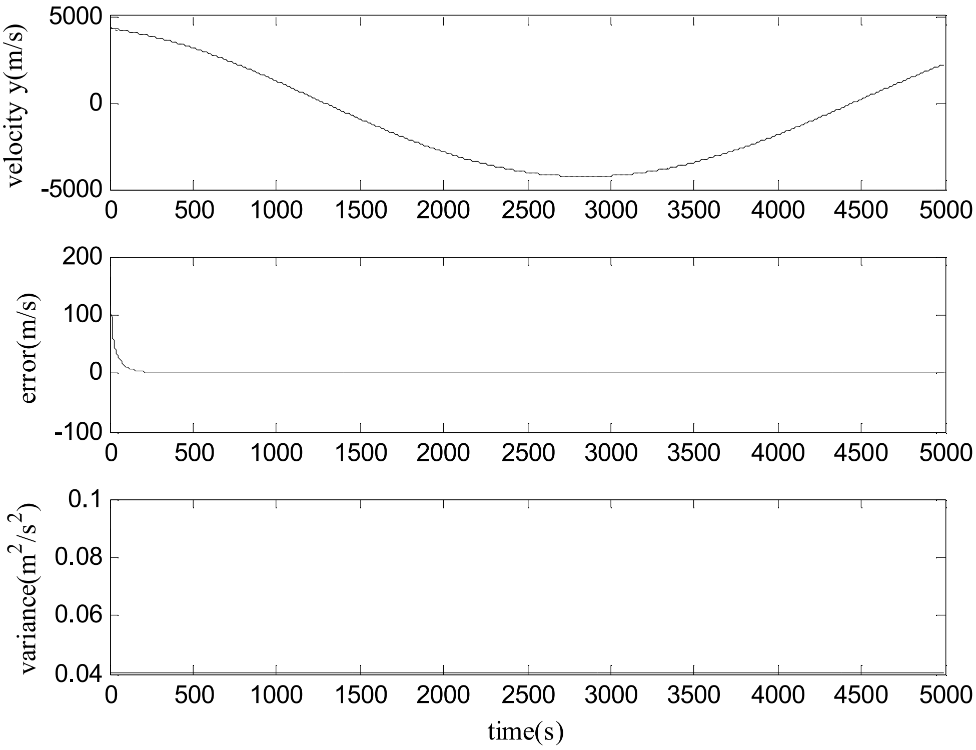

Figure C.119 : Y velocity est. via Regular UKF in case of zero out, GPS.

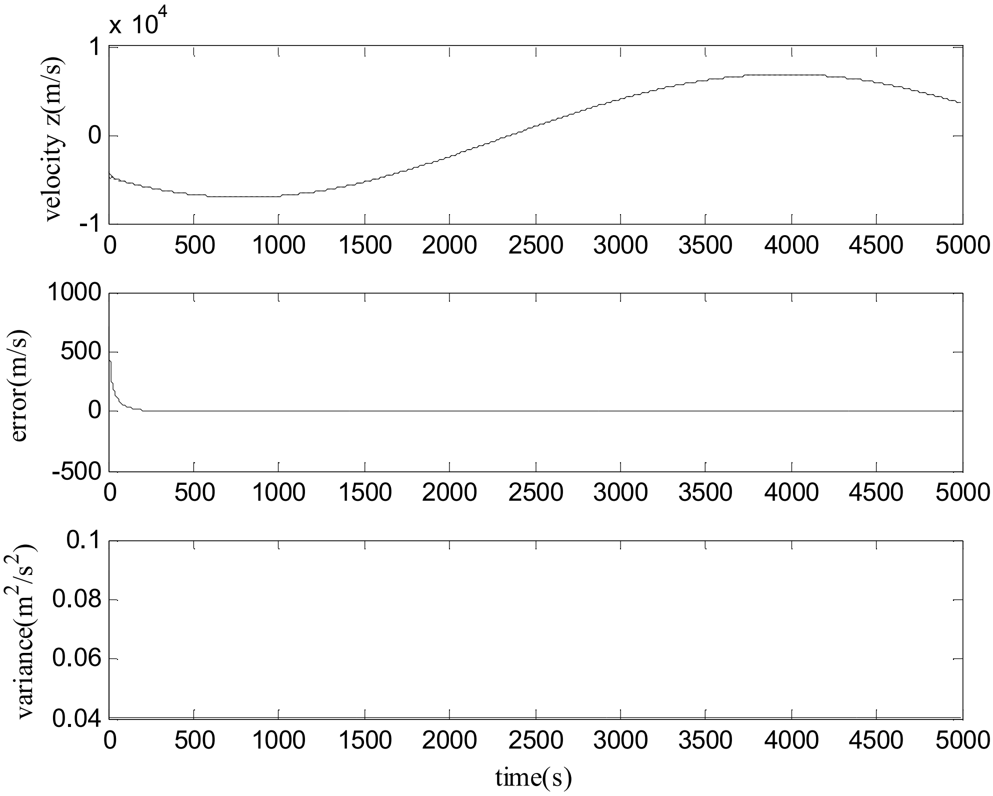

Figure C.120 : Z velocity est. via Regular UKF in case of zero out, GPS.

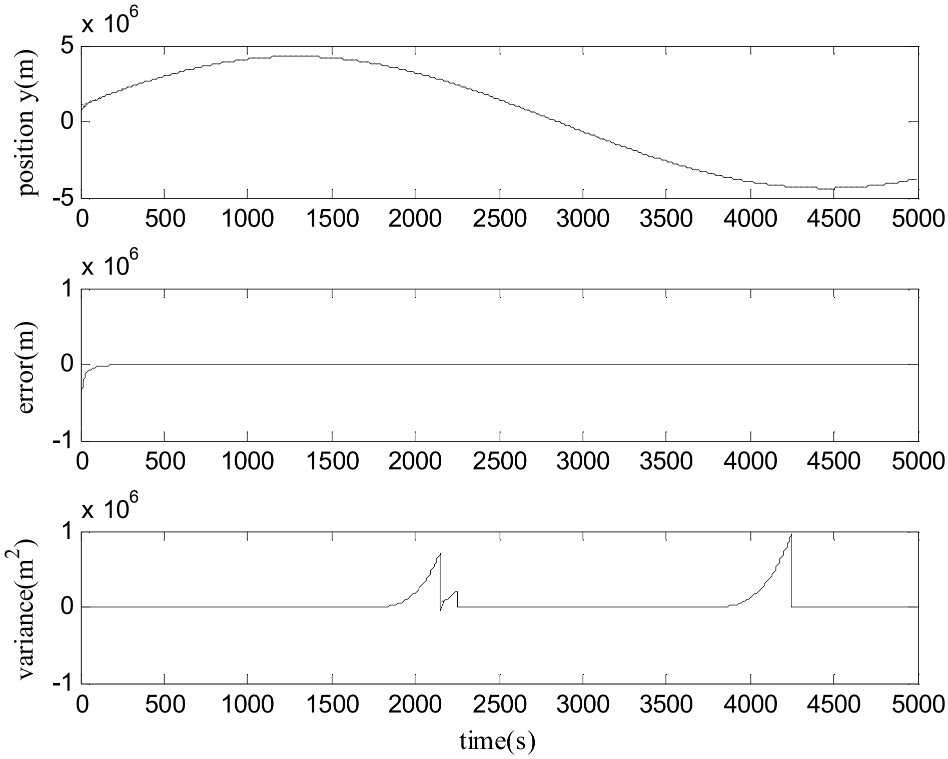

Figure C.121 : Y position est. via RUKF with SMNSF in case of zero out, GPS.

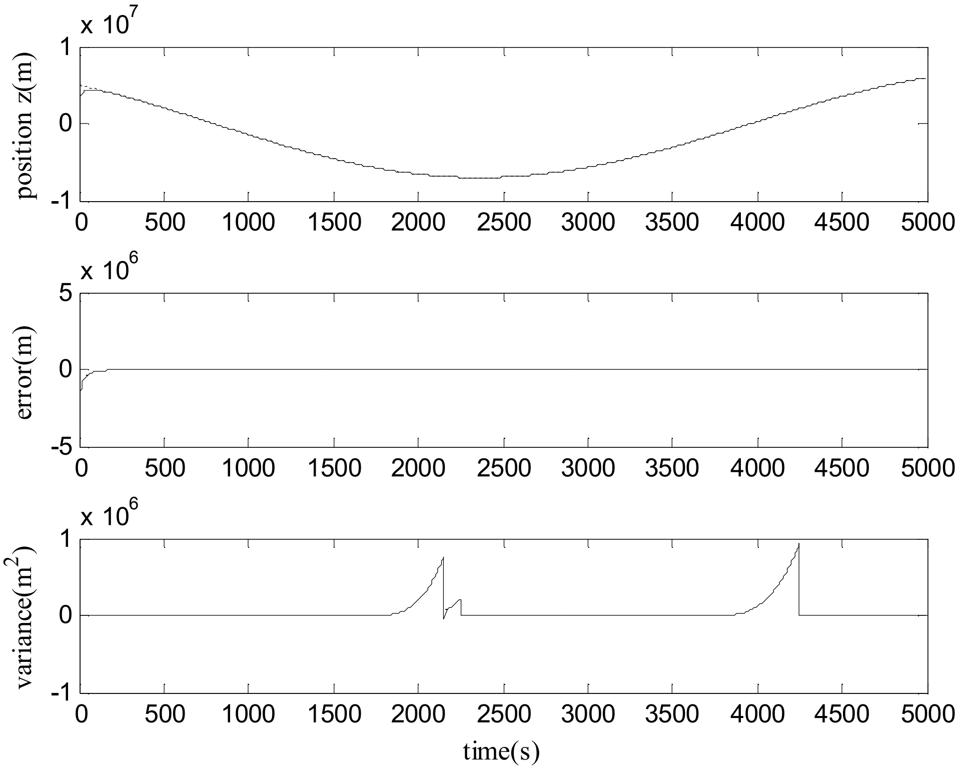

Figure C.122 : Z position est. via RUKF with SMNSF in case of zero out, GPS.

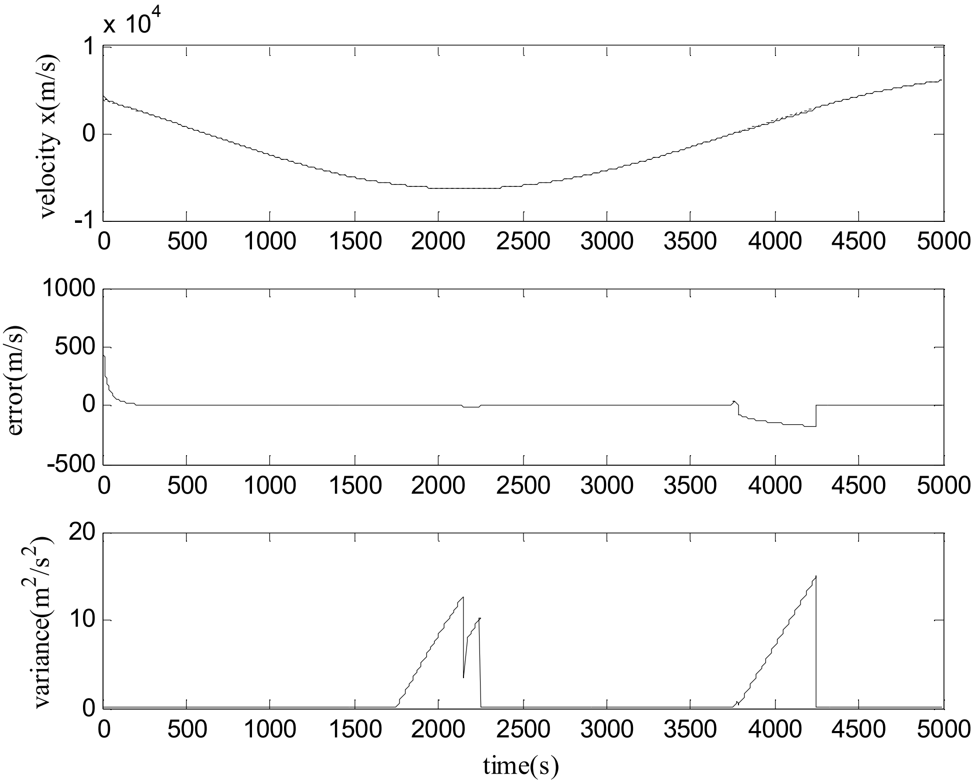

Figure C.123 : X velocity est. via RUKF with SMNSF in case of zero out, GPS.

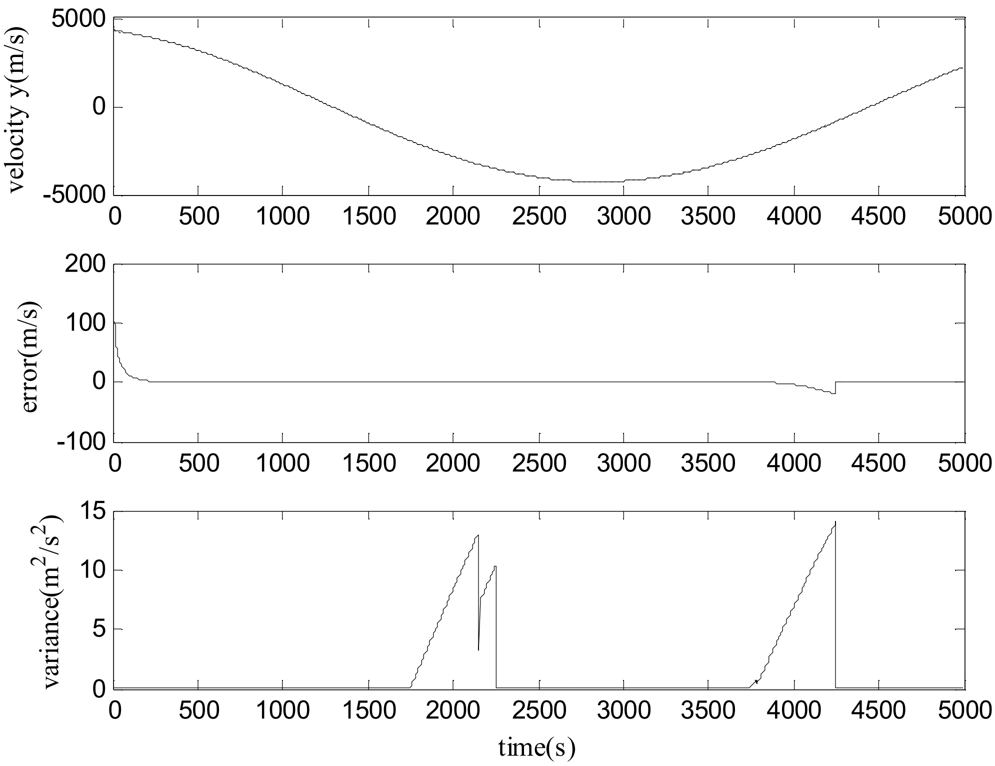

Figure C.124 : Y velocity est. via RUKF with SMNSF in case of zero out, GPS.

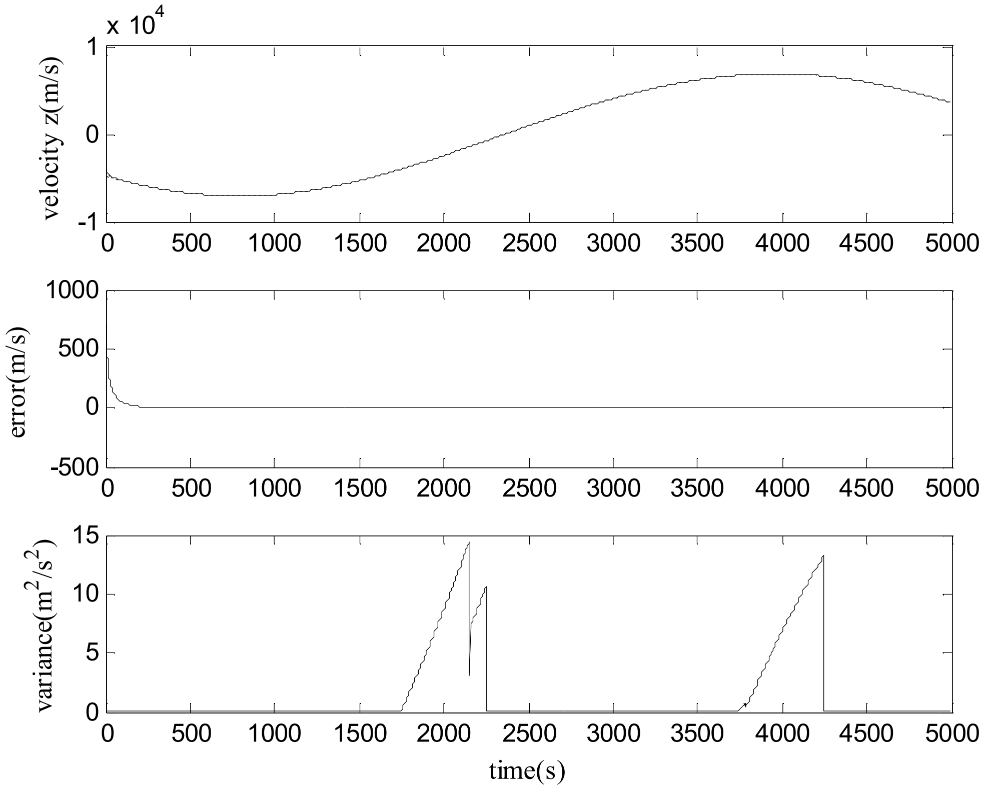

Figure C.125 : Z velocity est. via RUKF with SMNSF in case of zero out, GPS.

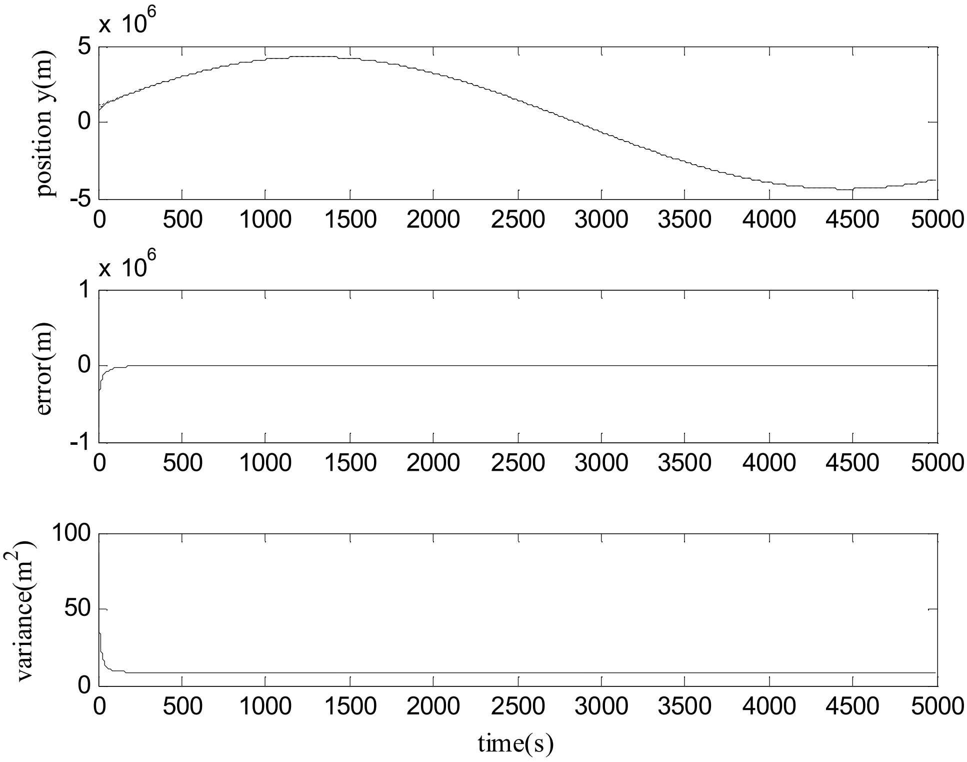

Figure C.126 : Y position est. via RUKF with MMNSF in case of zero out, GPS.

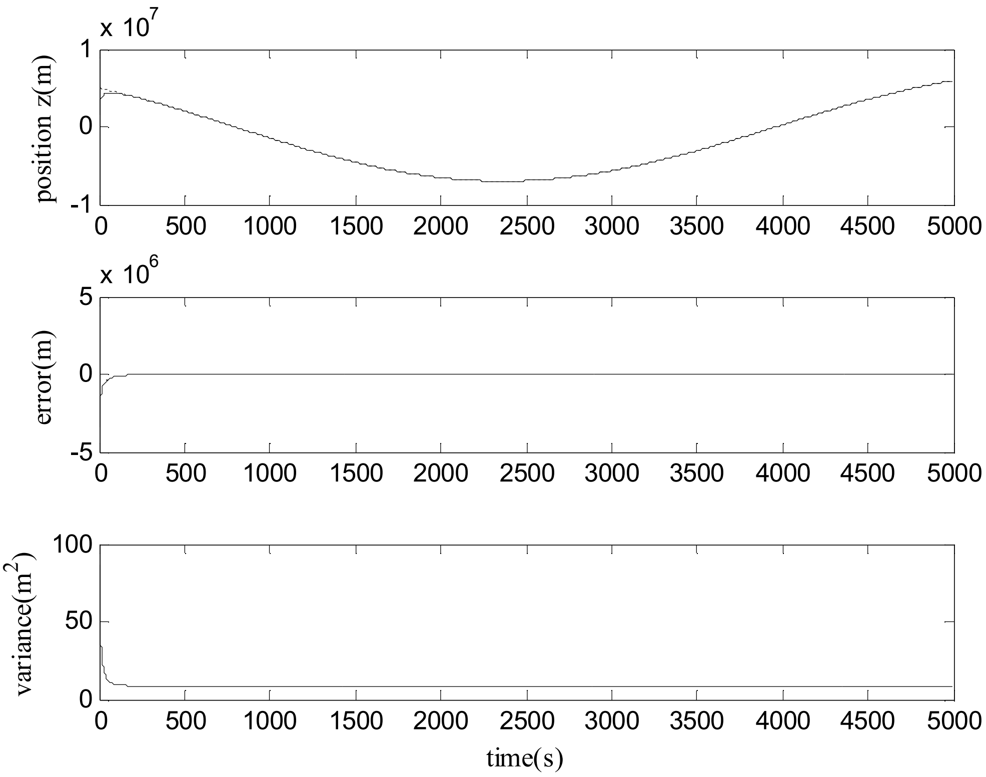

Figure C.127 : Z position est. via RUKF with MMNSF in case of zero out, GPS.

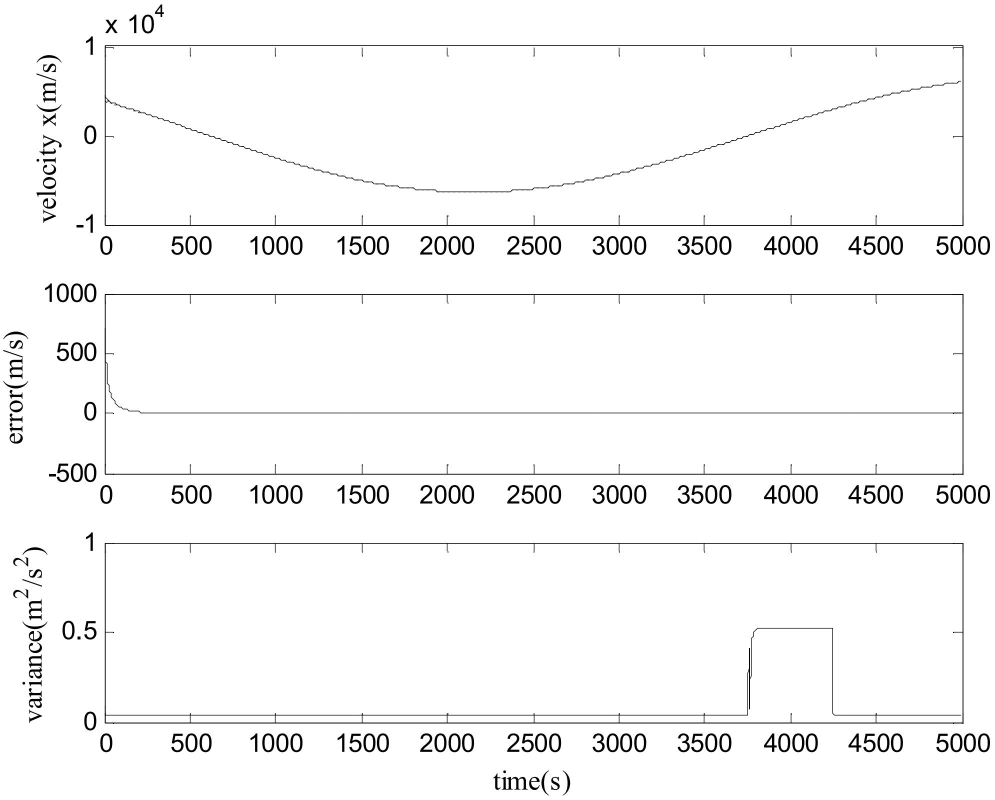

Figure C.128 : X velocity est. via RUKF with MMNSF in case of zero out, GPS.

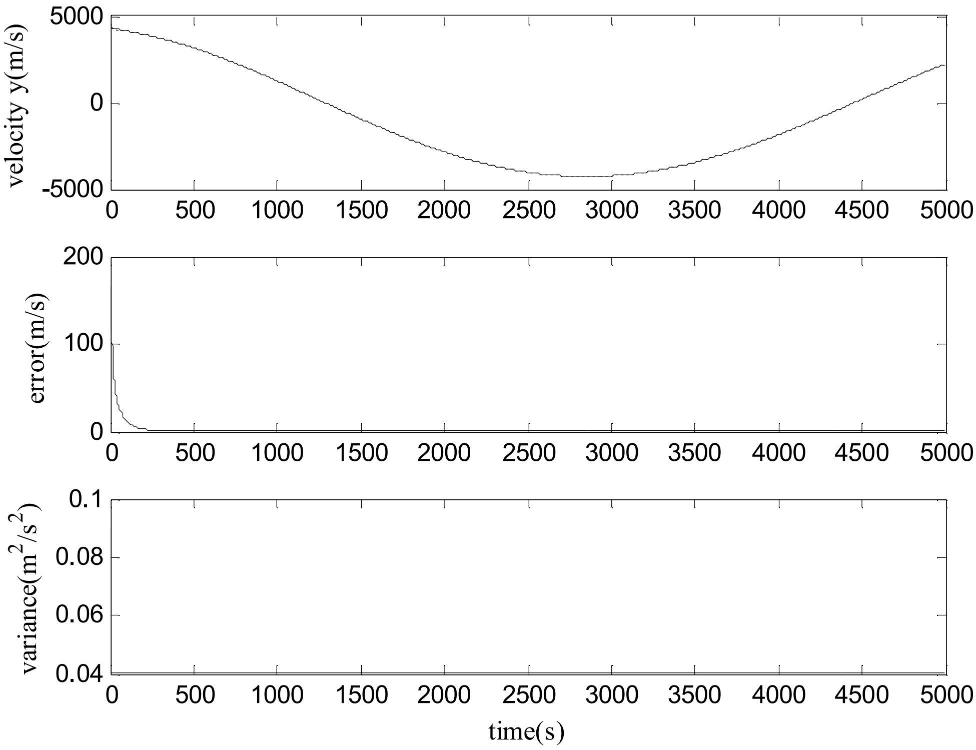

Figure C.129 : Y velocity est. via RUKF with MMNSF in case of zero out, GPS.

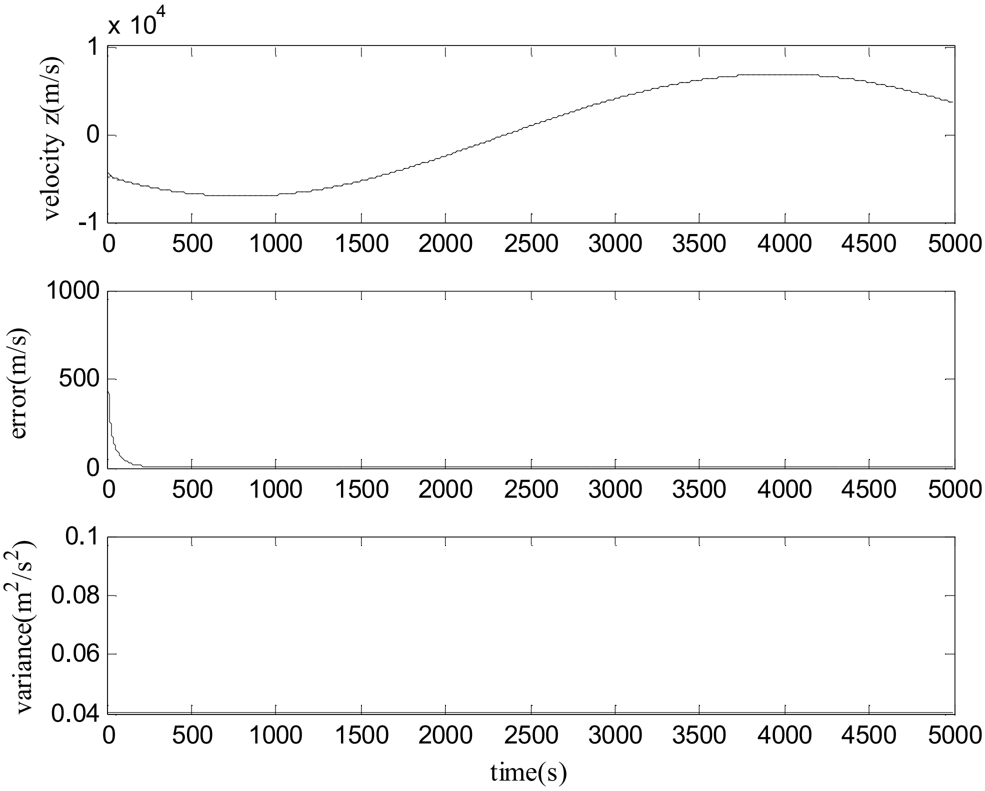

Figure C.130 : Z velocity est. via RUKF with MMNSF in case of zero out, GPS.

CURRICULUM VITAE

Name Surname: Melih Ata

Place and Date of Birth: Istanbul, 05.04.1988

E-Mail: atame@itu.edu.tr

B.Sc.: Astronautical Engineering, Faculty of Aeronautics and Astronautics, Istanbul Technical University, 2006-2011.

M.Sc: Aeronautical and Astronautical Engineering, Graduate School of Science Engineering and Technology, Istanbul Technical University, 2011- 2013.

List of Publications:

- C. Hajiyev, H.E. Soken, **M. Ata** and M. Dinç, 2012. "*FAULT TOLERANT ESTIMATION OF AUTONOMOUS UNDERWATER VEHICLE DYNAMICS VIA ROBUST UKF",* 13th International Carpathian Control Conference (ICCC), 28-31 May 2012, Podbanske, High Tatras, Slovakia.

PUBLICATIONS/PRESENTATIONS ON THE THESIS

- Hajiyev, C., and **Ata, M.** (2011). Error analysis of orbit determination for the geostationary satellite with single station antenna tracking data, *Positioning*, 2, 135-144, doi:10.4236/pos.2011.24013.
- **M. Ata** ve C. Hacıyev, "YER SABİT YÖRÜNGE UYDUSUNUN TEK ANTEN ÖLÇÜM VERİSİ İLE YÖRÜNGESİNİN BELİRLENMESİNİN HATA ANALİZİ", IV. Ulusal Havacılık ve Uzay Konferansı, 12-14 Eylül 2012, Hava Harp Okulu, İstanbul.